ISTITUTO NAZIONALE PER STUDI ED ESPERIENZE DI ARCHITETTURA NAVALE

Istituito con D.L. 23 giugno 1927, n. 1429 modificato con D.L. 24 maggio 1946, n. 530

- Technical Report

Title: PMM MODEL TEST WITH DDG51 INCLUDING UNCERTAINTY ASSESSMENT	Diffusion: *Internal* ☐ *Free* ⊗ *Reserved* ☐ *Classified* ☐
Authors: L.BENEDETTI, B.BOUSCASSE, R.BROGLIA, L.FABBRI, F. LA GALA, C. LUGNI	
Keywords: PMM test, uncertainty assessment	Security advisor:
Client: SIMMAN 2007	
Dir. U. O. R&S: U.P. BULGARELLI	Report n.:14/06 pagg. 180

INSEAN – Technical Report N°_14_

LIST OF CONTEST

1 Introduction 1

2 Facility 1

3 Model 1

4 Test conditions 2

5 Measured quantities 3

6 Brief description of the PMM motion generation 3

7 Uncertainty analysis 5

7.1 Limitations of the present method 6

7.2 Definition of bias limit 7

7.2.1 Non-dimensional longitudinal force, X' 7

7.2.2 Non-dimensional transverse force, Y' 9

7.2.3 Bias on the dimensional yaw moment, N' 10

7.3 Estimation of individual bias limits 11

7.3.1 Estimation of the bias for water density, ρ 11

7.3.2 Estimation of bias limit for carriage speed, U_c 12

7.3.3 Estimation of Bias limit for total model mass, M 13

7.3.4 Estimation of bias for the total moment of Inertia, I_z 13

7.3.5 Estimation of bias for mean draft, T_m 15

7.3.6 Estimation of bias on the perpendicular length, L_{pp} 15

7.3.7 Estimation of bias limit for X_G 15

7.3.8 Estimation of bias limit for Y_G 16

7.3.9 Estimation of bias limit for ψ in dynamic tests 16

7.3.10 Estimation of the bias limit for v_{PMM} in dynamic tests 18

7.3.11 Estimation of the bias limit for v in dynamic tests 18

7.3.12 Estimation of the bias limit for $\dot{v}_{PMM}$ in dynamic tests 19

7.3.13 Estimation of bias limit $\dot{v}$ in dynamic tests 19

7.3.14 Estimation of bias limit for r in dynamic tests 20

7.3.15 Estimation of bias limit for $\dot{r}$ in dynamic tests 21

7.3.16 Estimation of bias limit for u in dynamic tests 21

7.3.17 Estimation of bias limit for $\dot{u}$ in dynamic tests 22

7.3.18 Estimation of bias limit for the measured X-force, F_x 23

7.3.19 Estimation of the bias limit for the measured Y-force, F_Y 30

7.3.20 Estimation of bias limit for yaw moment, M_z 36

7.4 Precision limits 41

7.4.1 Longitudinal force, X' 41

7.4.2 Transverse force, Y' 42

7.4.3 Yaw moment, N' 42

8 Discussion of test results 42

8.1 Static tests 43

8.2 Dynamic tests (Pure Yaw) 46
8.3 Dynamic tests (Pure Sway) 50
8.4 Dynamic test (Yaw and drift) 53

9 Conclusion 55

10 Future works 57

11 Acknowledgement 57

References 59

Appendix A Test programs 60
A.1 Approach speed, Fn = 0.138 60
A.2 Approach speed, Fn = 0.280 61
A.3 Approach speed, Fn = 0.410 62

Appendix B Results from static tests 63

Appendix C Results from uncertainty assessment on dynamic test cases 65
C.1 Dynamic test (Pure yaw), Fr=0.280 65
C.1.1 Motion parameters 65
C.1.2 Longitudinal force 68
C.1.3 Transverse force 70
C.1.4 Yaw moment 71
C.2 Dynamic test (Pure sway), Fr=0.280 73
C.2.1 Motion parameters 73
C.2.2 Longitudinal force 76
C.2.3 Transverse force 78
C.2.4 Yaw moment 79
C.3 Dynamic test (Yaw and drift), Fr=0.280 81
C.3.1 Motion parameters 81
C.3.2 Longitudinal force 84
C.3.3 Transverse force 86
C.3.4 Yaw moment 87
C.4 Dynamic test (Pure yaw), Fr=0.138 89
C.4.1 Motion parameters 89
C.4.2 Longitudinal force 92
C.4.3 Transverse force 94
C.4.4 Yaw moment 95
C.5 Dynamic test (Pure yaw), Fr = 0.410 97
C.5.1 Motion parameters 97
C.5.2 Longitudinal force 100
C.5.3 Transverse force 102
C.5.4 Yaw moment 103
C.6 Results from dynamic tests without uncertainty assessment 105
C.6.1 List of Figures 106

INDEX OF FIGURE

FIGURE 7.2.1.1 SKETCH OF THE INSEAN LARGE AMPLITUDE PLANAR MECHANISM MOTION. 4
FIGURE C.1.1.1HEADING ANGLE (ON THE LEFT) AND BIAS LIMITS (ON THE RIGHT). 65
FIGURE C.1.1.2 TRANSVERSE PMM VELOCITY (ON THE LEFT) AND BIAS LIMITS (ON THE RIGHT). 65
FIGURE C.1.1.3 SWAY VELOCITY (ON THE LEFT) AND BIAS LIMITS (ON THE RIGHT). 66
FIGURE C.1.1.4 TRANSVERSE PMM ACCELERATION (ON THE LEFT) AND BIAS LIMITS (ON THE RIGHT). 66
FIGURE C.1.1.5 SWAY ACCELERATION (ON THE LEFT) AND BIAS LIMITS (ON THE RIGHT). 66
FIGURE C.1.1.6 YAW RATE (ON THE LEFT) AND BIAS LIMITS (ON THE RIGHT). 67
FIGURE C.1.1.7 YAW ACCELERATION (ON THE LEFT) AND BIAS LIMITS (ON THE RIGHT). 67
FIGURE C.1.1.8 SURGE VELOCITY (ON THE LEFT) AND BIAS LIMITS (ON THE RIGHT). 67
FIGURE C.1.1.9 SURGE ACCELERATION (ON THE LEFT) AND BIAS LIMITS (ON THE RIGHT). 68
FIGURE C.1.2.1 BIAS LIMITS FOR MEASURED X-FORCE. 68
FIGURE C.1.2.2 BIAS LIMITS FOR $X^{'}$. 69
FIGURE C.1.2.3 MEASURED F_X AND ITS BIAS LIMIT (ON THE LEFT); $X^{'}$ INCLUDING UNCERTAINTY (ON THE RIGHT). 69
FIGURE C.1.3.1 BIAS LIMITS FOR MEASURED Y-FORCE. 70
FIGURE C.1.3.2 BIAS LIMITS FOR $Y^{'}$. 70
FIGURE C.1.3.3 MEASURED F_Y AND ITS BIAS LIMIT (ON THE LEFT); $Y^{'}$ INCLUDING UNCERTAINTY (ON THE RIGHT). 71
FIGURE C.1.4.1 BIAS LIMITS FOR MEASURED YAW MOMENT M_Z. 71
FIGURE C.1.4.2 BIAS LIMITS FOR $N^{'}$. 72
FIGURE C.1.4.3 MEASURED M_Z AND ITS BIAS LIMIT (ON THE LEFT); $N^{'}$ INCLUDING UNCERTAINTY (ON THE RIGHT). 72
FIGURE C.2.1.1 HEADING ANGLE (ON THE LEFT) AND BIAS LIMITS (ON THE RIGHT). 73
FIGURE C.2.1.2 TRANSVERSE PMM VELOCITY (ON THE LEFT) AND BIAS LIMITS (ON THE RIGHT). 73
FIGURE C.2.1.3 SWAY VELOCITY (ON THE LEFT) AND BIAS LIMITS (ON THE RIGHT). 74
FIGURE C.2.1.4 TRANSVERSE PMM ACCELERATION (ON THE LEFT) AND BIAS LIMITS (ON THE RIGHT). 74
FIGURE C.2.1.5 SWAY ACCELERATION (ON THE LEFT) AND BIAS LIMITS (ON THE RIGHT). 74
FIGURE C.2.1.6 YAW RATE (ON THE LEFT) AND BIAS LIMITS (ON THE RIGHT). 75
FIGURE C.2.1.7 YAW ACCELERATION (ON THE LEFT) AND BIAS LIMITS (ON THE RIGHT). 75
FIGURE C.2.1.8 SURGE VELOCITY (ON THE LEFT) AND BIAS LIMITS (ON THE RIGHT). 75
FIGURE C.2.1.9 SURGE ACCELERATION (ON THE LEFT) AND BIAS LIMITS (ON THE RIGHT). 76
FIGURE C.2.2.1 BIAS LIMITS FOR MEASURED X-FORCE. 76
FIGURE C.2.2.2 BIAS LIMITS FOR $X^{'}$. 77
FIGURE C.2.2.3 MEASURED F_X AND ITS BIAS LIMIT (ON THE LEFT); $X^{'}$ INCLUDING UNCERTAINTY (ON THE RIGHT). 77
FIGURE C.2.3.1 BIAS LIMITS FOR MEASURED Y-FORCE. 78
FIGURE C.2.3.2 BIAS LIMITS FOR $Y^{'}$. 78
FIGURE C.2.3.3 MEASURED F_Y AND ITS BIAS LIMIT (ON THE LEFT); $Y^{'}$ INCLUDING UNCERTAINTY (ON THE RIGHT). 79
FIGURE C.2.4.1 BIAS LIMITS FOR MEASURED YAW MOMENT M_Z. 79
FIGURE C.2.4.2 BIAS LIMITS FOR $N^{'}$. 80
FIGURE C.2.4.3 MEASURED M_Z AND ITS BIAS LIMIT (ON THE LEFT); $N^{'}$ INCLUDING UNCERTAINTY (ON THE RIGHT). 80
FIGURE C.3.1.1 HEADING ANGLE (ON THE LEFT) AND BIAS LIMITS (ON THE RIGHT). 81
FIGURE C.3.1.2 TRANSVERSE PMM VELOCITY (ON THE LEFT) AND BIAS LIMITS (ON THE RIGHT). 81
FIGURE C.3.1.3 SWAY VELOCITY (ON THE LEFT) AND BIAS LIMITS (ON THE RIGHT). 82
FIGURE C.3.1.4 TRANSVERSE PMM ACCELERATION (ON THE LEFT) AND BIAS LIMITS (ON THE RIGHT). 82
FIGURE C.3.1.5 SWAY ACCELERATION (ON THE LEFT) AND BIAS LIMITS (ON THE RIGHT). 82
FIGURE C.3.1.6 YAW RATE (ON THE LEFT) AND BIAS LIMITS (ON THE RIGHT). 83
FIGURE C.3.1.7 YAW ACCELERATION (ON THE LEFT) AND BIAS LIMITS (ON THE RIGHT). 83
FIGURE C.3.1.8 SURGE VELOCITY (ON THE LEFT) AND BIAS LIMITS (ON THE RIGHT). 83
FIGURE C.3.1.9 SURGE ACCELERATION (ON THE LEFT) AND BIAS LIMITS (ON THE RIGHT). 84
FIGURE C.3.2.1 BIAS LIMITS FOR MEASURED X-FORCE. 84
FIGURE C.3.2.2 BIAS LIMITS FOR X'. 85
FIGURE C.3.2.3 MEASURED FX AND ITS BIAS LIMIT (ON THE LEFT); X' INCLUDING UNCERTAINTY (ON THE RIGHT). 85
FIGURE C.3.3.1 BIAS LIMITS FOR MEASURED Y-FORCE. 86
FIGURE C.3.3.2 BIAS LIMITS FOR Y'. 86
FIGURE C.3.3.3 MEASURED FY AND ITS BIAS LIMIT (ON THE LEFT); Y' INCLUDING UNCERTAINTY (ON THE RIGHT). 87
FIGURE C.3.4.1 BIAS LIMITS FOR MEASURED YAW MOMENT MZ. 87
FIGURE C.3.4.2 BIAS LIMITS FOR N'. 88
FIGURE C.3.4.3 MEASURED MZ AND ITS BIAS LIMIT (ON THE LEFT); N' INCLUDING UNCERTAINTY (ON THE RIGHT). 88
FIGURE C.4.1.1 HEADING ANGLE (ON THE LEFT) AND BIAS LIMITS (ON THE RIGHT). 89
FIGURE C.4.1.2 TRANSVERSE PMM VELOCITY (ON THE LEFT) AND BIAS LIMITS (ON THE RIGHT). 89
FIGURE C.4.1.3 SWAY VELOCITY (ON THE LEFT) AND BIAS LIMITS (ON THE RIGHT). 90
FIGURE C.4.1.4 TRANSVERSE PMM ACCELERATION (ON THE LEFT) AND BIAS LIMITS (ON THE RIGHT). 90
FIGURE C.4.1.5 SWAY ACCELERATION (ON THE LEFT) AND BIAS LIMITS (ON THE RIGHT). 90
FIGURE C.4.1.6 YAW RATE (ON THE LEFT) AND BIAS LIMITS (ON THE RIGHT). 91
FIGURE C.4.1.7 YAW ACCELERATION (ON THE LEFT) AND BIAS LIMITS (ON THE RIGHT). 91
FIGURE C.4.1.8 SURGE VELOCITY (ON THE LEFT) AND BIAS LIMITS (ON THE RIGHT). 91
FIGURE C.4.1.9 SURGE ACCELERATION (ON THE LEFT) AND BIAS LIMITS (ON THE RIGHT). 92
FIGURE C.4.2.1 BIAS LIMITS FOR MEASURED X-FORCE. 92
FIGURE C.4.2.2 BIAS LIMITS FOR X'. 93
FIGURE C.4.2.3 MEASURED FX AND ITS BIAS LIMIT (ON THE LEFT); X' INCLUDING UNCERTAINTY (ON THE RIGHT). 93
FIGURE C.4.3.1 BIAS LIMITS FOR MEASURED Y-FORCE. 94
FIGURE C.4.3.2 BIAS LIMITS FOR Y'. 94
FIGURE C.4.3.3 MEASURED FY AND ITS BIAS LIMIT (ON THE LEFT); Y' INCLUDING UNCERTAINTY (ON THE RIGHT). 95
FIGURE C.4.4.1 BIAS LIMITS FOR MEASURED YAW MOMENT MZ. 95
FIGURE C.4.4.2 BIAS LIMITS FOR N'. 96
FIGURE C.4.4.3 MEASURED MZ AND ITS BIAS LIMIT (ON THE LEFT); N' INCLUDING UNCERTAINTY (ON THE RIGHT). 96

FIGURE C.5.1.1 HEADING ANGLE (ON THE LEFT) AND BIAS LIMITS (ON THE RIGHT). 97
FIGURE C.5.1.2 TRANSVERSE PMM VELOCITY (ON THE LEFT) AND BIAS LIMITS (ON THE RIGHT). 97
FIGURE C.5.1.3 SWAY VELOCITY (ON THE LEFT) AND BIAS LIMITS (ON THE RIGHT). 98
FIGURE C.5.1.4 TRANSVERSE PMM ACCELERATION (ON THE LEFT) AND BIAS LIMITS (ON THE RIGHT). 98
FIGURE C.5.1.5 SWAY ACCELERATION (ON THE LEFT) AND BIAS LIMITS (ON THE RIGHT). 98
FIGURE C.5.1.6 YAW RATE (ON THE LEFT) AND BIAS LIMITS (ON THE RIGHT). 99
FIGURE C.5.1.7 YAW ACCELERATION (ON THE LEFT) AND BIAS LIMITS (ON THE RIGHT). 99
FIGURE C.5.1.8 SURGE VELOCITY (ON THE LEFT) AND BIAS LIMITS (ON THE RIGHT). 99
FIGURE C.5.1.9 SURGE ACCELERATION (ON THE LEFT) AND BIAS LIMITS (ON THE RIGHT). 100
FIGURE C.5.2.1 BIAS LIMITS FOR MEASURED X-FORCE. 100
FIGURE C.5.2.2 BIAS LIMITS FOR X'. 101
FIGURE C.5.2.3 MEASURED FX AND ITS BIAS LIMIT (ON THE LEFT); X' INCLUDING UNCERTAINTY (ON THE RIGHT). 101
FIGURE C.5.3.1 BIAS LIMITS FOR MEASURED Y-FORCE. 102
FIGURE C.5.3.2 BIAS LIMITS FOR Y'. 102
FIGURE C.5.3.3 MEASURED FY AND ITS BIAS LIMIT (ON THE LEFT); Y' INCLUDING UNCERTAINTY (ON THE RIGHT). 103
FIGURE C.5.4.1 BIAS LIMITS FOR MEASURED YAW MOMENT MZ. 103
FIGURE C.5.4.2 BIAS LIMITS FOR N'. 104
FIGURE C.5.4.3 MEASURED MZ AND ITS BIAS LIMIT (ON THE LEFT); N' INCLUDING UNCERTAINTY (ON THE RIGHT). 104
FIGURE C.6.1.1-YAW_138_1 (PART 1). 106
FIGURE C.6.1.2 YAW_138_1 (PART 2). 107
FIGURE C.6.1.3 YAW_138_2 (PART 1). 108
FIGURE C.6.1.4 YAW_138_2 (PART 2). 109
FIGURE C.6.1.5 YAW_138_3 (PART 1). 110
FIGURE C.6.1.6 YAW_138_3 (PART 2). 111
FIGURE C.6.1.7 YAW_138_4 (PART 1). 112
FIGURE C.6.1.8 YAW_138_4 (PART 2). 113
FIGURE C.6.1.9 YAW_138_5 (PART 1). 114
FIGURE C.6.1.10 YAW_138_5 (PART 2). 115
FIGURE C.6.1.11 YAW_138_6 (PART 1). 116
FIGURE C.6.1.12 YAW_138_6 (PART 2). 117
FIGURE C.6.1.13 YAW_280_1 (PART 1). 118
FIGURE C.6.1.14 YAW_280_1 (PART 2). 119
FIGURE C.6.1.15 YAW_280_2 (PART 1). 120
FIGURE C.6.1.16 YAW_280_2 (PART 2). 121
FIGURE C.6.1.17 YAW_280_3 (PART 1). 122
FIGURE C.6.1.18 YAW_280_3 (PART 2). 123
FIGURE C.6.1.19 YAW_280_4 (PART 1). 124
FIGURE C.6.1.20 YAW_280_4 (PART 2). 125
FIGURE C.6.1.21 YAW_280_5 (PART 1). 126
FIGURE C.6.1.22 YAW_280_5 (PART 2). 127
FIGURE C.6.1.23 YAW_280_6 (PART 1). 128
FIGURE C.6.1.24 YAW_280_6 (PART 2). 129
FIGURE C.6.1.25 YAW_280_7 (PART 1). 130
FIGURE C.6.1.26 YAW_280_7 (PART 2). 131
FIGURE C.6.1.27 YAW_280_8 (PART 1). 132
FIGURE C.6.1.28 YAW_280_8 (PART 2). 133
FIGURE C.6.1.29 YAW_280_9 (PART 1). 134
FIGURE C.6.1.30 YAW_280_9 (PART 2). 135
FIGURE C.6.1.31 YAW_280_10 (PART 1). 136
FIGURE C.6.1.32 YAW_280_10 (PART 2). 137
FIGURE C.6.1.33 YAW_280_11 (PART 1). 138
FIGURE C.6.1.34 YAW_280_11 (PART 2). 139
FIGURE C.6.1.35 YAW_280_12 (PART 1). 140
FIGURE C.6.1.36 YAW_280_12 (PART 2). 141
FIGURE C.6.1.37 YAW_410_1 (PART 1). 142
FIGURE C.6.1.38 YAW_410_1 (PART 2). 143
FIGURE C.6.1.39 YAW_410_1 (PART 2). 144
FIGURE C.6.1.40 YAW_410_2 (PART 2). 145
FIGURE C.6.1.41 YAW_410_3 (PART 1). 146
FIGURE C.6.1.42 YAW_410_3 (PART 2). 147
FIGURE C.6.1.43 YAW_410_4 (PART 1). 148
FIGURE C.6.1.44 YAW_410_4 (PART 2). 149
FIGURE C.6.1.45 YAW_410_5 (PART 1). 150
FIGURE C.6.1.46 YAW_410_5 (PART 2). 151
FIGURE C.6.1.47 SWAY_280_1 (PART 1). 152
FIGURE C.6.1.48 SWAY_280_1 (PART 2). 153
FIGURE C.6.1.49 SWAY_280_2 (PART 1). 154
FIGURE C.6.1.50 SWAY_280_2 (PART 2). 155
FIGURE C.6.1.51 SWAY_280_3 (PART 1). 156
FIGURE C.6.1.52 SWAY_280_3 (PART 2). 157
FIGURE C.6.1.53 SWAY_280_4 (PART 1). 158
FIGURE C.6.1.54 SWAY_280_4 (PART 2). 159
FIGURE C.6.1.55 SWAY_280_5 (PART 1). 160
FIGURE C.6.1.56 SWAY_280_5 (PART 2). 161
FIGURE C.6.1.57 SWAY_280_6 (PART 1). 162
FIGURE C.6.1.58 SWAY_280_6 (PART 2). 163
FIGURE C.6.1.59 SWAY_280_7 (PART 1). 164

FIGURE C.6.1.60 SWAY_280_7 (PART 2). 165
FIGURE C.6.1.61 SWAY_280_8 (PART 1). 166
FIGURE C.6.1.62 SWAY_280_8 (PART 2). 167
FIGURE C.6.1.63 SWAY_280_9 (PART 1). 168
FIGURE C.6.1.64 SWAY_280_9 (PART 2). 169
FIGURE C.6.1.65 YAW&DRIFT_280_1 (PART 1). 170
FIGURE C.6.1.66 YAW&DRIFT_280_2 (PART 1). 171
FIGURE C.6.1.67 YAW&DRIFT_280_2 (PART 2). 172
FIGURE C.6.1.68 YAW&DRIFT_280_3 (PART 1). 173
FIGURE C.6.1.69 YAW&DRIFT_280_3 (PART 2). 174

INDEX of TABLES

TABLE 3-1 FULL SCALE AND MODEL SCALE PARTICULARS 1
TABLE 5-1 OVERVIEW OF MEASURED QUANTITIES. 3
TABLE 7-1 BIAS LIMIT FOR WATER DENSITY. 12
TABLE 7-2 BIAS LIMIT FOR MODEL MASS. 13
TABLE 7-3 PERIOD DISCARDS OF THE LEAST SQUARE CURVE. 13
TABLE 7-4 BIAS LIMIT FOR MEAN DRAFT. 15
TABLE 7-5 BIAS LIMIT FOR THE SHIP LENGTH. 15
TABLE 7-6 BIAS LIMIT FOR X_G 16
TABLE 7-7 BIAS LIMIT FOR Y_G 16
TABLE 7-8 BIAS LIMITS FOR DRIFT ANGLE. 17
TABLE 7-9 BIAS LIMIT FOR THE FREQUENCY, THE TIME AND THE MAX ANGLE OF THE YAW MOTION. 17
TABLE 7-10 UNCERTAINTIES IN CONNECTION WITH THE ESTIMATE OF B_ψ 17
TABLE 7-11 BIAS LIMIT FOR THE AMPLITUDE OF THE SWAY MOTION. 18
TABLE 7-12 CONSIDERED TERMS. 23
TABLE 7-13 BIAS LIMIT DATA RELATED TO DRIFT ANGLE SETTING ($\beta = 10°$) IN STATIC TESTS. 24
TABLE 7-14 UNCERTAINTY OF WEIGHTS FOR AFTER TRANSDUCER. 25
TABLE 7-15 UNCERTAINTY OF WEIGHTS FOR FORE TRANSDUCER. 25
TABLE 7-16 WEIGHT RELATED BIAS LIMIT. 26
TABLE 7-17 ACQUISITION BIAS LIMIT. 26
TABLE 7-18 CONVERSION A/D BIAS LIMIT. 27
TABLE 7-19 TOTAL BIAS LIMIT FOR CALIBRATION AND ACQUISITION OF FORCE GAUGES. 27
TABLE 7-20 COEFFICIENT FOR POLYNOMIAL FAIRING IN PURE YAW. (DIMENSIONAL). 28
TABLE 7-21 COEFFICIENTS FOR POLYNOMIAL FAIRING IN PURE SWAY. (DIMENSIONAL). 28
TABLE 7-22 COEFFICIENTS FOR POLYNOMIAL FAIRING IN YAW AND DRIFT. (DIMENSIONAL). 29
TABLE 7-23 CONSIDERED TERMS. 30
TABLE 7-24 BIAS LIMIT DATA RELATED TO DRIFT ANGLE SETTING ($\beta = 10°$) IN STATIC TESTS. 31
TABLE 7-25 AFTER GAUGE: UNCERTAINTY OF WEIGHTS. 31
TABLE 7-26 FORE GAUGE: UNCERTAINTY OF WEIGHTS. 32
TABLE 7-27 WEIGHT RELATED BIAS LIMIT. 32
TABLE 7-28 ACQUISITION BIAS LIMIT. 32
TABLE 7-29 CONVERSION A/D BIAS LIMIT. 32
TABLE 7-30 TOTAL BIAS LIMIT FOR CALIBRATION AND ACQUISITION OF FORCE GAUGES. 33
TABLE 7-31 COEFFICIENT FOR POLYNOMIAL FAIRING IN PURE YAW (DIMENSIONAL). 33
TABLE 7-32 COEFFICIENTS FOR POLYNOMIAL FAIRING IN PURE SWAY (DIMENSIONAL). 34
TABLE 7-33 COEFFICIENTS FOR POLYNOMIAL FAIRING IN YAW AND DRIFT (DIMENSIONAL). 34
TABLE 7-34 CONSIDERED TERMS. 36
TABLE 7-35 BIAS LIMIT DATA RELATED TO DRIFT ANGLE SETTING, $\beta = 10^\circ$ IN STATIC TEST. 37
TABLE 7-36 COEFFICIENT FOR POLYNOMIAL FAIRING IN PURE YAW. (DIMENSIONAL). 38
TABLE 7-37 COEFFICIENT FOR POLYNOMIAL FAIRING IN PURE SWAY. (DIMENSIONAL) 38
TABLE 7-38 COEFFICIENT FOR POLYNOMIAL FAIRING IN YAW AND DRIFT. (DIMENSIONAL). 39
TABLE 8-1 SUMMARY OF BIAS LIMIT FOR THE MEASURED F_X AT 10 DEGREES DRIFT. 43
TABLE 8-2 SUMMARY OF BIAS LIMIT FOR THE MEASURED F_Y AT 10 DEGREES DRIFT. 43
TABLE 8-3 SUMMARY OF BIAS LIMIT FOR THE MEASURED M_Z AT 10 DEGREES DRIFT. 43
TABLE 8-4 SUMMARY OF UNCERTAINTIES FOR X' FROM THE STATIC DRIFT TEST, $\beta = 10^\circ$ 44
TABLE 8-5 SUMMARY OF UNCERTAINTIES FOR Y' FROM THE STATIC DRIFT TEST, $\beta = 10^\circ$ 44
TABLE 8-6 SUMMARY OF UNCERTAINTIES FOR N' FROM THE STATIC DRIFT TEST, $\beta = 10^\circ$ 45
TABLE 8-7 SINKAGE AT FP. 45
TABLE 8-8 SINKAGE AT AP. 45
TABLE 8-9 UNCERTAINTIES AND BIAS LIMITS RELATED TO THE X-FORCE, WHERE R = R_{MAX}. 49
TABLE 8-10 UNCERTAINTIES AND BIAS LIMITS RELATED TO THE Y-FORCE, WHERE R = R_{MAX}. 49
TABLE 8-11 UNCERTAINTIES AND BIAS LIMITS RELATED TO THE YAW MOMENT, WHERE R = R_{MAX}. 50
TABLE 8-12 UNCERTAINTIES AND BIAS LIMITS RELATED TO THE X-FORCE, WHERE V = V_{MAX}. 52
TABLE 8-13 UNCERTAINTIES AND BIAS LIMITS RELATED TO THE Y-FORCE, WHERE V = V_{MAX}. 52
TABLE 8-14 UNCERTAINTIES AND BIAS LIMITS RELATED TO THE YAW MOMENT, WHERE V = V_{MAX}. 53

TABLE 8-15 UNCERTAINTIES AND BIAS LIMITS RELATED TO THE X-FORCE, WHERE R = R_{MAX}. 54
TABLE 8-16 UNCERTAINTIES AND BIAS LIMITS RELATED TO THE Y-FORCE, WHERE R = R_{MAX}. 55
TABLE 8-17 UNCERTAINTIES AND BIAS LIMITS RELATED TO THE YAW MOMENT, WHERE R = R_{MAX}. 55

1 Introduction

The present report it is edited in the framework of the ITTC Manoeuvrability Committee activities in order to:

1. assess the experimental uncertainties related to the INSEAN Planar Motion Mechanism (PMM);
2. compare the INSEAN data with the IIHR and Force Technology towing tanks;
3. validate the CFD codes.

The scope of the work it is to develop a procedure for the uncertainty assessment to be used for the analysis of global forces acting on ship model during a PMM test. In this report are not considered the uncertainties on the traditional manoeuvring coefficients but are examined only the uncertainties on the hydrodynamic forces.
Tests are carried out with a 5.71 m between Lpp *DDG51 frigate* (INSEAN model C. 2340) that is a standard dimension for the INSEAN Large Amplitude PMM.
The uncertainty analysis carried out in the present work it is directly related to the scheme of the INSEAN PMM and some analytical development can be slightly different for different equipment.

2 Facility

The PMM tests are conducted in INSEAN towing tank in Roma, Italy. The towing tank is 500m long, 12.5m wide and 6.5m deep.

3 Model

The applied model is a 1:24.83 scale model of the hull of the *DDG51 frigate*. The full scale and model scale hull particulars are given in Table 3-1. The test is conducted with the bare hull appended with bilge keels only.

	Ship	Model
Scale	1 : 1	1: 24.83
L_{PP} [m]	142.00	5.7200
L_{WL} [m]	142.18	5.7273
B_{WL} [m]	19.10	0.7690
T_m [m]	6.16	0.2480
∇ [m^3]	8472	0.5540
Δ [Ton]	8684	0.5540
C_{b-}	0.506	0.507

Table 3-1 Full scale and model scale particulars

4 Test conditions

The work interested four different typologies of movement for the model in matter: the before is a «pure drift», a static test in which the model is drawn to speed costing and presents a defined angle of route; the other three are dynamic tests, «pure sway», «pure yaw» and «yaw and drift». In these last one, the model it comes done motive oscillating second defined lecterns.

"Pure drift":
The model travels through the tank in oblique flow due to a given drift angle β.

"Pure sway":
The model travels through the tank on straight ahead course while it is oscillated from side to side. With u , v and r being the surge velocity, the sway velocity and the yaw rate in the ships local coordinate system, the pure sway motion can also be expressed in terms of the velocities, i.e. $u = U_C$ (carriage speed), $r = 0$ and v oscillates harmonically.

"Pure Yaw":
The model travels through the tank while it performs a pure yaw motion, where it is forced to follow the tangent of the oscillating path. In terms of velocities this means that $v = 0$, while r and u oscillate harmonically. u oscillates, since the carriage speed in the present set-up is constant.

"Yaw and drift":
The model travels through the tank, while it performs a pure yaw motion as described above. However, a fixed and preset drift angle is overlaid on the motion in order to obtain a drift angle relative to the tangent of the oscillating path. In terms of velocities this means that $v \neq 0$, but constant, while r and u oscillate harmonically.

For all of the above conditions, the tests will be conducted according to FORCE's standard PMM testing procedures. This means that the model will be constrained in roll but free to heave and pitch. Further, three approach speeds corresponding to the Froude numbers: $Fr=0.138$, $Fr=0.280$ and $Fr=0.410$ are tested. The test programs for the three speeds, including repeat tests for uncertainty assessment are shown in Appendix A.

5 Measured quantities

For all of the conditions outlined in §4, the quantities listed in Table 5-1 are measured during each run, as is standard practice in INSEAN PMM tests. Measurements 1 through 3 and 8 trough 9 provide the instantaneous operating conditions for the ship and 4 through 7 provide the resultant forces. Moreover channels 11 and 12 provide the ship acceleration (transducers collocated inside the model).

All forces are measured in a coordinate system following the ship, meaning that *X*-components act in the longitudinal direction of the ship and *Y*-components perpendicular to this direction. The yaw moment is taken with respect to the mid-ship position at L_{pp} / 2. All hydrodynamic forces and moments presented in the present work are non-dimensionalized by the following data reduction equations

$$\left\{ X' = \frac{F_{X_{Hydro}}}{0.5\rho U^2 A_0} \; Y' = \frac{F_{Y_{Hydro}}}{0.5\rho U^2 A_0} \; N' = \frac{M_{Z_{Hydro}}}{0.5\rho U^2 A_0 L_{pp}} \right. \tag{5.1}$$

where:

- ρ is the water density;
- $U = \sqrt{u^2 + v^2}$ is the ship speed (constant in static tests, variable in the dynamic tests)
- A_0 is the lateral underwater area: $A_0 = L_{pp} T_m$ where T_m is the mean draft and L_{pp} is the length between perpendiculars.

ID	Quantity	Sampling frequency [Hz]
1	Ship speed	133
2	Sway amplitude	133
3	Yaw amplitude	133
4	X-force, forward	133
5	X-force aft	133
6	Y-force forward	133
7	Y-force aft	133
8	Sinkage, forward	133
9	Sinkage, aft	133
10	Trigger	133
11	X-acceleration	133
12	Y-acceleration	133

Table 5-1 Overview of measured quantities.

6 Brief description of the PMM motion generation

The large amplitude planar motion mechanism (LAHPMM) is a device which can impart combinations of transverse (sway), rotational (yaw) motions to surface ship models being tested in a ship model towing tank (see Figure 7.2.1.1).

The forces generated by these motions are measured by a set of transducers located in the models and these forces converted to hydrodynamic force and moment coefficients which are then used to study and predict ship manoeuvrability.

The primary components of the INSEAN's LAHPMM are:

- Motions base which provides capability for translational and rotational motions
- Two electric motors, with power supplies and controllers, which generate specified harmonic translational (sway) and rotational (yaw) motions of the model
- A PC to control motions of the two motors and provide operator input interface
- A pair of model support struts connecting the motions base to the ship model
- A set of four forces gauges to sense surge and sway forces and yaw moment acting on the ship model
- Signal condition units to convert all force transducer signals to a DC voltage

Both static and dynamic tests on a Planar Motion Mechanism impart to the model a motion which has predefined and precisely known components of velocity and acceleration.
A typical test sequence includes four types of tests described above.

The PMM test consists of static and dynamic motions. In the former case, the motion is purely dependent of the carriage speed U_c and the specified drift angle β relative to the towing direction

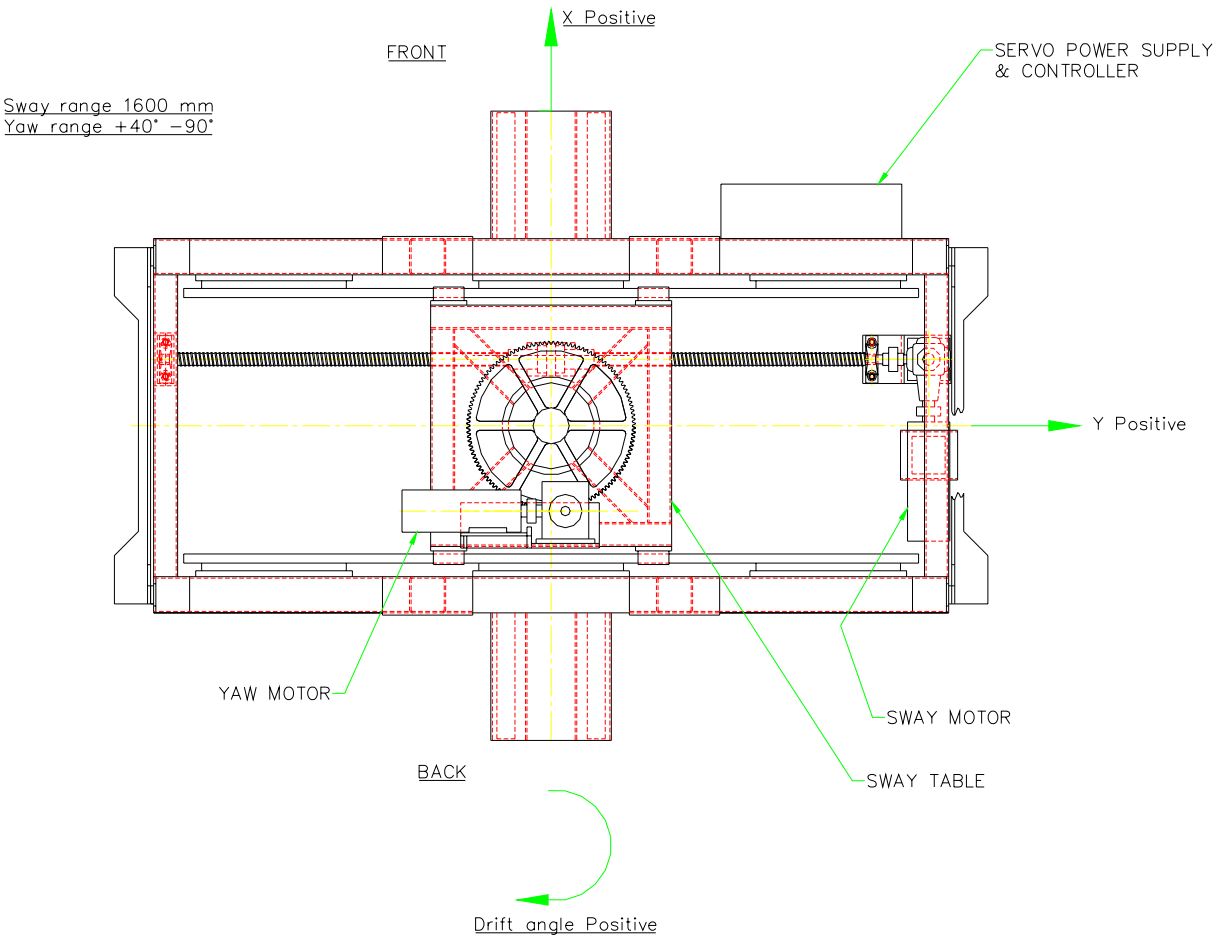

Figure 7.2.1.1 Sketch of the INSEAN Large Amplitude Planar Mechanism Motion.

In the dynamic case, the motion is realized through the combination of two sinusoidal motions with opportune phase shift. The motion turning out approximates the ideal one

HEADING:

$$\psi_{PMM} = \psi_{MAX} \sin(2\pi ft + \phi) + \beta \tag{6.1}$$

YAW RATE:

$$r_{PMM} = \psi_{MAX} (2\pi f) \cos(2\pi ft + \phi) \tag{6.2}$$

YAW ACCELERATION:

$$\dot{r}_{PMM} = -\psi_{MAX} (2\pi f)^2 \sin(2\pi ft + \phi) \tag{6.3}$$

TRANSVERSE TRANSLATION

$$\eta_{PMM} = \eta_{MAX} \sin(2\pi ft) \tag{6.4}$$

TRANSVERSE VELOCITY

$$v_{PMM} = \eta_{MAX} (2\pi f) \cos(2\pi ft) \tag{6.5}$$

TRANSVERSE ACCELERATION

$$\dot{v}_{PMM} = -\eta_{MAX} (2\pi f)^2 \sin(2\pi ft) \tag{6.6}$$

It must be observed that the angular velocity and acceleration are the same in the global and local reference system for all conditions, i.e. $r = r_{PMM}$ *and* $\dot{r} = \dot{r}_{PMM}$. For the sway velocity and acceleration, it is different. In pure sway the values are equal for both system but in pure yaw and yaw and drift $v \neq v_{PMM}$ and $\dot{v} \neq \dot{v}_{PMM}$. In particular,

$$v = v_{PMM} \cos\theta - U_C \sin\theta \tag{6.7}$$

$$\dot{v} = \dot{v}_{PMM} \cos\theta - r(U_C \cos\theta + v_{PMM}) \tag{6.8}$$

7 Uncertainty analysis

The uncertainty analysis follows the suitable approach in the ITTC 1999a and b. The global equations of the motion, written for a behind reference system to the ship, assume the form following (3 freedom degrees)

$$-F_{X_{measured}} + F_{X_{hydro}} = M\left(\dot{u} - rv - X_G r^2 - Y_G \dot{r}\right) \tag{7.1}$$

$$-F_{Y_{measured}} + F_{Y_{hydro}} = M\left(\dot{v} + ru - Y_G r^2 + X_G \dot{r}\right) \tag{7.2}$$

$$-M_{Z_{measured}} + M_{Z_{hydro}} = I_z \dot{r} + M\left[X_G\left(\dot{v} + ru\right) - Y_G\left(\dot{u} - rv\right)\right] \tag{7.3}$$

The total forces are measured where the contribution of the hydrodynamic member is added to that inertial one. It so separating the hydrodynamic force is necessary that opportunely non dimensionalized becomes:

$$X' = \frac{F_{X_{measured}} + M\left(\dot{u} - rv - X_G r^2 - Y_G \dot{r}\right)}{0.5\rho U^2 A_0} \tag{7.4}$$

$$Y' = \frac{F_{Y_{measured}} + M\left(\dot{v} + ru - Y_G r^2 + X_G \dot{r}\right)}{0.5\rho U^2 A_0} \tag{7.5}$$

$$N' = \frac{M_{Z_{measured}} + I_z \dot{r} + M\left[X_G\left(\dot{v} + ru\right) - Y_G\left(\dot{u} - rv\right)\right]}{0.5\rho U^2 A_0 L_{pp}} \tag{7.6}$$

u and v are the surge and the sway speed respectively, $F_{X_{measured}}$ and $F_{Y_{measured}}$ the measured total strengths, $M_{Z_{measured}}$ the measured yaw moment, M the mass of the model, ρ the water density, $U = \sqrt{u^2 + v^2}$ the total speed, r the yaw rate, $\dot{u}$, $\dot{v}$ and $\dot{r}$ the transverse and angular accelerations, X_G and Y_G the distances of the barycentre from the centre of rotation, A_0 the lateral underwater area and L_{pp} the length between the perpendiculars of the model. The general expressions written and valid for the dynamic case are strongly simplified in the static case where the components of speed and acceleration in the model reference are identically nothings, in this case the system of non dimensional equations is written more simply so:

$$X' = \frac{F_{X_{measured}}}{0.5\rho U^2 A_0} \tag{7.7}$$

$$Y' = \frac{F_{Y_{measured}}}{0.5\rho U^2 A_0} \tag{7.8}$$

$$N' = \frac{M_{Z_{measured}}}{0.5\rho U^2 A_0 L_{pp}} \tag{7.9}$$

in this case the expression for the speed U takes on the following shape $U = \sqrt{(U_C \cos\beta)^2 + (-U_C \sin\beta)^2} = U_C$ and therefore coincides with the speed of tow plans from the system.
Based on the multiple test approach, the total uncertainty for the average (calculated on the basis of a number of repeated tests) *X*- and *Y*-forces and yaw moment are given by :

$$U_{\overline{X'}}^2 = B_{X'}^2 + P_{\overline{X'}}^2 \tag{7.10}$$

$$U_{\overline{Y'}}^2 = B_{Y'}^2 + P_{\overline{Y'}}^2 \tag{7.11}$$

$$U_{\overline{N'}}^2 = B_{N'}^2 + P_{\overline{N'}}^2 \tag{7.12}$$

- $B_{X'}$ is the bias calculated for the F_X force
- $P_{\overline{X'}}$ is the precision which comes from a number of repeated tests

7.1 Limitations of the present method

All the data are sampled with a frequency of 133Hz, thus the time period between two samples will be $\Delta t = 1/133$ seconds. In the beginning of this time period the channels are scanned one after the other and nothing happens until the time of the next sampling. We consider that the time assigned

for all the channels reading is the same, nevertheless there will be for instance a time lack between the scan of the first channel and the one of the last. However, since the time lack is small, no corrections are applied. In the following uncertainty analysis it is assumed that the scanning takes place during the first $1/12\Delta t = 0.00063$ seconds of the time between two samples. This quantity will be used in bias limit calculates.

$$\varepsilon_t = 0.00063\,\text{sec} \tag{7.13}$$

The sinkage AP and FP is presented in this report, although no bias error estimates are made for its. However, though there data from precision limits were available, precision study on the sinkage is carried on.

7.2 Definition of bias limit

The bias limits will be assessed based on a study of the measuring system. According to (ITTC 1999a) they can be estimated on the basis of

$$B_r^2 = \sum_{i=1}^{J} \theta_i^2 B_i^2 + 2\sum_{i=1}^{J-1}\sum_{k=i+1}^{J} \theta_i \theta_k B_{ik} \tag{7.14}$$

where θ_i is the influence coefficient defined as

$$\theta_i = \frac{\partial r}{\partial X_i} \tag{7.15}$$

B_i are the bias limits in X_i and B_{ik} are the correlated bias limits in X_i and X_k

$$B_{ik} = \sum_{\alpha=1}^{L} \left(B_i\right)_\alpha \left(B_k\right)_\alpha \tag{7.16}$$

where L is the number of correlated bias error sources that are common for measurement of variables X_i and X_k.
The bias error for each variable in the data reduction equation may consist of a number of bias errors, so in order to calculate the combined bias error the root-sum-square is used

$$B_i^2 = \sum_{k=1}^{J} \left(B_i\right)_k^2 \tag{7.17}$$

i is the number of considered variable in the data reduction equation.

7.2.1 Non-dimensional longitudinal force, X'

For the dynamic tests the bias limit equation for X' is given by (7.14)

$$\begin{aligned} B_{X'}^2 = {} & \theta_{F_{Xmeasured}}^2 B_{F_{Xmeasured}}^2 + \theta_\rho^2 B_\rho^2 + \theta_{T_m}^2 B_{T_m}^2 + \theta_{L_{pp}}^2 B_{L_{pp}}^2 + \theta_M^2 B_M^2 + \theta_{X_G}^2 B_{X_G}^2 + \theta_{Y_G}^2 B_{Y_G}^2 + \theta_u^2 B_u^2 + \theta_{\dot{u}}^2 B_{\dot{u}}^2 + \theta_v^2 B_v^2 \\ & + \theta_r^2 B_r^2 + \theta_{\dot{r}}^2 B_{\dot{r}}^2 \end{aligned} \tag{7.18}$$

In this expression it is assumed that none of the variables are correlated. The influence coefficients are found from applying (7.15) on (7.4).

$$\theta_{F_{X_{measured}}} = \frac{\partial X'}{\partial F_{X_{measured}}} = \frac{2}{\rho(u^2+v^2)T_m L_{pp}} \tag{7.19}$$

$$\theta_{\rho} = \frac{\partial X'}{\partial \rho} = \frac{-2(F_{X_{measured}} + M(\dot{u} - rv - X_G r^2 - Y_G \dot{r}))}{\rho^2(u^2+v^2)T_m L_{pp}} \tag{7.20}$$

$$\theta_{T_m} = \frac{\partial X'}{\partial T_m} = \frac{-2(F_{X_{measured}} + M(\dot{u} - rv - X_G r^2 - Y_G \dot{r}))}{\rho(u^2+v^2){T_m}^2 L_{pp}} \tag{7.21}$$

$$\theta_{L_{pp}} = \frac{\partial X'}{\partial L_{pp}} = \frac{-2(F_{X_{measured}} + M(\dot{u} - rv - X_G r^2 - Y_G \dot{r}))}{\rho(u^2+v^2)T_m {L_{pp}}^2} \tag{7.22}$$

$$\theta_{M} = \frac{\partial X'}{\partial M} = \frac{2(\dot{u} - rv - X_G r^2 - Y_G \dot{r})}{\rho(u^2+v^2)T_m L_{pp}} \tag{7.23}$$

$$\theta_{X_G} = \frac{\partial X'}{\partial X_G} = \frac{-2Mr^2}{\rho(u^2+v^2)T_m L_{pp}} \tag{7.24}$$

$$\theta_{Y_G} = \frac{\partial X'}{\partial Y_G} = \frac{-2M\dot{r}}{\rho(u^2+v^2)T_m L_{pp}} \tag{7.25}$$

$$\theta_{u} = \frac{\partial X'}{\partial u} = \frac{-4u(F_{X_{measured}} + M(\dot{u} - rv - X_G r^2 - Y_G \dot{r}))}{\rho(u^2+v^2)^2 T_m L_{pp}} \tag{7.26}$$

$$\theta_{\dot{u}} = \frac{\partial X'}{\partial \dot{u}} = \frac{2M}{\rho(u^2+v^2)T_m L_{pp}} \tag{7.27}$$

$$\theta_{v} = \frac{\partial X'}{\partial v} = \frac{2}{\rho(u^2+v^2)T_m L_{pp}}\left[-Mr - \frac{2v(F_{X_{measured}} + M(\dot{u} - rv - X_G r^2 - Y_G \dot{r}))}{(u^2+v^2)}\right] \tag{7.28}$$

$$\theta_{r} = \frac{\partial X'}{\partial r} = \frac{-2M(v + 2X_G r)}{\rho(u^2+v^2)T_m L_{pp}} \tag{7.29}$$

$$\theta_{\dot{r}} = \frac{\partial X'}{\partial \dot{r}} = \frac{-2MY_G}{\rho(u^2+v^2)T_m L_{pp}} \tag{7.30}$$

For the static tests the bias limit can be reduced

$$B_{X'}^2 = \theta_{F_{Xmeasured}}^2 B_{F_{Xmeasured}}^2 + \theta_{\rho}^2 B_{\rho}^2 + \theta_{T_m}^2 B_{T_m}^2 + \theta_{L_{pp}}^2 B_{L_{pp}}^2 + \theta_{U_C}^2 B_{U_C}^2 \tag{7.31}$$

where the influence coefficients are found by applying (7.15) on (7.7):

$$\theta_{F_{X_{measured}}} = \frac{\partial X'}{\partial F_{X_{measured}}} = \frac{2}{\rho U_C^2 T_m L_{pp}} \tag{7.32}$$

$$\theta_{\rho} = \frac{\partial X'}{\partial \rho} = \frac{-2F_{X_{measured}}}{\rho^2 {U_C}^2 T_m L_{pp}} \tag{7.33}$$

$$\theta_{T_m} = \frac{\partial X'}{\partial T_m} = \frac{-2F_{X_{measured}}}{\rho {U_C}^2 {T_m}^2 L_{pp}} \tag{7.34}$$

$$\theta_{L_{pp}} = \frac{\partial X'}{\partial L_{pp}} = \frac{-2F_{X_{measured}}}{\rho U_C{}^2 T_m L_{pp}{}^2} \tag{7.35}$$

$$\theta_{U_C} = \frac{\partial X'}{\partial U_C} = \frac{-4F_{X_{measured}}}{\rho U_C{}^3 T_m L_{pp}} \tag{7.36}$$

7.2.2 Non-dimensional transverse force, Y'

The bias limit equation for Y' is given by :

$$B_{Y'}^2 = \theta_{F_{Ymeasured}}^2 B_{F_{Ymeasured}}^2 + \theta_\rho^2 B_\rho^2 + \theta_{T_m}^2 B_{T_m}^2 + \theta_{L_{pp}}^2 B_{L_{pp}}^2 + \theta_M^2 B_M^2 + \theta_{X_G}^2 B_{X_G}^2 + \theta_{Y_G}^2 B_{Y_G}^2 + \theta_u^2 B_u^2 + \theta_v^2 B_v^2 + \theta_{\dot{v}}^2 B_{\dot{v}}^2 + \theta_r^2 B_r^2 + \theta_{\dot{r}}^2 B_{\dot{r}}^2 \tag{7.37}$$

The influence coefficients are found from applying (7.15) on (7.5):

$$\theta_{F_{Y_{measured}}} = \frac{\partial Y'}{\partial F_{Y_{measured}}} = \frac{2}{\rho(u^2+v^2)T_m L_{pp}} \tag{7.38}$$

$$\theta_\rho = \frac{\partial Y'}{\partial \rho} = \frac{-2(F_{Y_{measured}} + M(\dot{v} - +ru - Y_G r^2 + X_G \dot{r}))}{\rho^2(u^2+v^2)T_m L_{pp}} \tag{7.39}$$

$$\theta_{T_m} = \frac{\partial Y'}{\partial T_m} = \frac{-2(F_{Y_{measured}} + M(\dot{v} + ru - Y_G r^2 + X_G \dot{r}))}{\rho(u^2+v^2)T_m{}^2 L_{pp}} \tag{7.40}$$

$$\theta_{L_{pp}} = \frac{\partial Y'}{\partial L_{pp}} = \frac{-2(F_{Y_{measured}} + M(\dot{v} + ru - Y_G r^2 + X_G \dot{r}))}{\rho(u^2+v^2)T_m L_{pp}{}^2} \tag{7.41}$$

$$\theta_M = \frac{\partial Y'}{\partial M} = \frac{2(\dot{v} + ru - Y_G r^2 + X_G \dot{r})}{\rho(u^2+v^2)T_m L_{pp}} \tag{7.42}$$

$$\theta_{X_G} = \frac{\partial Y'}{\partial X_G} = \frac{2M\dot{r}}{\rho(u^2+v^2)T_m L_{pp}} \tag{7.43}$$

$$\theta_{Y_G} = \frac{\partial Y'}{\partial Y_G} = \frac{-2Mr^2}{\rho(u^2+v^2)T_m L_{pp}} \tag{7.44}$$

$$\theta_u = \frac{\partial Y'}{\partial u} = \frac{2}{\rho(u^2+v^2)T_m L_{pp}} \left[Mr - \frac{2u(F_{Y_{measured}} + M(\dot{v} + ru - Y_G r^2 + X_G \dot{r}))}{(u^2+v^2)} \right] \tag{7.45}$$

$$\theta_v = \frac{\partial Y'}{\partial v} = \frac{-4v(F_{Y_{measured}} + M(\dot{v} + ru - Y_G r^2 + X_G \dot{r}))}{\rho(u^2+v^2)^2 T_m L_{pp}} \tag{7.46}$$

$$\theta_{\dot{v}} = \frac{\partial Y'}{\partial \dot{v}} = \frac{2M}{\rho(u^2+v^2)T_m L_{pp}} \tag{7.47}$$

$$\theta_r = \frac{\partial Y'}{\partial r} = \frac{2M(u - 2Y_G r)}{\rho(u^2+v^2)T_m L_{pp}} \tag{7.48}$$

$$\theta_{\dot{r}} = \frac{\partial Y'}{\partial \dot{r}} = \frac{2MY_G}{\rho(u^2+v^2)T_m L_{pp}} \tag{7.49}$$

For the static tests the bias limit can be reduced:

$$B_{Y'}^2 = \theta_{F_{Ymeasured}}^2 B_{F_{Ymeasured}}^2 + \theta_\rho^2 B_\rho^2 + \theta_{T_m}^2 B_{T_m}^2 + \theta_{L_{pp}}^2 B_{L_{pp}}^2 + \theta_{U_C}^2 B_{U_C}^2 \tag{7.50}$$

where the influence coefficients are found by applying (7.15) on (7.8):

$$\theta_{F_{Y_{measured}}} = \frac{\partial Y'}{\partial F_{Y_{measured}}} = \frac{2}{\rho U_C^2 T_m L_{pp}} \tag{7.51}$$

$$\theta_\rho = \frac{\partial Y'}{\partial \rho} = \frac{-2F_{Y_{measured}}}{\rho^2 U_C{}^2 T_m L_{pp}} \tag{7.52}$$

$$\theta_{T_m} = \frac{\partial Y'}{\partial T_m} = \frac{-2F_{Y_{measured}}}{\rho U_C{}^2 T_m{}^2 L_{pp}} \tag{7.53}$$

$$\theta_{L_{pp}} = \frac{\partial Y'}{\partial L_{pp}} = \frac{-2F_{Y_{measured}}}{\rho U_C{}^2 T_m L_{pp}{}^2} \tag{7.54}$$

$$\theta_{U_C} = \frac{\partial Y'}{\partial U_C} = \frac{-4F_{Y_{measured}}}{\rho U_C{}^3 T_m L_{pp}} \tag{7.55}$$

7.2.3 Bias on the dimensional yaw moment, N'

The bias limit equation for N' is given by :

$$\begin{aligned} B_{N'}^2 = {} & \theta_{M_{Z_{measured}}}^2 B_{M_{Z_{measured}}}^2 + \theta_\rho^2 B_\rho^2 + \theta_{T_m}^2 B_{T_m}^2 + \theta_{L_{pp}}^2 B_{L_{pp}}^2 + \theta_{I_Z}^2 B_{I_Z}^2 + \theta_{X_G}^2 B_{X_G}^2 + \theta_{Y_G}^2 B_{Y_G}^2 + \theta_u^2 B_u^2 + \theta_{\dot{u}}^2 B_{\dot{u}}^2 + \theta_v^2 B_v^2 + \\ & + \theta_{\dot{v}}^2 B_{\dot{v}}^2 + \theta_r^2 B_r^2 + \theta_{\dot{r}}^2 B_{\dot{r}}^2 \end{aligned} \tag{7.56}$$

The influence coefficients are found from applying (7.15) on(7.6):

$$\theta_{M_{Z_{measured}}} = \frac{\partial N'}{\partial M_{Z_{measured}}} = \frac{2}{\rho(u^2+v^2)T_m L_{pp}^2} \tag{7.57}$$

$$\theta_\rho = \frac{\partial N'}{\partial \rho} = \frac{-2\left(M_{Z_{measured}} + I_Z\dot{r} + M\left(X_G\left(\dot{v}+ru\right) - Y_G\left(\dot{u}-rv\right)\right)\right)}{\rho^2(u^2+v^2)T_m L_{pp}^2} \tag{7.58}$$

$$\theta_{T_m} = \frac{\partial N'}{\partial T_m} = \frac{-2\left(M_{Z_{measured}} + I_Z\dot{r} + M\left(X_G\left(\dot{v}+ru\right) - Y_G\left(\dot{u}-rv\right)\right)\right)}{\rho(u^2+v^2)T_m{}^2 L_{pp}^2} \tag{7.59}$$

$$\theta_{L_{pp}} = \frac{\partial N'}{\partial L_{pp}} = \frac{-4\left(M_{Z_{measured}} + I_Z\dot{r} + M\left(X_G\left(\dot{v}+ru\right) - Y_G\left(\dot{u}-rv\right)\right)\right)}{\rho(u^2+v^2)T_m^2 L_{pp}{}^2} \tag{7.60}$$

$$\theta_{I_Z} = \frac{\partial N'}{\partial I_Z} = \frac{2\dot{r}}{\rho(u^2+v^2)T_m L_{pp}^2} \tag{7.61}$$

$$\theta_{X_G} = \frac{\partial N'}{\partial X_G} = \frac{2M\left(\dot{v}+ru\right)}{\rho(u^2+v^2)T_m L_{pp}^2} \tag{7.62}$$

$$\theta_{Y_G} = \frac{\partial N'}{\partial Y_G} = \frac{-2M\left(\dot{u}-rv\right)}{\rho(u^2+v^2)T_m L_{pp}^2} \tag{7.63}$$

$$\theta_u = \frac{\partial N'}{\partial u} = \frac{2}{\rho(u^2+v^2)T_m L_{pp}^2}\left[MX_G r - \frac{2u\left(M_{Z_{measured}} + I_Z\dot{r} + M\left(X_G\left(\dot{v}+ru\right) - Y_G\left(\dot{u}-rv\right)\right)\right)}{(u^2+v^2)}\right] \tag{7.64}$$

$$\theta_{\dot{u}} = \frac{\partial N'}{\partial \dot{u}} = \frac{-2MY_G}{\rho(u^2+v^2)T_m L_{pp}^2} \tag{7.65}$$

$$\theta_v = \frac{\partial N'}{\partial v} = \frac{2}{\rho(u^2+v^2)T_m L_{pp}^2}\left[MY_G r - \frac{2v\left(M_{Z_{measured}} + I_Z\dot{r} + M\left(X_G\left(\dot{v}+ru\right) - Y_G\left(\dot{u}-rv\right)\right)\right)}{(u^2+v^2)}\right] \tag{7.66}$$

$$\theta_{\dot{v}} = \frac{\partial N'}{\partial \dot{v}} = \frac{2MX_G}{\rho(u^2+v^2)T_m L_{pp}^2} \tag{7.67}$$

$$\theta_r = \frac{\partial N'}{\partial r} = \frac{2M(X_G u + Y_G v)}{\rho(u^2+v^2)T_m L_{pp}} \tag{7.68}$$

$$\theta_{\dot{r}} = \frac{\partial N'}{\partial \dot{r}} = \frac{2I_Z}{\rho(u^2+v^2)T_m L_{pp}} \tag{7.69}$$

For the static tests the bias limit can be reduced:

$$B_{N'}^2 = \theta_{M_{Z_{measured}}}^2 B_{M_{Z_{measured}}}^2 + \theta_\rho^2 B_\rho^2 + \theta_{T_m}^2 B_{T_m}^2 + \theta_{L_{pp}}^2 B_{L_{pp}}^2 + \theta_{U_C}^2 B_{U_C}^2 \tag{7.70}$$

where the influence coefficients are found by applying (7.15) on (7.9):

$$\theta_{M_{Zmeasured}} = \frac{\partial N'}{\partial M_{Z_{measured}}} = \frac{2}{\rho U_C^2 T_m L_{pp}^2} \tag{7.71}$$

$$\theta_\rho = \frac{\partial N'}{\partial \rho} = \frac{-2M_{Z_{measured}}}{\rho^2 U_C{}^2 T_m L_{pp}^2} \tag{7.72}$$

$$\theta_{T_m} = \frac{\partial N'}{\partial T_m} = \frac{-2M_{Z_{measured}}}{\rho U_C{}^2 T_m{}^2 L_{pp}^2} \tag{7.73}$$

$$\theta_{L_{pp}} = \frac{\partial N'}{\partial L_{pp}} = \frac{-2M_{Z_{measured}}}{\rho U_C{}^2 T_m L_{pp}^3} \tag{7.74}$$

$$\theta_{U_C} = \frac{\partial N'}{\partial U_C} = \frac{-4M_{Z_{measured}}}{\rho U_C{}^3 T_m L_{pp}^2} \tag{7.75}$$

7.3 Estimation of individual bias limits

Below are estimated the bias limits for the quantities involved in the data reduction equations.

7.3.1 Estimation of the bias for water density, ρ

$$\rho = f(T) \text{ thus } B_\rho = \frac{\delta\rho(T)}{\delta T} B_T \bigg|_{T_0} \tag{7.76}$$

where $\rho(T)$ comes from an ITTC (1963) formulate and B_T from the type of thermometer used. Such a way,

$$\rho(T) = 999.784 + 0.0638 \cdot T - 0.00865 \cdot T^2 + 0.0000631 \cdot T^3 \tag{7.77}$$

assuming that B_T is equal to 0.1° C (uncertainty of the thermometer)

$$B_\rho = \frac{\delta\rho(T)}{\delta T} B_T \bigg|_{T_0} = \left(0.0638 - 0.173 \cdot T_0 + 0.0001893 \cdot T_0^2\right) \cdot 0.1 \tag{7.78}$$

T_0 [Deg.]	ρ [kg/m^3]	B_ρ^2 [(kg/m^3)^2]
21.55	997.8	0.0221

Table 7-1 Bias limit for water density.

7.3.2 Estimation of bias limit for carriage speed, U_c

The speed of the carriage is measured with a tachometric system consisting in an optical encoder. The expression for the carriage speed can be so defined:

$$U_C = \pi \frac{MD}{N\Delta t} \tag{7.79}$$

where

- N is the number of marks on the tachometric wheel;
- D is the diameter of the tachometric wheel;
- and M is the number of pulses generated by the encoder during time sample Δt

Thus

$$B_{U_C} = \sqrt{\theta_M^2 B_M^2 + \theta_D^2 B_D^2 + \theta_{\Delta t}^2 B_{\Delta t}^2} \tag{7.80}$$

and the influence coefficients are so determined:

$$\theta_M = \frac{\partial U_C}{\partial M} = \frac{\pi D}{N\Delta t} = \frac{U_C}{M} \tag{7.81}$$

$$\theta_D = \frac{\partial U_C}{\partial D} = \frac{\pi M}{N\Delta t} = \frac{U_C}{D} \tag{7.82}$$

$$\theta_{\Delta t} = \frac{\partial U_C}{\partial \Delta t} = -\frac{\pi DM}{N\Delta t^2} = \frac{U_C}{\Delta t} \tag{7.83}$$

The Bias limit for M is ± 1, the uncertainty of the diameter (D) is $\pm 0.0001m$ while the time basis is captured with much more precision and so, in consequence of this, it will be negligible in the calculation of the bias limit. As three different velocity are used in the tests, we have to consider three different bias limit (see Table 7.3.2-1).

U_c (m/s)	Θ_M	Θ_D	B_{Uc} (m/s)
1.034	0.0010	6.4952	0.0012
2.097	0.0021	13.179	0.0025
3.071	0.0031	19.297	0.0036

Table 7.3.2-1 Bias limit for carriage speed.

7.3.3 Estimation of Bias limit for total model mass, *M*

The model (bare hull plus ballast weights) is weighted on a balance once for all, in this way we can assume the systematic error of the balance as bias limit for total model mass. It is $\pm 10^{-1}\ kg$.

B_M [Kg]
0.100

Table 7-2 Bias limit for model mass.

7.3.4 Estimation of bias for the total moment of Inertia, I_z

The total moment of inertia of the model I_z has been measured with a balance which swings about to a vertical board. The balance, checked by two soft antagonists, is made swing and therefore the periods of swings are measured with a chronometer. The obtained value (it mediates on 30 repetitions) is converted in the moment of inertia through the curve of calibration of the balance. In this way the moment of inertia of the model is determined by the difference between the obtained one placing the saddle and the model $I_{Z_{TOT}}$ and that partner to the only saddle $I_{Z_{SAD}}$.

$$I_Z = I_{Z_{TOT}} - I_{Z_{SAD}} \tag{7.84}$$

The bias limit for the total moment of inertia cab be expressed as

$$B_{I_Z} = \sqrt{B_{I_{Z_{TOT}}}{}^2 + B_{I_{Z_{SAD}}}{}^2} \tag{7.85}$$

I_Z (Kg m^2)	$T_{measured}$ (msec)	T_{curve} (msec)	$\varepsilon\% = (T_{measured} - T_{curve})/T_{masured}$
0	600.4	579.2	7.42
82.265	707.1	697.5	0.25
166.09	811.9	812.5	2.36
252.82	916.3	925.7	2.62
335.08	1011.3	1027.6	2.03
505.66	1196.4	1221.9	0.61
587.95	1279.9	1307.4	0.04
671.72	1361	1389	0.5
758.52	1440.8	1440.8	0.96
840.81	1512.7	1512.7	0.85
924.62	1581.9	1601.8	0.86
1011.4	1649.5	1649.5	0.75
1093.7	1709.7	1715.9	0
1177.6	1767.2	1764.2	0.16
1264.3	1822.5	1808.2	1.17

Table 7-3 Period discards of the least square curve.

The single moment of inertia is determined through the curve of calibration of the balance obtained interpolating a diagram of well known points (theoretical moments -- swing periods) with a curve of the second order by the least square method ($T = aI_Z^2 + bI_Z + c$),

$$I_{Z_{TOT}} = \frac{-b \pm \sqrt{b^2 - 4a(c - T_{TOT})}}{2a} \tag{7.86}$$

$$I_{Z_{SAD}} = \frac{-b \pm \sqrt{b^2 - 4a(c - T_{SAD})}}{2a} \tag{7.87}$$

The bias will be determinate by the contribution of the T_{TOT} bias (or T_{SAD} bias), by the relative approximation of the interpolation curve ε_{int} and by the relative contribution due to the uncertainty of the theoretical moment used to build the calibration $\varepsilon_{I_{th}}$. The ε_{int} is experimentally obtained as middle quadratic discard between the value of the period given by the curve to leave for the moment of theorist inertia and the measured one as shown in the below and it is equal to 0,012.

The uncertainty $\varepsilon_{I_{th}}$ on the sample moments is due to bias of the masses and that on the positioning on the balance,

$$\varepsilon_{I_{th}} = \sqrt{\sum_{i=1}^{N} (\varepsilon_{I_{th,i}})^2} \tag{7.88}$$

where

$$\varepsilon_{I_{th,i}} = \sqrt{\left(\frac{\partial I_{th,i}}{\partial M_{th,i}} \varepsilon_{M_{th,i}} \frac{1}{I_{th,i}}\right)^2 + \left(\frac{\partial I_{th,i}}{\partial d_{th,i}} \varepsilon_{d_{th,i}} \frac{1}{I_{th,i}}\right)^2} = \sqrt{\left(\frac{\varepsilon_{M_{th,i}}}{M_{th,i}}\right)^2 + \left(\frac{2\varepsilon_{d_{th,i}}}{d_{th,i}}\right)^2} \tag{7.89}$$

considering that $I_{th,i} = M_{th,i} d_{th,i}^2$. The uncertainty $\varepsilon_{I_{th}}$ is equal to 0.0019. Summarizing:

$$B_{I_{Z_{TOT}}} = B_{T_{TOT}} \theta_{T_{TOT}} + (\varepsilon_{\text{int}} + \varepsilon_{th}) I_{Z_{TOT}} \tag{7.90}$$

$$B_{I_{Z_{SAD}}} = B_{T_{SAD}} \theta_{T_{SAD}} + (\varepsilon_{\text{int}} + \varepsilon_{th}) I_{Z_{SAD}} \tag{7.91}$$

The expression for the influence coefficients θ are,

$$\theta_{T_{TOT}} = \frac{1}{\sqrt{b^2 - 4a(c - T_{TOT})}} \tag{7.92}$$

$$\theta_{T_{SAD}} = \frac{1}{\sqrt{b^2 - 4a(c - T_{SAD})}} \tag{7.93}$$

The period is calculated repeating the measure on the balance 30 times and therefore the uncertainty on the time is bound to the mistake of the chronometer and the index of precision of the statistical average of the acquisitions. Then the expression for the bias B_{T_j} can be written in the following way,

$$B_{T_{TOT}} = B_T + t_{st} S_{T_{TOT}} \tag{7.94}$$

$$S_{T_{TOT}} = \sqrt{\frac{\sum_{j=1}^{M}(T_j - \bar{T})^2}{M(M-1)}} \tag{7.95}$$

where T_j and $\bar{T}$ are respectively the single acquired periods and the average. The calculation of the bias of the moment of inertia is summarized in the following tables:

	B_T (kgm^2/s)	t_{st}	S_T (s)	θ_T (kgm^2/s)	B_{I_Z} (kgm^2)
$I_{Z_{TOT}}$	0.011	2	5.132 s	2019.2	39.978
$I_{Z_{SAD}}$	0.005	2	1.984 s	712.8	4.736

Table 7.3.4-1 Total and saddle bias.

I_Z	B_{I_Z}
1151.4 kgm^2	40.257 kgm^2

Table 7.3.4-2 Iz and its bias limit.

7.3.5 Estimation of bias for mean draft, T_m

The hull has been realized with a numerical controlled machine, which accuracy is estimated at $\pm 1\,mm$. Thus, the bias limit on T_m will be taken at:

B_{T_m} [m]
0.001

Table 7-4 Bias limit for mean draft.

7.3.6 Estimation of bias on the perpendicular length, L_{pp}

The error in the length between perpendiculars is assessed based on the tolerance related to the model manufacturing. The reason is that this dimension is a pure geometrical definition, which does not change with loading condition, as was the case for the draft. As mentioned above the milling machine works with a tolerance of ± 1 mm in all directions. This means that L_{pp} can be in the range from L_{pp} - *2 mm.* to L_{pp} + *2 mm*, i.e. an uncertainty of 2 mm. Therefore, the bias limit for L_{pp} is assumed to be as shown in

$B_{L_{pp}}$ [m]
0.002

Table 7-5 Bias limit for the ship length.

7.3.7 Estimation of bias limit for X_G

X_G is the longitudinal distance between the mid-ship position and the axial location of the center of gravity of the model. The bias limit related to X_G originates from two sources. One is the

uncertainty $\varepsilon_{X_G,1}$ related to how accurate the model can be mounted in PMM set-up. This means how well the longitudinal point of rotation coincides with the mid-ship position. The other is the uncertainty of the location of the center of gravity $\varepsilon_{X_G,2}$. Therefore, the bias limit for X_G can be expressed as:

$$B_{X_G} = \sqrt{\varepsilon_{X_G,1} + \varepsilon_{X_G,2}}$$

The results are summarized in the Table 7-6

$\varepsilon_{X_G,1}$ [m]	$\varepsilon_{X_G,2}$ [m]	B_{X_G} [m]
0.002	0.004	0.0045

Table 7-6 Bias limit for X_G.

7.3.8 Estimation of bias limit for Y_G

Y_G is the transverse distance between the mid-ship position and the axial location of the center of gravity of the model. The bias limit related to Y_G originates from two sources. One is the uncertainty $\varepsilon_{Y_G,1}$ related to how accurate the model can be mounted in PMM set-up. This means how well the transverse point of rotation coincides with the mid-ship position. The other is the uncertainty of the location of the center of gravity $\varepsilon_{Y_G,2}$. Therefore, the bias limit for Y_G can be expressed as:

$$B_{Y_G} = \sqrt{\varepsilon_{Y_G,1} + \varepsilon_{Y_G,2}}$$

The results are summarized in the Table 7-7 Bias limit for Y_G.

$\varepsilon_{Y_G,1}$ [m]	$\varepsilon_{Y_G,2}$ [m]	B_{Y_G} [m]
0.002	0.004	0.0045

Table 7-7 Bias limit for Y_G.

7.3.9 Estimation of bias limit for ψ in dynamic tests

The bias of the heading (6.1)of the model for the PMM tests, is required for some of the following bias limit estimates. A resume of the motion applied is resumed in §6.

$$\psi(t) = \psi_{PMM}(t) = \psi_{MAX}\sin(2\pi ft + \phi) + \beta \tag{7.96}$$

The bias limit, $B_{heading}$, of the heading (7.96) is found from :

$$B_{heading} = \sqrt{B_{\psi_{MAX}}^2 + B_f^2 + B_t^2 + B_\beta^2 + B_\phi^2} \tag{7.97}$$

where :

$$B_{\psi_{MAX}} = \frac{\partial\psi}{\partial\psi_{MAX}}\varepsilon_{\psi_{MAX}} = \sin(2\pi ft + \phi)\varepsilon_{\psi_{MAX}} \tag{7.98}$$

$$B_f = \frac{\partial \psi}{\partial f}\varepsilon_f = \psi_{MAX} 2\pi t \cos\left(2\pi ft + \phi\right)\varepsilon_f \tag{7.99}$$

$$B_t = \frac{\partial \psi}{\partial t}\varepsilon_t = \psi_{MAX} 2\pi f \cos\left(2\pi ft + \phi\right)\varepsilon_t \tag{7.100}$$

$$B_\beta = \frac{\partial \psi}{\partial \beta}\varepsilon_\beta = \varepsilon_\beta \tag{7.101}$$

$$B_\phi = \frac{\partial \psi}{\partial \phi}\varepsilon_\phi = \psi_{MAX} \cos\left(2\pi ft + \phi\right)\varepsilon_\phi \tag{7.102}$$

$\varepsilon_{\psi_{MAX}}$, ε_f, ε_t, ε_β and ε_ϕ are the uncertainties of $\psi_{MAX}, f, t, \beta, \phi$ respectively.
We have to decompose the error committed on the drift angle ε_β with respect to three components.

- The first will be $\varepsilon_{\beta,hydro}$, the error made during the make of the hydrodynamic zero reference. It will be taken at 0.10°
- The second, $\varepsilon_{\beta,PMM}$ is the error due to the play of the PMM device during the angle setting, it has been estimated at 0.10°
- The third, $\varepsilon_{\beta,align}$ is the bias limit related to the alignment of the model when it is mounted in the PMM, will be taken at 0.04°

$\varepsilon_{\beta,hydro}$ [deg]	$\varepsilon_{\beta,PMM}$ [deg]	$\varepsilon_{\beta,align}$ [deg]	ε_β [deg]
0.10	0.10	0.04	0.15

Table 7-8 Bias limits for drift angle

ε_f [s^{-1}]	ε_t [s]	$\varepsilon_{\psi_{MAX}}$ [deg]
0.001	0.00063	0.1

Table 7-9 Bias limit for the frequency, the time and the max angle of the yaw motion.

Uncertainty	Magnitude
$\varepsilon_{\psi_{MAX}}$	0.10°
ε_ω	0.00628 s^{-1}
ε_t	0.00063 s
ε_β	0.15°

Table 7-10 Uncertainties in connection with the estimate of B_ψ.

The uncertainty on $\varepsilon_{\psi_{MAX}}$ is bound to the play of PMM; the uncertainty on the frequency ($\varepsilon_\omega = 2\pi\varepsilon_f$), which depends from how the system "board of generation-engine step by step" the signal manages, is in our equal to 0.001 s^{-1}; the uncertainty on the time ε_t is equal to 0.00063sec (see §7.1); the uncertainty on the phase ε_ϕ is inferable considering that we can write

$$\phi = 2\pi f T_0 \Rightarrow \varepsilon_\phi = \sqrt{\left(T_0\right)^2 \varepsilon_\omega^2 + \left(2\pi f\right)^2 \varepsilon_t^2} \tag{7.103}$$

where $T_0 = 1/4f$ and so it comes to depend on the uncertainty on the time and on the frequency at last.

7.3.10 Estimation of the bias limit for v_{PMM} in dynamic tests

$$v_{PMM} = \eta_{MAX}\omega\cos(\omega t) \tag{7.104}$$

where $\omega = 2\pi f$.
Thus, the bias for v_{Pmm} is found from:

$$\varepsilon_{v_{PMM}} = \sqrt{B_{\eta_{MAX}}^2 + B_\omega^2 + B_t^2} \tag{7.105}$$

where:

$$B_{\eta_{MAX}} = \frac{\partial V_{Pmm}}{\partial \eta_{MAX}}\varepsilon_{\eta_{MAX}} = \omega\cos(\omega t)\varepsilon_{\eta_{MAX}} \tag{7.106}$$

$$B_\omega = \frac{\partial V_{PMM}}{\partial \omega}\varepsilon_\omega = \left(\eta_{MAX}\cos(\omega t) - \eta_{MAX}\omega t\sin(\omega t)\right)\varepsilon_\omega \tag{7.107}$$

$$B_t = \frac{\partial V_{PMM}}{\partial t}\varepsilon_t = -\eta_{MAX}\omega^2\sin(\omega t)\varepsilon_t \tag{7.108}$$

The uncertainty of the amplitude of the sway motion depends by the play of the PMM mechanism (motion of a toothed wheel what engages on a denture) and it has been fixed in 4 mm. For the values relative to the uncertainties ε_i one sends again to the Table 7-10 Uncertainties in connection with the estimate of B_ψ.
$(\varepsilon_\omega = 2\pi\varepsilon_f)$.

$\varepsilon_{\eta_{MAX}}$ [m.]
0.001

Table 7-11 Bias limit for the amplitude of the sway motion.

7.3.11 Estimation of the bias limit for v in dynamic tests

$$v = v_{PMM}\cos(\psi) - U_C\sin(\psi) \tag{7.109}$$

Notice that if the considered test is pure sway, then $\psi = 0$. Thus, the bias for v is found from:

$$B_v = \sqrt{B_{U_C}^2 + B_\psi^2 + B_{v_{PMM}}^2} \tag{7.110}$$

where

$$B_{U_C} = \frac{\partial v}{\partial U_C}\varepsilon_{U_C} = -\sin(\psi)\varepsilon_{U_C} \tag{7.111}$$

$$B_{\psi} = \frac{\partial v}{\partial \psi}\varepsilon\psi = -\left(v_{PMM}\sin(\psi) + U_C\cos(\psi)\right)\varepsilon_{\psi} \tag{7.112}$$

$$B_{v_{PMM}} = \frac{\partial v}{\partial v_{PMM}}\varepsilon_{v_{PMM}} = \cos(\psi)\varepsilon_{v_{PMM}} \tag{7.113}$$

ε_{U_C} is the uncertainty of the carriage speed, already found in §7.3.2 $\left(\varepsilon_{U_C} = B_{U_C}\right)$; ε_{ψ} is the uncertainty of the heading, which was found in §7.3.9 $\left(\varepsilon_{\psi} = B_{heading}\right)$. The uncertainty $\varepsilon_{v_{PMM}}$ has been discussed in §7.3.10.

7.3.12 Estimation of the bias limit for $\dot{v}_{PMM}$ in dynamic tests

$$\dot{v}_{PMM} = -\eta_{MAX}\omega^2\sin(\omega t) \tag{7.114}$$

Thus, the bias for $\dot{v}_{PMM}$ is found from:

$$\varepsilon_{\dot{v}_{PMM}} = \sqrt{B_{\eta_{MAX}}^2 + B_{\omega}^2 + B_t^2} \tag{7.115}$$

where:

$$B_{\eta_{MAX}} = \frac{\partial \dot{v}_{Pmm}}{\partial \eta_{MAX}}\varepsilon_{\eta_{MAX}} = -\omega^2\sin(\omega t)\varepsilon_{\eta_{MAX}} \tag{7.116}$$

$$B_{\omega} = \frac{\partial \dot{v}_{PMM}}{\partial \omega}\varepsilon_{\omega} = \left(-\eta_{MAX}2\omega\sin(\omega t) - \eta_{MAX}\omega^2 t\cos(\omega t)\right)\varepsilon_{\omega} \tag{7.117}$$

$$B_t = \frac{\partial \dot{v}_{PMM}}{\partial t}\varepsilon_t = -\eta_{MAX}\omega^3\cos(\omega t)\varepsilon_t \tag{7.118}$$

For the values relative to the uncertainties ε_i one sends again to the Table 7-10 Uncertainties in connection with the estimate of B_{ψ}.
and Table 7-11 Bias limit for the amplitude of the sway motion.
$(\varepsilon_{\omega} = 2\pi\varepsilon_f)$.

7.3.13 Estimation of bias limit $\dot{v}$ in dynamic tests

The sway acceleration $\dot{v}$ of the model can be expressed as a function of the transverse PMM acceleration $\dot{v}_{PMM}$, the heading ψ, the transverse PMM velocity and the carriage acceleration $\dot{U}_C$. Nevertheless, the carriage acceleration is assumed to be zero, i.e. $\dot{U}_C = 0$, so the sway acceleration becomes:

$$\dot{v} = \dot{v}_{PMM}\cos\psi - r\left(U_C\cos\psi + v_{PMM}\sin\psi\right) \tag{7.119}$$

Based on this expression the bias limit for the models sway acceleration is found from

$$B_{\dot{v}} = \sqrt{B_{\psi}^2 + B_{\dot{v}_{PMM}}^2 + B_{v_{PMM}}^2 + B_r^2 + B_{U_c}^2} \tag{7.120}$$

where

$$B_{\psi} = \frac{\partial \dot{v}}{\partial \psi}\varepsilon_{\psi} = -\left(\dot{v}_{PMM}\sin(\psi) - r\left(-U_C\sin(\psi) + v_{PMM}\cos(\psi)\right)\right)\varepsilon_{\psi} \tag{7.121}$$

$$B_{\dot{v}_{PMM}} = \frac{\partial \dot{v}}{\partial \dot{v}_{PMM}}\varepsilon_{\dot{v}_{PMM}} = \cos(\psi)\varepsilon_{\dot{v}_{PMM}} \tag{7.122}$$

$$B_{v_{PMM}} = \frac{\partial \dot{v}}{\partial v_{PMM}}\varepsilon_{v_{PMM}} = r\sin(\psi)\varepsilon_{v_{PMM}} \tag{7.123}$$

$$B_r = \frac{\partial \dot{v}}{\partial r}\varepsilon_{v_{PMM}} = -\left(U_C\cos(\psi) + v_{PMM}\sin(\psi)\right)\varepsilon_r \tag{7.124}$$

$$B_{U_C} = \frac{\partial \dot{v}}{\partial U_C}\varepsilon_{U_C} = -r\cos(\psi)\varepsilon_{U_C} \tag{7.125}$$

ε_{ψ} is the uncertainty of the heading, which was found in §7.3.9, where $\varepsilon_{\psi} = B_{heading}$. [Note, when using the data from §7.3.9 it is necessary to take the value corresponding to the type of test, i.e. pure sway ($\psi = 0$) or pure yaw.]; $\varepsilon_{v_{PMM}}$ is the uncertainty on the transverse PMM velocity v_{PMM}, which has been found in §; ε_r is the uncertainty of the yaw rate, which will be discussed in the following section, where $\varepsilon_r = B_r$; ε_{U_C} is the velocity bias calculated in §7.3.2; the uncertainty $\varepsilon_{\dot{v}_{PMM}}$ is the one related to the transverse PMM acceleration $\dot{v}_{PMM}$, which is defined in §7.3.12.

7.3.14 Estimation of bias limit for *r* in dynamic tests

The expression of the PMM yaw rate r_{PMM} is given by (6.2) in §6. Since $r = r_{PMM}$, the uncertainty on r can be introduced trough ψ_{MAX}, ω, t and ϕ.

$$\boxed{r = \dot{\psi} = \psi_{MAX}\omega\cos(\omega t + \phi)} \tag{7.126}$$

Considering the motion, the bias limit for *r* can be given as

$$B_r = \sqrt{B_{\psi_{MAX}}^2 + B_{\omega}^2 + B_t^2 + B_{\phi}^2} \tag{7.127}$$

where the terms under the square root are defined by

$$B_{\psi_{MAX}} = \frac{\partial r}{\partial \psi_{MAX}}\varepsilon_{\psi_{MAX}} = \omega\cos(\omega t + \phi)\varepsilon_{\psi_{MAX}} \tag{7.128}$$

$$B_{\omega} = \frac{\partial r}{\partial \omega}\varepsilon_{\omega} = -\psi_{MAX}\omega t\sin(\omega t + \phi)\varepsilon_{\omega} \tag{7.129}$$

$$B_t = \frac{\partial r}{\partial t}\varepsilon_t = -\psi_{MAX}\omega^2\sin(\omega t + \phi)\varepsilon_t \tag{7.130}$$

$$B_\phi = \frac{\partial r}{\partial \phi}\varepsilon_\phi = -\psi_{MAX}\omega\sin\left(\omega t+\phi\right)\varepsilon_\phi \tag{7.131}$$

$\varepsilon_{\psi_{MAX}}$, ε_ω, ε_t and ε_ϕ are the uncertainties of ψ_{MAX}, ω, t and ϕ respectively (see §7.3.9).

7.3.15 Estimation of bias limit for $\dot{r}$ in dynamic tests

The expression of the PMM yaw acceleration $\dot{r}_{PMM}$ is given by (6.3) in §6. Since $\dot{r} = \dot{r}_{PMM}$, the uncertainty in $\dot{r}$ is introduced trough ψ_{MAX}, ω, t.

$$\boxed{\dot{r} = \ddot{\psi} = -\psi_{MAX}\omega^2\sin\left(\omega t+\phi\right) \qquad (7.132)}$$

Therefore, the bias limit can be expressed as

$$B_{\dot{r}} = \sqrt{B_{\psi_{MAX}}^2 + B_\omega^2 + B_t^2 + B_\phi^2} \tag{7.133}$$

The 4 terms needed for the calculate are given by

$$B_{\psi_{MAX}} = \frac{\partial \dot{r}}{\partial \psi_{MAX}}\varepsilon_{\psi_{MAX}} = -\omega^2\sin\left(\omega t+\phi\right)\varepsilon_{\psi_{MAX}} \tag{7.134}$$

$$B_\omega = \frac{\partial \dot{r}}{\partial \omega}\varepsilon_\omega = -\psi_{MAX}\omega^2 t\cos\left(\omega t+\phi\right)\varepsilon_\omega \tag{7.135}$$

$$B_t = \frac{\partial \dot{r}}{\partial t}\varepsilon_t = -\psi_{MAX}\omega^3\cos\left(\omega t+\phi\right)\varepsilon_t \tag{7.136}$$

$$B_\phi = \frac{\partial \dot{r}}{\partial \phi}\varepsilon_\phi = -\psi_{MAX}\omega^2\cos\left(\omega t+\phi\right)\varepsilon_\phi \tag{7.137}$$

$\varepsilon_{\psi_{MAX}}$, ε_ω, ε_t and ε_ϕ are the uncertainties of ψ_{MAX}, ω, t and ϕ respectively (see §7.3.9).

7.3.16 Estimation of bias limit for u in dynamic tests

u is the sum of the projections of the carriage speed U_C and the transverse PMM velocity v_{PMM} onto the models heading directions. So, it is possible to express u as

$$\boxed{u = U_C\cos\psi + v_{PMM}\sin\psi \qquad (7.138)}$$

Based on this expression, the bias limit of u is given by

$$B_u = \sqrt{B_{U_C}^2 + B_{v_{PMM}}^2 + B_\psi^2}$$

where

$$B_{v_{PMM}} = \frac{\partial u}{\partial v_{PMM}}\varepsilon_{v_{PMM}} = \sin\left(\psi\right)\varepsilon_{v_{PMM}} \tag{7.139}$$

$$B_{U_C} = \frac{\partial u}{\partial U_C}\varepsilon_{U_C} = \cos(\psi)\varepsilon_{U_C} \tag{7.140}$$

$$B_{\psi} = \frac{\partial u}{\partial \psi}\varepsilon_{\psi} = \left(-U_C \sin(\psi) + v_{PMM}\cos(\psi)\right)\varepsilon_{\psi} \tag{7.141}$$

$\varepsilon_{v_{PMM}}$ is the uncertainty of the transverse PMM velocity which has been estimated from (7.105); ε_{ψ} is the uncertainty of the heading which has been estimated from (7.97); ε_{U_C} is the uncertainty of the carriage speed which has been estimated from (7.80). In case of pure sway, one should observe that $\psi = 0$ and so $B_{v_{PMM}} = 0$.

7.3.17 Estimation of bias limit for $\dot{u}$ in dynamic tests

The surge acceleration $\dot{u}$ is the sum of the projections of the carriage acceleration, $\dot{U}_C$ and the transverse PMM acceleration $\dot{v}_{PMM}$ onto the models heading direction plus a cross coupling term. Therefore it is possible to express $\dot{u}$ as

$$\boxed{\dot{u} = \dot{U}_C \cos\psi + \dot{v}_{PMM}\sin\psi + r(v_{PMM}\cos\psi - U_C \sin\psi)} \tag{7.142}$$

and considering that the carriage acceleration is assumed to be zero, i.e. $\dot{U}_C = 0$

$$\boxed{\dot{u} = \dot{v}_{PMM}\sin\psi + r(v_{PMM}\cos\psi - U_C \sin\psi)} \tag{7.143}$$

Based on this expression, the bias limit of $\dot{u}$ is given by

$$B_{\dot{u}} = \sqrt{B_{\dot{v}_{PMM}}^2 + B_{v_{PMM}}^2 + B_r^2 + B_{\psi}^2 + B_{U_C}^2} \tag{7.144}$$

where

$$B_{\dot{v}_{PMM}} = \frac{\partial \dot{u}}{\partial \dot{v}_{PMM}}\varepsilon_{\dot{v}_{PMM}} = \sin(\psi)\varepsilon_{\dot{v}_{PMM}} \tag{7.145}$$

$$B_{v_{PMM}} = \frac{\partial \dot{u}}{\partial v_{PMM}}\varepsilon_{v_{PMM}} = r\cos(\psi)\varepsilon_{v_{PMM}} \tag{7.146}$$

$$B_{\psi} = \frac{\partial \dot{u}}{\partial \psi}\varepsilon_{\psi} = \left(\dot{v}_{PMM}\cos(\psi) - r\left(v_{PMM}\sin(\psi) + U_C\cos(\psi)\right)\right)\varepsilon_{\psi} \tag{7.147}$$

$$B_r = \frac{\partial \dot{u}}{\partial r}\varepsilon_r = \left(v_{PMM}\cos(\psi) - U_C\sin(\psi)\right)\varepsilon_r \tag{7.148}$$

$$B_{U_C} = \frac{\partial \dot{u}}{\partial U_C}\varepsilon_{U_C} = -r\sin(\psi)\varepsilon_{U_C} \tag{7.149}$$

$\varepsilon_{\dot{v}_{PMM}}$ is the uncertainty of the transverse PMM acceleration which has been estimated from (7.115); $\varepsilon_{v_{PMM}}$ is the uncertainty of the transverse PMM velocity which has been estimated from (7.105); ε_{ψ} is the uncertainty of the heading which has been estimated from (7.97); ε_r is the uncertainty of the yaw rate which has been estimated from (7.127); ε_{U_C} is the uncertainty of the carriage speed which

has been estimated from (7.80). In case of pure sway, one should observe that $\psi = 0$ and so $B_{\dot{v}_{PMM}} = 0$.

7.3.18 Estimation of bias limit for the measured *X*-force, F_x

The bias limit of the X-force measured at the gauges is assumed to consist of eleven components, which cover

- The error in the drift angle setting in the PMM
- The error introduced through the volt-force conversion during data acquisition
- The error introduced in the calibration of the force gauges due to uncertainties in the applied weights
- The error in the positioning of the measure cell when mounted in the model
- The error introduced through the uncertainties in the surge velocities during the dynamic test.
- This error introduced through the uncertainties in the sway velocities during the dynamic test.
- The error introduced due to uncertainty in the obtained yaw rate during dynamic tests
- The error introduced through the uncertainties in the surge acceleration during the dynamic test.
- The error introduced through the uncertainties in the sway acceleration during the dynamic test.
- The error introduced through the uncertainties in the yaw acceleration during the dynamic test.
- The error introduced through the uncertainty in time

These error contributions can be collected in following expression for the bias limit

$$B_{Fx}^2 = B_{\beta,Fx}^2 + B_{conv,Fx}^2 + B_{calib,Fx}^2 + B_{acquis,Fx}^2 + B_{u,Fx}^2 + B_{v,Fx}^2 + B_{r,Fx}^2 + B_{\dot{u},Fx}^2 + B_{\dot{v},Fx}^2 + B_{\dot{r},Fx}^2 + B_{t,Fx}^2 \qquad (7.150)$$

Term	Static	Dynamic
$B_{\beta,Fx}^2$	X	
$B_{cal\&acq,Fx}^2$	X	X
$B_{u,Fx}^2$		X
$B_{v,Fx}^2$		X
$B_{r,Fx}^2$		X
$B_{\dot{u},Fx}^2$		X
$B_{\dot{v},Fx}^2$		X
$B_{\dot{r},Fx}^2$		X
$B_{t,Fx}^2$		X

Table 7-12 Considered terms.

Depending of the type of test considered, different terms will be included in the uncertainty assessment. The table above shows the terms, which are included in the static and dynamic tests. The individual terms are described and estimated below.

Drift angle setting

$B_{\beta,Fx}$ is the force bias limit related to how accurate the drift angle can be set in the PMM. It is estimated from

$$B_{\beta,Fx} = \frac{dF_X}{d\beta}\varepsilon_\beta \tag{7.151}$$

where the influence coefficient $\frac{dF_X}{d\beta}$ is the derivative of the measured F_X with respect to β and ε_β is the uncertainty related to the accuracy of the drift angle setting. With respect to the uncertainty, ε_β which is related to the drift angle setting in the test, is estimated to be 0.15 degree.

Fn	$dF_X/d\beta$ [N/rad]	ε_β [rad]	$B_{\beta,Fx}$ [N]
0.138	-13.13	0.00262	-0.034
0.280	-125.1	0.00262	-0.328
0.410	-153.3	0.00262	-0.401

Table 7-13 Bias limit data related to drift angle setting ($\beta = 10°$) in static tests

Concerning the influence coefficient, it is taken from the static drift test results, but it is taken around a specific β value in order to match the considered test type. Therefore, since the static test uncertainty analysis is conducted for $\beta = 10°$, the slopes are evaluated around this drift angle. Table 7-13 Bias limit data related to drift angle setting ($\beta = 10°$) in static tests shows the applied slopes. For the dynamic test uncertainty assessment, the drift angle uncertainty is included via the heading uncertainty, which again is included in the uncertainties related to the surge and sway velocities and accelerations, see later subsections. Therefore, in order not to include the drift angle uncertainty twice $B_{\beta,Fx} = 0$ in all dynamic tests.

Calibration and acquisition of force gauges

The bound uncertainty to the use of the force gauges is due to three fundamental factors:

1. B_{calib,F_X}, the uncertainty on the weights used for the building of the curve of calibration,
2. B_{acquis,F_X}, the uncertainty on the positioning of the measure cells in the model (in practical the capacity to appreciate, by the force gauge, the whole applied strength),
3. B_{conv,F_X}, the mistake introduced in the measure chain during the conversion of the signal from analogic to digital (Kg in Volt).

The total uncertainty can so be express as:

$$B_{cal\&acq,F_X} = \sqrt{B_{cal,F_X}^2 + B_{acq,F_X}^2 + B_{conv,F_X}^2} \tag{7.152}$$

The curve of calibration of the transducer has been obtained loading the sample cell with some weights. The control on the perfect perpendicularity of the load (load coaxial with the measure sensor axis) has been executed measuring the angle with respect to the vertical one of the loaded

agent. In practice the sample weight has understood equal the applied weight ($P_{appl} = Mg$) for the cosine of the measured angle θ. This procedure has been repeated for a series of loads as shown in the relative tables (Table 7-14 and Table 7-15). In this way the uncertainty on the weights comes to depend on uncertainty on the sample masses and on that on the angle measured according to the relation:

$$P_{calib} = P_{appl} \cos\theta \tag{7.153}$$

$$B_{calib,i} = \sqrt{\theta_M^2 B_M^2 + \theta_\theta^2 B_\theta^2} = \sqrt{(g\cos\theta)^2 B_M^2 + (Mg\sin\theta)^2 B_\theta^2} \tag{7.154}$$

P_{appl} (N)	θ (°)	P_{calib} **(N)**	θ_M	B_M	θ_θ	B_θ	$B_{calib,i}$ (N)
98,1	5,4	**97,7**	**9,766**	**0,0016**	**9,232**	**0,0087**	0,0821
196,2	3,8	**195,8**	**9,788**	**0,0023**	**13,005**	**0,0087**	0,1156
294,3	3,4	**293,8**	**9,793**	**0,0029**	**17,456**	**0,0087**	0,1549
392,4	3	**391,9**	**9,797**	**0,0033**	**20,538**	**0,0087**	0,1820
490,5	2,3	**490,1**	**9,802**	**0,0036**	**19,684**	**0,0087**	0,1754
588,6	2,3	**588,1**	**9,802**	**0,0039**	**23,622**	**0,0087**	0,2097
686,7	2,3	**686,2**	**9,802**	**0,0042**	**27,559**	**0,0087**	0,2440
784,8	2	**784,4**	**9,804**	**0,0045**	**27,391**	**0,0087**	0,2430
882,9	1,9	**882,4**	**9,805**	**0,0047**	**29,273**	**0,0087**	0,2597
981,0	1,8	**980,5**	**9,805**	**0,0050**	**30,815**	**0,0087**	0,2734
1079,1	1,8	**1078,6**	**9,805**	**0,0053**	**33,896**	**0,0087**	0,3003

Table 7-14 Uncertainty of weights for after transducer.

P_{appl} (N)	θ (°)	P_{calib} **(N)**	θ_M	B_M	θ_θ	B_θ	$B_{calib,i}$ (N)
98,1	5,6	**97,6**	**9,763**	**0,0016**	**9,573**	**0,0087**	0,0850
196,2	4,2	**195,7**	**9,784**	**0,0023**	**14,371**	**0,0087**	0,1274
294,3	3,9	**293,6**	**9,787**	**0,0029**	**20,019**	**0,0087**	0,1770
392,4	3,5	**391,7**	**9,792**	**0,0033**	**23,957**	**0,0087**	0,2115
490,5	2,9	**489,9**	**9,797**	**0,0036**	**24,815**	**0,0087**	0,2195
588,6	3	**587,8**	**9,797**	**0,0039**	**30,805**	**0,0087**	0,2716
686,7	3	**685,8**	**9,797**	**0,0042**	**35,940**	**0,0087**	0,3163
784,8	2,6	**784,0**	**9,800**	**0,0045**	**35,603**	**0,0087**	0,3138
882,9	2,6	**882,0**	**9,800**	**0,0047**	**40,052**	**0,0087**	0,3526
981,0	2,5	**980,1**	**9,801**	**0,0050**	**42,791**	**0,0087**	0,3767
1079,1	2,6	**1078,0**	**9,800**	**0,0053**	**48,952**	**0,0087**	0,4303

Table 7-15 Uncertainty of weights for fore transducer.

The table takes back the values of the theoretical weight and of the real one, for every sample mass the relative bias and influence coefficient is suitable, so for the measure of the angle, at last the total bias are also taken back. The total bias is given by the standard deviation of the distribution assuming the middle reference value as 0.

$$B_{calib} = \sqrt{\frac{\sum_{i=1}^{n} B_{calib,i}^2}{N-1}} \tag{7.155}$$

Obviously, considered that the strength is obtained adding the measures of a couple of force gauges positioned on the after and fore post of the PMM, the total weight uncertainty is:

$$B_{calib,F_X} = \sqrt{B^2_{calib,aft} + B^2_{calib,for}} \tag{7.156}$$

B_{calib,F_X} [N]
0.371

Table 7-16 Weight related bias limit.

For the calculation of the uncertainty due to the second factor B_{acquis,F_X}, we have considered that the fundamental mistakes that it is possible to perform during the assembly of the cells on the model are two: the mistake in the alignment of the two cells with respect to the ideal mean line of the model which is translated in a misalignment of the model with respect to 0, the mistake due to the positioning of the single transducer which can bring a light angular rotation of the sensor axis with respect to the ideal direction. The estimate of the first contribution can be done considering that a mistake of two millimetres can be performed on a distance of 1334 mm (distance between both post), that of the second, analogously, thinking that it is possible to perform a mistake of one millimetre on 150 mm (side of the force gauges).

$$\varepsilon_1 = F_{appl} - F^*_{measured} = \frac{F^*_{measured}}{\cos\gamma_1} - F^*_{measured} = F^*_{measured}\frac{(1-\cos\gamma_1)}{\cos\gamma_1} \tag{7.157}$$

$$\varepsilon_2 = F^*_{measured} - F_{measured} = \frac{F_{measured}}{\cos\gamma_2} - F_{measured} = F_{measured}\frac{(1-\cos\gamma_2)}{\cos\gamma_2}$$

$$\varepsilon_{12} = \varepsilon_1 + \varepsilon_2 = F_{X_{measured}}\frac{1-\cos\gamma_1\cos\gamma_2}{\cos\gamma_1\cos\gamma_2} \tag{7.158}$$

where $\cos\gamma_1 = \cos(arctg(\frac{2}{1334}))$ and $\cos\gamma_2 = \cos(arctg(\frac{1}{150}))$. Finally we have:

$$B_{acquis,F_X} = \sqrt{\varepsilon_{12}^2 + \varepsilon_{12}^2} = \sqrt{2}\varepsilon_{12} \tag{7.159}$$

B_{acquis,F_X} [N]
2.335E-5 $F_{X_{measured}}$

Table 7-17 Acquisition bias limit.

The third factor is bound to the mistake introduced in the conversion of the signal from analogic to digital, the factor will also be given by the combination of the uncertainty of the single transducer,

$$B_{conv,F_X} = \sqrt{B^2_{conv,F_{X_{aft}}} + B^2_{conv,F_{X_{fore}}}} \tag{7.160}$$

The single contribution is soon determinate considering that the measured strength will be given by the signal in tension (signal (v)) multiplied for the sensitivity (S) of the transducer and then,

$$F_{X_{measured}} = S \cdot signal(V) \tag{7.161}$$

$$B_{conv,F_{X_{aft}}} = S \cdot B_{signal} \tag{7.162}$$

the resolution error in acquisition for the signal is given, the adopted cards acquire to 16 bits, from the ratio between the maximum tension (10 volts) e 2^{16}. Hence $B_{signal} = \frac{10}{2^{16}} = 0.000153$,

B_{conv,F_X} [N]
0.075

Table 7-18 Conversion A/D bias limit.

In conclusion the total bias limiti is indicated in Table 7-19:

$B_{cal\&acq,F_X}$ [N]
$\sqrt{0.378^2 + (0.00002335 \cdot F_{X_{measured}})^2}$

Table 7-19 Total bias limit for calibration and acquisition of force gauges.

Surge velocity of the model

B_{u,F_X} is the bias of the *X*-force related to the surge velocity of the model: The bias limit is defined as

$$B_{u,F_X} = \frac{\partial F_X}{\partial u} \varepsilon_{surge} \tag{7.163}$$

The influence coefficient in this expression is the partial derivative of the measured *X*-force F_X with respect to *u*. ε_{surge} is the uncertainty of surge velocity, which equals B_u, which was found in §7.3.16. In order to determine the influence coefficient, the time series for F_X is transformed into a function, $\tilde{F}_X$, of the velocities and accelerations by means of a polynomial approximation, which is faired trough the data points and which can be differentiated with respect to *u*. With $\tilde{F}_X$ known it is possible to estimate B^2_{u,F_X} by means of the approximation

$$B_{u,F_X} \approx \frac{\partial \tilde{F}_X}{\partial u} \varepsilon_{surge} \tag{7.164}$$

The development of $\tilde{F}_X$ is determined to match the considered type of test.

Pure Yaw:

$$\tilde{F}_X = X_0 + X_u u + X_r r + X_{rr} r^2 + X_{\dot{u}} \dot{u} + X_{\dot{r}} \dot{r} + X_v v + X_{\dot{v}} \dot{v} \tag{7.165}$$

Pure Sway:

$$\tilde{F}_X = X_0 + X_u u + X_r r + X_{\dot{u}} \dot{u} + X_{\dot{r}} \dot{r} + X_v v + X_{\dot{v}} \dot{v} + X_{vv} v^2 \tag{7.166}$$

Yaw and drift:

$$\tilde{F}_X = X_0 + X_u u + X_r r + X_{rr} r^2 + X_{\dot{u}} \dot{u} + X_{\dot{r}} \dot{r} + X_v v + X_{\dot{v}} \dot{v} + X_{uu} u^2 + X_{vv} v^2 + X_{uv} uv \tag{7.167}$$

The coefficients for the three polynomials are shown in Table 7-20 toTable 7-22.

Fn	0.138	0.280	0.410
X_0	-11.99	-54.59	-162.6
X_u	0.36	0.34	0.07
X_r	8.05	0.51	9.98
X_{rr}	-248.7	-99.22	-75.91
$X_{\dot{u}}$	-629.0	-587.31	-649.42
$X_{\dot{r}}$	-5.07	-11.84	5.47
X_v	0	0	0
$X_{\dot{v}}$	0	0	0

Table 7-20 Coefficient for polynomial fairing in pure yaw. (Dimensional).

Fn	0.280
X_0	-59.22
X_u	2.63
X_r	0
$X_{\dot{u}}$	0
$X_{\dot{r}}$	0
X_v	-2.33
$X_{\dot{v}}$	8.37
X_{vv}	-93.22

Table 7-21 Coefficients for polynomial fairing in pure sway. (Dimensional).

Fn	0.280
X_0	-54.59
X_u	0.34
X_r	0.51
X_{rr}	-99.22
$X_{\dot{u}}$	-587.3
$X_{\dot{r}}$	-11.84
X_v	-2.33
$X_{\dot{v}}$	8.37
X_{uu}	3.69
X_{vv}	529.9

X_{uv}	-246.6

Table 7-22 Coefficients for polynomial fairing in yaw and drift. (Dimensional).

Please notice that the error related to the polynomial fairing is for this study not included into the analysis.

Sway velocity of the model

B_{v,F_X} is the bias limit of the *X*-force related to the sway velocity of the model. The bias limit is defined as

$$B_{v,F_X} = \frac{\partial F_X}{\partial v}\varepsilon_{sway} \approx \frac{\partial \tilde{F}_X}{\partial v}\varepsilon_{sway} \tag{7.168}$$

As was the case for B_{u,F_X} the polynomial approximation is applied in order to estimate the influence coefficient. $\tilde{F}_X$ is given by expressions (7.165) to (7.167). ε_{sway} is the uncertainty of the sway rate, which equals B_v found in §7.3.12.

Yaw rate of the model

B_{r,F_X} is the bias limit of the *X*-force related to yaw rate of the model. The bias limit is defined as

$$B_{r,F_X} = \frac{\partial F_X}{\partial r}\varepsilon_{yawrate} \approx \frac{\partial \tilde{F}_X}{\partial r}\varepsilon_{yawrate} \tag{7.169}$$

$\tilde{F}_X$ is given by expressions (7.165) to (7.167). $\varepsilon_{yawrate}$ is the uncertainty of the yaw rate, which equals B_r found in §7.3.14.

Surge acceleration of Model

$B_{\dot{u},F_X}$ is the bias limit of the *X*-force related to the surge acceleration of the model. The bias limit is defined as

$$B_{\dot{u},F_X} = \frac{\partial F_X}{\partial \dot{u}}\varepsilon_{surge\,acc.} \approx \frac{\partial \tilde{F}_X}{\partial \dot{u}}\varepsilon_{surge\,acc.} \tag{7.170}$$

$\tilde{F}_X$ is given by expressions (7.165) to (7.167). $\varepsilon_{surge\,acc.}$ is the uncertainty of the surge acceleration, which equals $B_{\dot{u}}$ found in §7.3.17.

Sway acceleration of the model

$B_{\dot{v},F_X}$ is the bias limit of the *X*-force related to the surge acceleration of the model. The bias limit is defined as

$$B_{\dot{v},F_X} = \frac{\partial F_X}{\partial \dot{v}}\varepsilon_{sway\,acc.} \approx \frac{\partial \tilde{F}_X}{\partial \dot{v}}\varepsilon_{sway\,acc.} \tag{7.171}$$

$\tilde{F}_X$ is given by expressions (7.165) to (7.167). $\varepsilon_{sway\,acc.}$ is the uncertainty of the sway acceleration, which equals $B_{\dot{v}}$ found in §7.3.13.

Yaw acceleration of the model

$B_{\dot{r},F_X}$ is the bias limit of the *X*-force related to the yaw acceleration of the model. The bias limit is defined as

$$B_{\dot{r},F_X} = \frac{\partial F_X}{\partial \dot{r}} \varepsilon_{yaw\,acc.} \approx \frac{\partial \tilde{F}_X}{\partial \dot{r}} \varepsilon_{yaw\,acc.} \tag{7.172}$$

$\tilde{F}_X$ is given by expressions (7.165) to (7.167). $\varepsilon_{yaw\,acc.}$ is the uncertainty of the yaw acceleration, which equals $B_{\dot{r}}$ found in §7.3.15.

Time

B_{t,F_X} is the bias limit of the *X*-force related to the time at which the data is measured. The bias limit is defined as

$$B_{t,F_X} = \frac{\partial F_X}{\partial t} \varepsilon_t \tag{7.173}$$

The influence coefficient is determined by means of differentiation of the time series for F_X with respect to time. $\varepsilon_t = 0.00063$ second is the uncertainty related to time.

7.3.19 Estimation of the bias limit for the measured Y-force, F_Y

The same error sources are considered for F_Y as for F_X: it must be mentioned that the total Y-force is considered for most of the bias limit (the sum of the data given by the two force gauges).

$$B_{F_Y}^2 = B_{\beta,F_Y}^2 + B_{conv,F_Y}^2 + B_{calib,F_Y}^2 + B_{acquis,F_Y}^2 + B_{u,F_Y}^2 + B_{v,F_Y}^2 + B_{r,F_Y}^2 + B_{\dot{u},F_Y}^2 + B_{\dot{v},F_Y}^2 + B_{\dot{r},F_Y}^2 + B_{t,F_Y}^2 \tag{7.174}$$

Term	Static	Dynamic
B_{β,F_Y}^2	X	
$B_{cal\&acq,F_Y}^2$	X	X
B_{u,F_Y}^2		X
B_{v,F_Y}^2		X
B_{r,F_Y}^2		X
$B_{\dot{u},F_Y}^2$		X
$B_{\dot{v},F_Y}^2$		X
$B_{\dot{r},F_Y}^2$		X
B_{t,F_Y}^2		X

Table 7-23 Considered terms.

The table above shows the terms, which are included in the static and dynamic tests. The individual terms are described and estimated below.

Drift angle setting

B_{β,F_Y} is the force bias limit related to how accurate the drift angle can be set in the PMM. It is estimated from

$$B_{\beta,F_Y} = \frac{dF_Y}{d\beta}\varepsilon_\beta \tag{7.175}$$

where the influence coefficient $\frac{dF_Y}{d\beta}$ is the derivative of the measured F_Y with respect to β and ε_β is the uncertainty related to the accuracy of the drift angle setting. With respect to the uncertainty, ε_β which is related to the drift angle setting in the test, is estimated to be 0.15 degree. As or the case of B_{β,F_X} the influence coefficient is taken around a specific β in order to match the considered test. Once again $B_{\beta,F_Y} = 0$ for the dynamic tests.

Fn	$dF_Y/d\beta$ [N/rad]	ε_β [rad]	$B_{\beta,Fx}$ [N]
0.138	380.9	0.00262	0.997
0.280	1715.7	0.00262	4.492
0.410	5327.78	0.00262	13.95

Table 7-24 Bias limit data related to drift angle setting ($\beta = 10°$) in static tests.

Calibration and acquisition of force gauges

P_{appl} (N)	θ (°)	P_{calib} **(N)**	θ_M	B_M	θ_θ	B_θ	$B_{calib,i}$ (N)
98,1	4,5	**97,8**	**9,780**	**0,0016**	**7,697**	**0,0087**	0,0690
196,2	3	**196,0**	**9,797**	**0,0023**	**10,270**	**0,0087**	0,0923
294,3	2,8	**294,0**	**9,798**	**0,0029**	**14,378**	**0,0087**	0,1286
392,4	2,5	**392,0**	**9,801**	**0,0033**	**17,117**	**0,0087**	0,1527
490,5	1,8	**490,2**	**9,805**	**0,0036**	**15,407**	**0,0087**	0,1391
588,6	2	**588,2**	**9,804**	**0,0039**	**20,542**	**0,0087**	0,1833
686,7	1,9	**686,3**	**9,805**	**0,0042**	**22,768**	**0,0087**	0,2029
784,8	1,7	**784,5**	**9,806**	**0,0045**	**23,283**	**0,0087**	0,2078
882,9	1,5	**882,6**	**9,807**	**0,0047**	**23,112**	**0,0087**	0,2070
981,0	1,8	**980,5**	**9,805**	**0,0050**	**30,815**	**0,0087**	0,2734
1079,1	1,8	**1078,6**	**9,805**	**0,0053**	**33,896**	**0,0087**	0,3003

Table 7-25 After gauge: uncertainty of weights.

P_{appl} (N)	θ (°)	P_{calib} **(N)**	θ_M	B_M	θ_θ	B_θ	$B_{calib,i}$ (N)
98,1	4,5	**97,8**	**9,7798**	**0,0016**	**7,6967**	**0,0087**	0,0690
196,2	3,1	**195,9**	**9,7956**	**0,0023**	**10,6116**	**0,0087**	0,0952
294,3	2,9	**294,0**	**9,7974**	**0,0029**	**14,8909**	**0,0087**	0,1330
392,4	2,5	**392,0**	**9,8007**	**0,0033**	**17,1172**	**0,0087**	0,1527
490,5	1,8	**490,2**	**9,8052**	**0,0036**	**15,4067**	**0,0087**	0,1391
588,6	2,1	**588,2**	**9,8034**	**0,0039**	**21,5685**	**0,0087**	0,1921
686,7	2	**686,3**	**9,8040**	**0,0042**	**23,9660**	**0,0087**	0,2132

784,8	1,5	**784,6**	**9,8066**	**0,0045**	**20,5447**	**0,0087**	0,1846
882,9	1,8	**882,5**	**9,8052**	**0,0047**	**27,7331**	**0,0087**	0,2464
981,0	1,6	**980,6**	**9,8062**	**0,0050**	**27,3916**	**0,0087**	0,2441
1079,1	1,6	**1078,7**	**9,8062**	**0,0053**	**30,1310**	**0,0087**	0,2679

Table 7-26 Fore gauge: uncertainty of weights.

The calculation of this bias is completely analogous to the one executed for the case F_X, the strengths in y direction are acquired with a couple of gauges which work to the same way. Only the tables and the values obtained for the single factors which contribute to the total uncertainty are, afterwards, taken back.

The total uncertainty can so be express as:

$$B_{cal\&acq,F_Y} = \sqrt{B^2_{calib,F_Y} + B^2_{acquis,F_Y} + B^2_{conv,F_Y}} \tag{7.176}$$

The total bias is given by the standard deviation of the distribution assuming the middle reference value as 0.

$$B_{calib} = \sqrt{\frac{\sum_{i=1}^{n} B^2_{calib,i}}{N-1}} \tag{7.177}$$

$$B_{calib,F_Y} = \sqrt{B^2_{calib,aft} + B^2_{calib,for}} \tag{7.178}$$

B_{calib,F_Y} [N]
0.279

Table 7-27 Weight related bias limit.

For the calculation of the uncertainty due to the second factor B_{acquis,F_Y},

$$B_{acquis,F_Y} = \sqrt{\varepsilon^2_{12} + \varepsilon^2_{12}} = \sqrt{2}\varepsilon_{12} \tag{7.179}$$

B_{acquis,F_Y} [N]
2.335E-5 $F_{Y_{measured}}$

Table 7-28 Acquisition bias limit.

The third factor is

$$B_{conv,F_Y} = \sqrt{B^2_{conv,F_{Y_{aft}}} + B^2_{conv,F_{Y_{fore}}}} \tag{7.180}$$

B_{conv,F_Y} [N]
0.090

Table 7-29 Conversion A/D bias limit.

In conclusion the total bias limit is indicated in Table 7-30:

$B_{cal\&acq,F_Y}$ [N]
$\sqrt{0.293^2 + (0.00002335 \cdot F_{Y_{measured}})^2}$

Table 7-30 Total bias limit for calibration and acquisition of force gauges.

Surge velocity of the model

B_{u,F_Y} is the bias of the *Y*-force related to the surge velocity of the model: The bias limit is defined as

$$B_{u,F_Y} = \frac{\partial F_Y}{\partial u} \varepsilon_{surge} \tag{7.181}$$

The influence coefficient in this expression is the partial derivative of the measured *Y*-force F_Y with respect to u. ε_{surge} is the uncertainty of surge velocity, which equals B_u, which was found in §7.3.16. Once again, in order to determine the influence coefficient, the time series for F_Y is transformed into a function, $\tilde{F}_Y$, then the same polynomial approximation is used in connection with B_{u,F_X} in §7.3.18, thus it will not be described here. The following approximation for

$$B_{u,F_Y} \approx \frac{\partial \tilde{F}_X}{\partial u} \varepsilon_{surge} \tag{7.182}$$

Fn	0.138	0.280	0.410
Y_0	-1.45	-1.53	-2.83
Y_u	0.43	-0.19	-0.39
Y_r	-647.6	-1535.9	-2713
Y_{rrr}	-20137	-12513	10905
$Y_{\dot{u}}$	-15.30	24.93	-88.60
$Y_{\dot{r}}$	-435.2	-368.19	-419.8
Y_v	0	0	0
$Y_{\dot{v}}$	0	0	0

Table 7-31 Coefficient for polynomial fairing in pure yaw (Dimensional).

Fn	0.280
Y_0	-1.74
Y_u	-0.19
Y_r	0
$Y_{\dot{r}}$	0
$Y_{\dot{u}}$	0

Y_v	-413.15
$Y_{\dot{v}}$	-1047.1
$Y_{v\|v\|}$	-315.86

Table 7-32 Coefficients for polynomial fairing in pure sway (Dimensional).

$\tilde{F}_Y$ is represented by different polynomials in order to match the considered tests.

Pure Yaw:

$$\tilde{F}_Y = Y_0 + Y_u u + Y_r r + Y_{rrr} r^3 + Y_{\dot{u}} \dot{u} + Y_{\dot{r}} \dot{r} + Y_v v + Y_{\dot{v}} \dot{v} \tag{7.183}$$

Pure Sway:

$$\tilde{F}_Y = Y_0 + Y_u u + Y_r r + Y_{\dot{u}} \dot{u} + Y_{\dot{r}} \dot{r} + Y_v v + Y_{\dot{v}} \dot{v} + Y_{vv} v^2 + Y_{v|v|} v|v| \tag{7.184}$$

Yaw and drift:

$$\begin{aligned}\tilde{F}_Y = {} & Y_0 + Y_u u + Y_r r + Y_{\dot{r}} \dot{r} + Y_{rrr} r^3 + Y_{\dot{u}} \dot{u} + Y_v v + Y_{\dot{v}} \dot{v} + Y_{vu} vu + Y_{v|v|} v|v| + Y_{v|r|} v|r| + \\ & Y_{r|v|} r|v| + Y_{rvv} rv^2 + Y_{vrr} vr^3\end{aligned} \tag{7.185}$$

The coefficients for the three polynomials are shown in Table 7-31 to Table 7-33.

Fn	0.280
Y_0	-1.53
Y_u	-0.19
Y_r	-1535.9
$Y_{\dot{r}}$	-368.19
Y_{rrr}	-12513
$Y_{\dot{u}}$	24.93
Y_v	-413.15
$Y_{\dot{v}}$	-1047.1
Y_{vu}	2.63
$Y_{v\|v\|}$	-315.86
$Y_{v\|r\|}$	-71.97
$Y_{r\|v\|}$	19147
Y_{rvv}	-55247
Y_{vrr}	-13249

Table 7-33 Coefficients for polynomial fairing in yaw and drift (Dimensional).

Sway velocity of the model

B_{v,F_Y} is the bias limit of the *Y*-force related to the sway velocity of the model. The bias limit is defined as

$$B_{v,F_Y} = \frac{\partial F_Y}{\partial v}\varepsilon_{sway} \approx \frac{\partial \tilde{F}_Y}{\partial v}\varepsilon_{sway} \tag{7.186}$$

As was the case for B_{u,F_Y} the polynomial approximation is applied in order to estimate the influence coefficient. $\tilde{F}_Y$ is given by expressions (7.183) to (7.185). ε_{sway} is the uncertainty of the sway rate, which equals B_v found in §7.3.10.

Yaw rate of the model

B_{r,F_Y} is the bias limit of the *Y*-force related to yaw rate of the model. The bias limit is defined as

$$B_{r,F_Y} = \frac{\partial F_Y}{\partial r}\varepsilon_{yawrate} \approx \frac{\partial \tilde{F}_Y}{\partial r}\varepsilon_{yawrate} \tag{7.187}$$

The influence coefficient is approximated by the derivative of $\tilde{F}_Y$ with respect to r. $\varepsilon_{yawrate}$ is the uncertainty of the yaw rate, which equals B_r found in §7.3.12.

Surge acceleration of Model

$B_{\dot{u},F_Y}$ is the bias limit of the *Y*-force related to the surge acceleration of the model. The bias limit is defined as

$$B_{\dot{u},F_Y} = \frac{\partial F_Y}{\partial \dot{u}}\varepsilon_{surge\,acc.} \approx \frac{\partial \tilde{F}_Y}{\partial \dot{u}}\varepsilon_{surge\,acc.} \tag{7.188}$$

$\tilde{F}_Y$ is given by expressions (7.183) to (7.185). $\varepsilon_{surge\,acc.}$ is the uncertainty of the surge acceleration, which equals $B_{\dot{u}}$ found in §7.3.15.

Sway acceleration of the model

$B_{\dot{v},F_Y}$ is the bias limit of the *Y*-force related to the surge acceleration of the model. The bias limit is defined as

$$B_{\dot{v},F_Y} = \frac{\partial F_Y}{\partial \dot{v}}\varepsilon_{sway\,acc.} \approx \frac{\partial \tilde{F}_Y}{\partial \dot{v}}\varepsilon_{sway\,acc.} \tag{7.189}$$

$\tilde{F}_Y$ is given by expressions (7.183) to (7.185). $\varepsilon_{sway\,acc.}$ is the uncertainty of the sway acceleration, which equals $B_{\dot{v}}$ found in §7.3.11.

Yaw acceleration of the model

$B_{\dot{r},F_Y}$ is the bias limit of the *Y*-force related to the yaw acceleration of the model. The bias limit is defined as

$$B_{\dot{r},F_Y} = \frac{\partial F_Y}{\partial \dot{r}}\varepsilon_{yaw\,acc.} \approx \frac{\partial \tilde{F}_Y}{\partial \dot{r}}\varepsilon_{yaw\,acc.} \tag{7.190}$$

$\tilde{F}_X$ is given by expressions (7.183) to (7.185). $\varepsilon_{yawacc.}$ is the uncertainty of the yaw acceleration, which equals $B_{\dot{r}}$ found in §7.3.13.

Time

B_{t,F_Y} is the bias limit of the *Y*-force related to the time at which the data is measured. The bias limit is defined as

$$B_{t,F_Y} = \frac{\partial F_Y}{\partial t}\varepsilon_t \tag{7.191}$$

The influence coefficient is determined by means of differentiation of the time series for F_Y with respect to time. $\varepsilon_t = 0.00063$ second is the uncertainty related to time.

7.3.20 Estimation of bias limit for yaw moment, M_z

In connection with estimation of the bias limit, B_{M_Z} for the yaw moment, the same error sources as for the *X*- and *Y*-forces are considered.

Term	Static	Dynamic
B^2_{β,M_Z}	X	
$B^2_{cal\&acq,M_Z}$	X	X
B^2_{u,M_Z}		X
B^2_{v,M_Z}		X
B^2_{r,M_Z}		X
$B^2_{\dot{u},M_Z}$		X
$B^2_{\dot{v},M_Z}$		X
$B^2_{\dot{r},M_Z}$		X
B^2_{t,M_Z}		X

Table 7-34 Considered terms.

It must be mentioned that the yaw moment, which is taken around the mid-ship position, is calculated on the basis of the two *Y*-forces and the distance between the gauges and the mid-ship position, i.e.

$$M_Z = M_{Z,fore} + M_{Z,aft} = L_{fore}F_{Y,fore} + L_{aft}F_{Y,aft} \tag{7.192}$$

However, for most of the bias limits for M_Z the total moment is considered. The only exceptions are in connection with the calibration and acquisition contributions, where the moment contributions from the fore and aft *Y*-forces are considered individually. The expression for the total bias limit is

$$B_{M_Z}^2 = B_{\beta,M_Z}^2 + B_{conv,M_Z}^2 + B_{calib,M_Z}^2 + B_{acquis,M_Z}^2 + B_{u,M_Z}^2 + B_{v,M_Z}^2 + B_{r,M_Z}^2 + B_{\dot{u},M_Z}^2 + B_{\dot{v},M_Z}^2 + B_{\dot{r},M_Z}^2 + B_{t,M_Z}^2 \quad (7.193)$$

Drift angle setting

B_{β,M_Z} is the force bias limit related to how accurate the drift angle can be set in the PMM. It is estimated from

$$B_{\beta,M_Z} = \frac{dM_Z}{d\beta}\varepsilon_\beta \quad (7.194)$$

where the influence coefficient $\frac{dM_Z}{d\beta}$ is the derivative of the measured M_Z with respect to β and ε_β is the uncertainty related to the accuracy of the drift angle setting. With respect to the uncertainty, ε_β which is related to the drift angle setting in the test, is estimated to be 0.15 degree. As it was the case for B_{β,F_X} the influence coefficient is taken from the static drift test results at $\beta = 10°$ in order to match the considered test. Again B_{β,F_X} is set to 0 for dynamic test.

Fn	$dM_Z/d\beta$ [N/rad]	ε_β [rad]	B_{β,M_Z} [N]
0.138	826.43	0.00263	2.164
0.280	4395	0.00263	11.506
0.410	12716	0.00263	33.290

Table 7-35 Bias limit data related to drift angle setting, $\beta = 10^\circ$ in static test.

Calibration and acquisition

The total moment is given from:

$$M_Z = L_{fore}F_{Y_{measured,fore}} - L_{aft}F_{Y_{measured,aft}} \quad (7.195)$$

since in our case $L_{fore} = L_{aft}$ we have $M_Z = L_{post}(F_{Y_{measured,fore}} - F_{Y_{measured,aft}})/2$, for which the bias limit will be

$$B_{cal\&acq,M_Z} = \sqrt{\theta_{L_{post}}^2 B_{L_{post}}^2 + \theta_{F_{Y_{measured,fore}}}^2 B_{cal\&acq,F_{Y_{measured,fore}}}^2 + \theta_{F_{Y_{measured,aft}}}^2 B_{cal\&acq,F_{Y_{measured,aft}}}^2} \quad (7.196)$$

$$\theta_{F_{Y_{measured,fore}}}^2 = \theta_{F_{Y_{measured,aft}}}^2 = \left(\frac{L_{post}}{2}\right)^2 \quad (7.197)$$

$$\theta_{L_{post}} = \frac{(F_{Y_{measured,fore}} - F_{Y_{measured,aft}})}{2} = \frac{M_Z}{L_{post}} \quad (7.198)$$

$$B_{cal\&acq,M_Z} = \sqrt{\theta_{L_{post}}^2 B_{L_{post}}^2 + 2\theta_{F_Y}^2 B_{cal\&acq,F_Y}^2} \quad (7.199)$$

considering that $B_{L_{post}} = 0.001m$ and $L_{post} = 1.334m$ we can arrange the limit bias as

$$B_{M_Z}^2 = \frac{(L_{post} B_{cal\&acq,F_Y})^2}{2} + \left(\frac{B_{L_{post}}}{L_{post}}\right)^2 M_Z^2 \qquad (7.200)$$
$$= 0.89 B_{cal\&acq,F_Y}{}^2 + 5.619^{-7} M_Z^2$$

Surge velocity of the model

B_{u,M_Z} is the bias of the yaw moment related to the surge velocity of the model: The bias limit is defined as

$$B_{u,M_Z} = \frac{\partial M_Z}{\partial u} \varepsilon_{surge} \qquad (7.201)$$

The influence coefficient in this expression is the partial derivative of the measured M_Z with respect to u. ε_{surge} is the uncertainty of surge velocity, which equals B_u, which was found in §7.3.16. Once again, in order to determine the influence coefficient, for M_Z, the same polynomial approximation is used in connection with B_{u,F_X} in §7.3.18, thus it will not be described here. The following approximation for

$$B_{u,M_Z} \approx \frac{\partial \tilde{M}_Z}{\partial u} \varepsilon_{surge} \qquad (7.202)$$

Fn	0.138	0.280	0.410
M_0	0.26	-0.17	1.19
M_u	-0.43	0.39	-1.16
M_r	-778.6	-2311.4	-5264
$M_{\dot{r}}$	-2407.2	-2591.6	-2228.7
M_{rrr}	-38186	-14739	11706
$M_{\dot{u}}$	-36.23	70.71	-144.1
M_v	0	0	0
$M_{\dot{v}}$	0	0	0

Table 7-36 Coefficient for polynomial fairing in pure yaw. (Dimensional)

Fn	0.280
M_0	1.26
M_u	-0.95
M_r	0
$M_{\dot{r}}$	0
$M_{\dot{u}}$	0
M_v	-1328
$M_{\dot{v}}$	-406.5
$M_{v\|v\|}$	-954.2

Table 7-37 Coefficient for polynomial fairing in pure sway. (Dimensional)

$\tilde{M}_Z$ is represented by different polynomials in order to match the considered tests.

Pure Yaw:

$$\tilde{M}_Z = M_0 + M_u u + M_r r + M_{rrr} r^3 + M_{\dot{u}} \dot{u} + M_{\dot{r}} \dot{r} + M_v v + M_{\dot{v}} \dot{v} \tag{7.203}$$

Pure Sway:

$$\tilde{M}_Z = M_0 + M_u u + M_r r + M_{\dot{u}} \dot{u} + M_{\dot{r}} \dot{r} + M_v v + M_{\dot{v}} \dot{v} + M_{v|v|} v|v| \tag{7.204}$$

Yaw and drift:

$$\begin{aligned}\tilde{M}_Z = {} & M_0 + M_u u + M_r r + M_{\dot{r}} \dot{r} + M_{rrr} r^3 + M_{\dot{u}} \dot{u} + M_v v + M_{\dot{v}} \dot{v} + M_{vu} vu + M_{v|v|} v|v| \\ & + M_{v|r|} v|r| + M_{r|v|} r|v| + M_{rvv} rv^2 + M_{vrr} vr^3\end{aligned} \tag{7.205}$$

The coefficients for the three polynomials are shown in Table 7-36 to Table 7-38.

Fn	0.280
M_0	-0.17
M_u	0.39
M_r	-2311.4
$M_{\dot{r}}$	-2591.6
M_{rrr}	-14739
$M_{\dot{u}}$	70.71
M_v	-1328
$M_{\dot{v}}$	-406.53
M_{vu}	66.7
$M_{v\|v\|}$	-954.19
$M_{v\|r\|}$	-69.02
$M_{r\|v\|}$	37721
M_{rvv}	-111480
M_{vrr}	-19859

Table 7-38 Coefficient for polynomial fairing in yaw and drift. (Dimensional)

Sway velocity of the model

B_{v,M_Z} is the bias limit of yaw moment related to the sway velocity of the model. The bias limit is defined as

$$B_{v,M_Z} = \frac{\partial M_Z}{\partial v} \varepsilon_{sway} \approx \frac{\partial \tilde{M}_Z}{\partial v} \varepsilon_{sway} \tag{7.206}$$

As was the case for B_{u,M_Z} the polynomial approximation is applied in order to estimate the influence coefficient. $\tilde{M}_Z$ is given by expressions (7.203) to (7.205). ε_{sway} is the uncertainty of the sway rate, which equals B_v found in §7.3.11.

Yaw rate of the model

B_{r,M_Z} is the bias limit of yaw moment related to yaw rate of the model. The bias limit is defined as

$$B_{r,M_Z} = \frac{\partial M_Z}{\partial r}\varepsilon_{yawrate} \approx \frac{\partial \tilde{M}_Z}{\partial r}\varepsilon_{yawrate} \tag{7.207}$$

The influence coefficient is approximated by the derivative of $\tilde{M}_Z$ with respect to r. $\varepsilon_{yawrate}$ is the uncertainty of the yaw rate, which equals B_r found in §7.3.14.

Surge acceleration of Model

$B_{\dot{u},M_Z}$ is the bias limit of yaw moment related to the surge acceleration of the model. The bias limit is defined as

$$B_{\dot{u},M_Z} = \frac{\partial M_Z}{\partial \dot{u}}\varepsilon_{surgeacc.} \approx \frac{\partial \tilde{M}_Z}{\partial \dot{u}}\varepsilon_{surgeacc.} \tag{7.208}$$

$\tilde{M}_Z$ is given by expressions (7.203) to (7.205). $\varepsilon_{surgeacc.}$ is the uncertainty of the surge acceleration, which equals $B_{\dot{u}}$ found in §7.3.17.

Sway acceleration of the model

$B_{\dot{v},M_Z}$ is the bias limit of yaw moment related to the surge acceleration of the model. The bias limit is defined as

$$B_{\dot{v},M_Z} = \frac{\partial M_Z}{\partial \dot{v}}\varepsilon_{swayacc.} \approx \frac{\partial \tilde{M}_Z}{\partial \dot{v}}\varepsilon_{swayacc.} \tag{7.209}$$

$\tilde{M}_Z$ is given by expressions (7.203) to (7.205). $\varepsilon_{swayacc.}$ is the uncertainty of the sway acceleration, which equals $B_{\dot{v}}$ found in §7.3.15.

Yaw acceleration of the model

$B_{\dot{r},M_Z}$ is the bias limit of yaw moment related to the yaw acceleration of the model. The bias limit is defined as

$$B_{\dot{r},M_Z} = \frac{\partial M_Z}{\partial \dot{r}}\varepsilon_{yawacc.} \approx \frac{\partial \tilde{M}_Z}{\partial \dot{r}}\varepsilon_{yawacc.} \tag{7.210}$$

$\tilde{M}_Z$ is given by expressions (7.203) to (7.205). $\varepsilon_{yawacc.}$ is the uncertainty of the yaw acceleration, which equals $B_{\dot{r}}$ found in §7.3.15.

Time

B_{t,M_Z} is the bias limit of yaw moment related to the time at which the data is measured. The bias limit is defined as

$$B_{t,M_Z} = \frac{\partial M_Z}{\partial t}\varepsilon_t \tag{7.211}$$

The influence coefficient is determined by means of differentiation of the time series for M_Z with respect to time. $\varepsilon_t = 0.00063$ seconds is the uncertainty related to time.

7.4 Precision limits

The precision limits are assessed through repeated tests. The repeated tests have been mixed with the other tests of the matrix. According to (ITTC 1999a) the precision limit is estimated with:

$$P_{\bar{r}} = \frac{2S_{\bar{r}}}{\sqrt{M}} \tag{7.212}$$

where M is the number of repeats and the factor of 2 is applied for M>10. $S_{\bar{r}}$ is the standard deviation defined as

$$S_{\bar{r}} = \left[\sum_{1}^{M}\frac{(r_k - \bar{r})^2}{M-1}\right]^{1/2} \tag{7.213}$$

Here r_k is the value from each repeat test and $\bar{r}$ is the mean value of all the quantities from the repeated tests. $\bar{r}$ is thus defined as

$$\bar{r} = \frac{1}{M}\sum_{1}^{M} r_k \tag{7.214}$$

For the present application the focus is placed on the non-dimensional forces X', Y' and moment N' defined in equations (7.4) to (7.6). With $M = 12$ the following equations can be used for the three quantities.

7.4.1 Longitudinal force, X'

$$P_{\bar{X}} = \frac{2S_{\bar{X}}}{\sqrt{12}} \tag{7.215}$$

$$S_{\bar{X}} = \left[\sum_{1}^{12}\frac{(X'_k - \bar{X}')^2}{11}\right]^{1/2} \tag{7.216}$$

$$\overline{X}' = \frac{1}{12}\sum_{1}^{12} X'_k \tag{7.217}$$

7.4.2 Transverse force, Y'

$$P_{\overline{Y}} = \frac{2S_{\overline{Y}}}{\sqrt{12}} \tag{7.218}$$

$$S_{\overline{Y}} = \left[\sum_{1}^{12} \frac{\left(Y'_k - \overline{Y}'\right)^2}{11}\right]^{1/2} \tag{7.219}$$

$$\overline{Y}' = \frac{1}{12}\sum_{1}^{12} Y'_k \tag{7.220}$$

7.4.3 Yaw moment, N'

$$P_{\overline{N}} = \frac{2S_{\overline{N}}}{\sqrt{12}} \tag{7.221}$$

$$S_{\overline{N}} = \left[\sum_{1}^{12} \frac{\left(N'_k - \overline{N}'\right)^2}{11}\right]^{1/2} \tag{7.222}$$

$$\overline{N}' = \frac{1}{12}\sum_{1}^{12} N'_k \tag{7.223}$$

For the Static tests all the quantities in the expressions above are time averaged and are thus constant. But, in the dynamic tests, they are all varying in time. This mean that the expressions are being applied on time series data, averaged on a PMM period.

8 Discussion of test results

The results of the PMM tests are presented in the following pages. The results related to the static tests are shown in Appendix B, while that of the dynamic tests, which concern the uncertainty analysis, are shown in the Appendix C. At last the Appendix D takes back the remaining results of the dynamic tests.

8.1 Static tests

The static tests, which are pure drift tests, are conducted at three Froude Numbers, equal to 0.138, 0.280 and 0.410. The test matrix in Table A.1. 1, Table A.2. 1, Table A.3. 1 shows the angles considered. For the two first Froude numbers, the drift angle range is from –20 to 20 degrees, nevertheless at Froude 0.410; it was only possible to cover –12 to 12 degrees.
With respect to the precision limit part of the uncertainty analysis described earlier, the condition chosen for the repeatability is $\beta = 10°$, condition which is repeated 12 times at each speed to estimate the precision limits. The tables showed below (Table 8-1 to Table 8-3), give the bias limits related to the measured dimensional forces and moment. The bias limit is composed of two components: one from the accuracy of the drift angle setting, B_β, one from the accuracy of the force gauges used in the system $B_{cal\&acq}$ (see (7.152)).

Term	Fn=0.138	Fn=0.280	Fn=0.410
$B_{\beta,Fx}$ [N]	0.0344	0.3278	0.4016
$B_{cal\&acq,Fx}$ [N]	0.3785	0.3785	0.3785
$B_{F_{X_{measured}}} = B_{F_X}$ [N]	0.3801	0.5007	0.5519

Table 8-1 Summary of bias limit for the measured F_X at 10 degrees drift.

Term	Fn=0.138	Fn=0.280	Fn=0.410
B_{β,F_Y} [N]	0.998	4.4951	13.9588
$B_{cal\&acq,F_Y}$ [N]	0.2932	0.2932	0.2934
$B_{F_{Y_{measured}}} = B_{F_Y}$ [N]	1.0401	4.5047	13.9619

Table 8-2 Summary of bias limit for the measured F_Y at 10 degrees drift.

Term	Fn=0.138	Fn=0.280	Fn=0.410
B_{β,M_Z} [Nm]	2.1652	11.5149	33.3159
$B_{cal\&acq,M_Z}$ [Nm]	0.2894	0.4969	1.0764
$B_{M_{Z_{measured}}} = B_{M_Z}$ [Nm]	2.1845	11.5256	33.3333

Table 8-3 Summary of bias limit for the measured M_Z at 10 degrees drift.

The bias on the X-force is dominated to low speed from the contribution due to the calibration and acquisition while to increase by speed the error due to the drift angle setting prevails. The relative bias to the side force and the moment are instead widely dominates from the error due to the drift angle already to the lower speed.
Moving to non-dimensional quantities, Table 8-4 to Table 8-6 show the results of the uncertainty analysis for the non-dimensional forces and moments obtained for the considered speeds. In the Table 8-4 to Table 8-6 the first 5 rows show the bias related error sources. The next three rows show the total bias limit, the precision limit (based on the expressions from (7.10) to (7.12)) and finally the total uncertainty. Finally, the last two rows show the force or moment coefficients and the uncertainty in percent of the coefficients, respectively.
The total uncertainty on the hydrodynamic X' is altogether contained (less of 4%) and stretches quickly to decrease to increasing of the Froude. In particular, both the bias error and the precision index are small to the higher speeds and, large way, of the same order of magnitude. In detail on the

components of the bias of the X, one looks at as the dominant contribution is that data from the measured force that is reduced to growing of the speed in how much the lessening of the influence coefficient prevails on the increase of the bias of the X-force. To the higher speed the uncertainty on the immersion of the model and, in smaller measure, that one on the speed, become prevailing.
The total uncertainty on the hydrodynamic Y' is mainly constant even though it shows a little increase behaviour with the speed. Respect to the single components of the uncertainty, the bias error dominates on the precision limit, nonetheless as the speed increases the growing of the precision is much more large than the bias. As the X' case, the main component of the bias error is related to the measured force, but this time the value becomes higher with the velocity.
As far as the moment N', we notice that the error of Bias stretches to increase growing of the speed while the precision index remains enough stable. Altogether the not varied uncertainty total with the Froude. For the single contributions to the Bias limit they are worth the express considerations for Y'.

Term	Fn=0.138	Fn=0.280	Fn=0.410
$\theta^2_{F_{xmeasured}} B^2_{F_{xmeasured}}$	2.5119 10^{-7}	2.577 10^{-8}	6.8074 10^{-9}
$\theta^2_{\rho} B^2_{\rho}$	1.39 10^{-13}	1.7432 10^{-13}	3.9641 10^{-13}
$\theta^2_{Tm} B^2_{Tm}$	4.6273 10^{-9}	5.8032 10^{-9}	1.3197 10^{-8}
$\theta^2_{Lpp} B^2_{Lpp}$	3.4793 10^{-11}	4.3636 10^{-11}	9.9227 10^{-11}
$\theta^2_{U_C} B^2_{U_C}$	1.5332 10^{-9}	2.0292 10^{-9}	4.4614 10^{-9}
$B_{X'}$	0.00051	0.00018	0.00016
$P_{X'}$	0.00043	0.00019	0.00011
$U_{X'}$	0.00067	0.00026	0.00019
X'	0.0169	0.0189	0.0285
$U_{X'}$ in % X'	3.9	1.4	0.7

Table 8-4 Summary of uncertainties for X' from the static drift test, $\beta = 10^{\circ}$.

Term	Fn=0.138	Fn=0.280	Fn=0.410
$\theta^2_{F_{Ymeasured}} B^2_{F_{Ymeasured}}$	1.8813 10^{-6}	2.086 10^{-6}	4.3564 10^{-6}
$\theta^2_{\rho} B^2_{\rho}$	1.4888 10^{-12}	1.9125 10^{-12}	2.5137 10^{-12}
$\theta^2_{Tm} B^2_{Tm}$	4.9562 10^{-8}	6.3667 10^{-8}	8.368 10^{-8}
$\theta^2_{Lpp} B^2_{Lpp}$	3.7267 10^{-10}	4.7873 10^{-10}	6.292 10^{-10}
$\theta^2_{U_C} B^2_{U_C}$	1.6422 10^{-8}	2.2262 10^{-8}	2.829 10^{-8}
$B_{Y'}$	0.00140	0.00150	0.00210
$P_{Y'}$	0.00098	0.00144	0.00181
$U_{Y'}$	0.00171	0.00206	0.00278
Y'	0.0552	0.0626	0.0717
$U_{Y'}$ in % Y'	3.1	3.3	3.9

Table 8-5 Summary of uncertainties for Y' from the static drift test, $\beta = 10^{\circ}$.

Before the final discuss on the static tests, a pause has to be made to analyze the sinkage of the model, measured during the tests. According to the fact that the present analysis focus on the forces, no bias limit estimates are made for the sinkage. However, since the sinkage results are available for the static tests, the precision limits have been estimated. The results are estimated for three cases and are shown in Tables 8.1.7 and 8.1.8, where positive sinkage means that the draft increases.

Term	Fn=0.138	Fn=0.280	Fn=0.410
$\theta^2_{M_{Zmeasured}} B^2_{M_{Zmeasured}}$	2.5362 10^{-7}	4.1736 10^{-7}	7.5894 10^{-7}
$\theta^2_{\rho} B^2_{\rho}$	3.3379 10^{-13}	4.6534 10^{-13}	6.4242 10^{-13}
$\theta^2_{Tm} B^2_{Tm}$	1.1112 10^{-8}	5.8032 10^{-9}	2.1386 10^{-8}
$\theta^2_{Lpp} B^2_{Lpp}$	3.3421 10^{-10}	4.6592 10^{-10}	6.4323 10^{-10}
$\theta^2_{U_C} B^2_{U_C}$	3.6819 10^{-9}	5.4166 10^{-9}	7.2301 10^{-9}
$B_{N'}$	0.00052	0.00066	0.00089
$P_{N'}$	0.00040	0.00068	0.00052
$U_{N'}$	0.00065	0.00095	0.00103
N'	0.0261	0.0309	0.0363
$U_{N'}$ in % N'	2.5	3.1	2.8

Table 8-6 Summary of uncertainties for N' from the static drift test, $\beta = 10^{\circ}$.

Uncertainty	Fn=0.138	Fn=0.280	Fn=0.410
S_{FP} [m]	0.002	0.015	0.027
$P_{S_{FP}}$	0.00036	0.00029	0.00051
$P_{S_{FP}}$ in % of S_{FP}	18.0	1.9	1.8

Table 8-7 Sinkage at FP.

Uncertainty	Fn=0.138	Fn=0.280	Fn=0.410
S_{AP} [m]	-0.0007	-0.0043	0.0046
$P_{S_{AP}}$	0.00010	0.00008	0.00014
$P_{S_{AP}}$ in % of S_{AP}	14.0	1.8	3.1

Table 8-8 Sinkage at AP.

Finally, the results for the whole static tests are shown in Figure B. 1,Figure B. 2 and Figure B. 3. in Appendix B together with the error bands from the conditions described above. Observing the diagram up of Figure B. 1 that extension the course of the X' to varying of the drift angle, famous one light asymmetry. The cause of this could be due to the uncertainty total (if the bands to two opposite angles were overlapped), but since to increasing of the speed the band considerably stretches to reduce rendering impossible the superimposition, one can think that the asymmetry is due to geometric errors of construction of the model not considered in the present analysis of uncertainty. Figure B. 1 low shows, always in function of the drift angle, the course of the Y',

analogous for N' in Figure B. 2. The behavior of the curves, linear around to the 0 and not linear ones for increasing angles, appears corrected. Finally Figure B. 3 shows the courses of the sinkage ahead and behind the model (FP and AP respectively). To low speed the order variations are small. These stretch quickly to increase already to medium speed and still more to high speed. It is interesting to observe that to high speed the breast to small angles of drift reassumes next values to those of the lower speed.

8.2 Dynamic tests (Pure Yaw)

According to the test program in Appendix A, the PMM test covers a number of pure yaw conditions. Nevertheless, only one condition, $r' = 0.3$, at each of the Froude numbers 0.138, 0.280 and 0.410 are considered for uncertainty assessment. The three cases are marked with a * in the test matrix. The results are presented in the Appendix C. The time series for the remaining tests are plotted in C.6.

Starting with the results in C.1, the section is subdivided into four subsections. Section C.1.1 shows the time series over one period for all the motion parameters, i.e. the heading, the velocities and the accelerations plus the uncertainty components related to these quantities. Section C.1.2 shows the measured and the non-dimensionalized *X*-force plus the uncertainty contributions from the error sources described earlier in the report. Sections C.1.3 and C.1.4 do the same, but instead of the *X*-force they show the *Y*-force and the yaw moment, respectively. In connection with the presented data two things should be noted:

1. When the term "measured" is used for the forces and moments it means the quantity as measured at the gauge, i.e. it is the quantity, which goes into the data reduction equations, which again means that it consists of both hydrodynamic and inertial contributions.
2. The heading, the velocities, the accelerations values are all mean values based on the average of the 12 repeat tests. This means that the plotted value at some time t_0 is obtained as the average of 12 values, which are taken out of the time series at t_0.

The heading ψ is shown in **Error! Reference source not found.** (left side) together with the uncertainty band representing $B_{heading}$. If the error composition is studied closer (right side), one notes that the dominating source originates from the uncertainty B_{β_head} in the drift angle, i.e. the errors related to the setting of the drift angle on the PMM and the alignment of the model.

The transverse PMM velocity v_{PMM} is shown in Figure C.1.1.2 (left side) together with the total uncertainty band ε_{vpmm}. Looking at the right side of the figure one can note that there is no dominating error source since the errors are of approximately the same size. Though, it should be noted, that the contribution from the PMM oscillations B_{ω_vpmm} tend to become stronger throughout the period.

The sway velocity v is shown in Figure C.1.1.3 (left side) together with the total uncertainty band B_v. Ideally, v should be zero for pure yaw during the whole PMM cycle. However, due the motion law imposed to the PMM which is pure sine in our case instead of an arctan, v is slightly different from zero. In any case, v is included in the reduction equations and so its contribution is considered in the inertial forces. Respect to the bias components, it is clear from the right side of the figure that B_{ψ_v} dominates. Recalling the drift angle dominated result of ψ it therefore turns out that v to a certain degree is dominated by the uncertainty related to the drift angle.

The transverse PMM acceleration $\dot{v}_{PMM}$ is shown in Figure C.1.1.4 (left side) together with the total uncertainty $\varepsilon_{vpmmdot}$. Analyzing the components, we can observe that are all of the same magnitude (right side). Again, as was the case for v_{PMM}, the contribution which depends by the frequency, $B_{\omega_vpmmdot}$, increases in the second part of the period.

The sway acceleration $\dot{v}$ is shown in Figure C.1.1.5 (left side) together with the total uncertainty B_{vdot}. Ideally $\dot{v}$ must be always zero as v. The effects of the measured $\dot{v}$ are taken in account in the reduction equations to determine the hydrodynamic forces. Between the single components of the total uncertainty, B_{r_vdot} is the largest (right side). As ψ has the prevalent role on the uncertainty of the v, here r has the prevalent role for $\dot{v}$.

The yaw rate r is shown in Figure C.1.1.6 (left side) together with the total uncertainty B_r.Between the contributions to the error total that due to the maximum angle, $B_{\psi\max_r}$, prevails whose effect is greater in correspondence to the maximum amplitudes of the motion. Also here, as for the previous cases (v_{PMM} and $\dot{v}_{PMM}$) we have the error which had to the frequency that grows during the period (B_{ω_r} in the right side of the figure).

The yaw acceleration $\dot{r}$ is shown in Figure C.1.1.7 (left side) together with the total uncertainty B_{rdot}. Both for the factors that determine the error total, than for the course of the member who depends on the frequency is worth considerations similar to those described for the case of r.

The surge velocity u is shown in Figure C.1.1.8 (left side) together with the total uncertainty B_u. u is variable when it would have ideally to be null. This why the motion of pure "yaw" is obtained to constant speed of the carriage, it is logical therefore to expect (right part of the figure) that the term of main error is that induced from the speed of the carriage (B_{Uc_u}).

Finally, the surge acceleration $\dot{u}$ is shown in Figure C.1.1.9 (left side) together with the total uncertainty B_{udot}. Observing the various contributions to the uncertainty to the total bias, one looks at as it does not come considered that relative one to the acceleration of the carriage. For the rest, the bias widely it is dominated from the errors induced from the transverse speed and the acceleration of the PMM (right side of the figure).

The next quantity is the longitudinal force, for which the bias limit contributions related to the measured force F_X and to the non-dimensional force coefficient X' are described in §7.3.18 and §7.2.1, respectively.

Figure C.1.2.1 show the total uncertainty of F_X plus all the individual bias limit contributions. Widely dominant is the contribution which had to the uncertainty of the calibration, acquisition and conversion of signal measured from the force transducers (B_{cac_Fx}). Towards the end of the cycle it is only appreciable, even if altogether still negligible, the contribution which had to the longitudinal acceleration of the model (B_{udot_Fx}). Finally, Figure C.1.2.3 (left side) shows F_X together with the uncertainty band given by B_{Fx}.

With respect to the non-dimensional X-force X', Figure C.1.2.2 shows all the individual contributions to the uncertainty $U_{X'}$ of X'. Various they are the terms that influence the total bias of the hydrodynamic resistance: those determined from the uncertainty on the longitudinal velocity and acceleration (u and $\dot{u}$), on the transverse velocity v, on the F_X measured, on the draft (T_m) and on the transverse position of the centre gravity (Y_G). Finally, Figure C.1.2.3 (right side) summarizes the results. It shows X' together with the bias and precision limits and the total uncertainty. The precision limit is quite small, which indicates a good repeatability of the measurements. The result is that the total uncertainty mainly consists of bias error.

Concerning the transverse Y-force the bias limit contributions related to the measured force F_Y and to the non-dimensional force coefficient Y' are described in §7.3.19 and §7.2.2, respectively. Figure C.1.3.1 show the total uncertainty of F_Y plus all the individual bias limit contributions. The prevailing contributions to the "bias" error have had to the velocity and to the acceleration of the "yaw" motion (B_{r_Fy} and B_{rdot_Fy}) and in part to the calibration, acquisition and conversion of the measured side force from the gauges (B_{cac_Fy}). The incidence of this uncertainty on that total is smaller regarding the case of the longitudinal force (probably why, in this, the measured medium values are larger). Finally, Figure C.1.3.3 (left side) summarizes the results by showing F_Y together with the uncertainty band given by B_{Fy}.
With respect to the non-dimensional Y-force Y', Figure C.1.3.2 shows all the individual contributions to the uncertainty $U_{Y'}$ of Y'. They are the three factors of more important errors that they influence the measure of the lateral hydrodynamic force: those due to the uncertainty on the angular velocity (r), the lateral acceleration ($\dot{v}$) and the measured force (F_Y). By tracing the sources of errors one looks at as the all three factors listed are strongly conditioned from the uncertainty on the maximum angle of "yaw" fixed during the motion. This can therefore be thought the root cause of error in the measures of the side force Y'. Finally, Figure C.1.3.3 (right side) shows Y' together with the bias and precision limits and the total uncertainty. This time, to difference of the case for X', we notice that the precision index influences the band of error more of the bias error (for how much the two quantity are, large way, of the same order of magnitude). The cause of this worse accuracy in the repeatability tests seems to have had to the greater importance that it covers for Y' rather than for X' the uncertainty on the maximum angle of yaw.
The final quantities to be discussed, covers the yaw moment. However, based on Figure C.1.4.1 it turns out that the behavior of the bias limit related to the measured yaw moment M_Z is similar to the behavior of B_{Fy}. The thing is logical if we think that the measured moment is obtained like combination of the measured side forces. In the case of the single part hydrodynamic N', we observe (Figure C.1.4.2) that the role of the uncertainty on the moment measured and that one on the moment of inertia of the model are dominant. Finally, Figure C.1.4.3 (right side) shows N' together with the bias and precision limits and the total uncertainty. The index of precision is small in all the cycle and confirms one good degree of repeatability.

The two remaining cases of "pure yaw" to Fr=0.138 and Fr=0.410 are illustrated respectively from sections C.4.1 to C.4.4 and sections C.5.1 to C.5.4. Similar considerations to those made for the case to Fr=0.280 can be repeated. To great lines, the sources of errors that determine the uncertainties on the forces and the moments for the cases to higher and lower speed are still the same ones.

In connection with the static test results the uncertainties were expressed as percentages of the considered force or moment, but with the time varying and zero crossing forces this will lead to percentages which vary from a finite value to infinity throughout the period. Therefore, in order to take out some values which can be used for a quantitative comparison between the three conditions, the value at maximum yaw rate will be used.

	Fr=0.138	Fr=0.280	Fr=0.410
r_{max} [rad/s]	0.055	0.111	0.160
B_{F_X} [N]	0.381	0.397	0.404
F_X [N]	-11.074	-49.587	-155.83

B_{F_X} in % of F_X [%]	3.4	0.8	0.3
$B_{X'}$ [--]	0.00053	0.00019	0.00017
$P_{X'}$ [--]	0.00029	0.00018	0.00011
$U_{X'}$ [--]	0.00060	0.00027	0.00020
X' [--]	-0.01450	-0.01580	-0.02330
$U_{X'}$ in % of X' [%]	4.2	1.7	0.9

Table 8-9 Uncertainties and bias limits related to the X-force, where r = r_{max}.

Table 8-9 shows the data for the X-force and the related uncertainties. The bias limit of the measured force grows with the speed but it remains much small per cent. In this way the uncertainty on the part hydrodynamics, that it is influenced mostly from the contribution of the bias, decreases quickly with the speed.
Table 8-10 shows the data for the Y-force and the related uncertainties. B_{F_Y} grows with the speed but it remains per cent stable. Observing the course of the uncertainty total on the part hydrodynamics, famous as mostly it is influenced from the bias, above all to high Froude. This uncertainty generates elevates values percentages, in particular to low Froude. This great difference between the values percentages of the error on the measured force and the force hydrodynamics is explained noticing like, to difference of the case of the resistance (X'), the hydrodynamics part of the side force is one fraction the much smallest one of the total.

	Fr=0.138	Fr=0.280	Fr=0.410
r_{max} [rad/s]	0.055	0.111	0.160
B_{F_Y} [N]	0.501	1.686	5.204
F_Y [N]	-39.165	-186.73	-393.21
B_{F_Y} in % of F_Y [%]	1.3	0.9	1.3
$B_{Y'}$ [--]	0.00095	0.00080	0.00110
$P_{Y'}$ [--]	0.00062	0.00033	0.00044
$U_{Y'}$ [--]	0.00110	0.00087	0.00110
Y' [--]	-0.01110	-0.01880	-0.01830
$U_{Y'}$ in % of Y' [%]	10.3	4.6	6.2

Table 8-10 Uncertainties and bias limits related to the Y-force, where r = r_{max}.

Table 8-11 shows the data for the yaw moment and the related uncertainties. The considerations on the moment bias limit are much similar to those made for the side force. An interesting difference is found in the composition of the uncertainty total on the hydrodynamic moment. Here, to difference of the other cases, the contribution of the bias limit is quite comparable with the precision index. To the lower speed the effect of the precision index prevails while the inverse succeed to the higher speed.

	Fr=0.138	Fr=0.280	Fr=0.410
r_{max} [rad/s]	0.055	0.111	0.160
B_{M_Z} [N]	0.690	2.672	10.17
M_Z [N]	-49.790	-280.74	-790.51

B_{M_Z} in % of M_Z [%]	1.4	1.0	1.3
$B_{N'}$ [--]	0.00018	0.00017	0.00029
$P_{N'}$ [--]	0.00025	0.00014	0.00023
$U_{N'}$ [--]	0.00031	0.00022	0.00037
N' [--]	-0.01170	-0.01590	-0.02090
$U_{N'}$ in % of N' [%]	2.6	1.4	1.8

Table 8-11 Uncertainties and bias limits related to the yaw moment, where r = r_{max}.

8.3 Dynamic tests (Pure Sway)

According to Appendix A, the PMM test covers three pure sway conditions at the Froude number 0.280. One of them is considered for uncertainty assessment, which means that it is repeated twelve times in order to be able to estimate the precision limits. The condition is marked with "*" in the test program. The discussion of the results will be focused on the uncertainty assessment case, which is presented in section C.2 in Appendix C. The time series for the remaining conditions are plotted in C.6.

The heading ψ is shown in Figure C.2.1.1(left side) together with the uncertainty band representing $B_{heading}$. As was the case for pure yaw, if the error composition is studied closer (right side), one notes that the dominating source originates from the uncertainty B_{β_head} in the drift angle, i.e. the errors related to the setting of the drift angle on the PMM and the alignment of the model. This band of amplitude comes modulated from the action produced from bias of the route angle B_{ψ_head}.
The transverse PMM velocity v_{PMM} is shown in Figure C.2.1.2 (left side) together with the total uncertainty band ε_{vpmm}. As was the case for pure yaw, looking at the right side of the figure one can note that there is no dominating error source since the errors are of approximately the same size. Though, it should be noted, that the contribution from the PMM oscillations B_{ω_vpmm} tend to become stronger throughout the period.
The sway velocity v is shown in Figure C.2.1.3 (left side) together with the total uncertainty band B_v. In this case, v is different from zero. Respect to the bias components, it is clear from the right side of the figure that B_{ψ_v} dominates. Recalling the drift angle dominated result of ψ it therefore turns out that v to a certain degree is dominated by the uncertainty related to the yaw angle.
The transverse PMM acceleration $\dot{v}_{PMM}$ is shown in Figure C.2.1.4 (left side) together with the total uncertainty $B_{vpmmdot}$. Analyzing the components, we can observe that are all of the same magnitude (right side). Again, as was the case for v_{PMM}, the contribution which depends by the frequency, $B_{\omega_vpmmdot}$, increases in the second part of the period.
The sway acceleration $\dot{v}$ is shown in Figure C.2.1.5(left side) together with the total uncertainty B_{vdot}. As a pure sway motion is investigated, $\dot{v}$ is no longer zero. The effects of the measured $\dot{v}$ are taken in account in the reduction equations to determine the hydrodynamic forces. Between the single components of the total uncertainty, B_{r_vdot} is the largest (right side). As ψ has the prevalent role on the uncertainty of the v, here r has the prevalent role for $\dot{v}$. The tendency of the uncertainty to grow in the period is due to the contribution given from the error on $B_{vpmmdot_vdot}$.

The yaw rate r, which is zero for pure sway, is shown in Figure C.2.1.6 (left side) together with the total uncertainty B_r. The only one bias limit that it affects the uncertainty is that related to $B_{\psi \max_r}$.
The yaw acceleration $\dot{r}$, which is obviously zero, is shown in Figure C.2.1.7 (left side) together with the total uncertainty B_{rdot}. Regard to the total uncertainty they are worth the same considerations exposed for r.
The surge velocity u, which for pure sway equals the carriage speed, is shown in Figure C.2.1.8 (left side) together with the total uncertainty B_u. The value measured for u has almost constant trend in all the period, its uncertainty band comes determined, of fact, from the uncertainty on the speed of the carriage, B_{Uc_u} (right side of the figure) and only in marginal way (modulation of the band of error) from the angle of yaw, B_{ψ_u}.
Finally, the surge acceleration $\dot{u}$ is shown in Figure C.2.1.9 (left side) together with the total uncertainty B_{udot}. The uncertainty total (right side of the figure) is determined, fundamentally, from the uncertainty on the angle of yaw (heading). Also, like for the pure yaw case, it is here well to emphasize that it has not been taken in account the contribution of the error on the carriage acceleration (considered null) during the analysis.

The next quantity is the longitudinal force, for which the bias limit contributions related to the measured force F_X and to the non-dimensional force coefficient X' are described in §7.3.18 and §7.2.1, respectively.
Figure C.2.2.1 show the total uncertainty of F_X plus all the individual bias limit contributions. From the figure it is seen that the uncertainty mainly consists of the contribution from the calibration, acquisition and conversion of signal measured from the force transducers (B_{cac_Fx}). Finally, Figure C.2.2.3 (left side) shows F_X together with the uncertainty band given by B_{Fx}.
With respect to the non-dimensional X-force X', Figure C.2.2.2 shows all the individual contributions to the uncertainty $U_{X'}$ of X'. The total uncertainty mainly turns out determined from the error on the force measured and from the error on the longitudinal acceleration ($\dot{u}$). Holding account of the determining factors on the uncertainty of these two last quantities, we can conclude that the uncertainty on the heading and the chain of acquisition are the main causes of uncertainty on the hydrodynamic transverse force. The Figure C.2.2.3 shows the course in the period of the force and looks at as, in the complex, the error band total (precision index and bias limit) is small.
Concerning the transverse Y-force the bias limit contributions related to the measured force F_Y and to the non-dimensional force coefficient Y' are described in §7.3.19 and §7.2.2, respectively. Figure C.2.3.1 show the total uncertainty of F_Y plus all the individual bias limit contributions. F_Y, contrarily to F_X, does not depend as well as on B_{cac_Fy} how much on the v and $\dot{v}$. Taking in account that the uncertainties on these two variable ones are legacy to the heading angle and the frequency of the sway motion, we can conclude that these two quantities are the main sources on the uncertainty for the measured force. Finally, Figure C.2.3.3 (left side) summarizes the results by showing F_Y together with the uncertainty band given by B_{Fy}.
With respect to the non-dimensional Y-force Y', Figure C.2.3.2 shows all the individual contributions to the uncertainty $U_{Y'}$ of Y'. The uncertainty on the Y' is determined nearly integrally from the contribution of the uncertainty on the measured force F_Y and therefore, resuming the appraisals as soon as made, the uncertainty on the frequency of the PMM and the angle of route is the sources of errors for Y'. Finally, Figure C.2.3.3 (right side) shows Y' together with the bias and precision limits and the total uncertainty. The total uncertainty in the entire period is smaller regarding the case of X' and it evidences altogether a good repeatability.

The final quantities to be discussed, covers the yaw moment. However, based on Figure C.2.4.1 it turns out that the behavior of the bias limit related to the measured yaw moment M_Z is similar to the behavior of B_{Fy}. The thing is logical if we think that the measured moment is obtained like combination of the measured transverse forces. In the case of the single part hydrodynamic N', we observe (Figure C.2.4.2) that the role of the uncertainty on the moment measured is dominant. Finally, Figure C.2.4.3 (right side) shows N' together with the bias and precision limits and the total uncertainty.

	Fr=0.280
$v_{\max}$ [rad/s]	0.366
B_{F_X} [N]	0.379
F_X [N]	-53.108
B_{F_X} in % of F_X [%]	0.7
$B_{X'}$ [--]	0.00014
$P_{X'}$ [--]	0.00015
$U_{X'}$ [--]	0.00021
X' [--]	-0.01650
$U_{X'}$ in % of X' [%]	1.3

Table 8-12 Uncertainties and bias limits related to the X-force, where v = v_{max}.

	Fr=0.280
$v_{\max}$ [rad/s]	0.366
B_{F_Y} [N]	3.151
F_Y [N]	-207.49
B_{F_Y} in % of F_Y [%]	1.5
$B_{Y'}$ [--]	0.00110
$P_{Y'}$ [--]	0.00079
$U_{Y'}$ [--]	0.00130
Y' [--]	-0.0645
$U_{Y'}$ in % of Y' [%]	2.1

Table 8-13 Uncertainties and bias limits related to the Y-force, where v = v_{max}.

	Fr=0.280
$v_{\max}$ [rad/s]	0.366
B_{M_Z} [N]	8.862
M_Z [N]	-614.92
B_{M_Z} in % of M_Z [%]	1.4
$B_{N'}$ [--]	0.00051
$P_{N'}$ [--]	0.00031
$U_{N'}$ [--]	0.00060

N' [--]	-0.0335
$U_{N'}$ in % of N' [%]	1.8

Table 8-14 Uncertainties and bias limits related to the yaw moment, where v = v_{max}.

In connection with the pure yaw results above data was extracted at characteristic conditions in order to find data, which could be used for a quantitative study. In the case of the pure yaw we had taken in consideration the point of the cycle in which the angular velocity it is maximum, analogous for the case of pure sway we focus the attention on the point in which the cross-sectional speed is maximum, i.e. $v = v_{\max}$.

The analysis of the three tables (Table 8-13 to Table 8-14) evidences that for the X-force and the yaw moment the results are similar to the case of pure yaw at the same Froude. In truth, the values of the uncertainties for the moment are here larger in absolute terms, but they return to be comparable if being referred to the value of the measured moment. Various the things for the Y-force. Here the values of the bias limit and the index of precision are proportionally more small regarding the case of pure yaw. The relative error on the measure of the hydrodynamics part nearly turns out halved. The reason of this is in the fact that, this time, the percentage ratio of the part hydrodynamics regarding the measured total force is the much largest one (in fact if we go to see the error on the measured force we notice that this is quite increased regarding the case of pure yaw).

8.4 Dynamic test (Yaw and drift)

The finale test type covers the yaw and drift test shown in the test program in Appendix A. Three yaw and drift tests are conducted at the Froude number 0.280 and one of them are considered for uncertainty assessment, i.e. it s repeated twelve times in order to estimate the precision limits. The condition is marked with "*" in the test program. The discussion of the results will be focused on the uncertainty assessment case, which is presented in section C.3 in Appendix C. The time series for the remaining conditions are plotted in C.6.

The similarity between the case of yaw and drift with that one of pure yaw is easy intuitable. In this case in fact we will have consequently a static drift angle various from zero and therefore a cross-sectional speed ($v = \sin\beta$) different from zero. From this, the analysis of the cinematic quantities and the relative uncertainties is leaded again to that one made for the case of pure yaw.

Figure C.3.2.1 show the total uncertainty of F_X plus all the individual bias limit contributions. The comparison with pure yaw shows that we have here a larger uncertainty on the measured force because of a greater contribution of the bias limit of B_{v_Fx} and B_{vdot_Fx} The Figure C.3.2.2 shows that the various contributions to the uncertainty total of the hydrodynamics force repeat the courses of the pure yaw one. Only θB_{T_m} is slightly emphasized. We can say, therefore, that the measure of the resistance, in the case of yaw and drift, is only little more sensitive to the error on the heading angle and on the PMM frequency (i.e. they influence v and v_{pmm} and, through these, B_{F_X}).

Concerning the transverse Y-force the bias limit contributions related to the measured force F_Y and to the non-dimensional force coefficient Y' are described in §7.3.19 and §7.2.2, respectively. Figure C.3.3.1 show the total uncertainty of F_Y plus all the individual bias limit contributions. They are the three factors that mainly influence the error on F_Y : in the first place $B_{r_F_y}$ and $B_{rdot_F_y}$ then,

but in smaller measure, $B_{cac_F_y}$. From the cinematic analysis it emerges that the error on $B_{r_F_y}$ and $B_{rdot_F_y}$ is determined mainly from the uncertainty on the route angle (ψ). The examination of the Figure C.3.3.2 reveals to us that F_Y assumes greater importance in the uncertainty of the hydrodynamic part regarding the case of pure yaw. On the base of the observations made for F_Y then we can conclude that the uncertainty on the heading angle has a crucial role here.
Finally, Figure C.3.3.3 (right side) shows Y' together with the bias and precision limits and the total uncertainty. The total uncertainty in the entire period is smaller regarding the case of X' and it evidences altogether a good repeatability.

The final quantities to be discussed, covers the yaw moment (Figure C.3.4.1). The bias limit of the measured moment it is in the case of "yaw and drift" much largest one regarding the case "pure yaw" (approximately 4 times). This why the importance of $B_{v_M_z}$ grows enormously. Considering (see Figure C.3.4.2) that the error on N' is more sensitive to the contribution of M_Z (analogous to how much as soon as seen for Y') we can repeat the same conclusion deducted for the transverse force: the importance of the heading angle uncertainty is emphasized in the case of "yaw and drift".

The characteristic condition chosen for “yaw and drift” in order to find data, which can be used for a quantitative study, is the same as for pure yaw, i.e. at the maximum yaw rate, $r = r_{\max}$. During the PMM cycle, there are two positions, where the yaw rate has a maximum, but due to the preset drift angle, they are different. The situation where the model points into the turn is the most realistic seen from a manoeuvring point of view.

	Fr=0.280
$r_{\max}$ [rad/s]	0.111
B_{F_X} [N]	0.464
F_X [N]	-102.22
B_{F_X} in % of F_X [%]	0.5
$B_{X'}$ [--]	0.00026
$P_{X'}$ [--]	0.00018
$U_{X'}$ [--]	0.00032
X' [--]	-0.0255
$U_{X'}$ in % of X' [%]	1.3

Table 8-15 Uncertainties and bias limits related to the X-force, where r = r_{max}.

	Fr=0.280
$r_{\max}$ [rad/s]	0.111
B_{F_Y} [N]	3.873
F_Y [N]	20.312
B_{F_Y} in % of F_Y [%]	19.1
$B_{Y'}$ [--]	0.00140
$P_{Y'}$ [--]	0.00083
$U_{Y'}$ [--]	0.00160

Y' [--]	0.0469
$U_{Y'}$ in % of Y' [%]	3.5

Table 8-16 Uncertainties and bias limits related to the Y-force, where r = r_{max}.

The analysis of the three tables (Table 8-15 to Table 8-17) shows that the bias limits and the precision indices are larger than that one estimated for the case "pure yaw".(once and half for the X', 2 times for the Y' and 2,5 times for N'). Also the precision index gets worse. The effects on the total uncertainty for the hydrodynamics part are that U_X and U_Y are relatively more small (because of the greater incidence percentage of the resistance hydrodynamics and the transverse force on the total measured one from the transducers) while remarkably grows the uncertainty percentage of the moment.

	Fr=0.280
r_{max} [rad/s]	0.111
B_{M_Z} [N]	8.487
M_Z [N]	241.93
B_{M_Z} in % of M_Z [%]	3.5
$B_{N'}$ [--]	0.00048
$P_{N'}$ [--]	0.00036
$U_{N'}$ [--]	0.00060
N' [--]	0.0135
$U_{N'}$ in % of N' [%]	4.4

Table 8-17 Uncertainties and bias limits related to the yaw moment, where r = r_{max}.

9 Conclusion

In the present report the uncertainty analysis has been carried out for PMM test and it has been applied on three static and five dynamic test cases on INSEAN model C.2340.
Three static tests have been considered in correspondence to pure drift condition at different Froude numbers: *Fr = 0.138* and *Fr = 0.410*. Five dynamic test cases reproduce pure yaw at three different conditions (*Fr = 0.138 Fr = 0.280* and *Fr = 0.410*), pure sway at one condition (*Fr = 0.280*) and yaw with drift at one condition (*Fr = 0.280*).
The analytical development are focused on the X and Y forces and on the yaw moment (N) based on a set of traditional reduction equation for manoeuvrability. The uncertainty assessment, as usual, covers the estimates of the bias limit error sources (the part of the global error that can be not treated with statistic) and the precision limit error sources (the part of the global error that can be treated with statistic).
The first component is determined on the basis of an accurate study on the test equipment respect to the all possible systematic error sources, while the second component is determined on the basis of repeated tests.
The following conclusion and consideration are now possible:

(I) For both static and dynamic test cases, the precision limit is quite good, stable between static and dynamic test type and comparable with bias limit in magnitude although slightly small than the bias itself.

(II) In the static tests for the non-dimensional forces X', Y' and N', the total bias is dominated by the error in the measured forces compared to the error due to water density, draft, Lpp and the carriage velocity. The minimum difference between these two sets of error sources is of $O(10^{-2})$.
Going into the measured forces bias errors components it has been shown that in the X' force the bias depending by the accuracy of the drift angle setting increases with the velocity. Further for higher speeds it becomes slightly greater than the bias related to the data acquisition and calibration that is, instead, constant respect to the velocity. The Y' force and yaw moment N' components present the same trend as for the X' force for the bias error that depends on the drift angle accuracy but, in a much more evident way; in this case the drift angle setting error dominates clearly respect to the data acquisition and calibration bias error.
Respect to the total uncertainty it has been shown that the error decrease with increasing the velocity for the X' force. For the Y' force and yaw moment there is not this trend with the velocity and the bias and precision limits are of the same order of magnitude.
The bias limit is dominated, however, by the accuracy of drift angle setting and a special attention should be paid to this operation. Furthermore a transducer with a lower full scale value should be used for the tests that have to be carried out at lower speed in order to reduce the total uncertainty in that condition.

(III) In the pure yaw test cases for the X' force component the total uncertainty is very low in magnitude and it is decreasing with the velocity increasing. The precision limit is quite small and for X' the error is dominated by the bias; this circumstance demonstrate the very good repeatability of the experiment. The bias error is the combination of many different cinematic and dynamic parameters and those that are greater are related to the F_X (thus to drift angle, acquisition and calibration biases) and related to the surge velocity. For the Y' force the bias and precision are of the same order of magnitude but differently to the X' case this time the precision limit influences the measure in a more significant way although the magnitude of the precision error is same as for X' case. For the yaw moment N' similar consideration as Y' can be stated for the magnitude of the errors sources but in this case the behaviour of the precision limit shows a very good repeatability of the experiment. The percentage error, finally, is decreasing with the velocity increasing. The greater error source for these two quantities is detectable in the setting of the yaw angle at the beginning of the pure yaw experiment. It should be notice, comparing the absolute values of the X', Y' and N' with the values measured in the static tests, that the percentage errors seems to be higher in pure yaw case due to the inertial contribution to the force that in the dynamic case has been subtracted from the total force; in such way the total uncertainty it is in relation only with the hydrodynamic force that is lower in the dynamic case.
Based on the above consideration we can stated the following consideration:

- the hydrodynamic forces are lower than in the static test case and the percentage error can became relevant at low speed;
- the total uncertainty is small if related to the measured force but can be relevant at low speed if compared with the hydrodynamic force;
- major error components come from the setting of the drift angle (for X', Y' and N') and from the surge velocity (for X').

(IV) In the case of sway test, as for the pure yaw, the errors that dominate are the ones on measured forces, sway velocity and acceleration and in a less significant amount on surge velocity. The X' force uncertainty is dominated by the error on measured force; in

particular on the bias related to the data acquisition calibration and conversion and on the bias related to the drift angle setting. The total error is globally small. The total uncertainty on Y' force does not depend on the bias acquisition, calibration and conversion as X' depends but it is dominated by sway velocity and acceleration and thus it is dominated by the drift angle setting and by the sway frequency. Similar considerations can be done for the yaw moment N'. Respect to the pure yaw case here the hydrodynamic force is much more high and similar in magnitude at the static tests and this is the main reason for a percentage error lower respect to the yaw case. In order to reduce the total uncertainty action must be done mostly on the drift angle setting.

(V) The last tests case is the dynamic yaw with drift. As for the pure yaw case, the uncertainty is dominated by the heading angle i.e. by the drift angle setting and by the test frequency for the hydrodynamic resistance. For the lateral force Y' and for the yaw moment N' the main contribution to the total uncertainty is due to the yaw rate and yaw acceleration i.e. to drift angle setting. A very good repeatability of the experiment is evident from the precision limit values. Respect to the pure yaw case both the bias limit and the precision limit increase in absolute value but the effect of the total uncertainty is reduced by the increasing of the hydrodynamic forces. In a more evident way for the present case seems to be crucial the quality of the initial drift angle setting.

The following final consideration can be done:

- the level of total uncertainty is widely good both for dynamic and static test cases although at low speed the percentage error can be in some test condition bigger than in the higher velocity cases;
- the uncertainty is generally dominated by the drift angle setting, by the surge velocity and by the calibration and acquisition bias error source;
- all the other geometric (*Lpp, Tm*, etc.), cinematic (*u, v, r,* etc.) and dynamic (mass and inertia) parameters are not so relevant in the bias error composition;
- the repeatability is quite good and generally lower in absolute value respect bias error.

10 Future works

The results obtained by the uncertainty assessment on the PMM tests suggest the future investigations:

(1) to develop a new set of transducers of a lower full scale value in order to improve the quality of the measure at the low speed test;
(2) to modify the law of the forced yaw motion in order to get a pure harmonic motion and to reduce consequently (although in a non-decisive amount) the total uncertainty;
(3) to introduce the roll degree of freedom and extend the uncertainty assessment to the heel angle and also to the roll force;
(4) to extend the uncertainty assessment to the traditional hydrodynamic coefficients studying the effect of the error on the hydrodynamic derivatives.

11 Acknowledgement

This work has been carried out under the Naval Hydrodynamics Research Program sponsored by the Ministry of Infrastructure and Transportation and within the framework of the activities of the 24th ITTC Manoeuvrability Committee.

References

Simonsen, C. D.
"ONR II 187 01 PMM model test with DDG51 including uncertainty assessment",
Force Technology, Lyngby, Denmark, 2004.

Barr, R. A.
"Some notes on conduct of LAHPMM (Planar Motion Mechanism) tests",
Technical note 2109-1 Hydronautics Research, Inc., Gaithersburg, MD U.S. 2001

Appendix A Test programs

In the present appendix the test matrices used for the various tests are listed. The nomenclature, what has been used, is the same adopted in the report. The only difference regards the maximum value of the speed and acceleration of the motions of yaw and sway which are given in non-dimensional form. In particular, they have been non-dimensionalized through the following relations: $r'_{\max} = r_{\max} L_{pp}/U$, $v'_{\max} = v_{\max}/U$, $\dot{r}'_{\max} = \dot{r}_{\max} (L_{pp}/U)^2$, $\dot{v}'_{\max} = \dot{v}'_{\max} L_{pp}/U^2$.

In the last column of the tables of the dynamic tests a "RunID" abbreviation which corresponds to the time history taken back in Appendix D is suitable.

A.1 *Approach speed, Fn = 0.138*

Froude number, Fn [-]	Carriage speed, U_C [m/s]	Drift angle, β [deg.]
0.138	1.755	-20, -16, -12, -11, -10, -9, -6, -2, 0, 20 , 16, 12, 11, 10*,9 ,6 ,2

Table A.1. 1 Test program for the static tests. "*" Indicates the test, for which uncertainty analysis is conducted.

Fn [-]	U_C [m/s]	β [deg.]	$r'_{\max}$	$\dot{r}'_{\max}$	S_{mm} [m]	fr [Hz]	Θ_{max} [deg.]	*No. of repeat.*	Run ID
0.138	1.034	0	0.050	0.097	0.077	0.056	1.5	1	Yaw_138_1
0.138	1.034	0	0.150	0.291	0.227	0.056	4.4	1	Yaw_138_2
0.138	1.034	0	0.300	0.581	0.458	0.056	8.9	12*	Yaw_138_3
0.138	1.034	0	0.450	0.872	0.685	0.056	13.3	1	Yaw_138_4
0.138	1.034	0	0.600	1.293	0.741	0.062	16	1	Yaw_138_5
0.138	1.034	0	0.750	1.817	0.729	0.070	17.7	1	Yaw_138_6

Table A.1. 2 Test program for the dynamic pure yaw test. "*" Indicates the test, for which uncertainty analysis is conducted.

A.2 *Approach speed, Fn = 0.280*

Froude number, Fn [-]	Carriage speed, U_C [m/s]	Drift angle, β [deg.]
0.280	1.755	-20, -16, -12, -11, -10, -9, -6, -2, 0, 20 , 16, 12, 11, 10*,9 ,6 ,2

Table A.2. 1 Test program for the static test. "*" Indicates condition, for which , for which uncertainty analysis is conducted.

Fn [-]	U_C [m/s]	β [deg.]	v'_{max}	$\dot{v}'_{max}$	S_{mm} [m]	fr [Hz]	Θ_{max} [deg.]	*No. Of repeat.*	Run ID
0.280	2.097	0	0.035	0.058	0.119	0.098	0	1	*Sway_280_1*
0.280	2.097	0	0.070	0.117	0.729	0.056	0	1	*Sway_280_2*
0.280	2.097	0	0.070	0.117	0.383	0.077	0	1	*Sway_280_3*
0.280	2.097	0	0.070	0.117	0.238	0.098	0	1	*Sway_280_4*
0.280	2.097	0	0.174	0.232	0.743	0.078	0	1	*Sway_280_5*
0.280	2.097	0	0.174	0.262	0.659	0.088	0	1	*Sway_280_6*
0.280	2.097	0	0.193	0.290	0.730	0.088	0	1	*Sway_280_7*
0.280	2.097	0	0.182	0.290	0.654	0.093	0	1	*Sway_280_8*
0.280	2.097	0	0.174	0.290	0.594	0.098	0	12*	*Sway_280_9*

Table A.2. 2 Test program for the dynamic pure sway test. "*" Indicates the test, for which uncertainty analysis is conducted. Note that the β setting on the PMM is 0 for pure sway.

Fn [-]	U_C [m/s]	β [deg.]	r'_{max}	$\dot{r}'_{max}$	S_{mm} [m]	fr [Hz]	Θ_{max} [deg.]	*No. Of repeat.*	Run ID
0.280	2.097	0	0.050	0.084	0.101	0.098	1.7	1	*Yaw_280_1*
0.280	2.097	0	0.150	0.251	0.304	0.098	5.1	1	*Yaw_280_2*
0.280	2.097	0	0.300	0.502	0.615	0.098	10.3	12*	*Yaw_280_3*
0.280	2.097	0	0.450	0.833	0.750	0.108	13.9	1	*Yaw_280_4*
0.280	2.097	0	0.600	1.290	0.743	0.125	16	1	*Yaw_280_5*
0.280	2.097	0	0.750	1.800	0.745	0.140	17.9	1	*Yaw_280_6*
0.280	2.097	0	0.150	0.162	0.740	0.063	8	1	*Yaw_280_7*
0.280	2.097	0	0.150	0.206	0.459	0.080	6.3	1	*Yaw_280_8*
0.280	2.097	0	0.150	0.206	0.459	0.080	6.3	1	*Yaw_280_9*
0.280	2.097	0	0.150	0.251	0.304	0.098	5.1	1	*Yaw_280_10*
0.280	2.097	0	0.201	0.251	0.734	0.073	9.2	1	*Yaw_280_11*
0.280	2.097	0	0.183	0.251	0.553	0.080	7.6	1	*Yaw_280_12*

Table A.2. 3 Test program for the dynamic pure yaw test. "*" Indicates the test, for which uncertainty analysis is conducted.

Fn [-]	U_C [m/s]	β [deg.]	r'_{max}	$\dot{r}'_{max}$	S_{mm} [m]	fr [Hz]	Θ_{max} [deg.]	*No. Of repeat.*	Run ID
0.280	2.097	9	0.300	0.502	0.615	0.098	10.3	1	*Yaw_Drift_280_1*
0.280	2.097	11	0.300	0.502	0.615	0.098	10.3	1	*Yaw_Drift_280_2*
0.280	2.097	10	0.300	0.502	0.615	0.098	10.3	12*	*Yaw_Drift_280_3*

Table A.2. 4 Test program for the dynamic yaw and drift test. . "*" Indicates the test, for which uncertainty analysis is conducted.

A.3 *Approach speed, Fn = 0.410*

Froude number, Fn [-]	Carriage speed, U_C [m/s]	Drift angle, β [deg.]
0.410	1.755	-12, -11, -10, -9, -6, -2, 0, 12, 11, 10*,9 ,6 ,2

Table A.3. 1 Test program for the static tests. "*" Indicates the test, for which uncertainty analysis is conducted.

Fn [-]	U_C [m/s]	β [deg.]	r'_{max}	$\dot{r}'_{max}$	S_{mm} [m]	fr [Hz]	Θ_{max} [deg.]	*No. Of repeat.*	Run ID
0.410	3.071	0	0.05	0.057	0.219	0.098	2.5	1	*Yaw_410_1*
0.410	3.071	0	0.150	0.171	0.656	0.098	7.5	1	*Yaw_410_2*
0.410	3.071	0	0.300	0.612	0.411	0.175	8.4	12*	*Yaw_410_3*
0.410	3.071	0	0.450	0.918	0.617	0.174	12.6	1	*Yaw_410_4*
0.410	3.071	0	0.600	1.292	0.742	0.184	16	1	*Yaw_410_5*

Table A.3. 2 Test program for the dynamic pure yaw test. "*" Indicates the test, for which uncertainty analysis is conducted.

Appendix B Results from static tests

The current appendix shows the forces and moments measured in the static drift tests

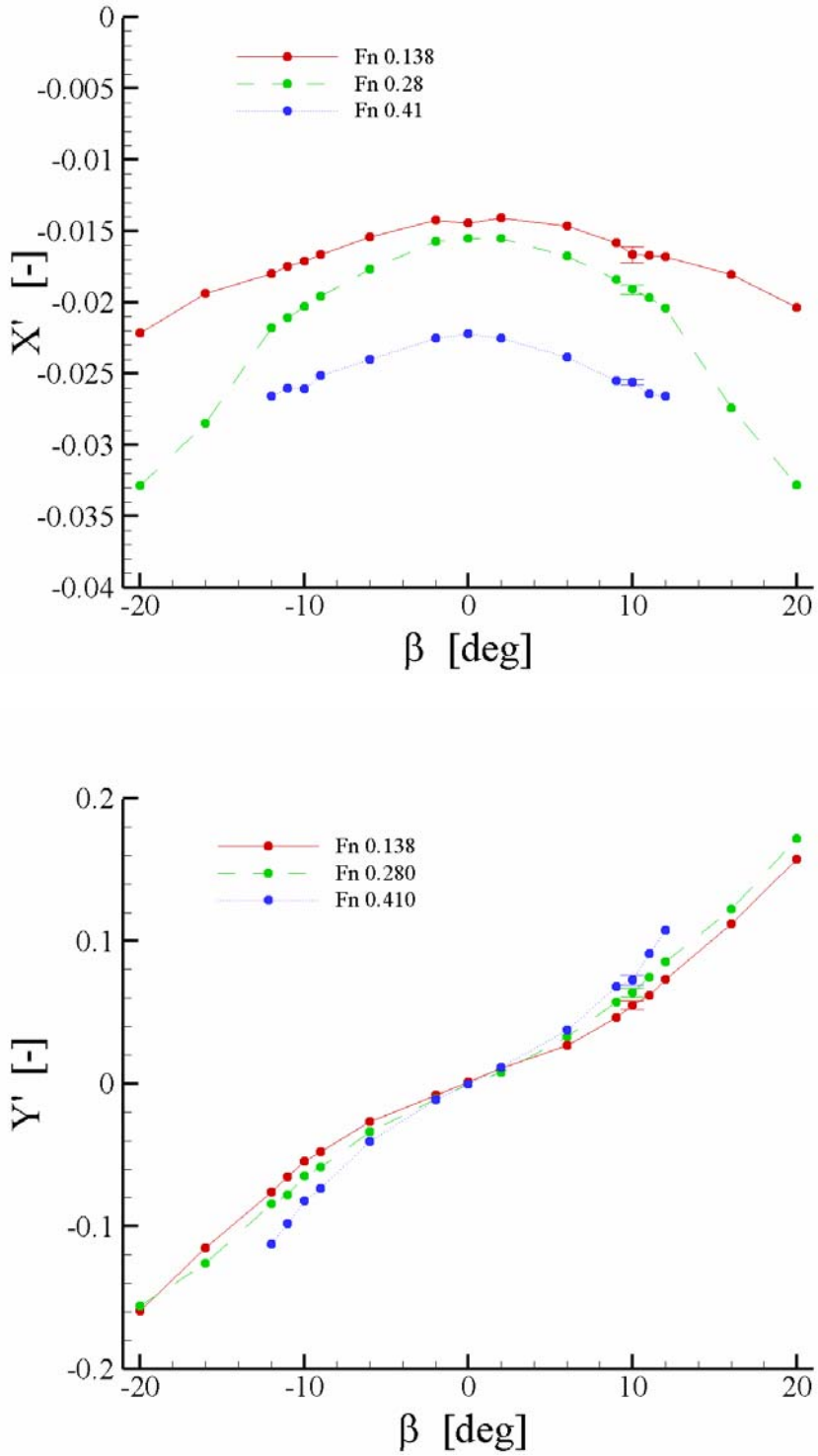

Figure B. 1 X- and Y-forces measured in pure drift at three different Froude numbers

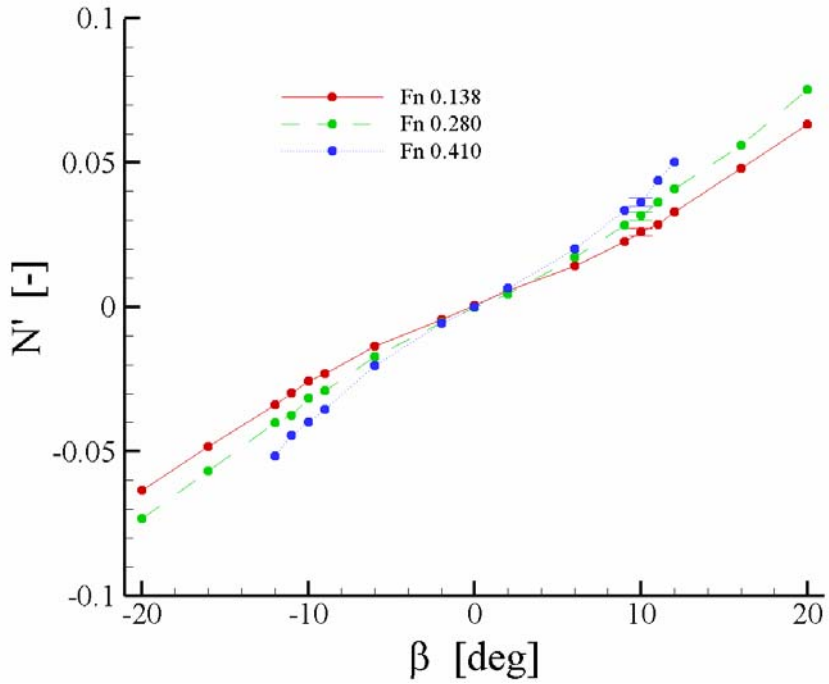

Figure B. 2 Yaw moment in pure drift.

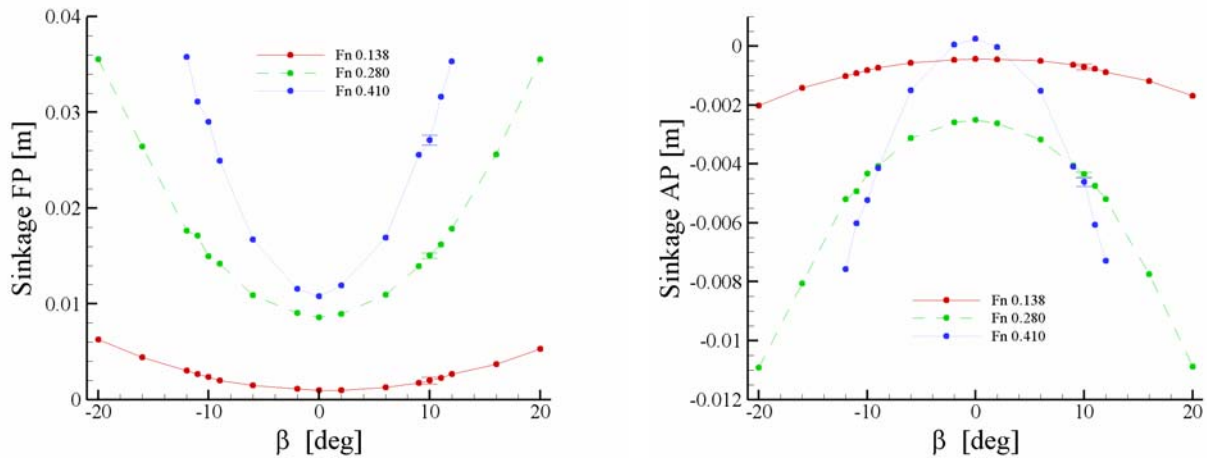

Figure B. 3 Sinkage.

Appendix C Results from uncertainty assessment on dynamic test cases

The present appendix shows the time series for the dynamic test cases, which are dealt with in the uncertainty analysis. The shown quantities cover motion parameters forces and moments and the uncertainties related to these quantities.

C.1 *Dynamic test (Pure yaw), Fr=0.280*

C.1.1 Motion parameters

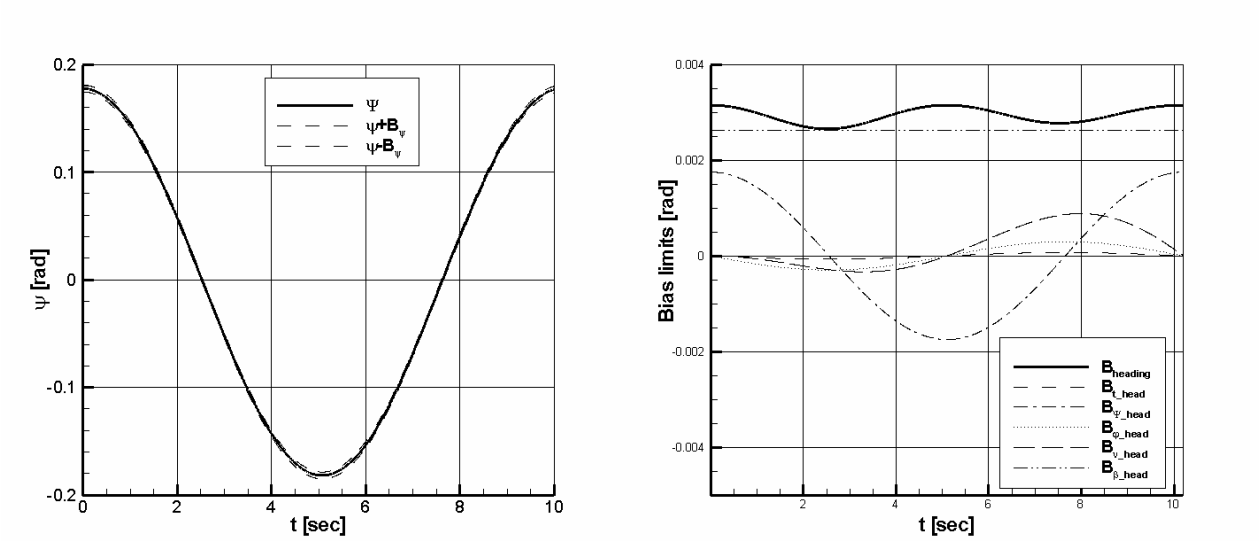

Figure C.1.1.1Heading angle (on the left) and bias limits (on the right).

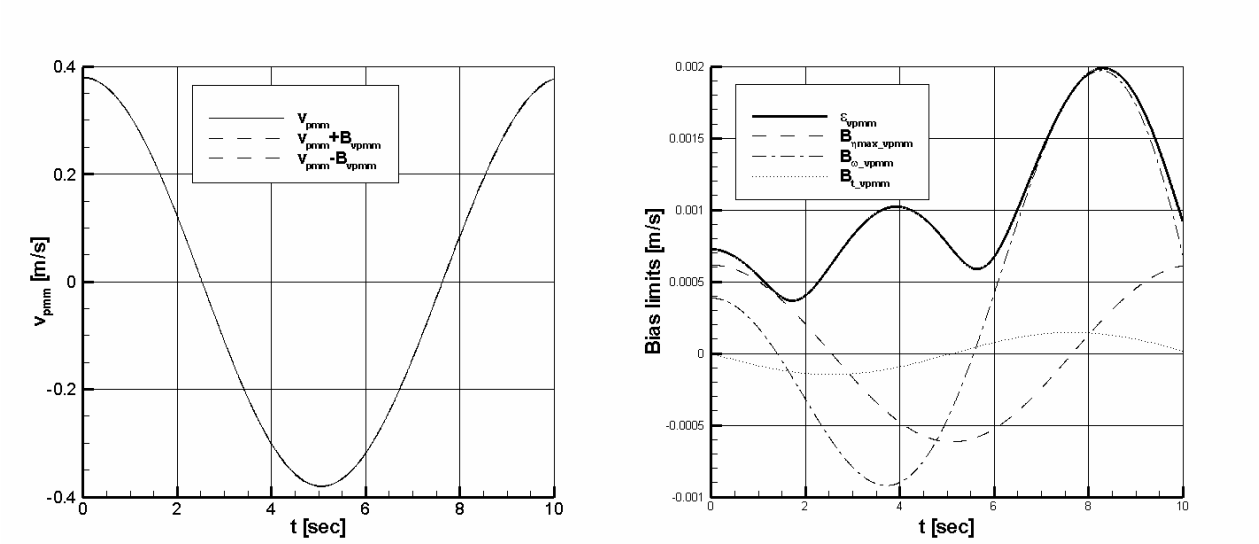

Figure C.1.1.2 Transverse PMM velocity (on the left) and bias limits (on the right).

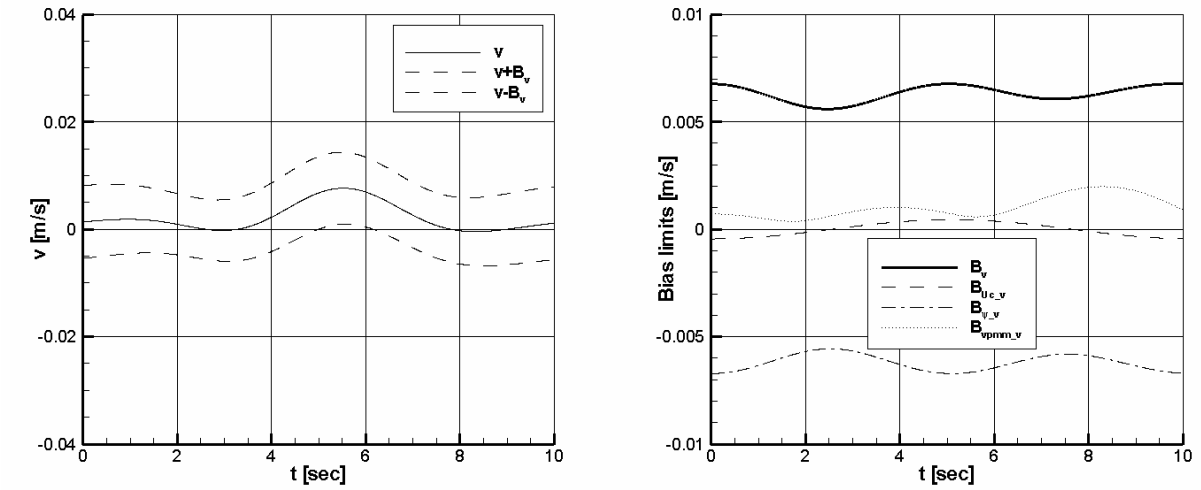

Figure C.1.1.3 Sway velocity (on the left) and bias limits (on the right).

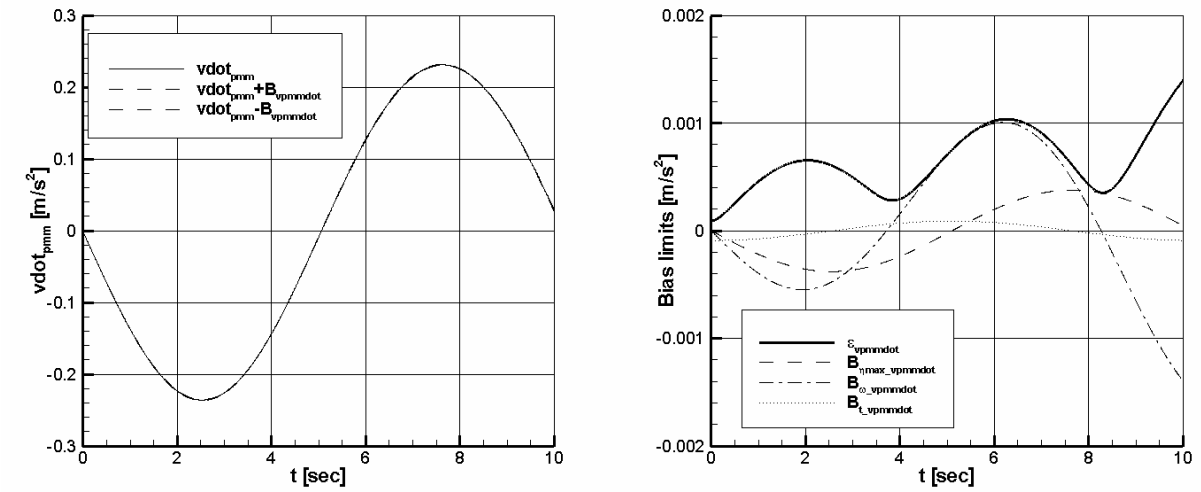

Figure C.1.1.4 Transverse PMM acceleration (on the left) and bias limits (on the right).

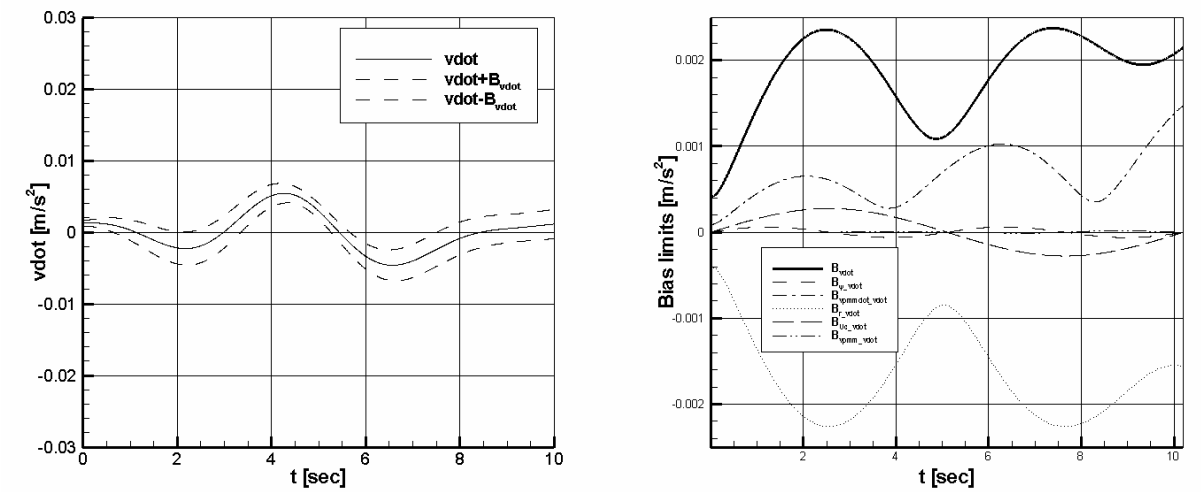

Figure C.1.1.5 Sway acceleration (on the left) and bias limits (on the right).

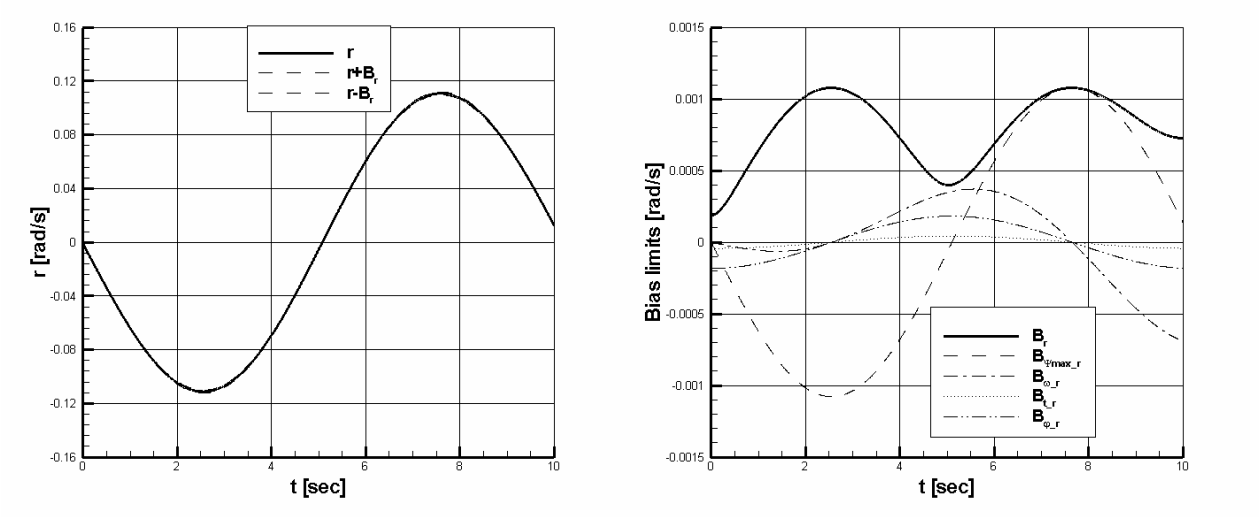

Figure C.1.1.6 Yaw rate (on the left) and bias limits (on the right).

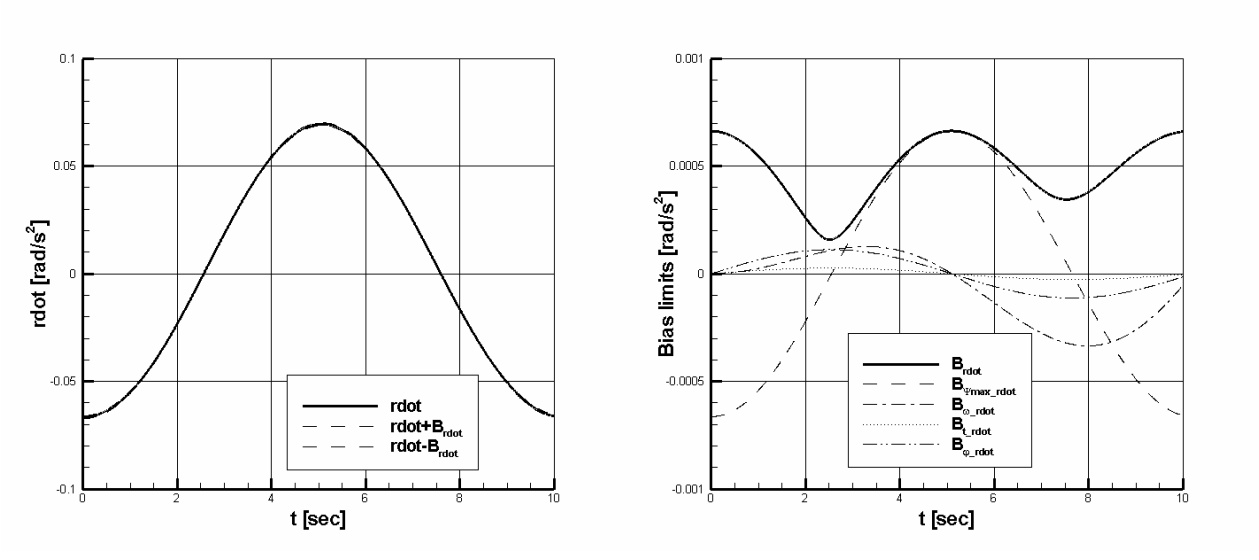

Figure C.1.1.7 Yaw acceleration (on the left) and bias limits (on the right).

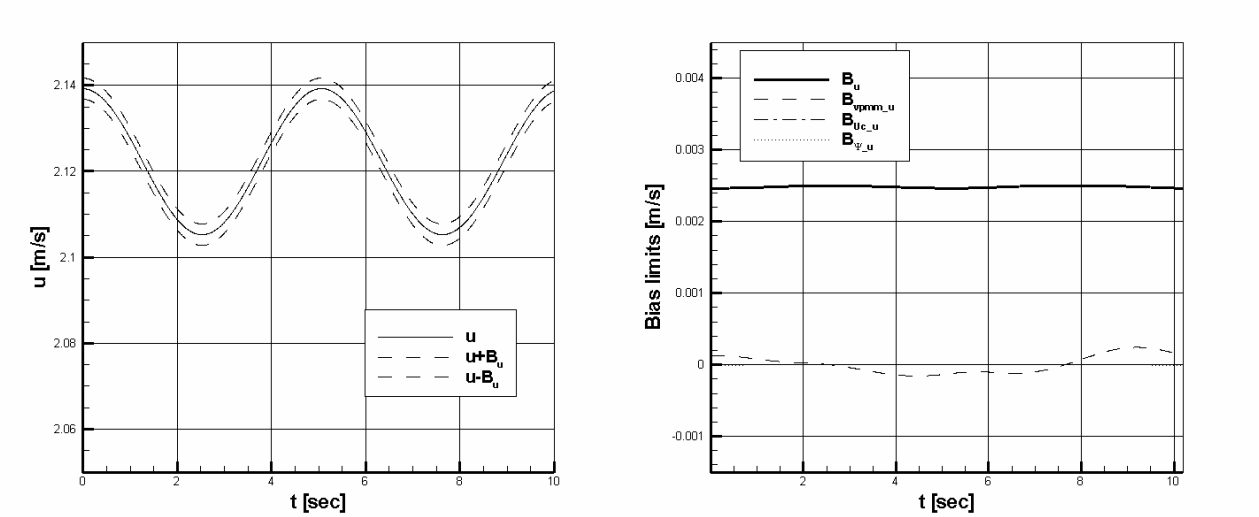

Figure C.1.1.8 Surge velocity (on the left) and bias limits (on the right).

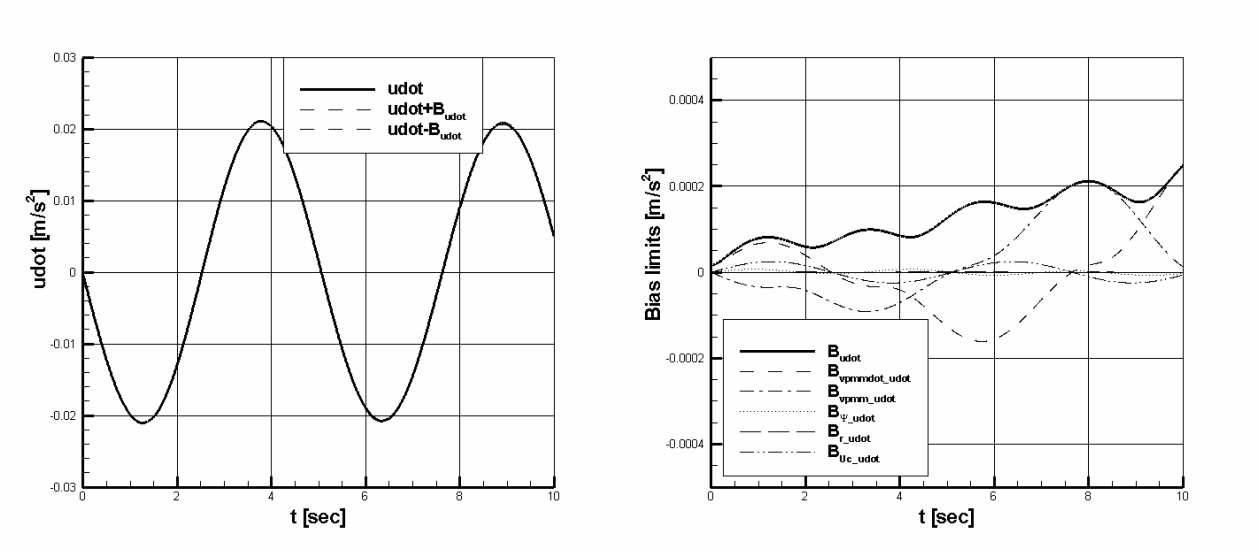

Figure C.1.1.9 Surge acceleration (on the left) and bias limits (on the right).

C.1.2 Longitudinal force

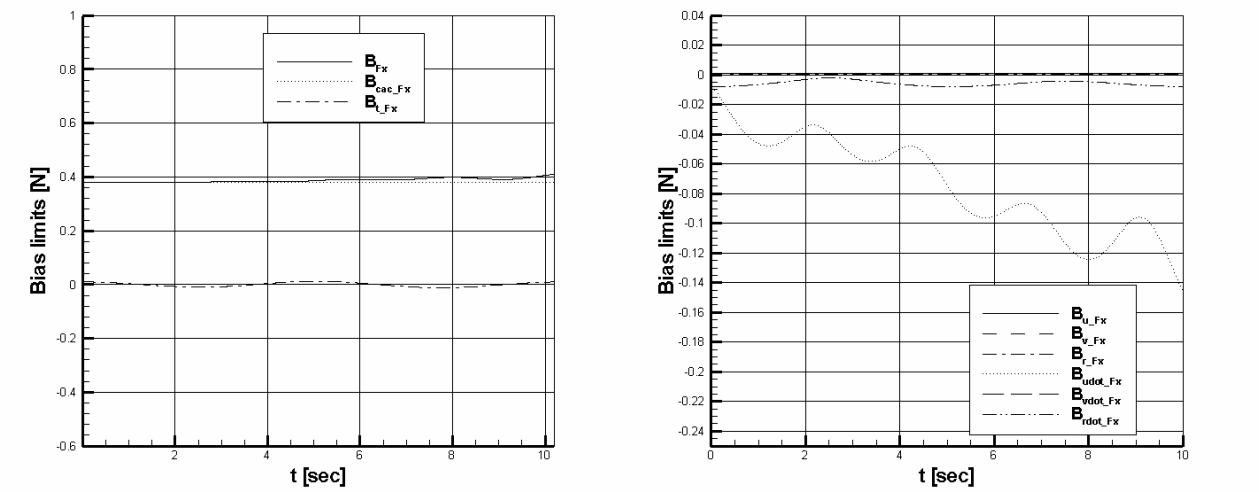

Figure C.1.2.1 Bias limits for measured X-force.

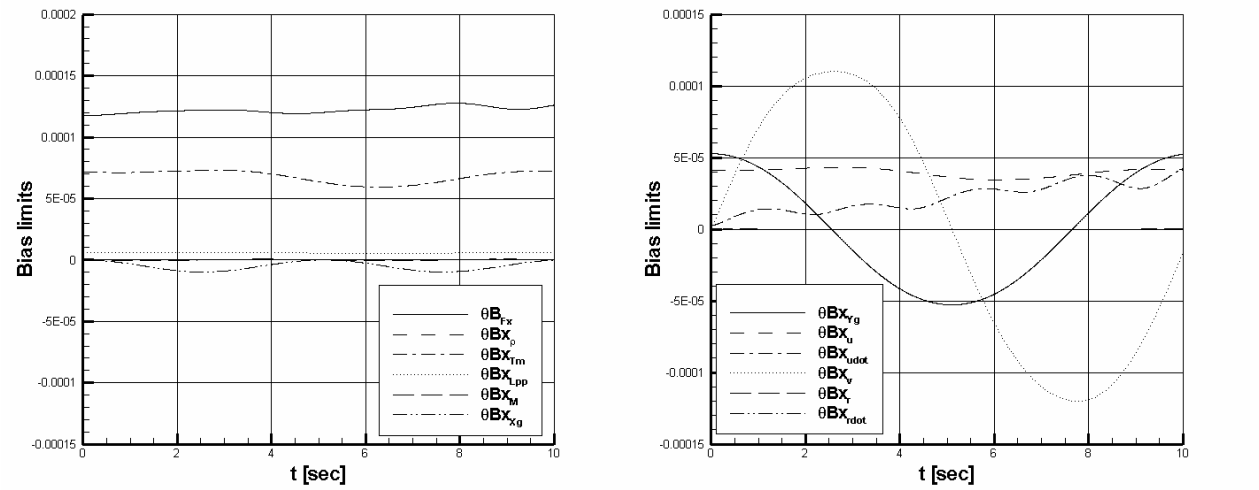

Figure C.1.2.2 Bias limits for X'.

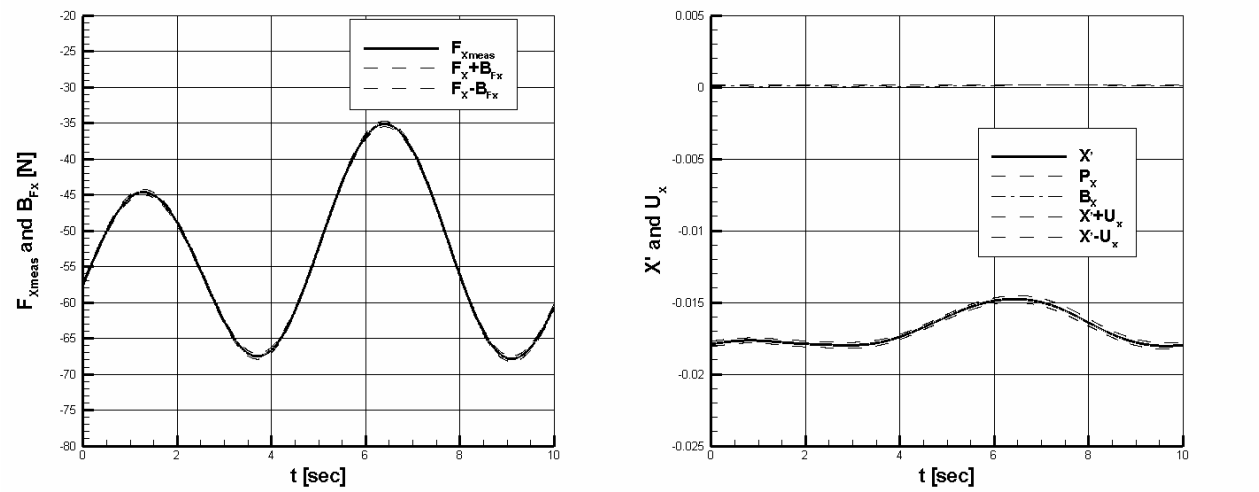

Figure C.1.2.3 Measured F_x and its bias limit (on the left); X' including uncertainty (on the right).

C.1.3 Transverse force

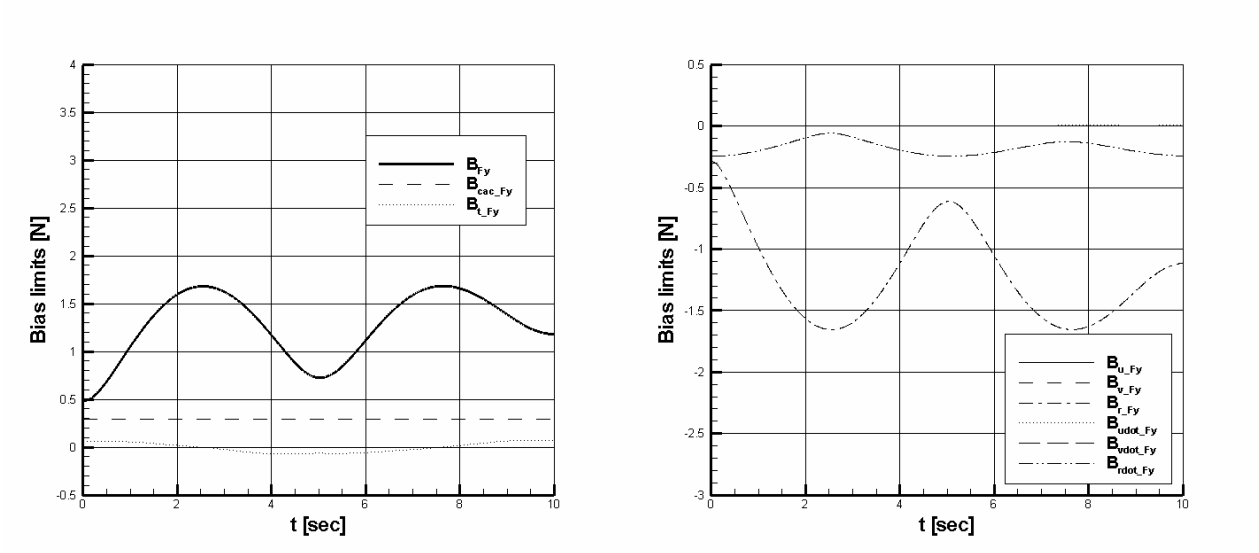

Figure C.1.3.1 Bias limits for measured Y-force.

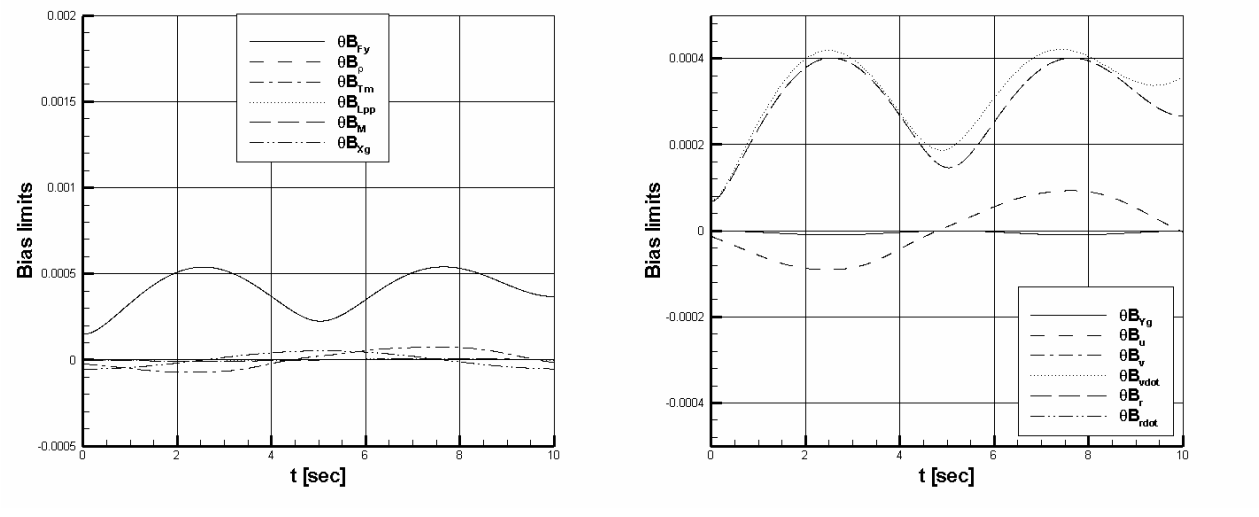

Figure C.1.3.2 Bias limits for Y'.

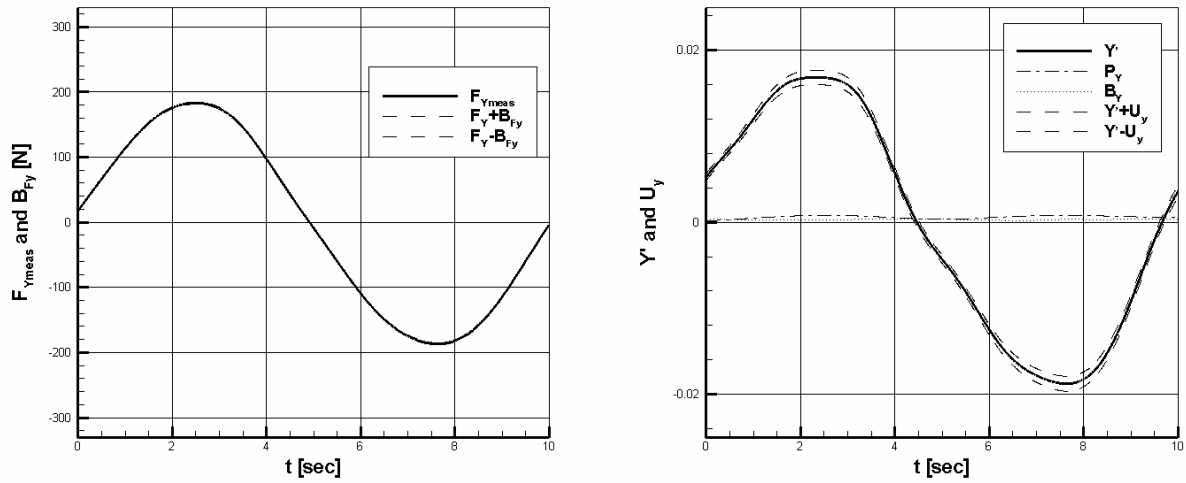

Figure C.1.3.3 Measured F_y and its bias limit (on the left); $Y^{'}$ including uncertainty (on the right).

C.1.4 Yaw moment

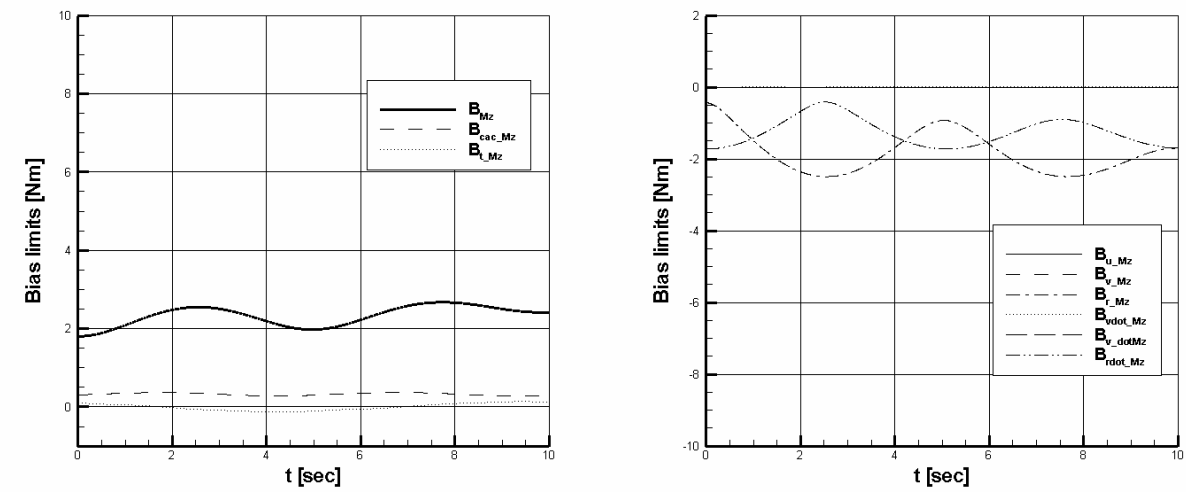

Figure C.1.4.1 Bias limits for measured yaw moment M_Z.

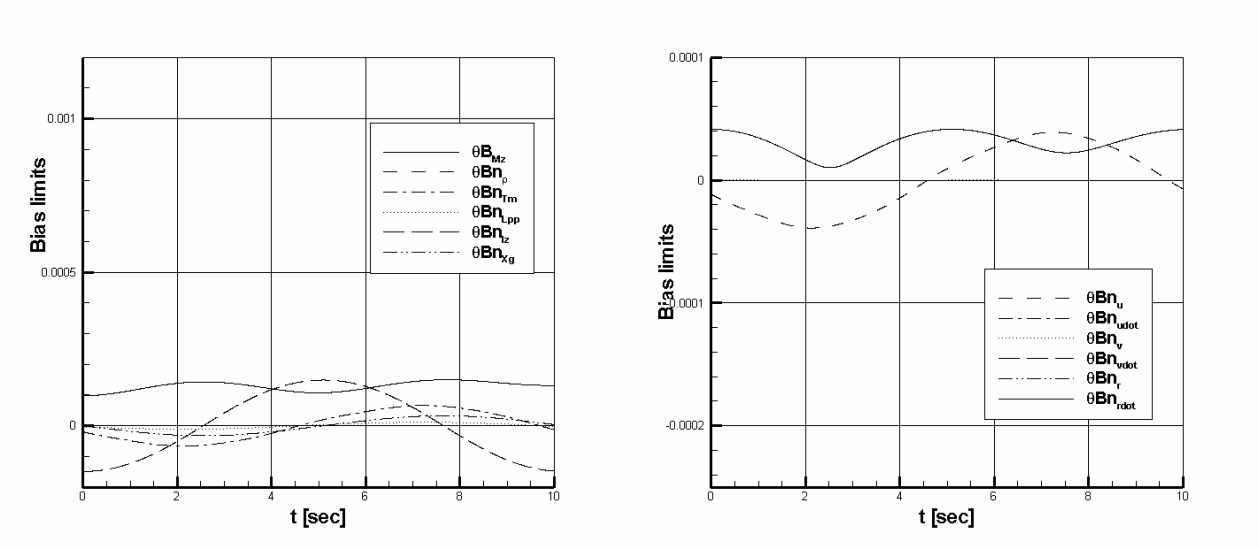

Figure C.1.4.2 Bias limits for N'.

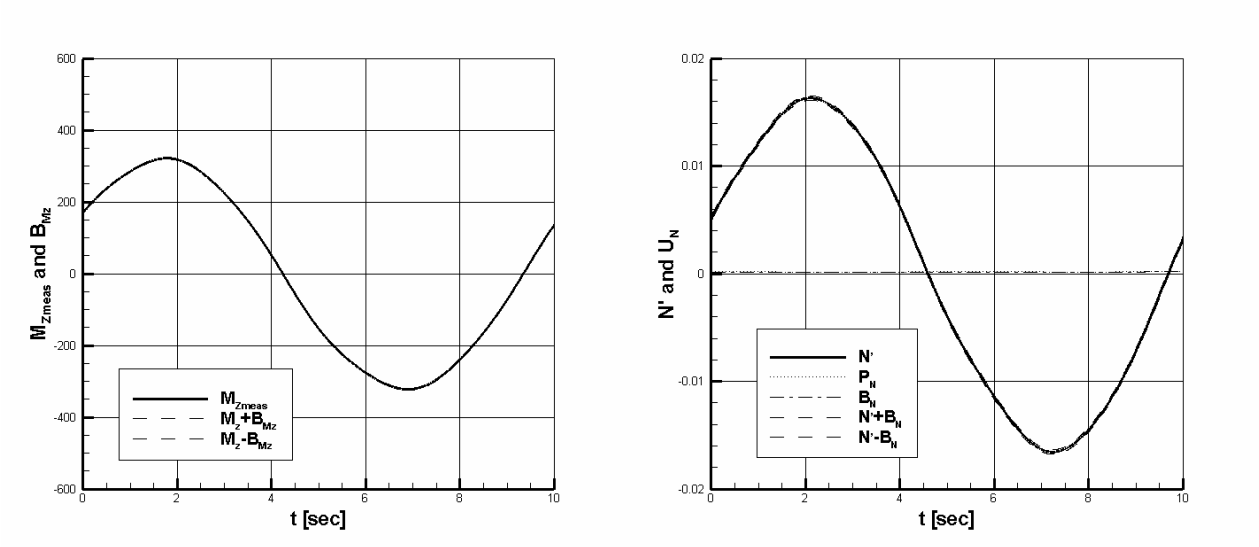

Figure C.1.4.3 Measured M_z and its bias limit (on the left); N' including uncertainty (on the right).

C.2 *Dynamic test (Pure sway), Fr=0.280*

C.2.1 Motion parameters

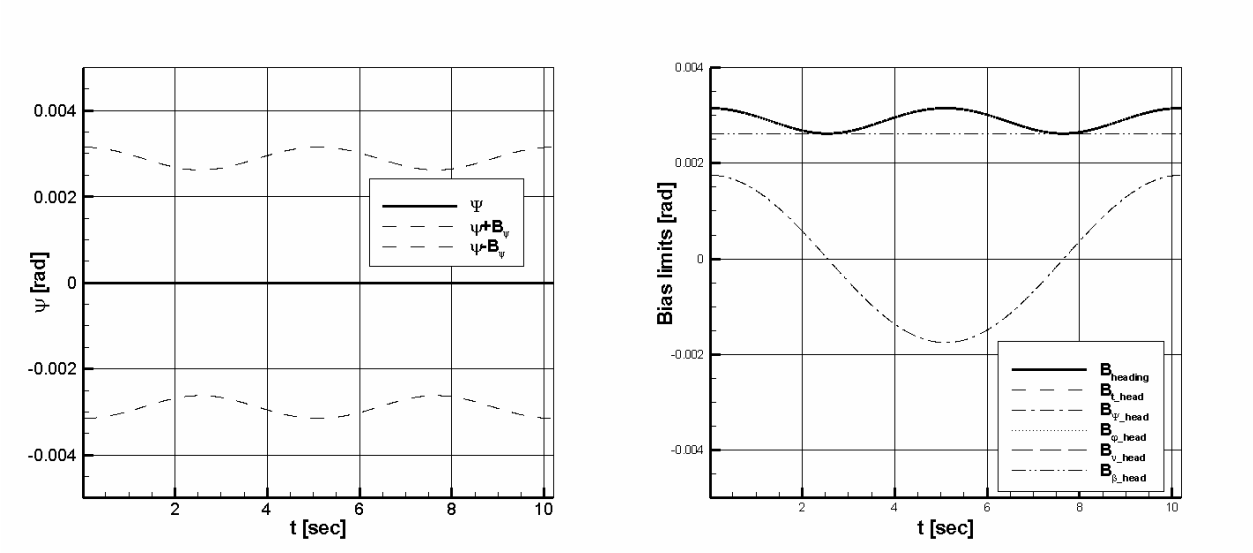

Figure C.2.1.1 Heading angle (on the left) and bias limits (on the right).

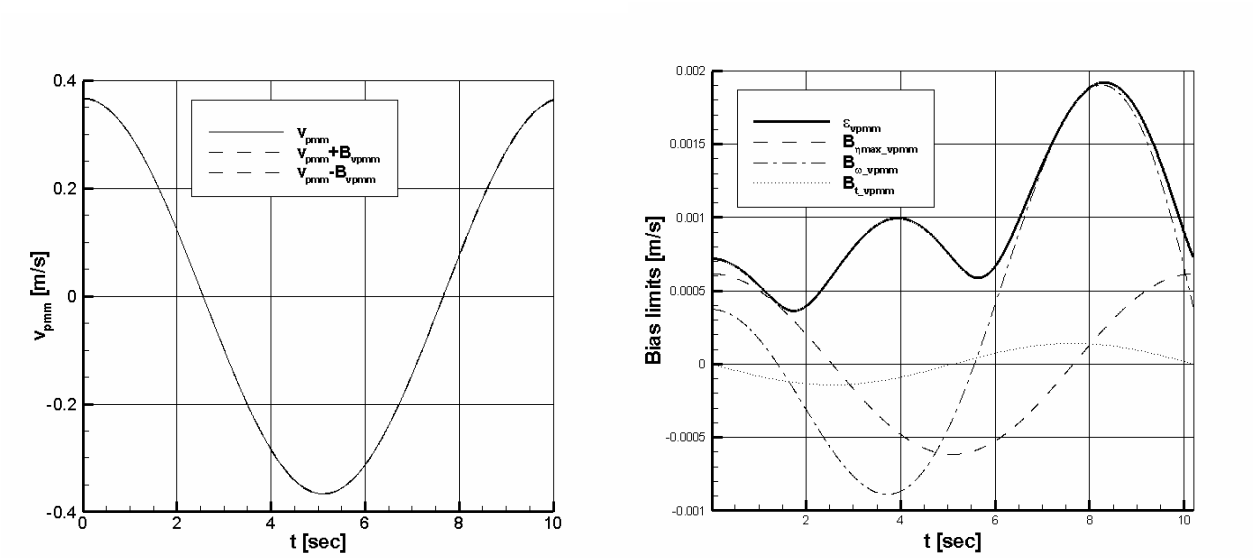

Figure C.2.1.2 Transverse PMM velocity (on the left) and bias limits (on the right).

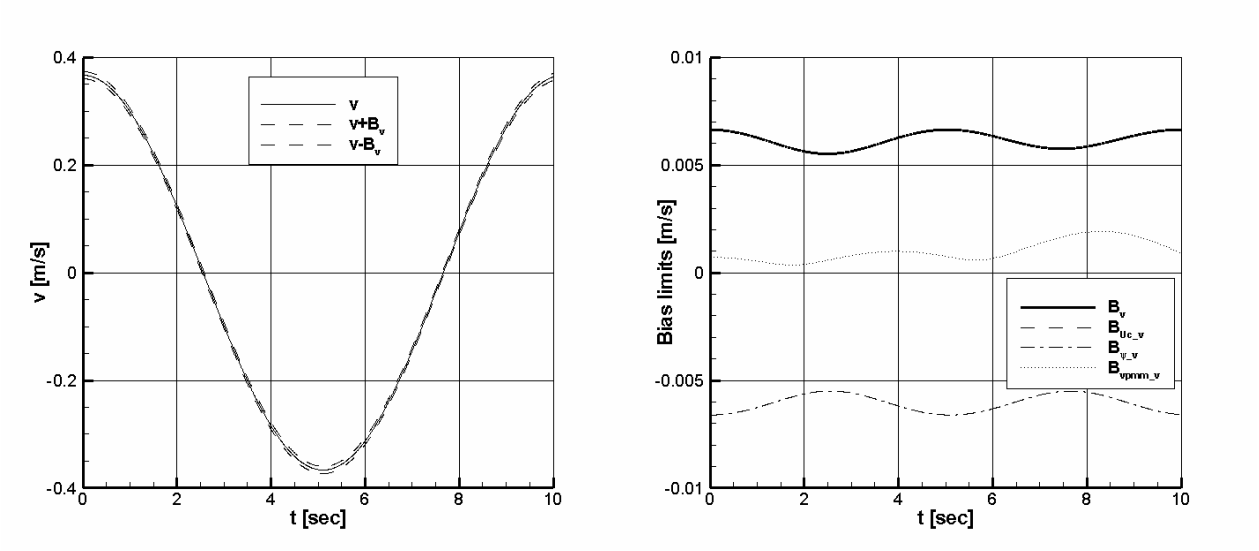

Figure C.2.1.3 Sway velocity (on the left) and bias limits (on the right).

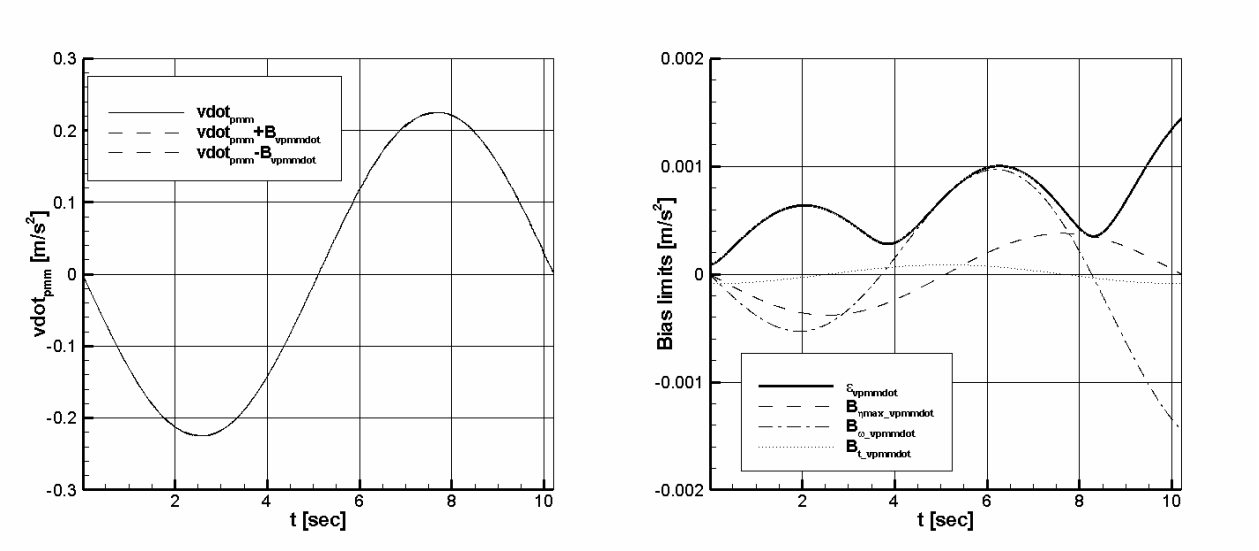

Figure C.2.1.4 Transverse PMM acceleration (on the left) and bias limits (on the right).

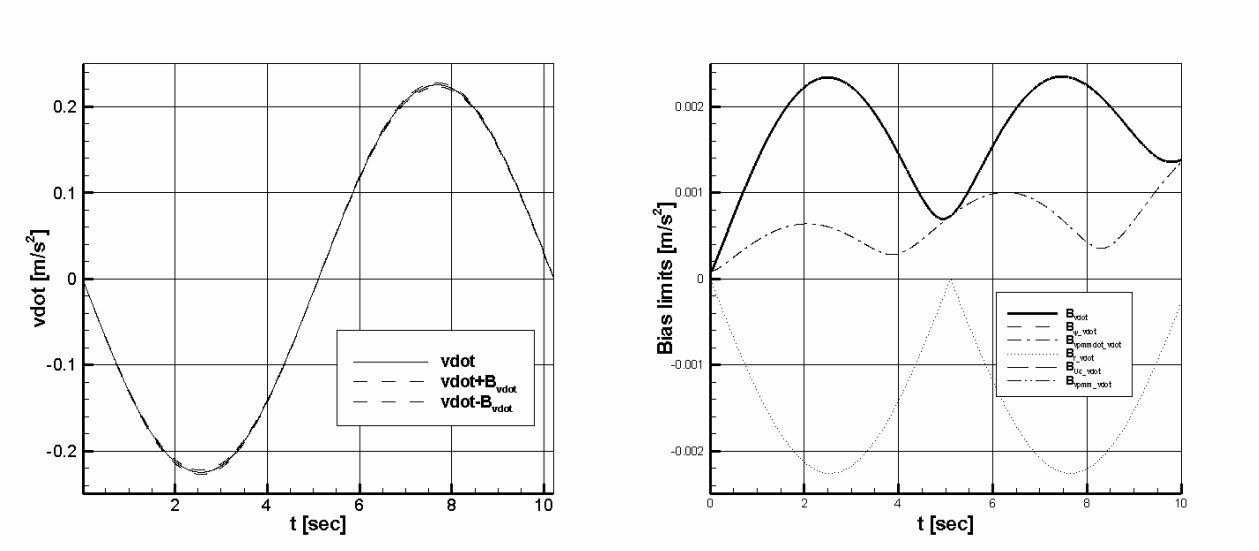

Figure C.2.1.5 Sway acceleration (on the left) and bias limits (on the right).

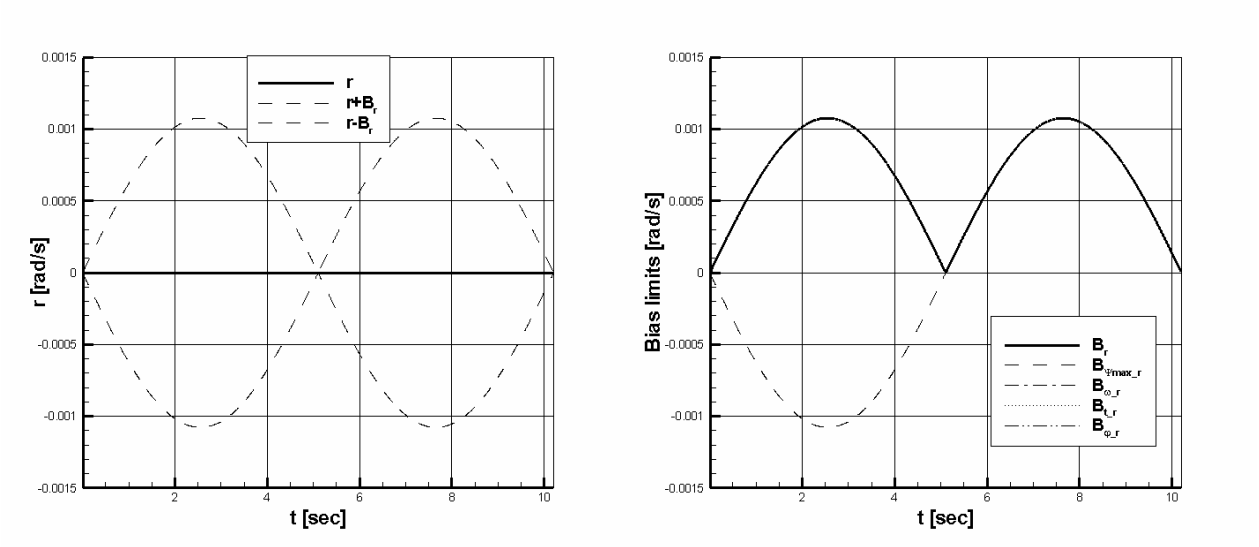

Figure C.2.1.6 Yaw rate (on the left) and bias limits (on the right).

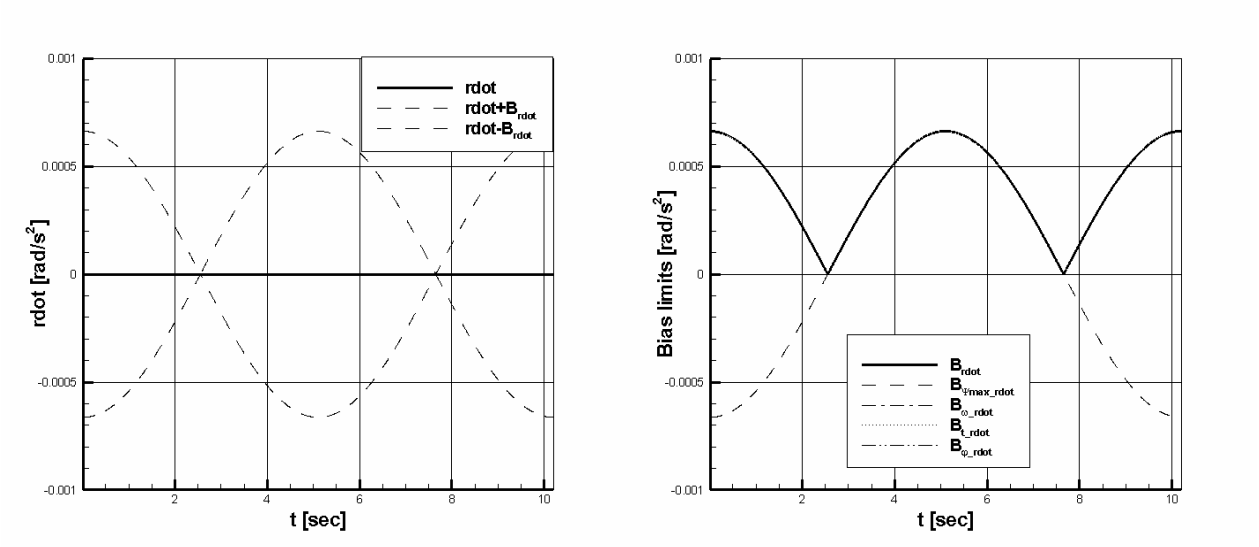

Figure C.2.1.7 Yaw acceleration (on the left) and bias limits (on the right).

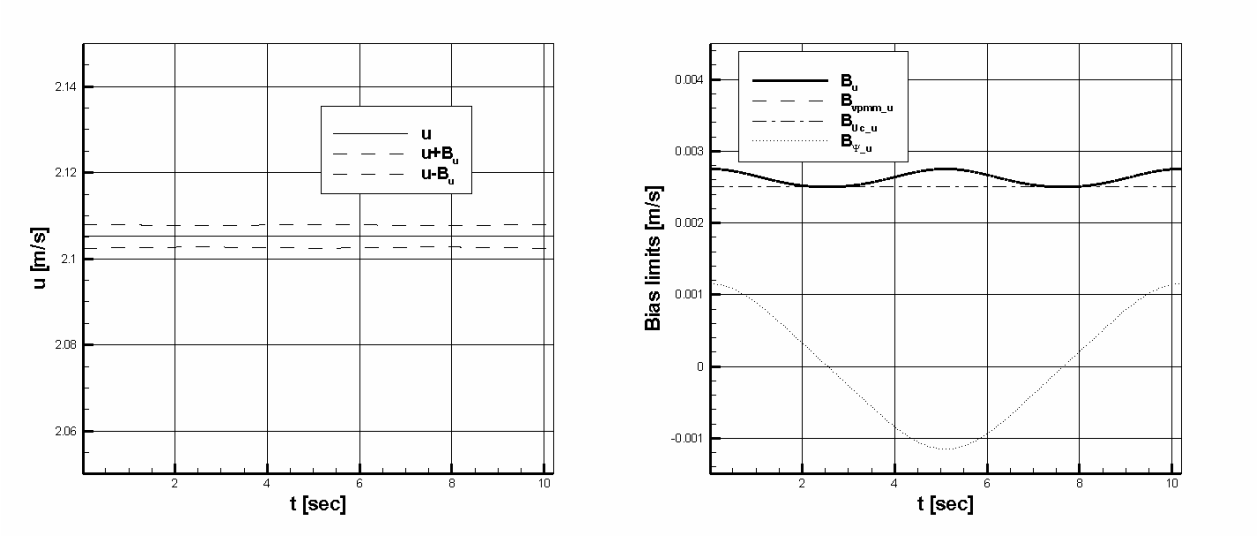

Figure C.2.1.8 Surge velocity (on the left) and bias limits (on the right).

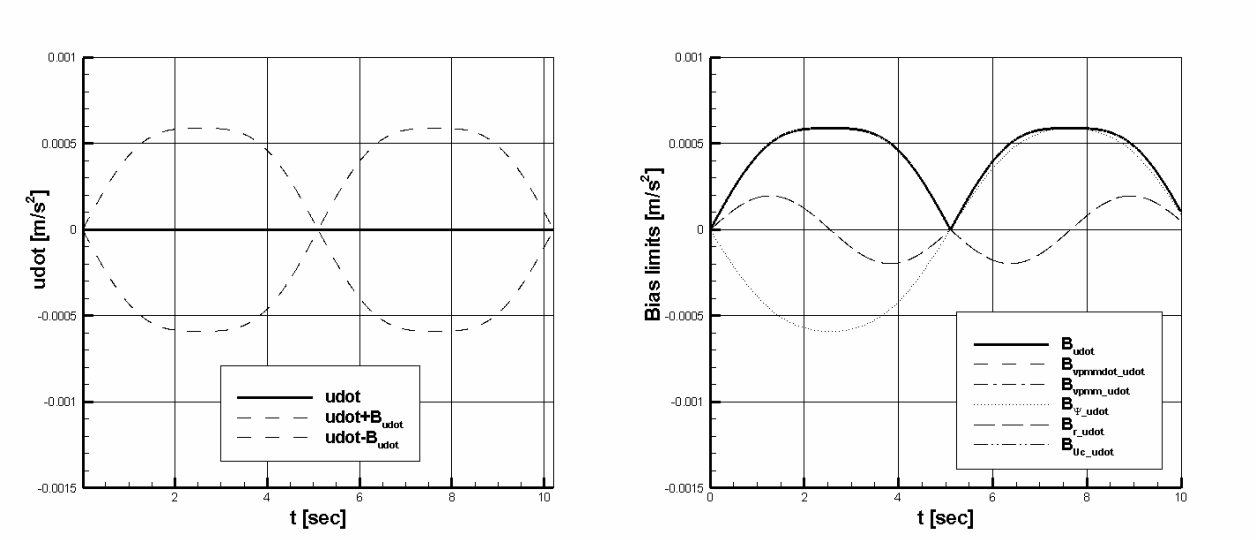

Figure C.2.1.9 Surge acceleration (on the left) and bias limits (on the right).

C.2.2 Longitudinal force

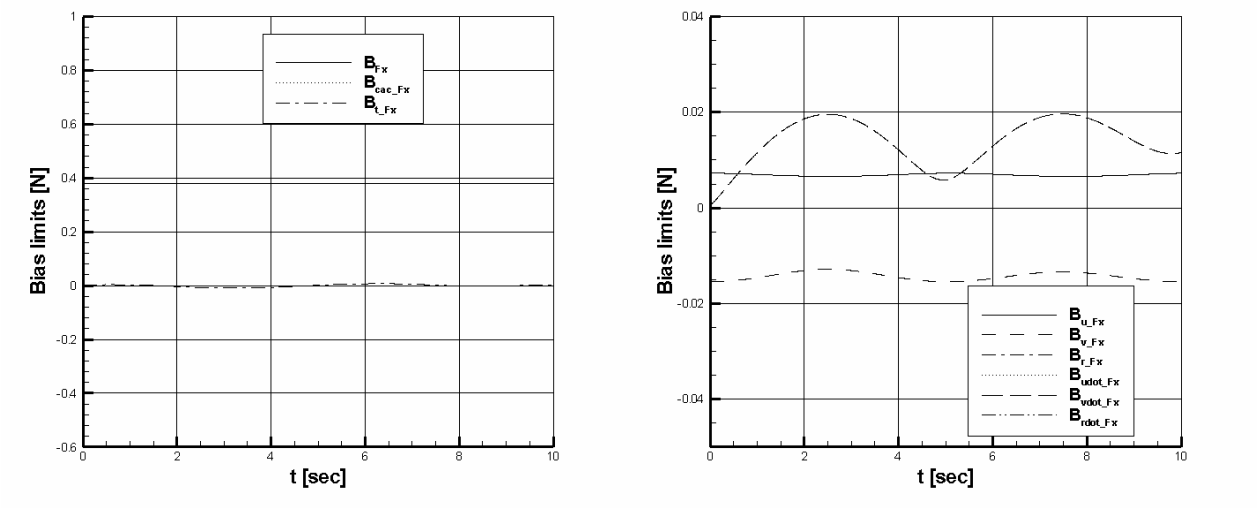

Figure C.2.2.1 Bias limits for measured X-force.

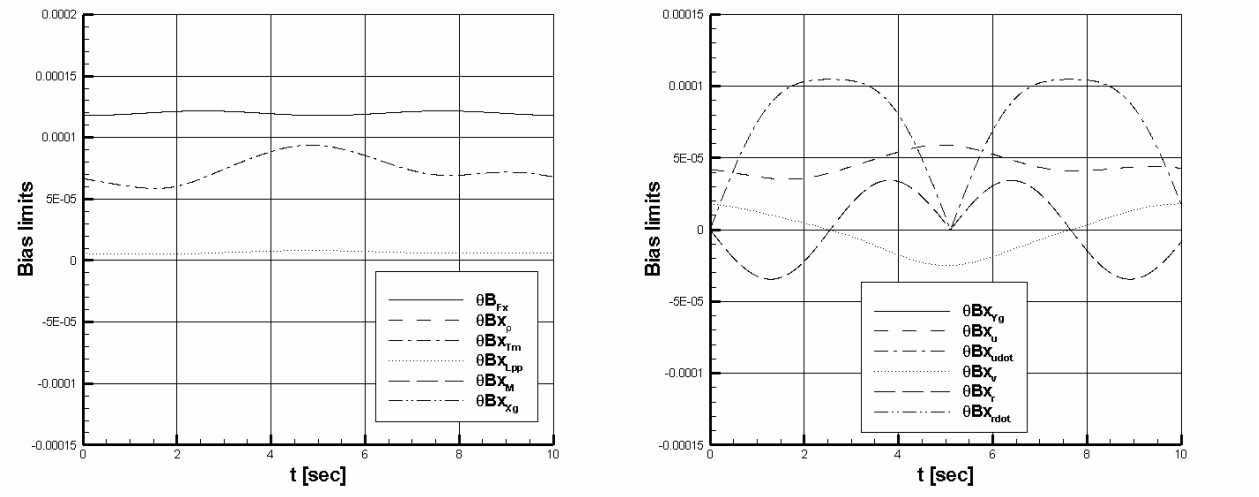

Figure C.2.2.2 Bias limits for X'.

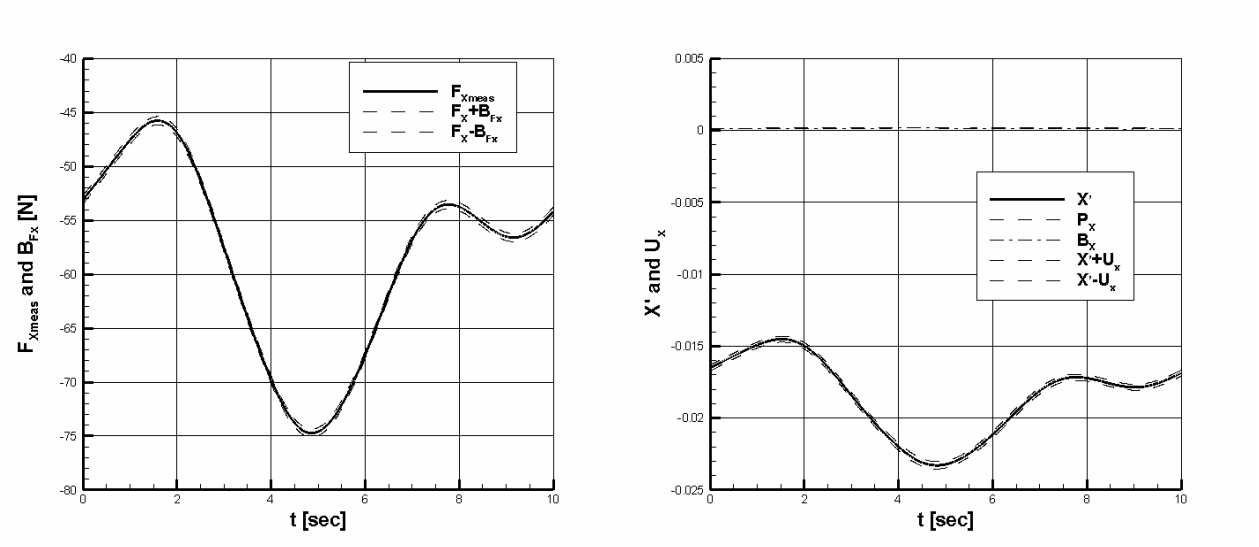

Figure C.2.2.3 Measured F_x and its bias limit (on the left); X' including uncertainty (on the right).

C.2.3 Transverse force

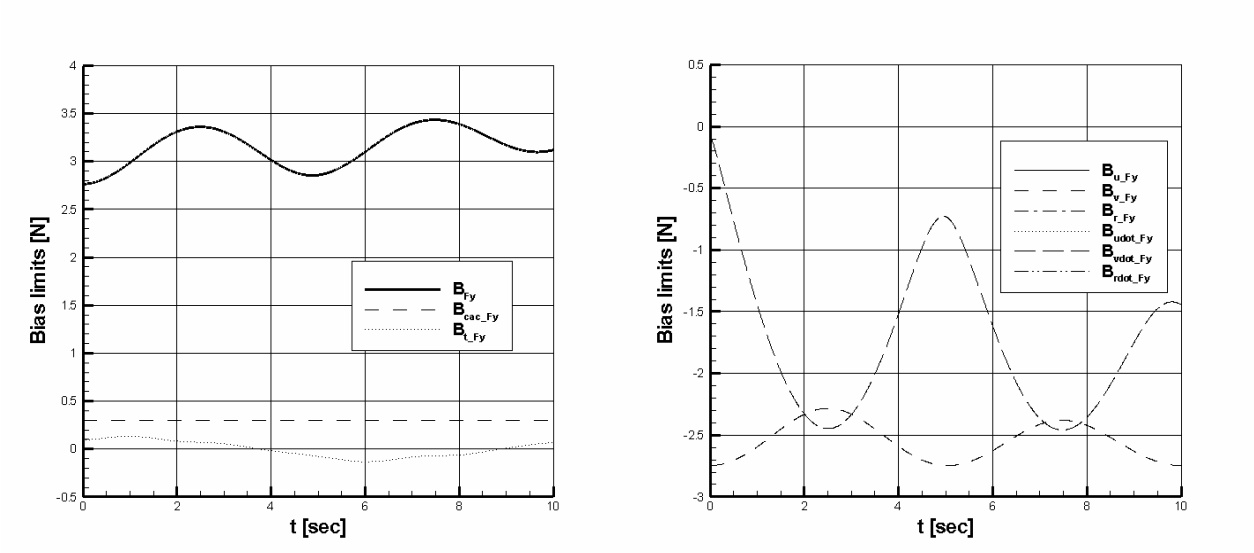

Figure C.2.3.1 Bias limits for measured Y-force.

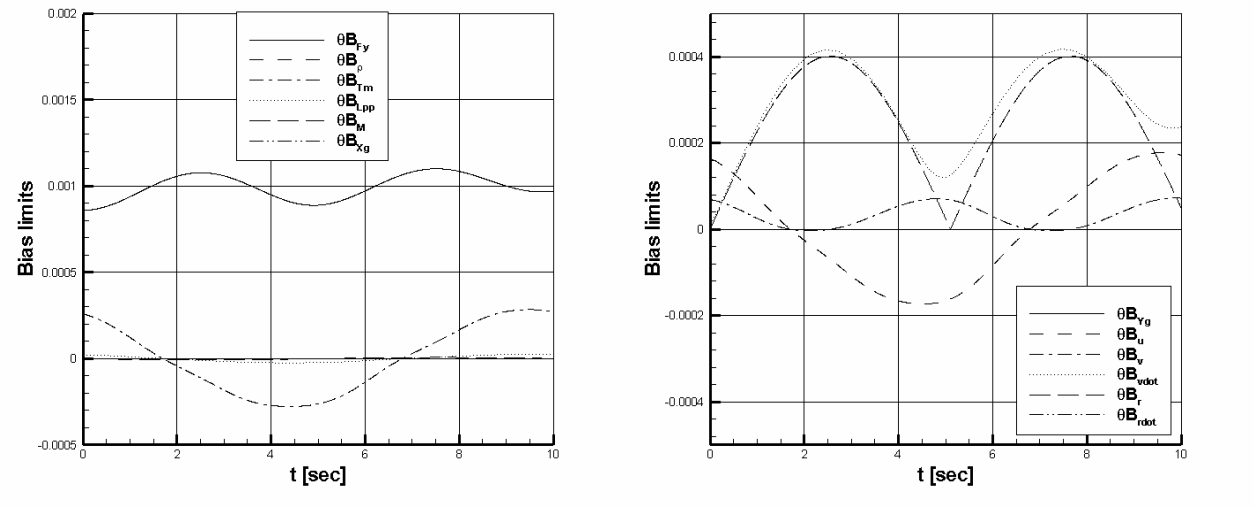

Figure C.2.3.2 Bias limits for Y'.

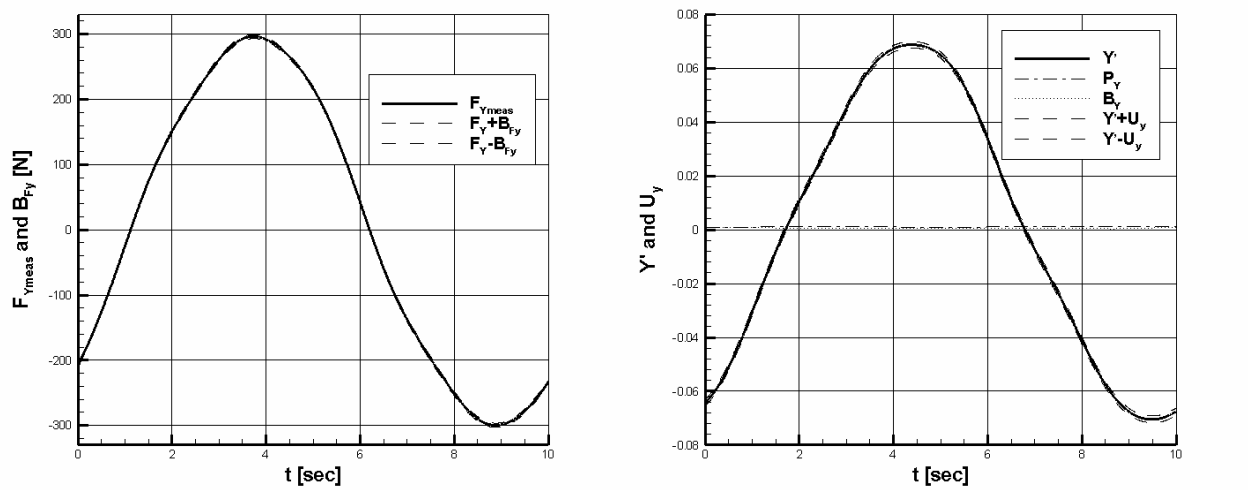

Figure C.2.3.3 Measured F_y and its bias limit (on the left); Y' including uncertainty (on the right).

C.2.4 Yaw moment

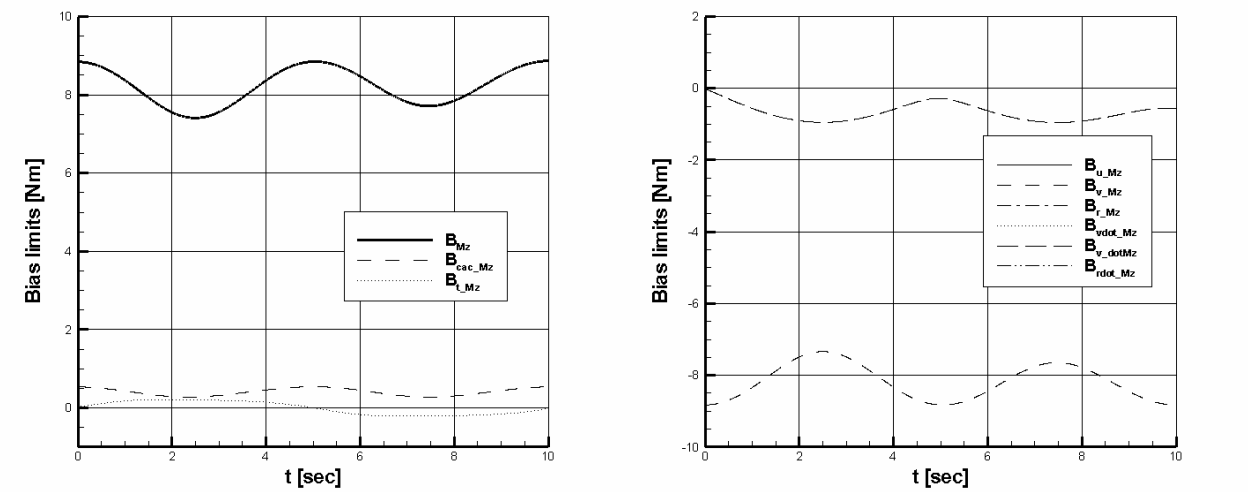

Figure C.2.4.1 Bias limits for measured yaw moment M_Z.

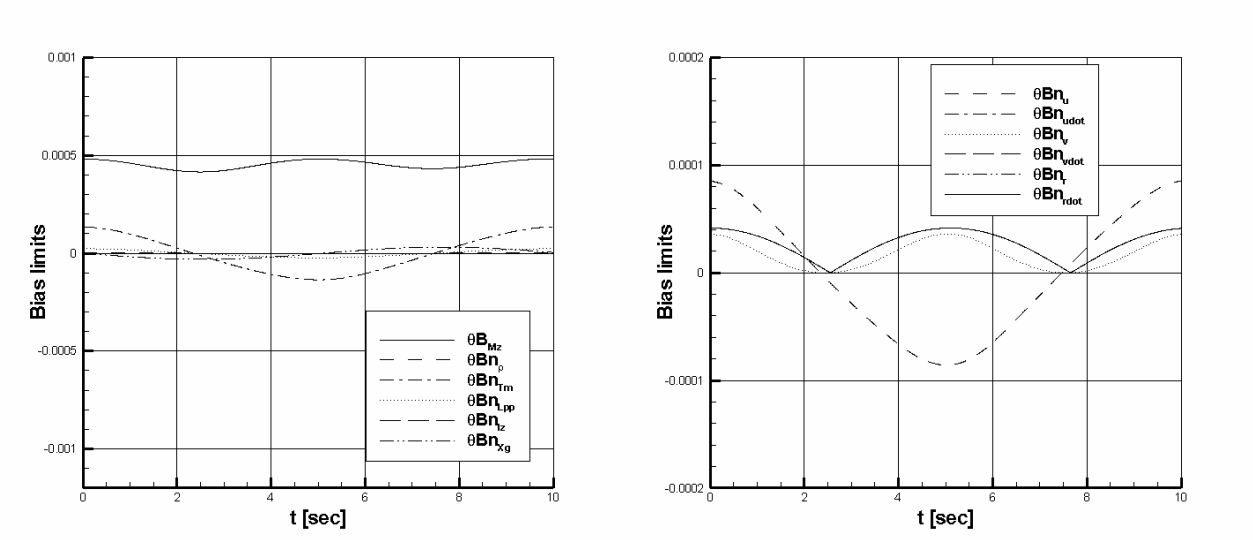

Figure C.2.4.2 Bias limits for N'.

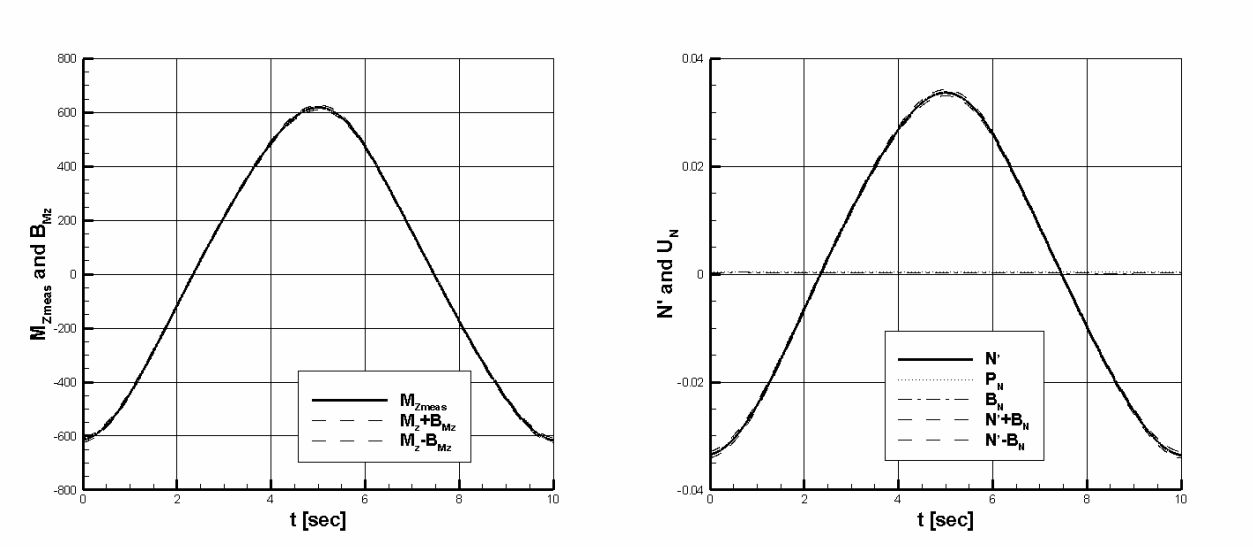

Figure C.2.4.3 Measured M_z and its bias limit (on the left); N' including uncertainty (on the right).

C.3 *Dynamic test (Yaw and drift), Fr=0.280*

C.3.1 Motion parameters

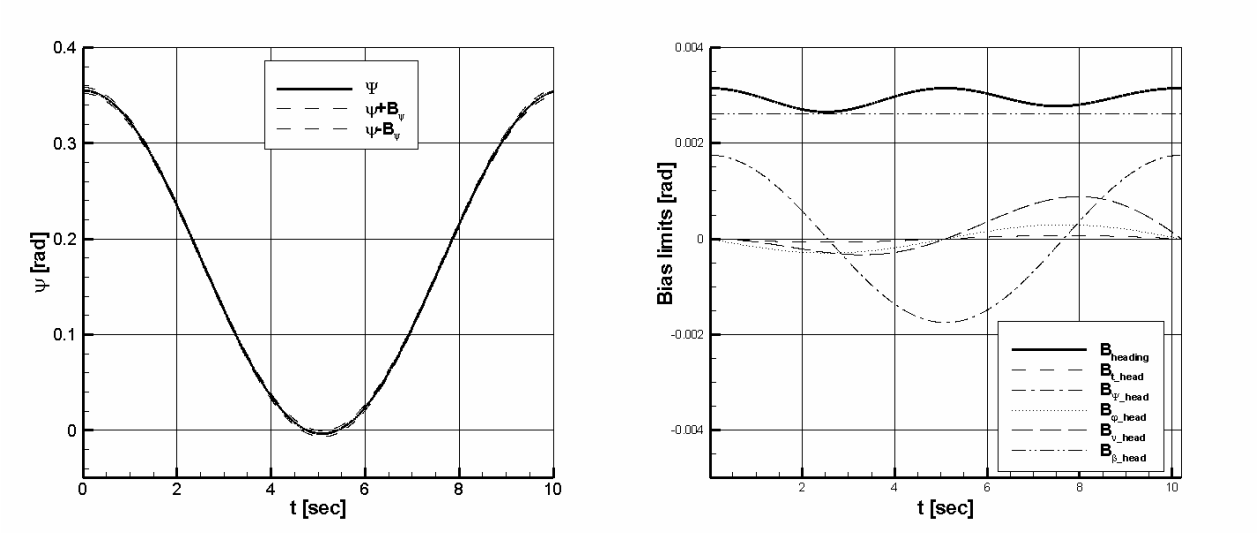

Figure C.3.1.1 Heading angle (on the left) and bias limits (on the right).

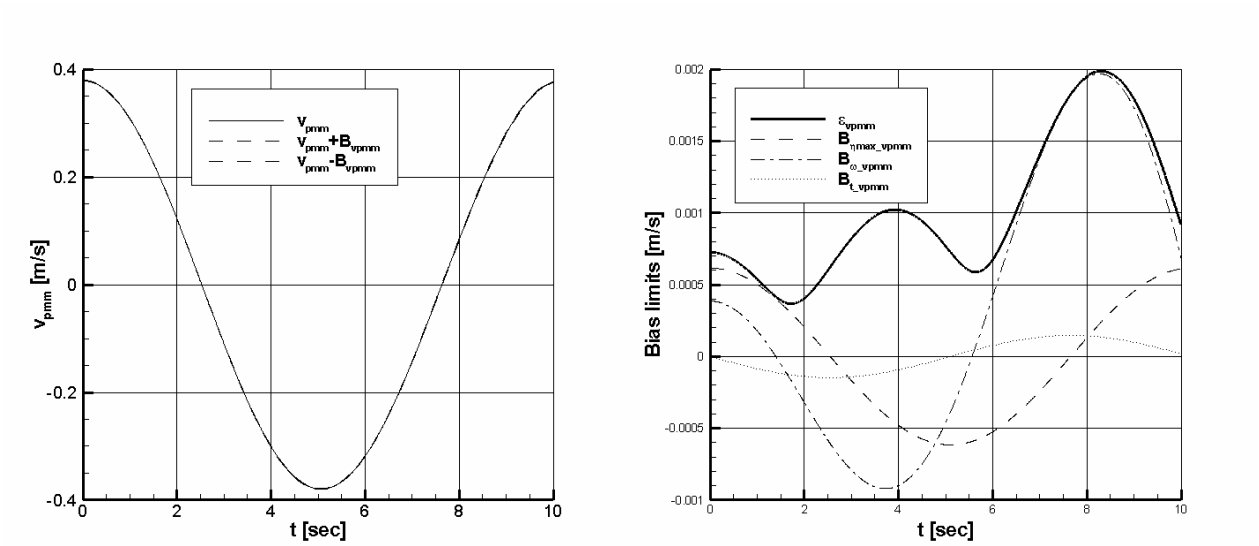

Figure C.3.1.2 Transverse PMM velocity (on the left) and bias limits (on the right).

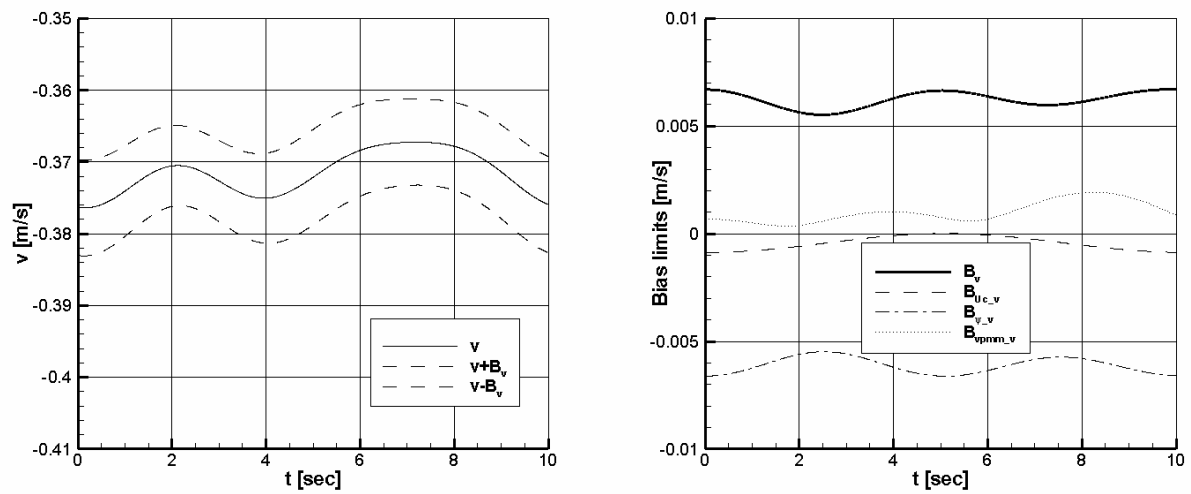

Figure C.3.1.3 Sway velocity (on the left) and bias limits (on the right).

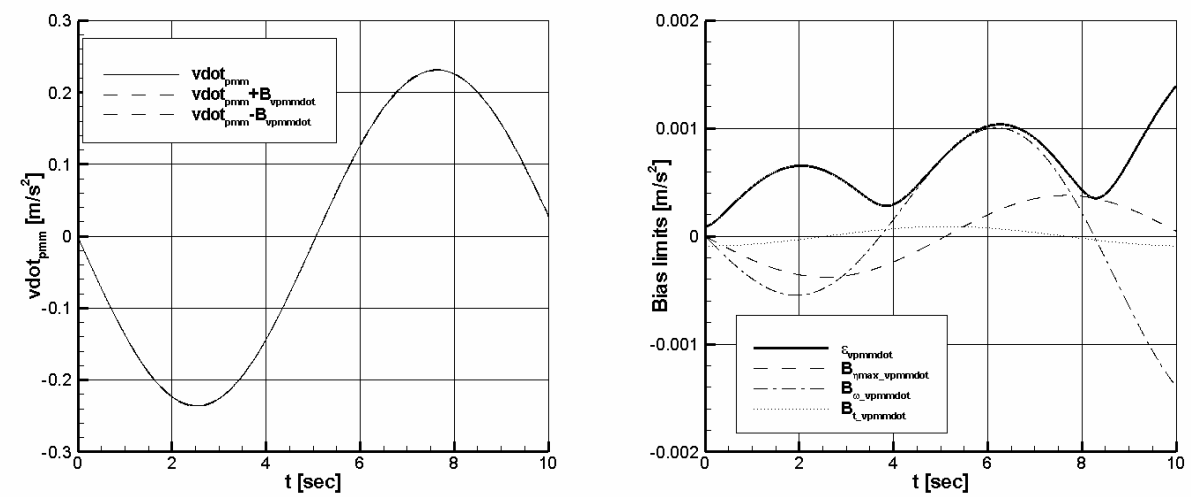

Figure C.3.1.4 Transverse PMM acceleration (on the left) and bias limits (on the right).

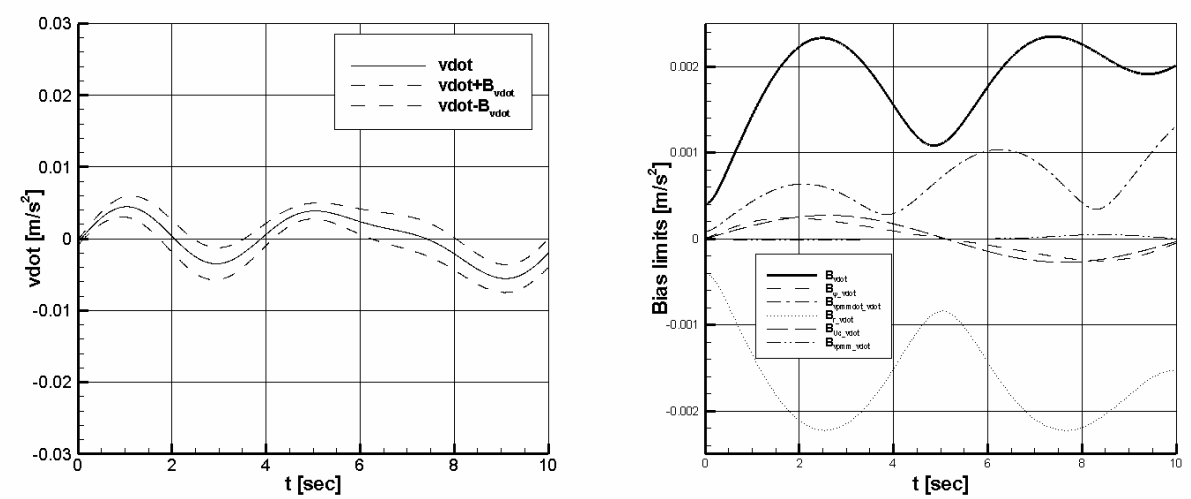

Figure C.3.1.5 Sway acceleration (on the left) and bias limits (on the right).

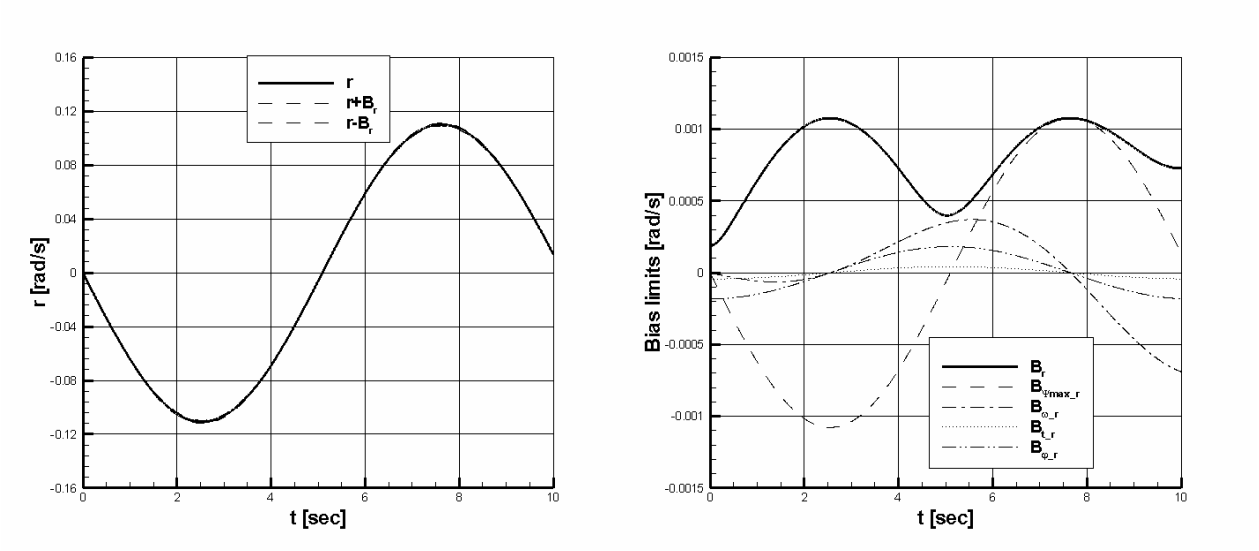

Figure C.3.1.6 Yaw rate (on the left) and bias limits (on the right).

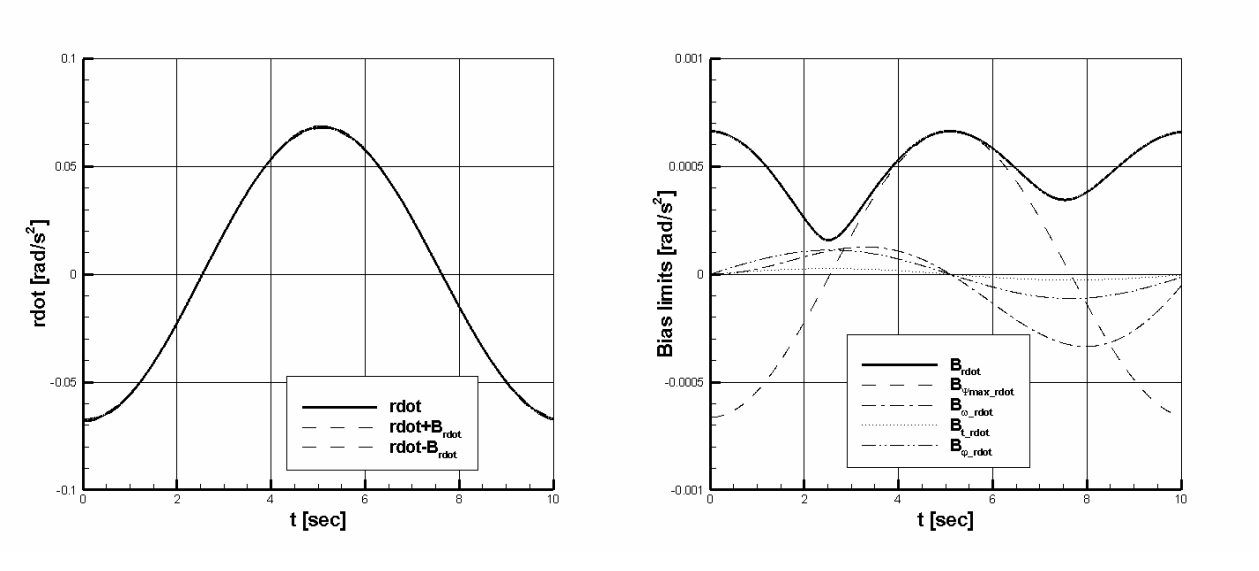

Figure C.3.1.7 Yaw acceleration (on the left) and bias limits (on the right).

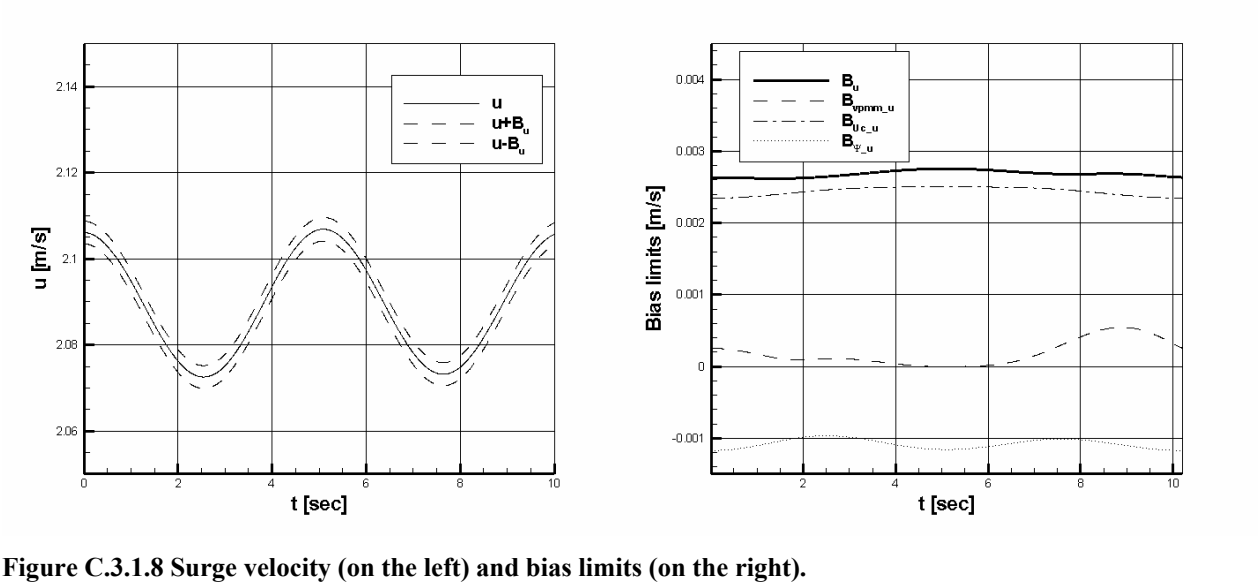

Figure C.3.1.8 Surge velocity (on the left) and bias limits (on the right).

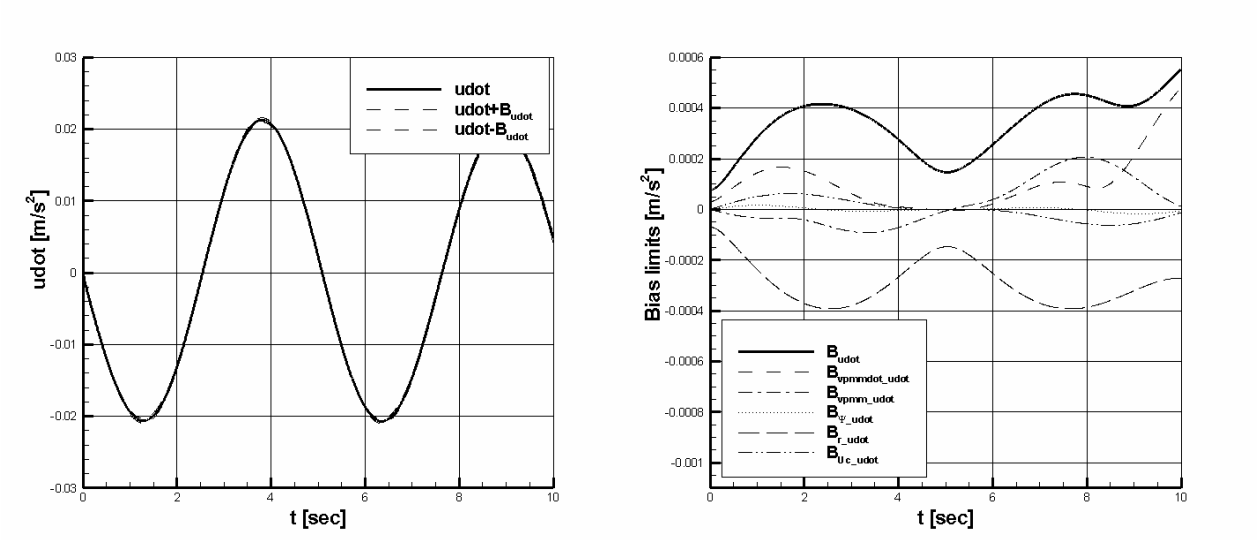

Figure C.3.1.9 Surge acceleration (on the left) and bias limits (on the right).

C.3.2 Longitudinal force

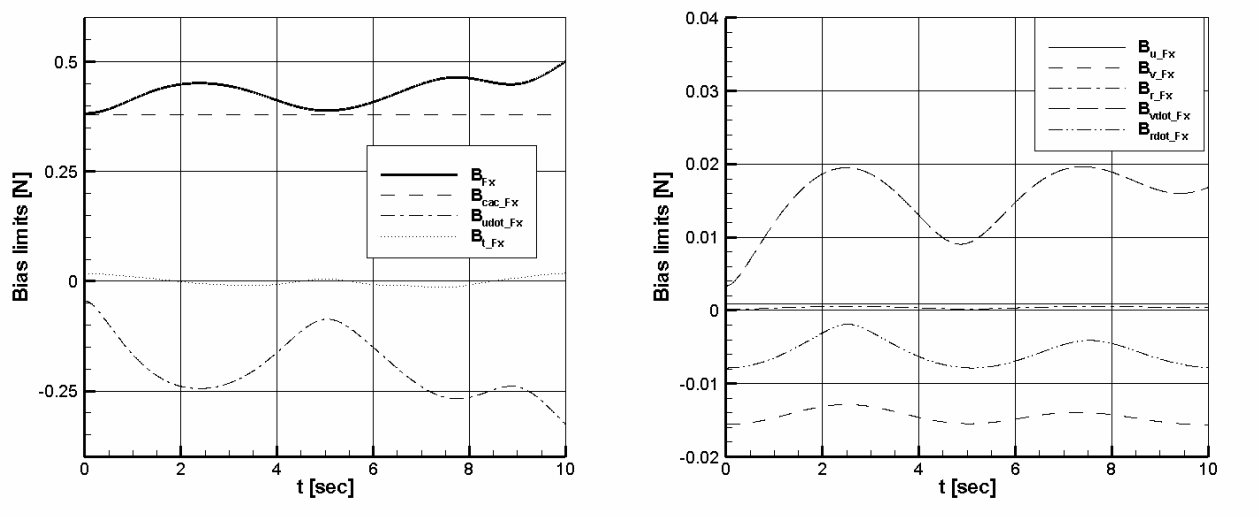

Figure C.3.2.1 Bias limits for measured X-force.

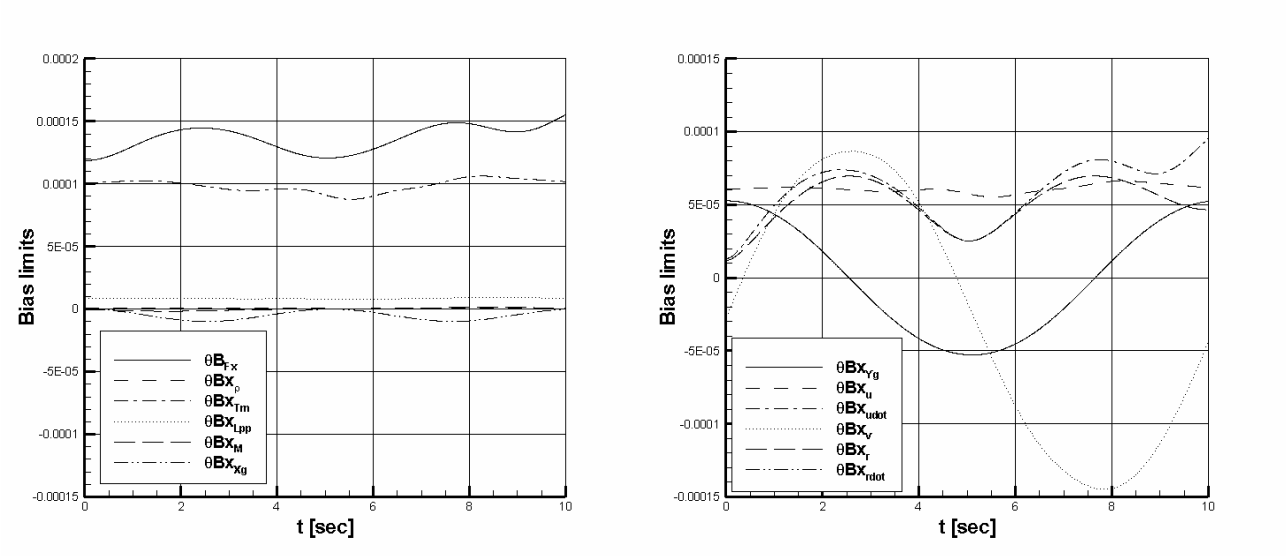

Figure C.3.2.2 Bias limits for X'.

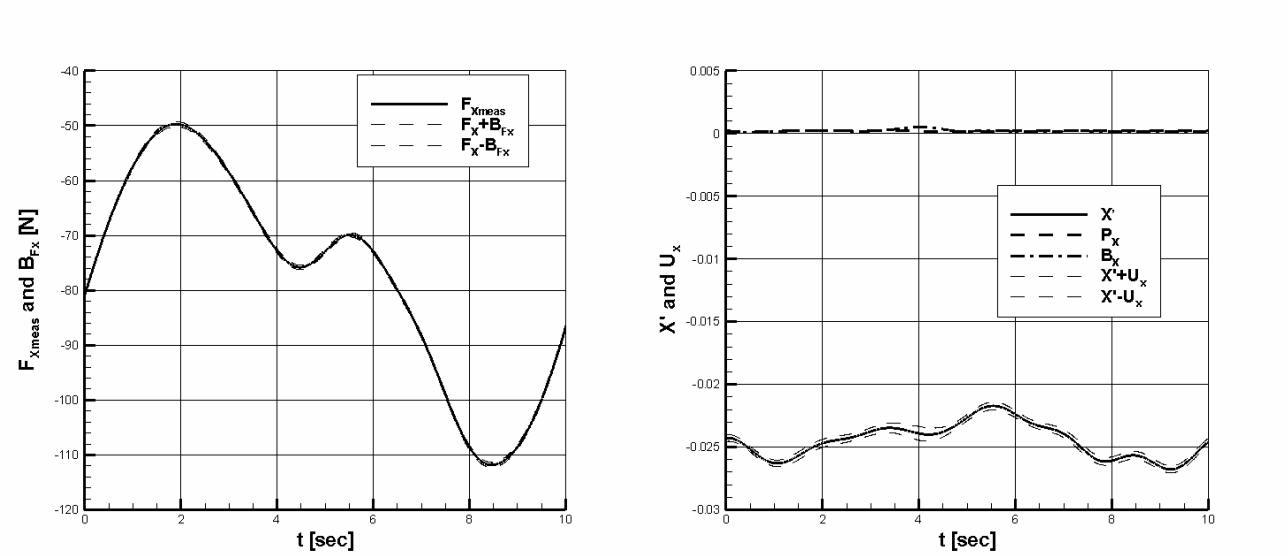

Figure C.3.2.3 Measured Fx and its bias limit (on the left); X' including uncertainty (on the right).

C.3.3 Transverse force

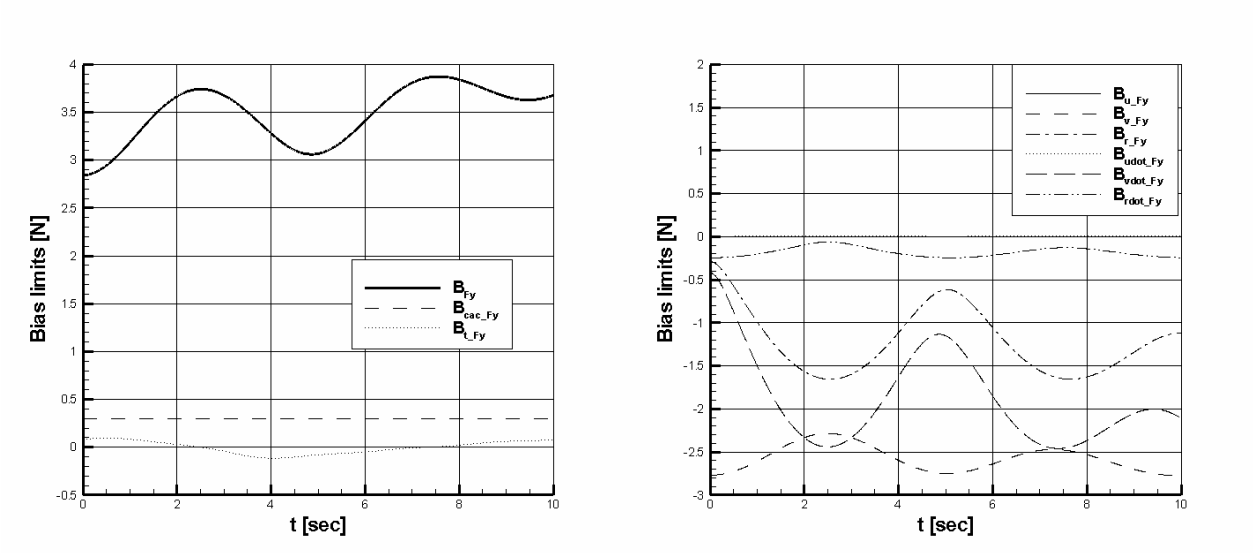

Figure C.3.3.1 Bias limits for measured Y-force.

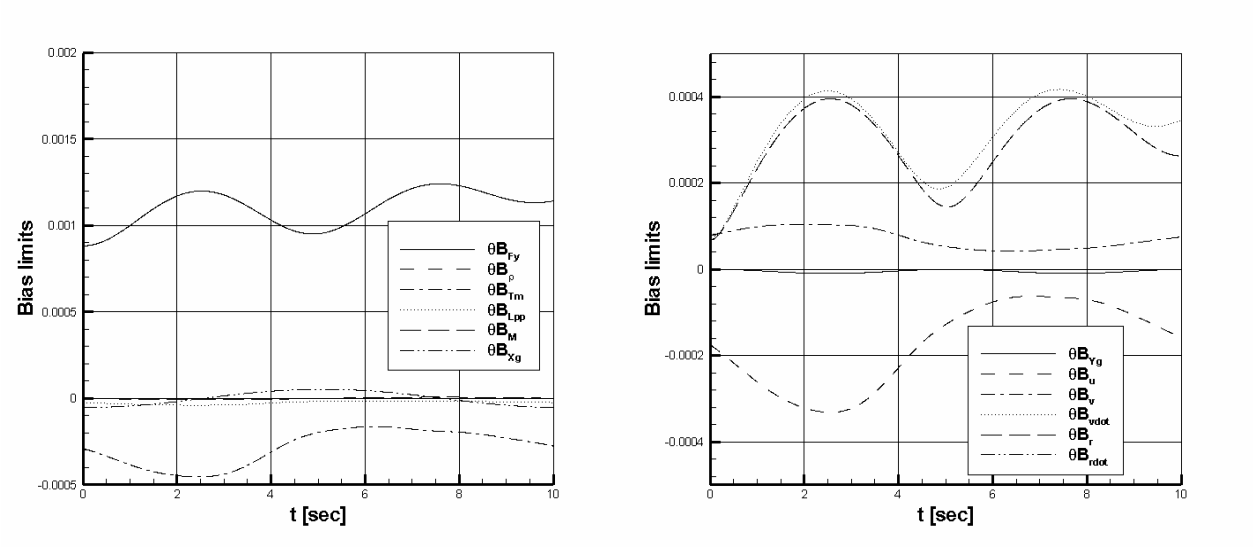

Figure C.3.3.2 Bias limits for Y'.

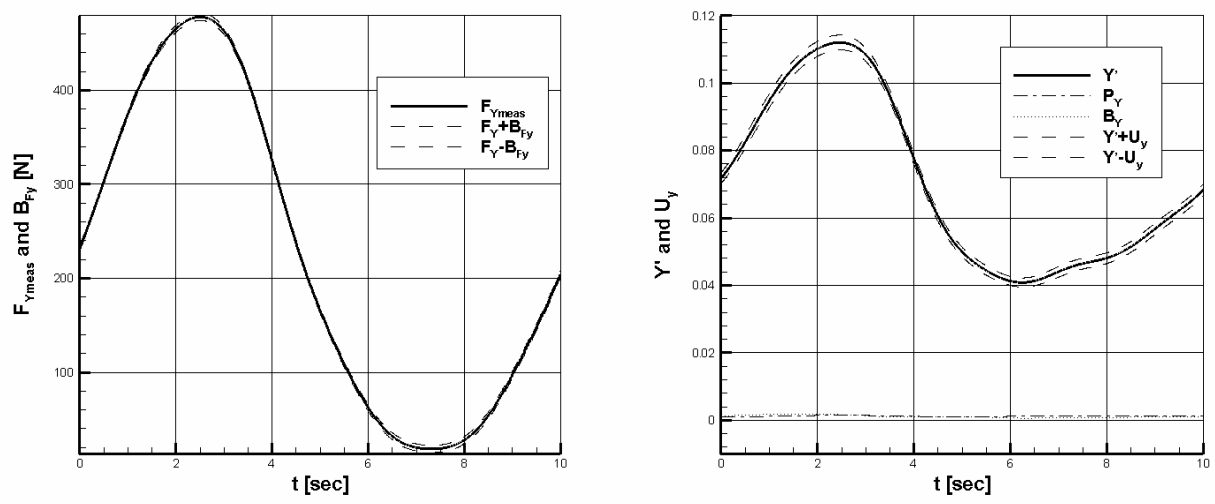

Figure C.3.3.3 Measured Fy and its bias limit (on the left); Y' including uncertainty (on the right).

C.3.4 Yaw moment

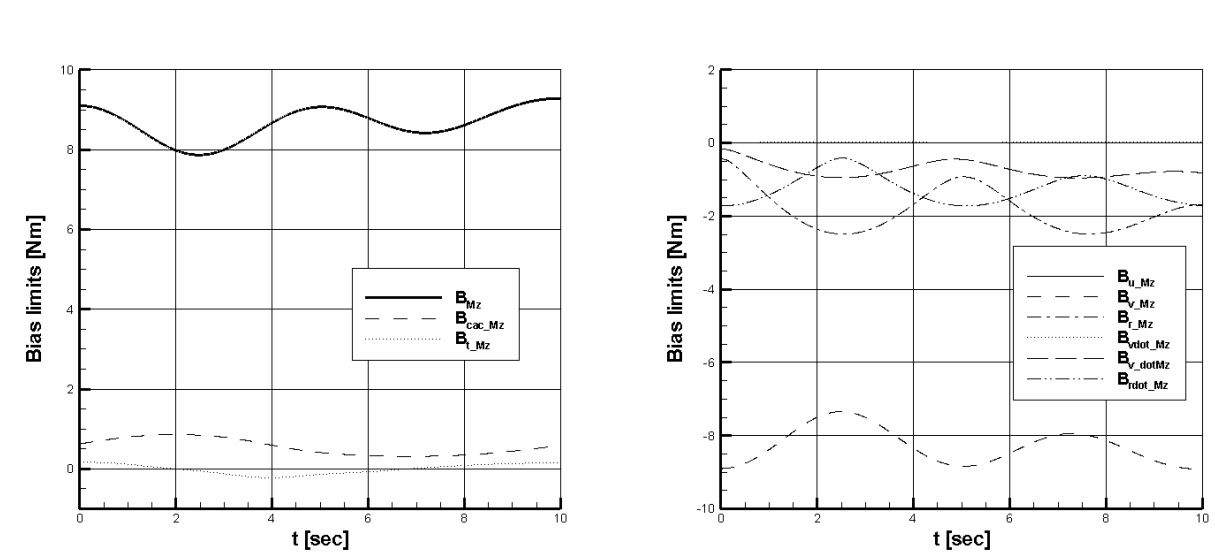

Figure C.3.4.1 Bias limits for measured yaw moment Mz.

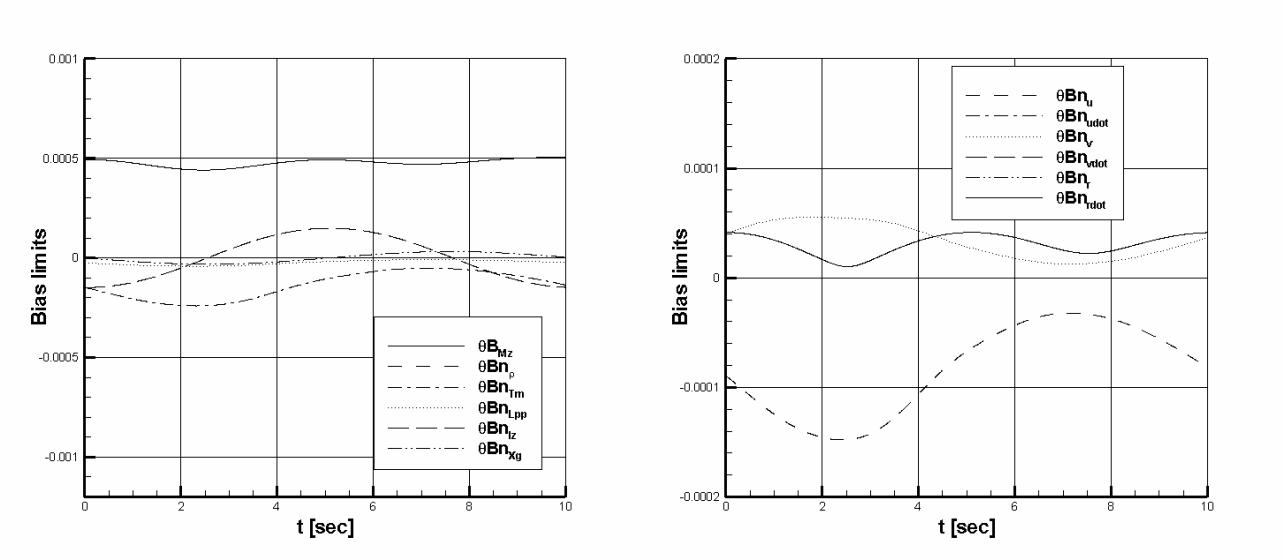

Figure C.3.4.2 Bias limits for N'.

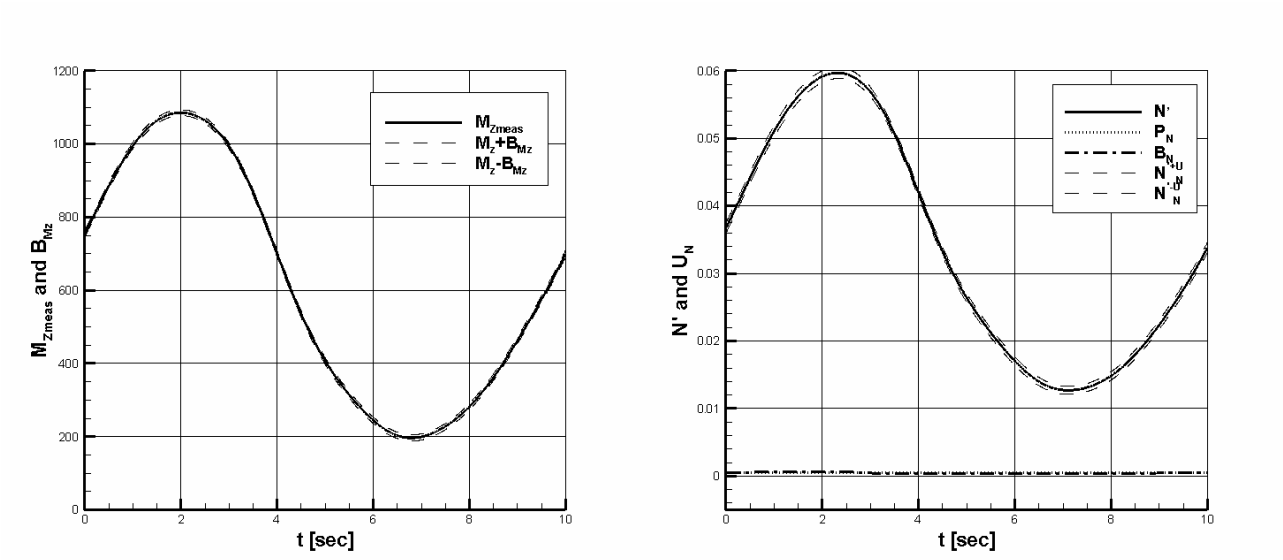

Figure C.3.4.3 Measured Mz and its bias limit (on the left); N' including uncertainty (on the right).

C.4 *Dynamic test (Pure yaw), Fr=0.138*

C.4.1 Motion parameters

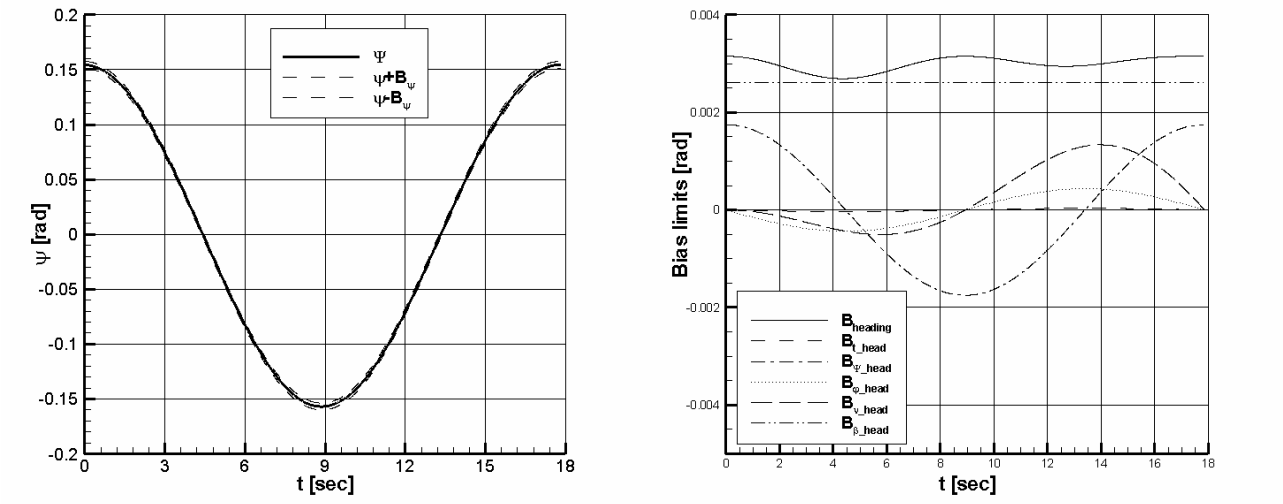

Figure C.4.1.1 Heading angle (on the left) and bias limits (on the right).

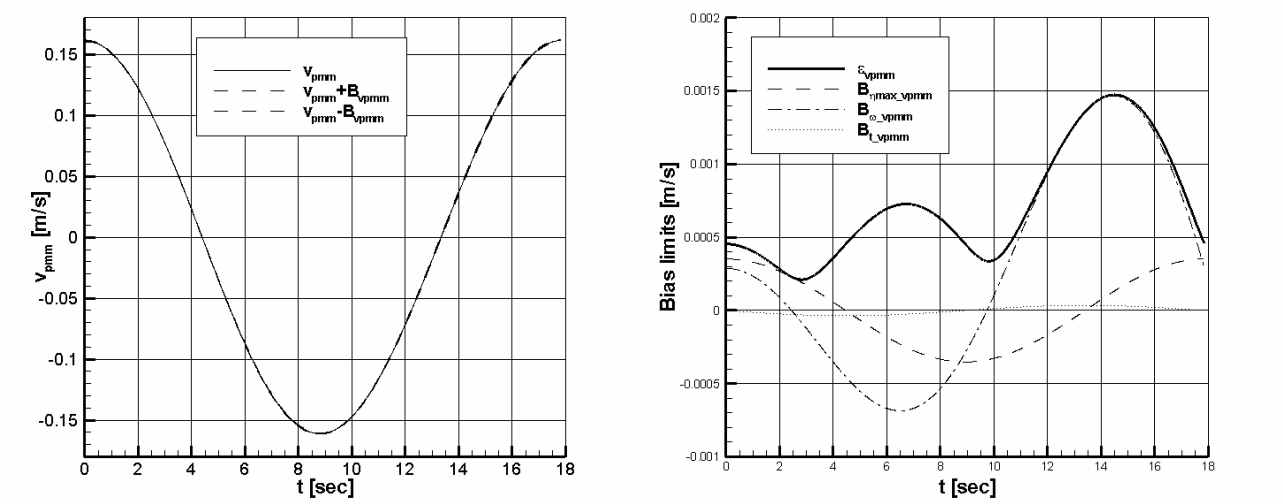

Figure C.4.1.2 Transverse PMM velocity (on the left) and bias limits (on the right).

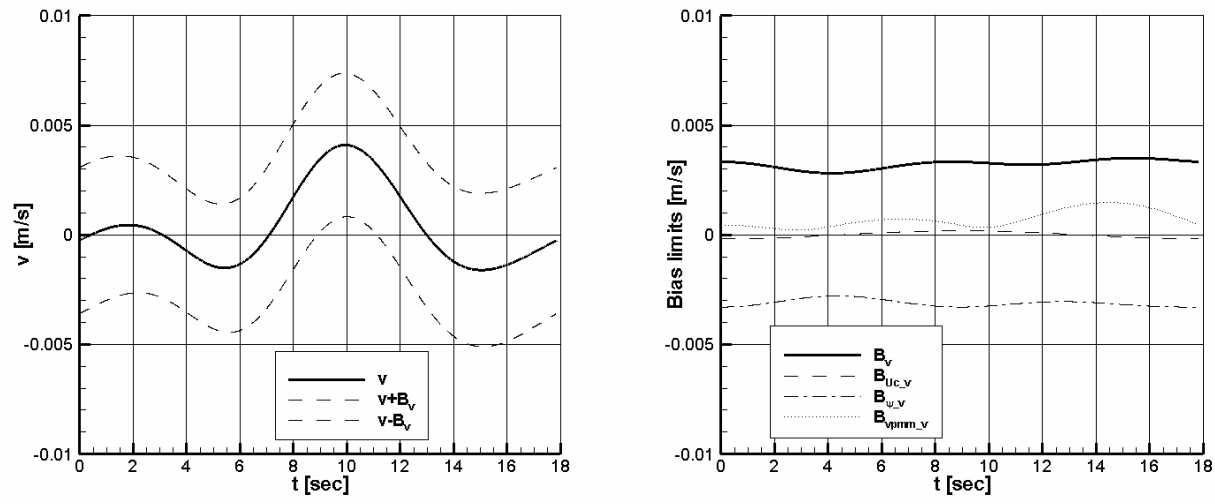

Figure C.4.1.3 Sway velocity (on the left) and bias limits (on the right).

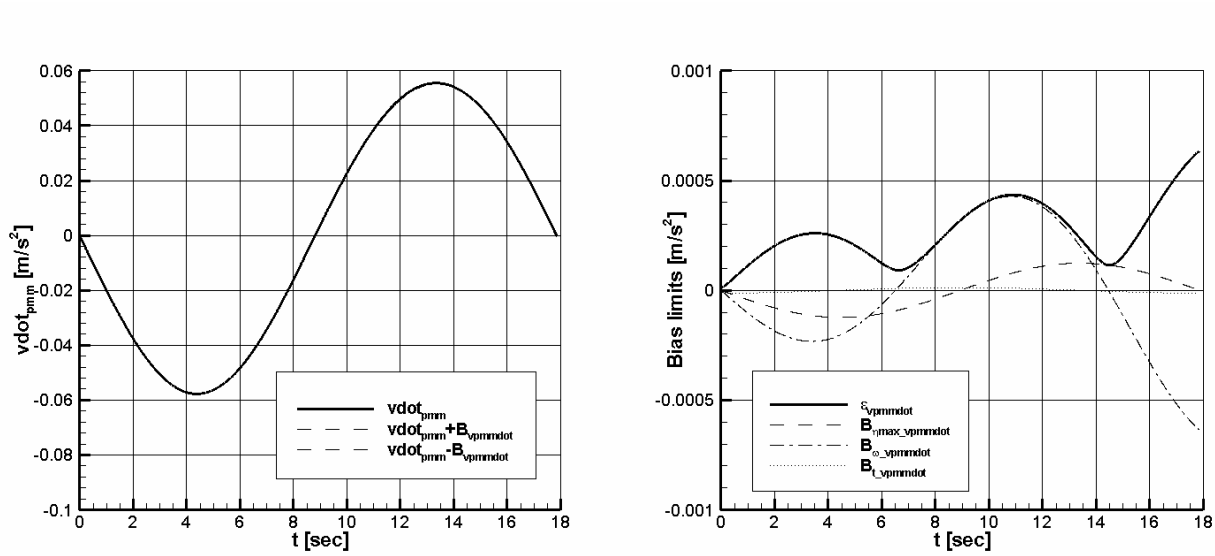

Figure C.4.1.4 Transverse PMM acceleration (on the left) and bias limits (on the right).

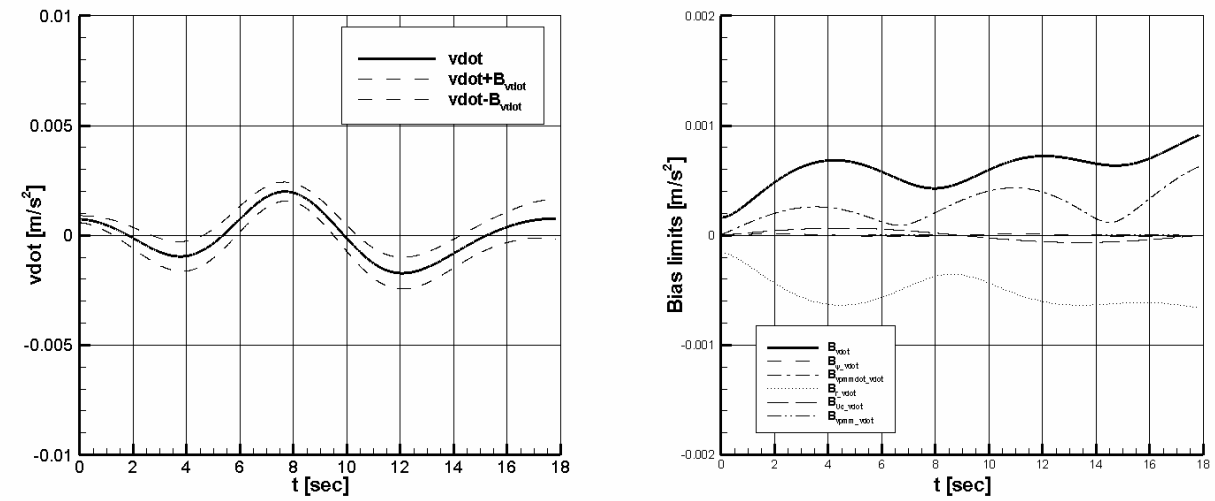

Figure C.4.1.5 Sway acceleration (on the left) and bias limits (on the right).

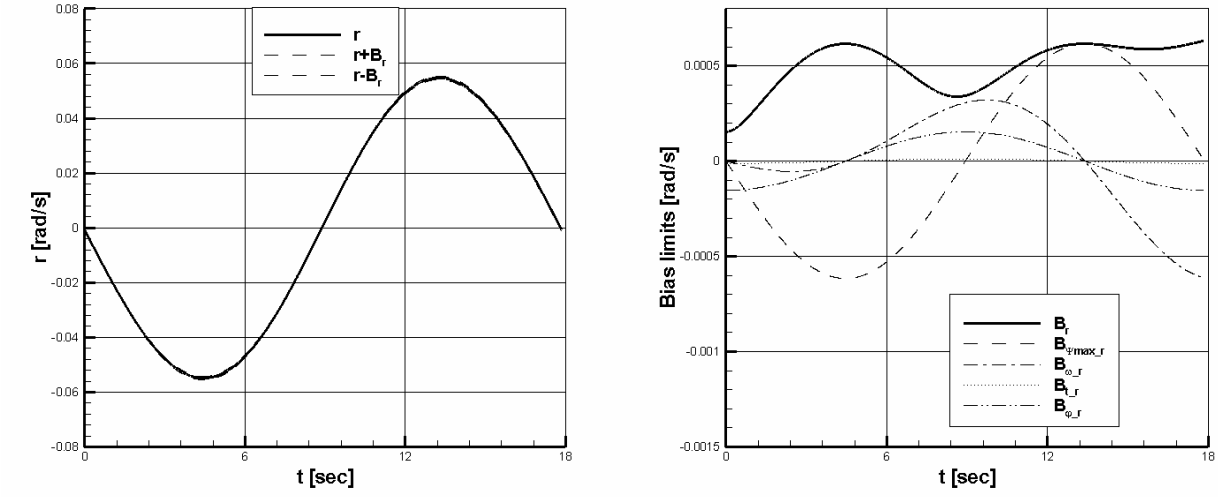

Figure C.4.1.6 Yaw rate (on the left) and bias limits (on the right).

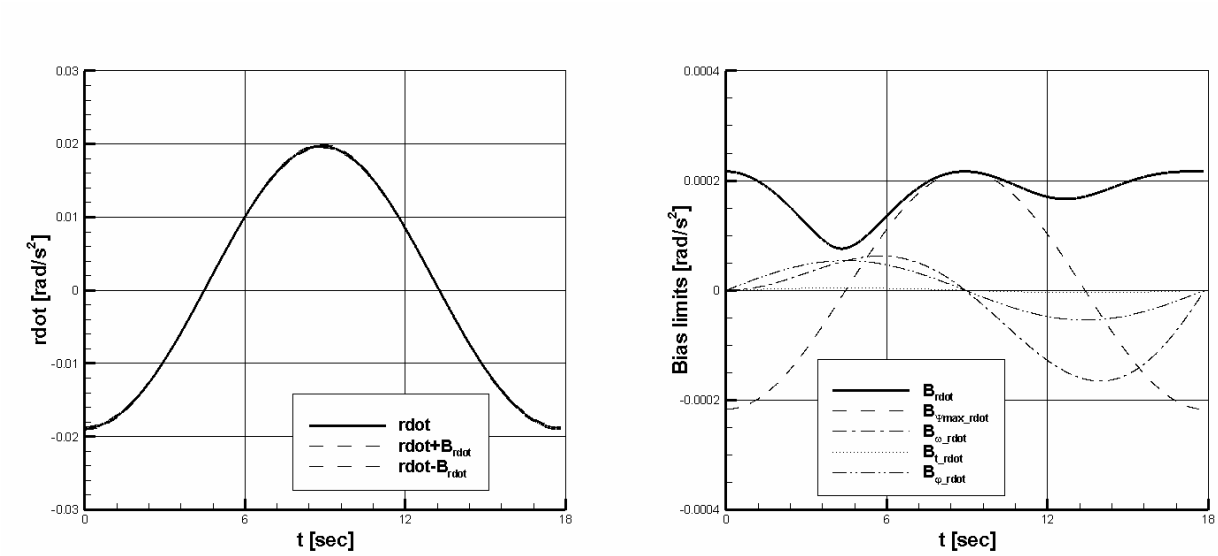

Figure C.4.1.7 Yaw acceleration (on the left) and bias limits (on the right).

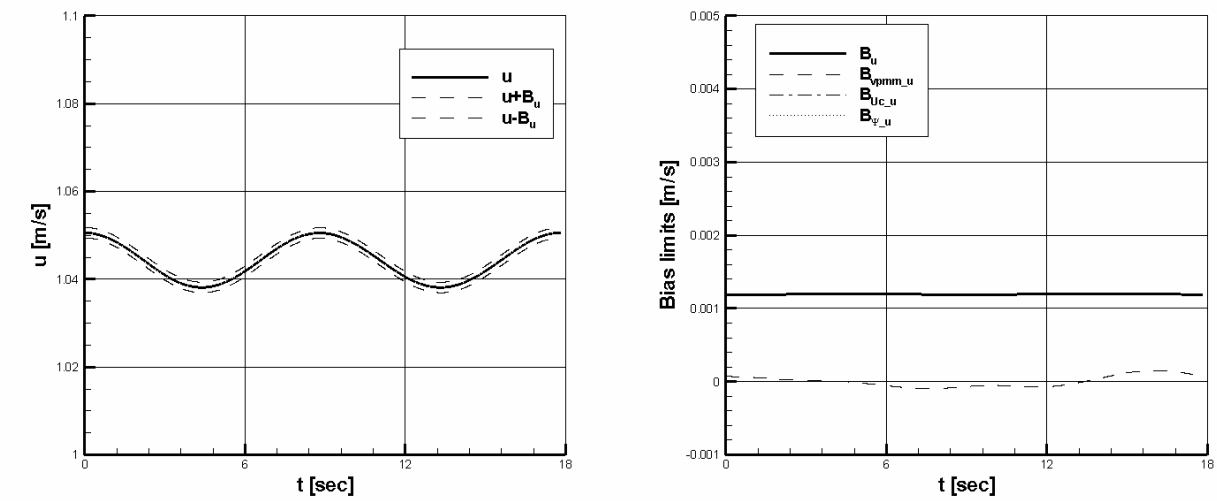

Figure C.4.1.8 Surge velocity (on the left) and bias limits (on the right).

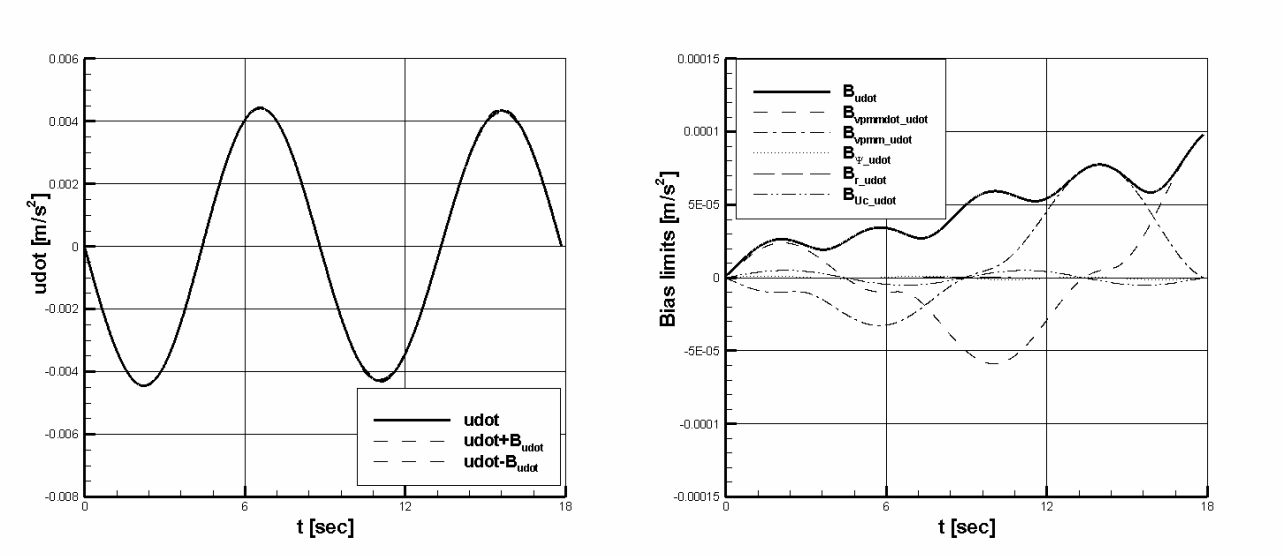

Figure C.4.1.9 Surge acceleration (on the left) and bias limits (on the right).

C.4.2 Longitudinal force

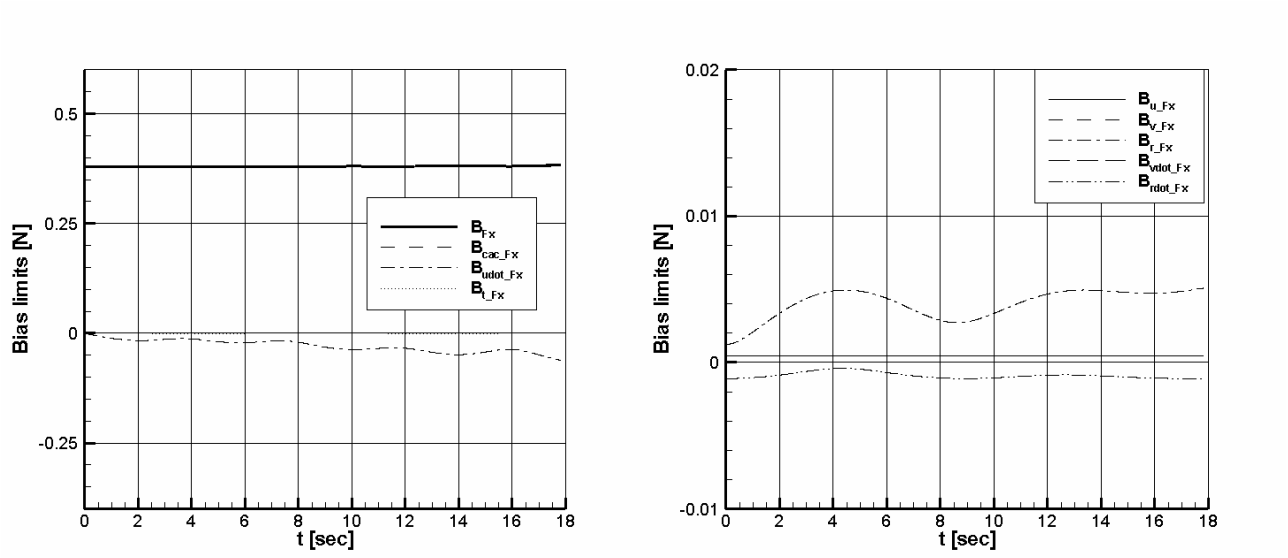

Figure C.4.2.1 Bias limits for measured X-force.

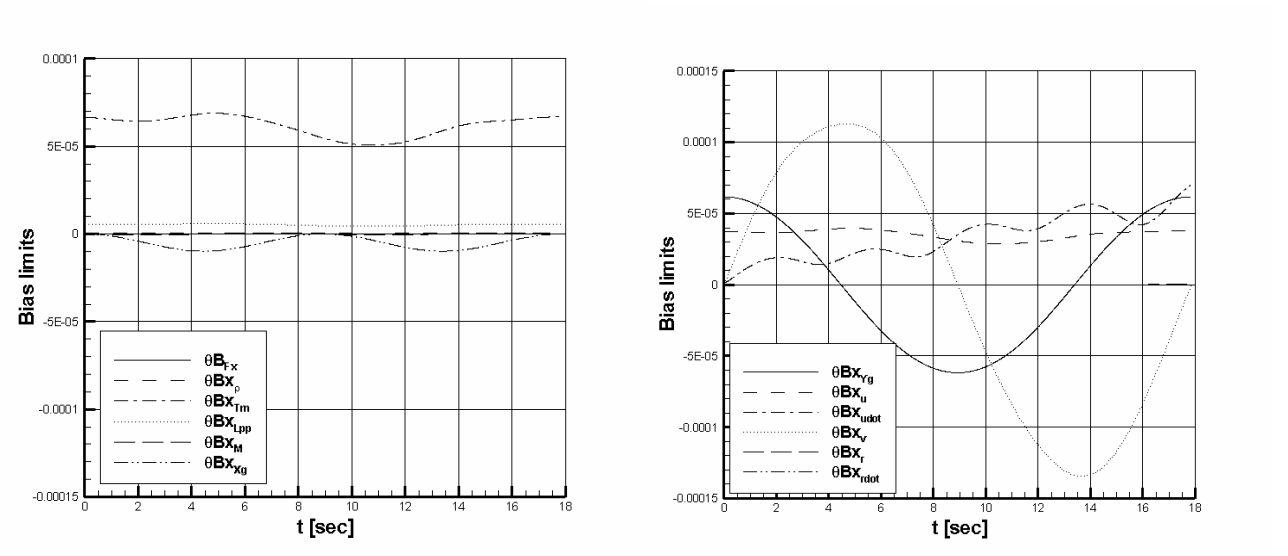

Figure C.4.2.2 Bias limits for X'.

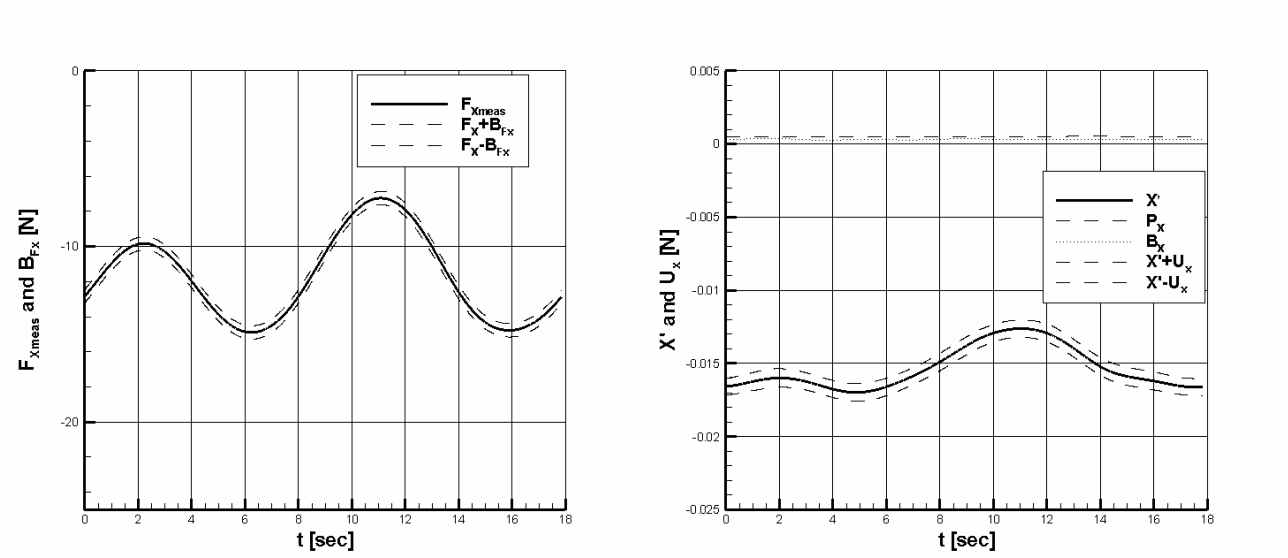

Figure C.4.2.3 Measured Fx and its bias limit (on the left); X' including uncertainty (on the right).

C.4.3 Transverse force

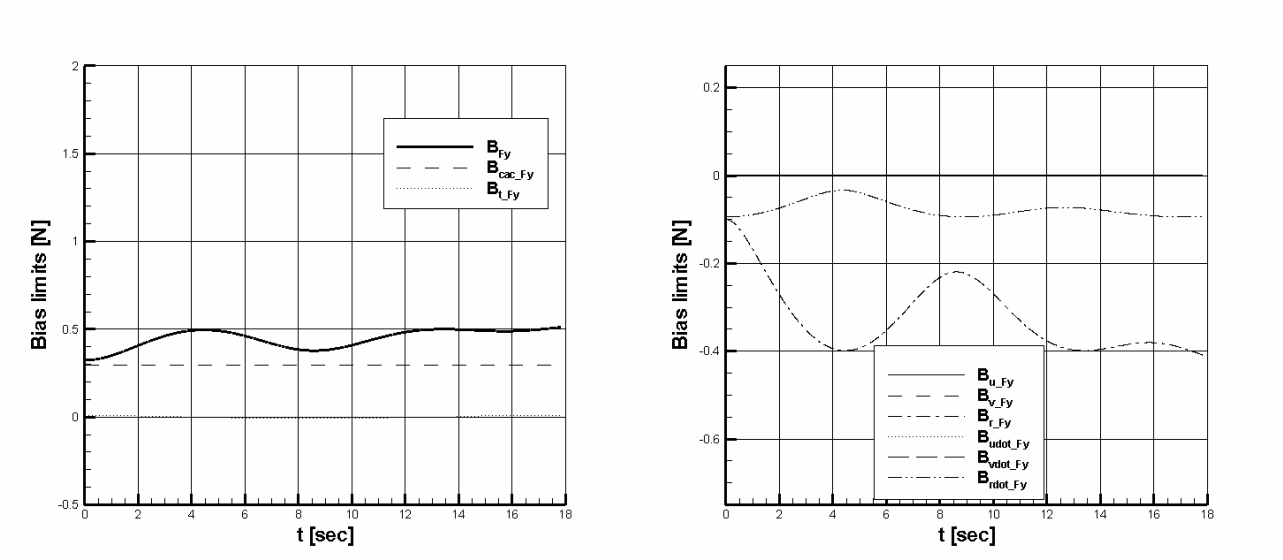

Figure C.4.3.1 Bias limits for measured Y-force.

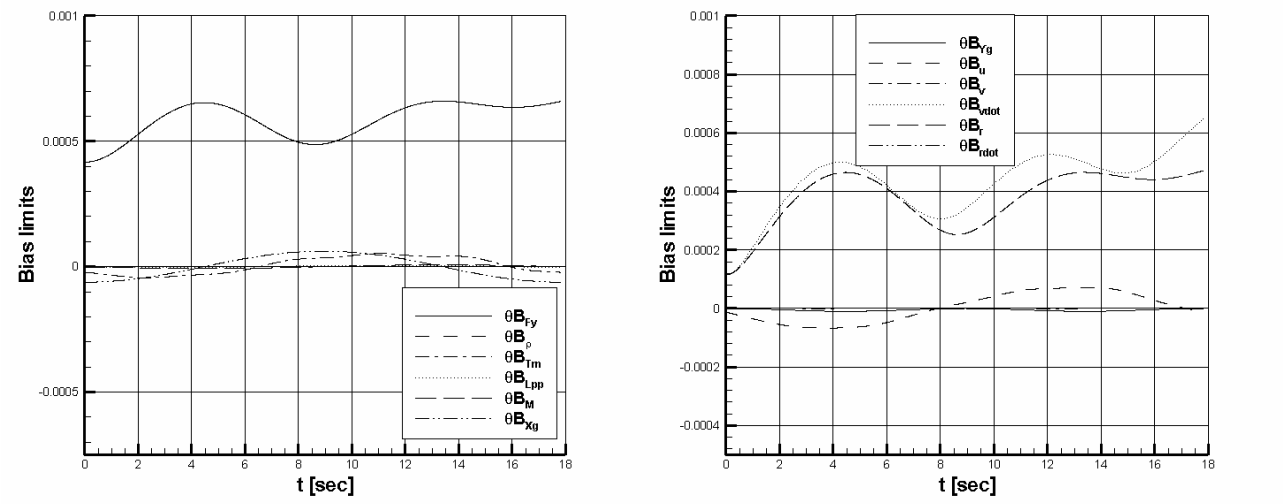

Figure C.4.3.2 Bias limits for Y'.

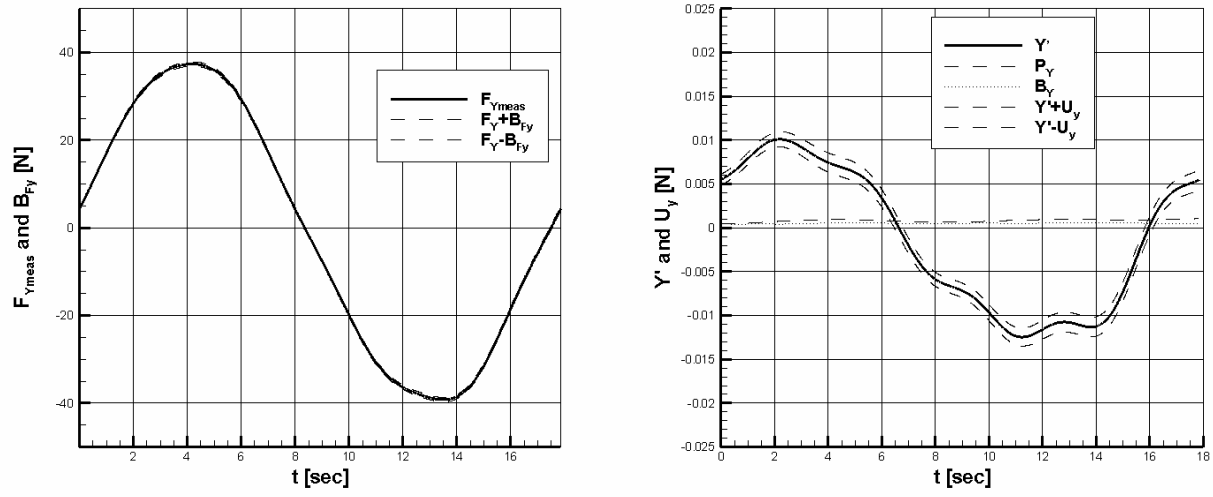

Figure C.4.3.3 Measured Fy and its bias limit (on the left); Y' including uncertainty (on the right).

C.4.4 Yaw moment

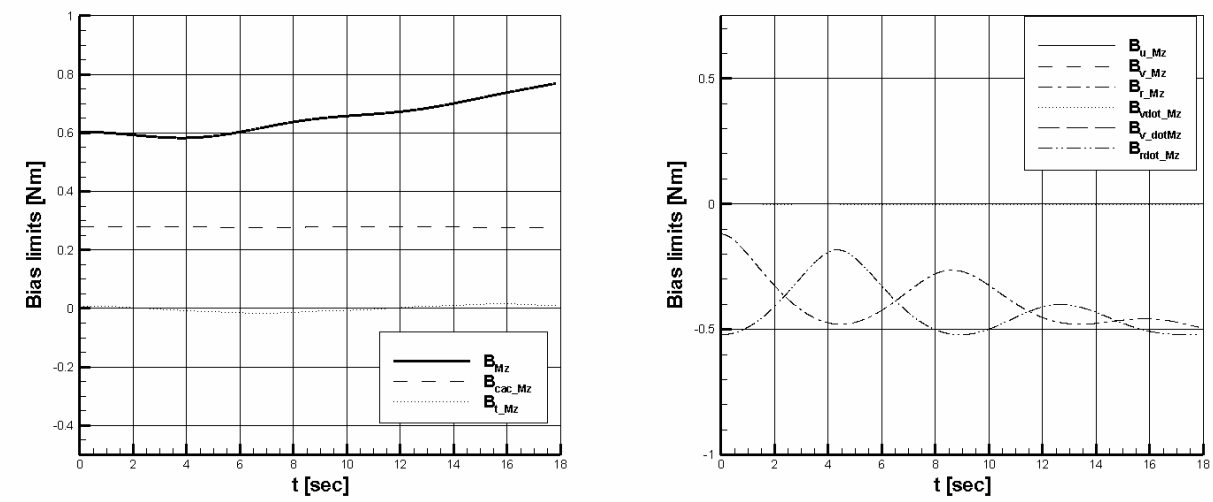

Figure C.4.4.1 Bias limits for measured yaw moment Mz.

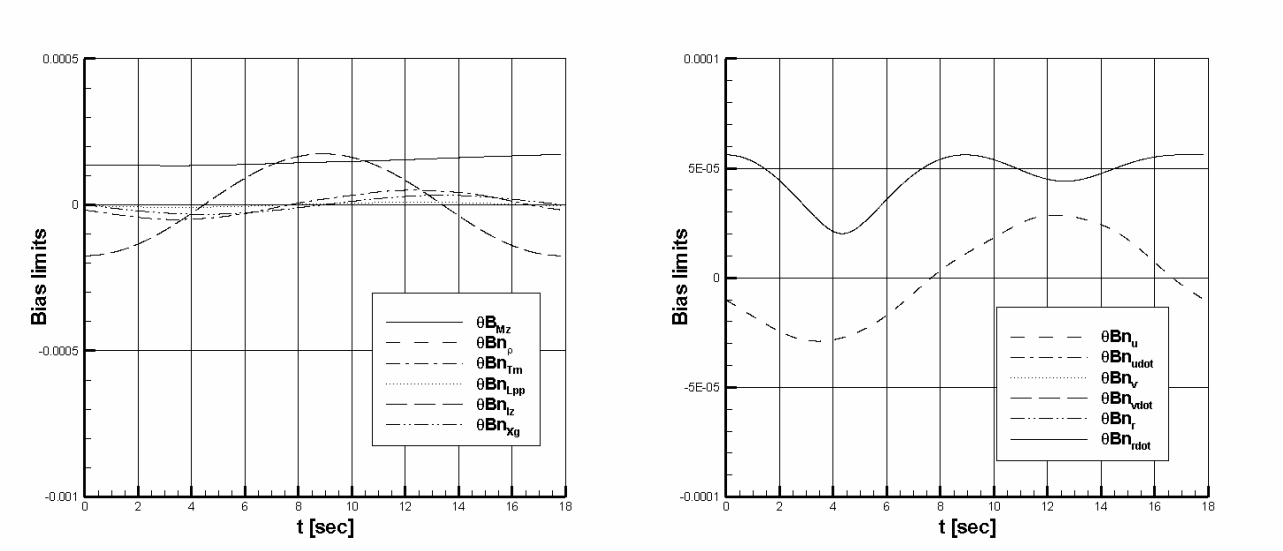

Figure C.4.4.2 Bias limits for N'.

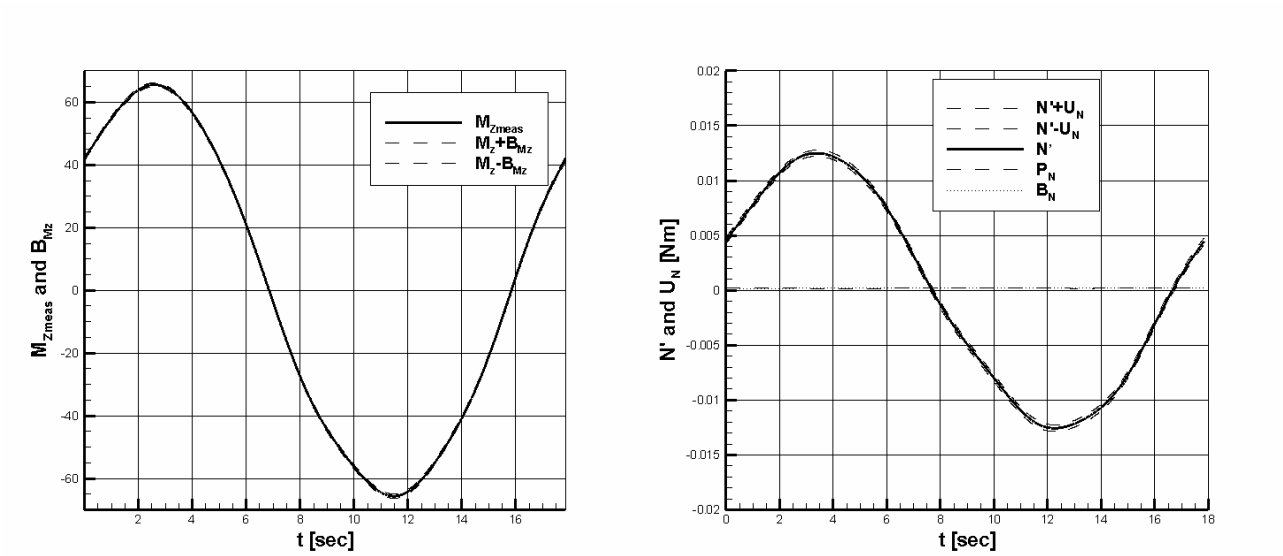

Figure C.4.4.3 Measured Mz and its bias limit (on the left); N' including uncertainty (on the right).

C.5 *Dynamic test (Pure yaw), Fr = 0.410*

C.5.1 Motion parameters

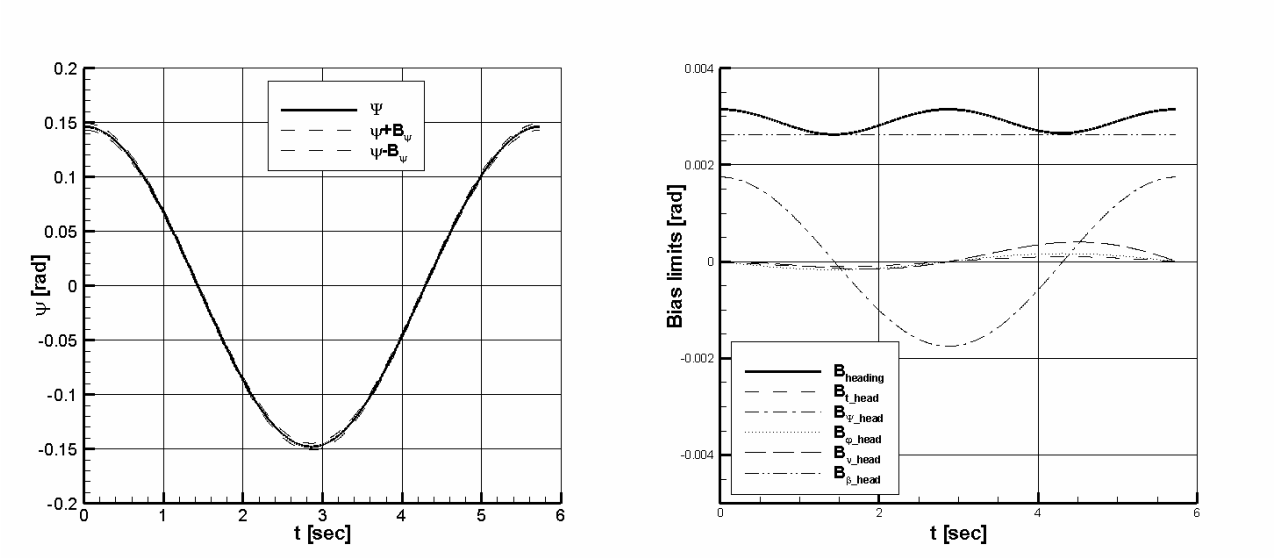

Figure C.5.1.1 Heading angle (on the left) and bias limits (on the right).

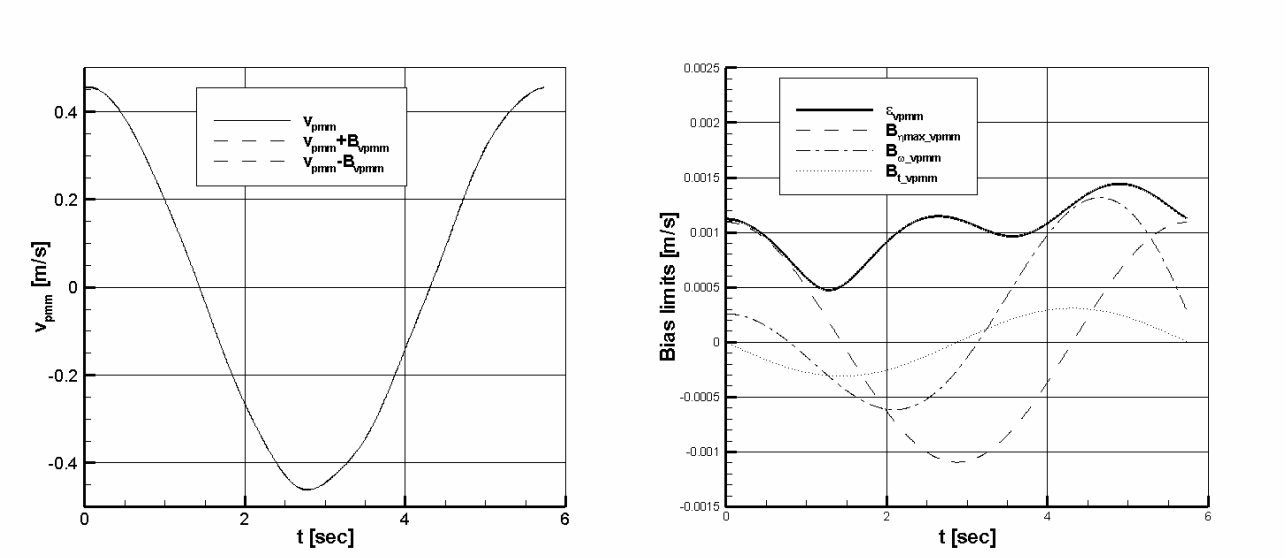

Figure C.5.1.2 Transverse PMM velocity (on the left) and bias limits (on the right).

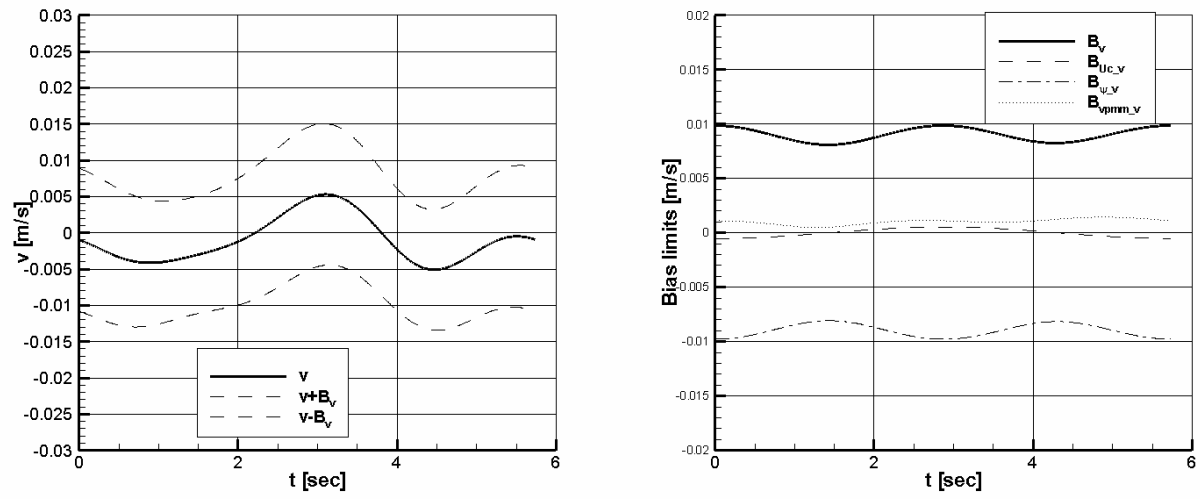

Figure C.5.1.3 Sway velocity (on the left) and bias limits (on the right).

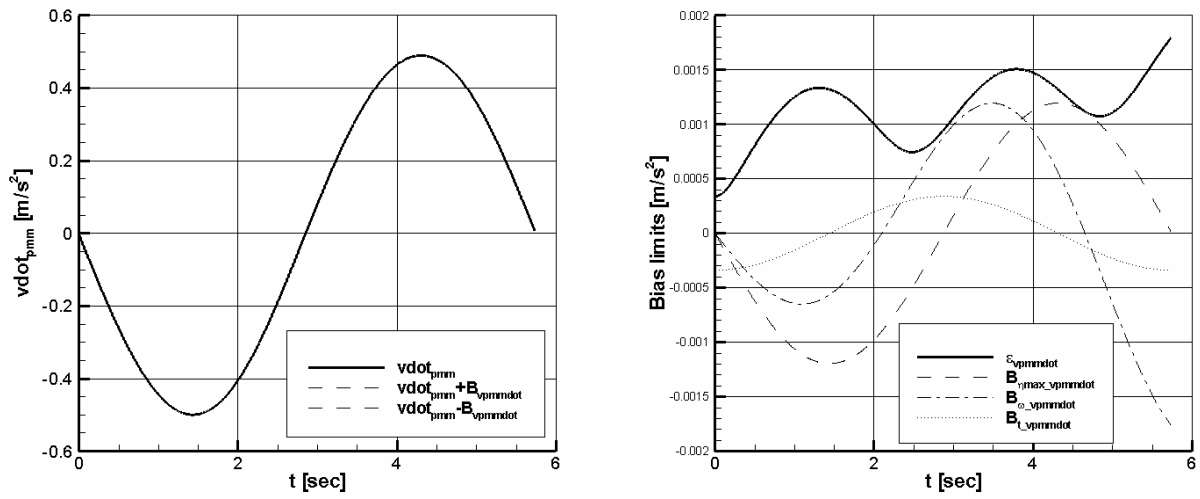

Figure C.5.1.4 Transverse PMM acceleration (on the left) and bias limits (on the right).

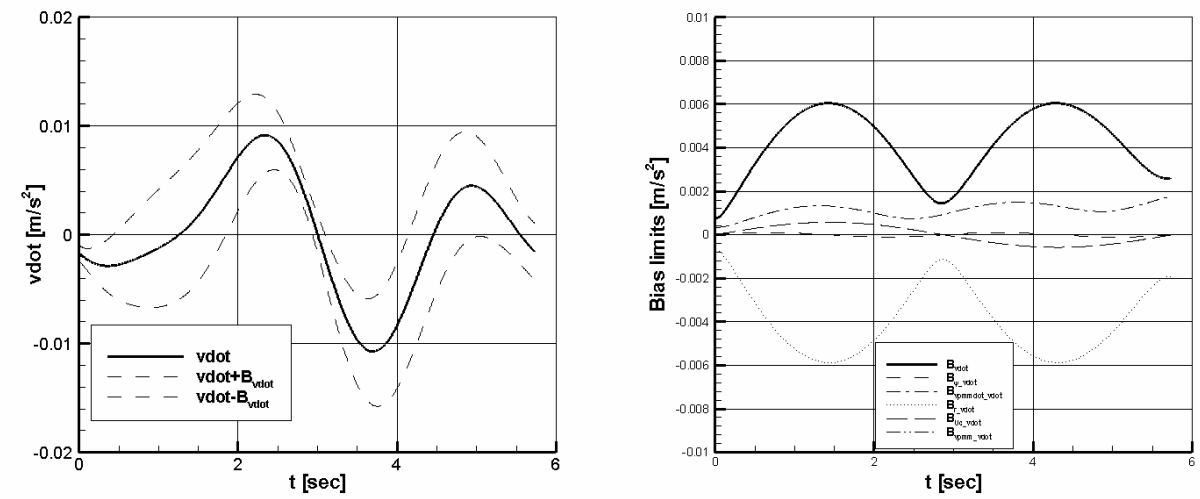

Figure C.5.1.5 Sway acceleration (on the left) and bias limits (on the right).

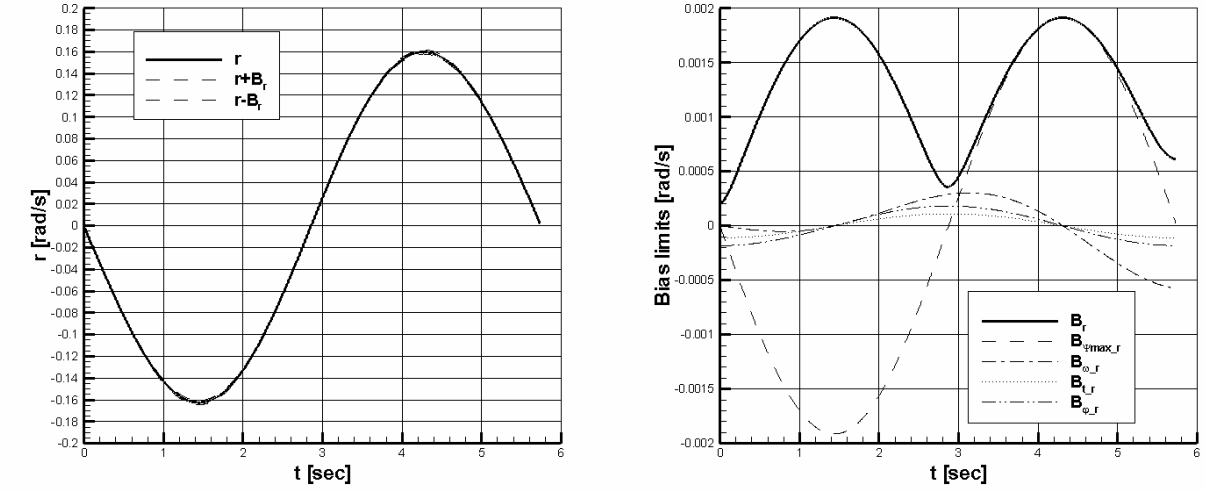

Figure C.5.1.6 Yaw rate (on the left) and bias limits (on the right).

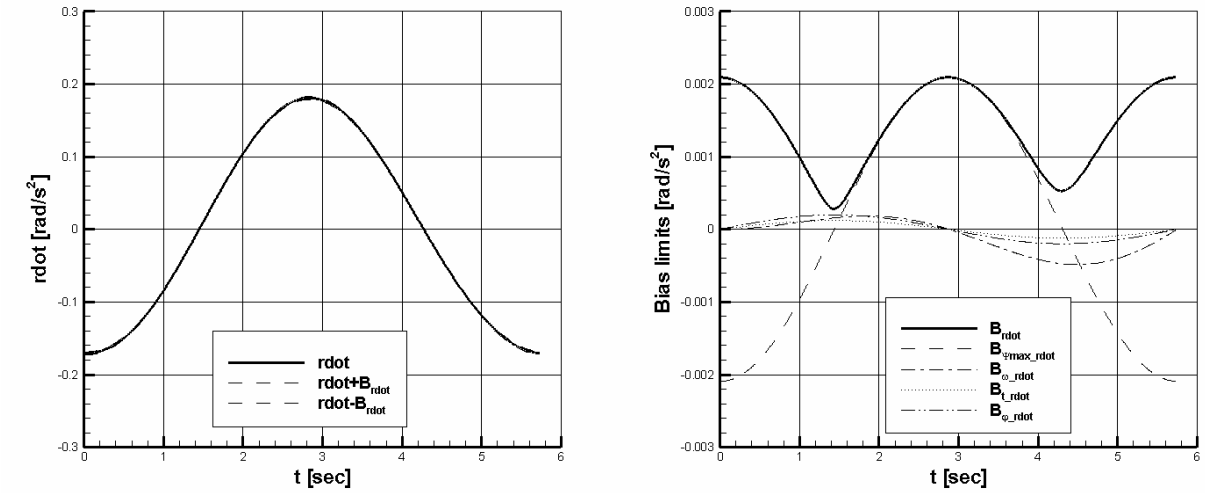

Figure C.5.1.7 Yaw acceleration (on the left) and bias limits (on the right).

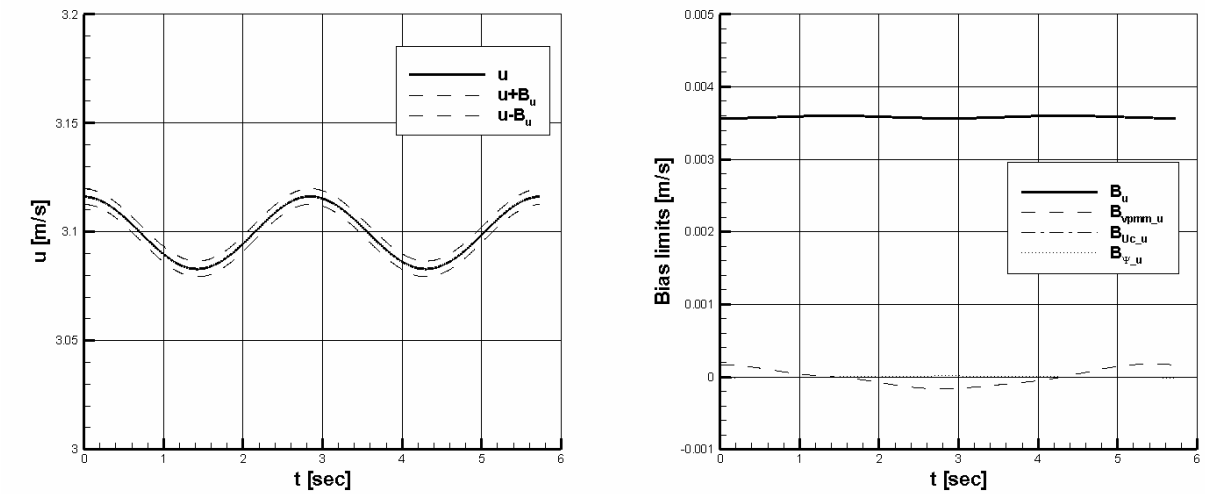

Figure C.5.1.8 Surge velocity (on the left) and bias limits (on the right).

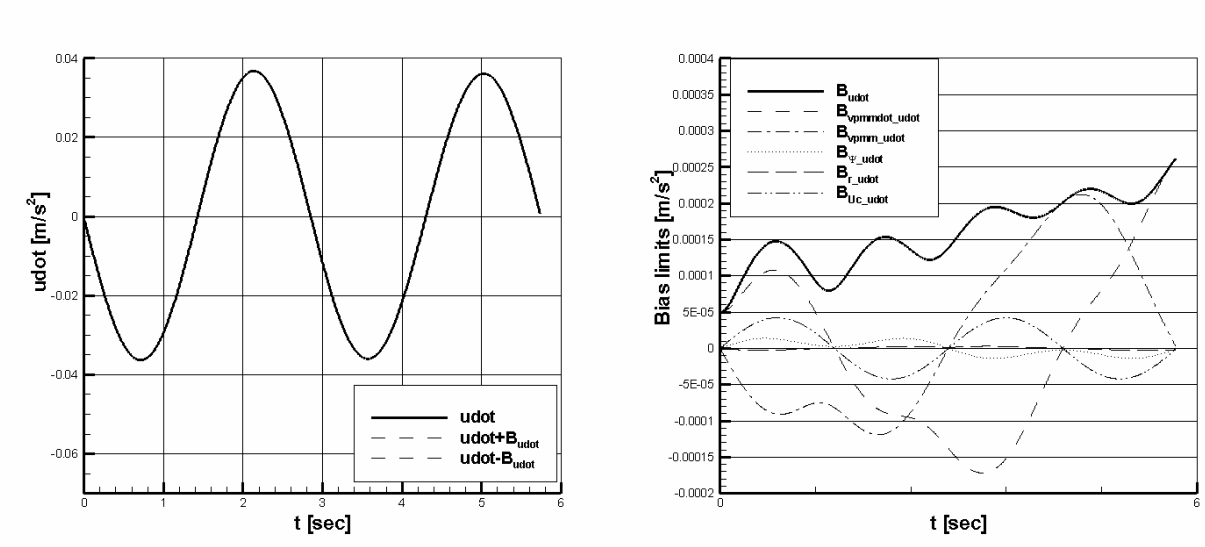

Figure C.5.1.9 Surge acceleration (on the left) and bias limits (on the right).

C.5.2 Longitudinal force

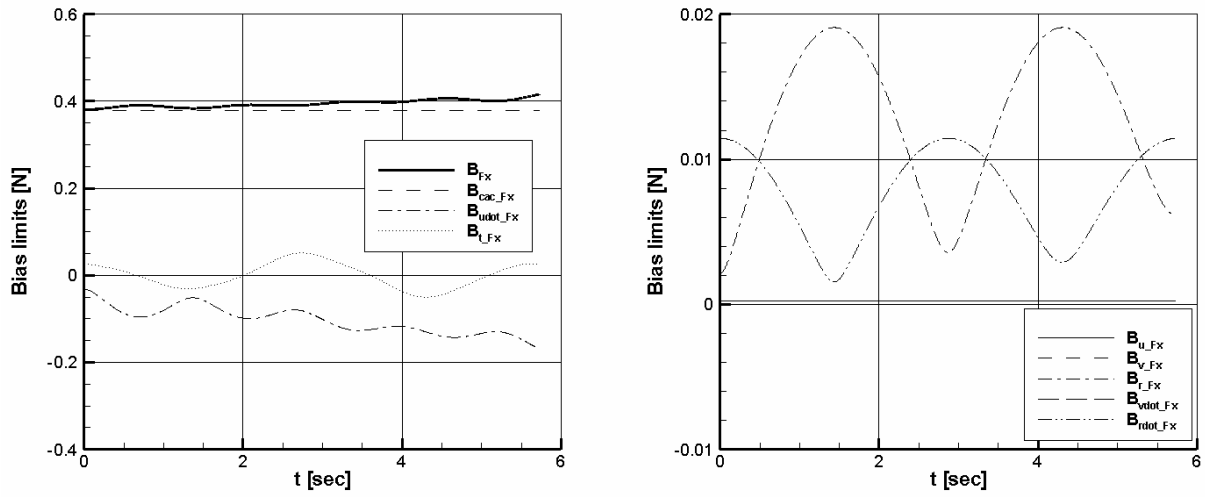

Figure C.5.2.1 Bias limits for measured X-force.

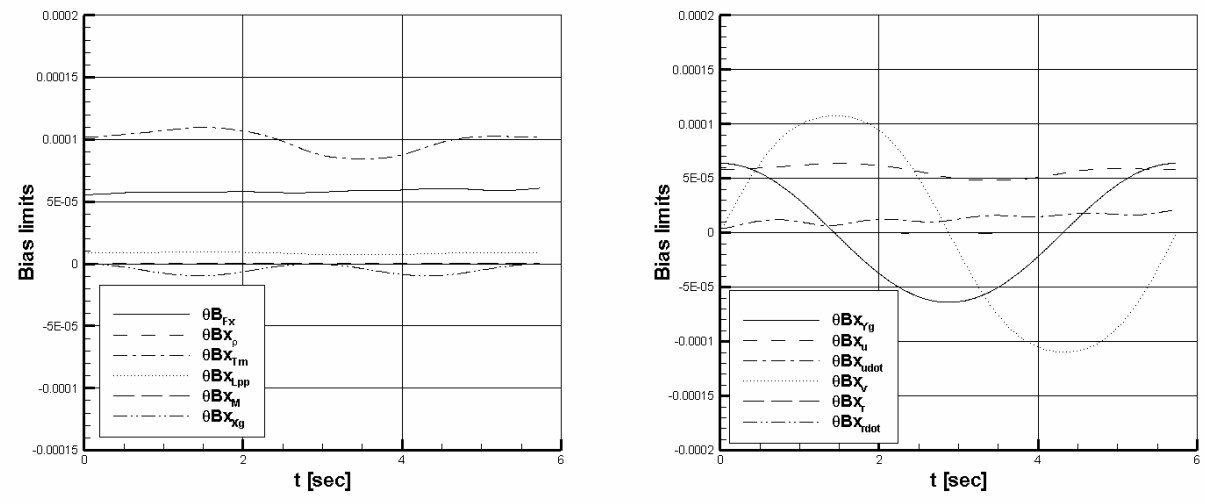

Figure C.5.2.2 Bias limits for X'.

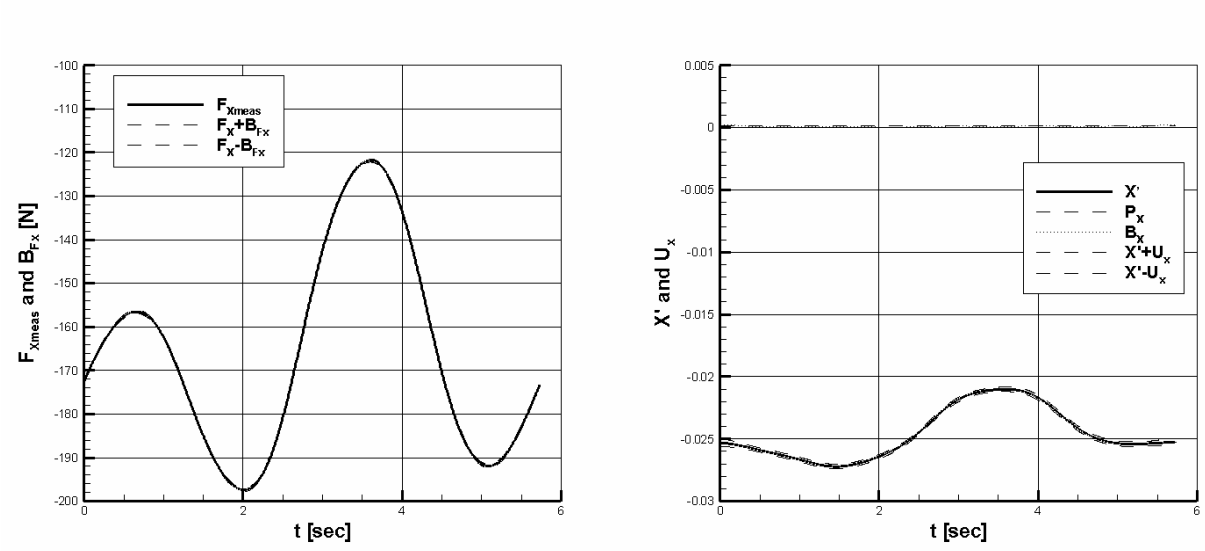

Figure C.5.2.3 Measured Fx and its bias limit (on the left); X' including uncertainty (on the right).

C.5.3 Transverse force

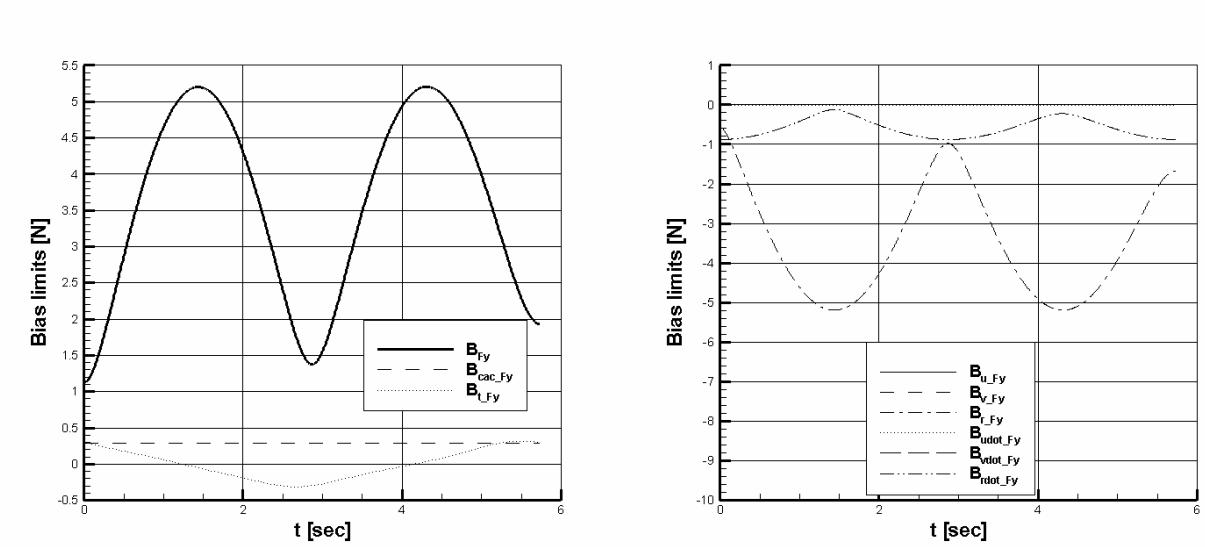

Figure C.5.3.1 Bias limits for measured Y-force.

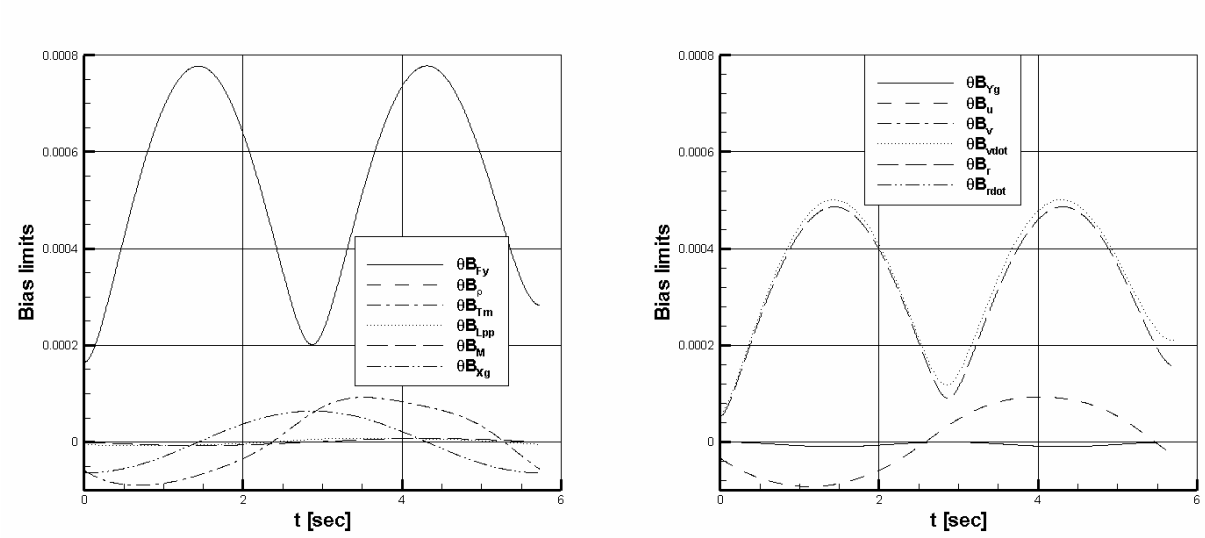

Figure C.5.3.2 Bias limits for Y'.

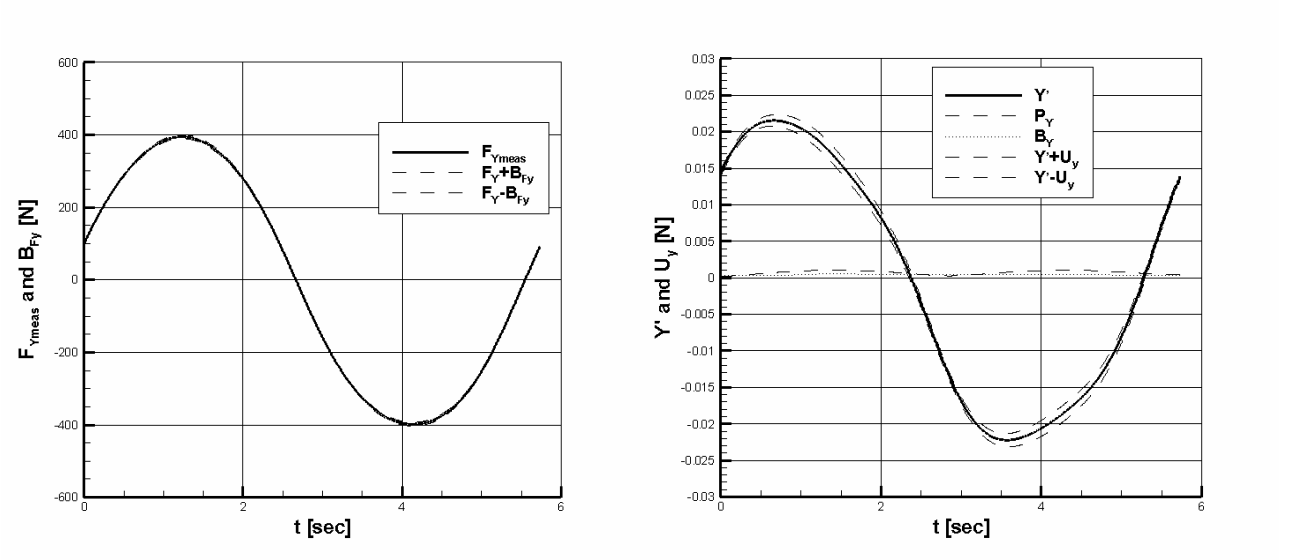

Figure C.5.3.3 Measured Fy and its bias limit (on the left); Y' including uncertainty (on the right).

C.5.4 Yaw moment

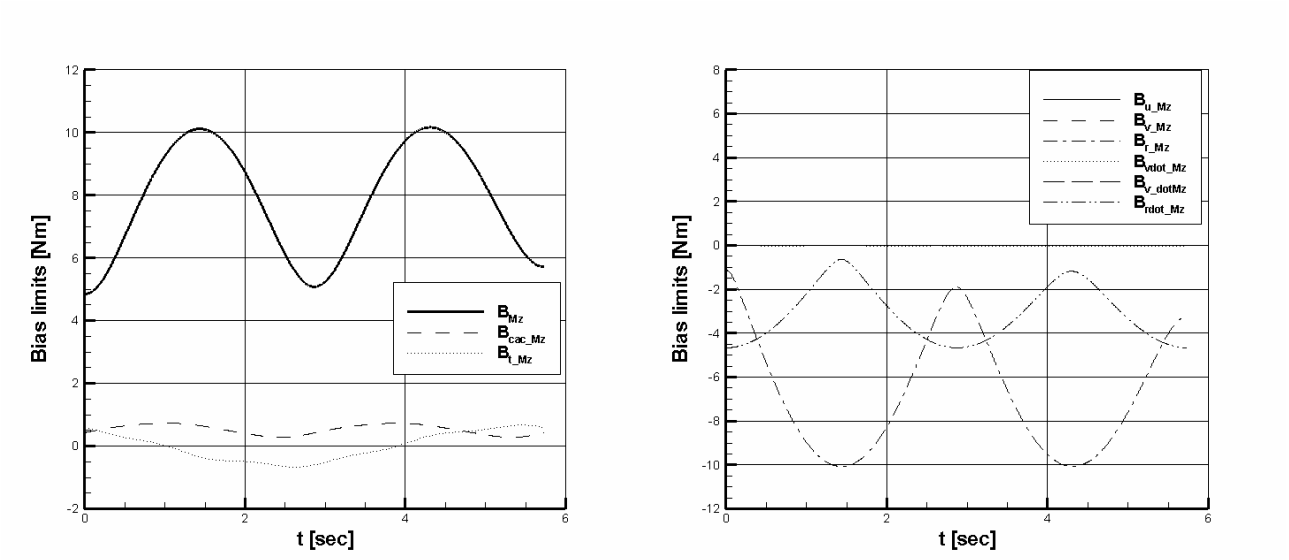

Figure C.5.4.1 Bias limits for measured yaw moment Mz.

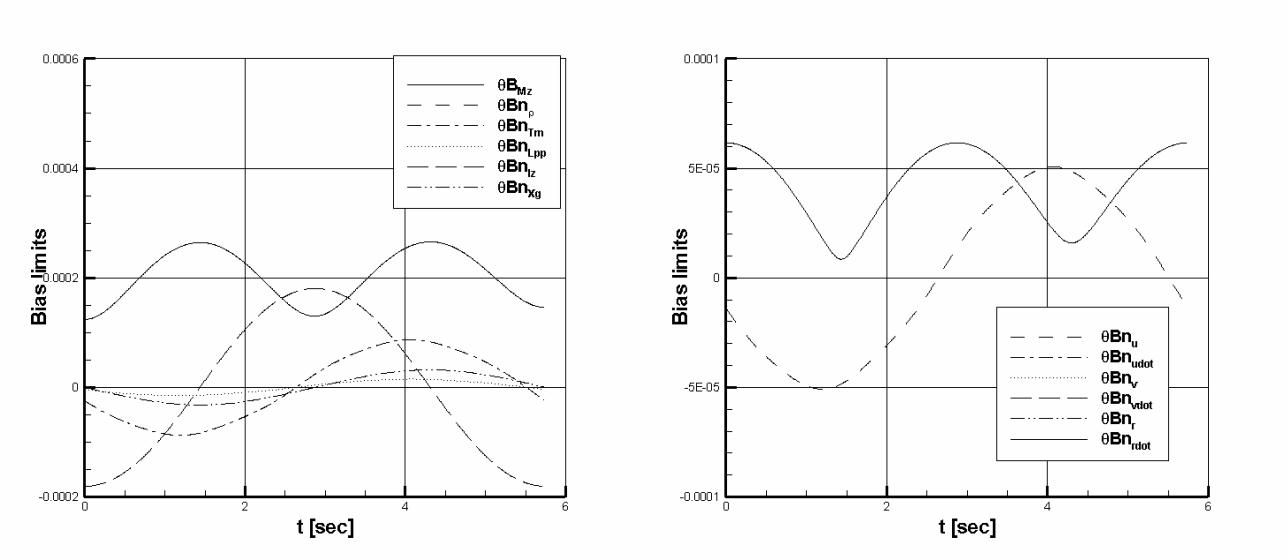

Figure C.5.4.2 Bias limits for N'.

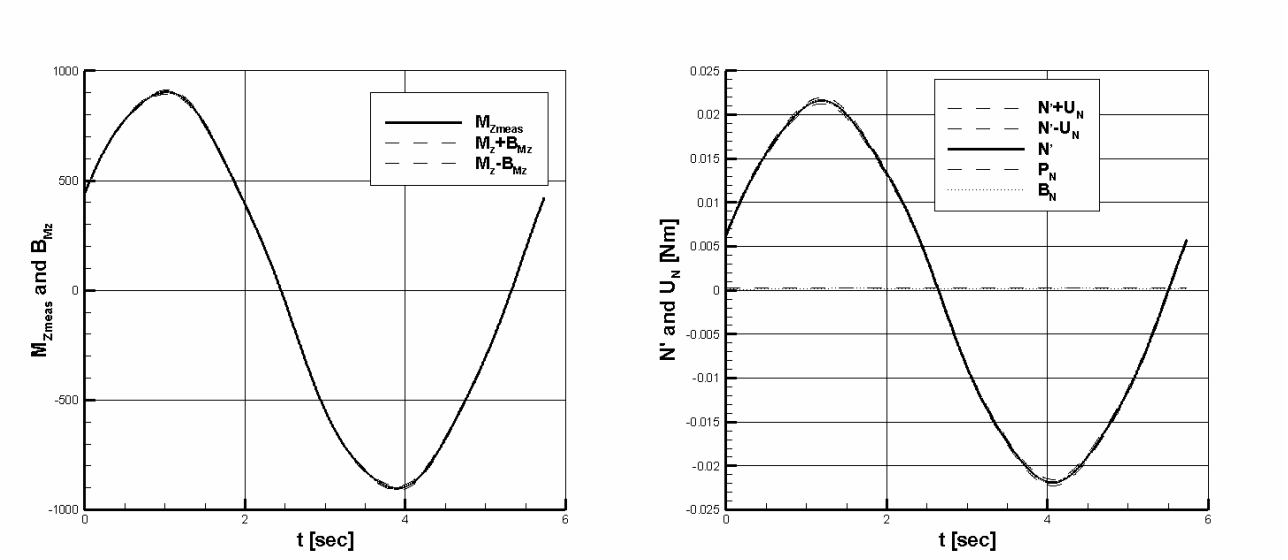

Figure C.5.4.3 Measured Mz and its bias limit (on the left); N' including uncertainty (on the right).

C.6 *Results from dynamic tests without uncertainty assessment*

This appendix shows the time series for all the dynamic cases which are not dealt with in the uncertainty analysis. Each condition is marked with a time series number printed at the bottom of each page. This number refers to the Run ID shown in the test program in Appendix A.

Quantities	Units
ψ	[rad]
y	[m]
r	[rad/s]
v	[m/s]
rdot	[rad/s^2]
vdot	[m/s^2]
u	[m/s]
Xp	[-]
Yp	[-]
Np	[-]
SinkAF	[m]
SinkFP	[m]

Table D. 1

C.6.1 List of Figures

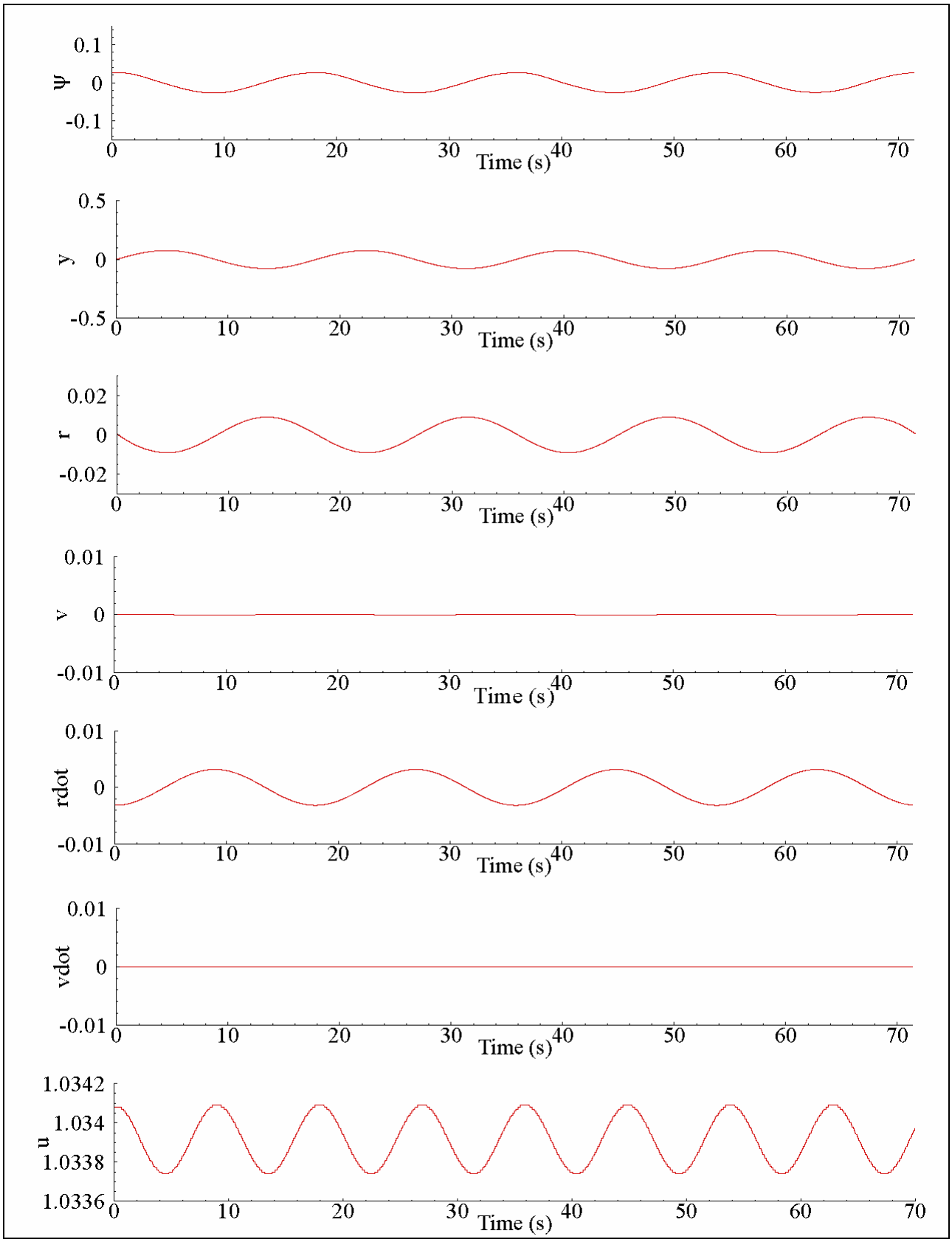

Figure C.6.1.1-Yaw_138_1 (part 1).

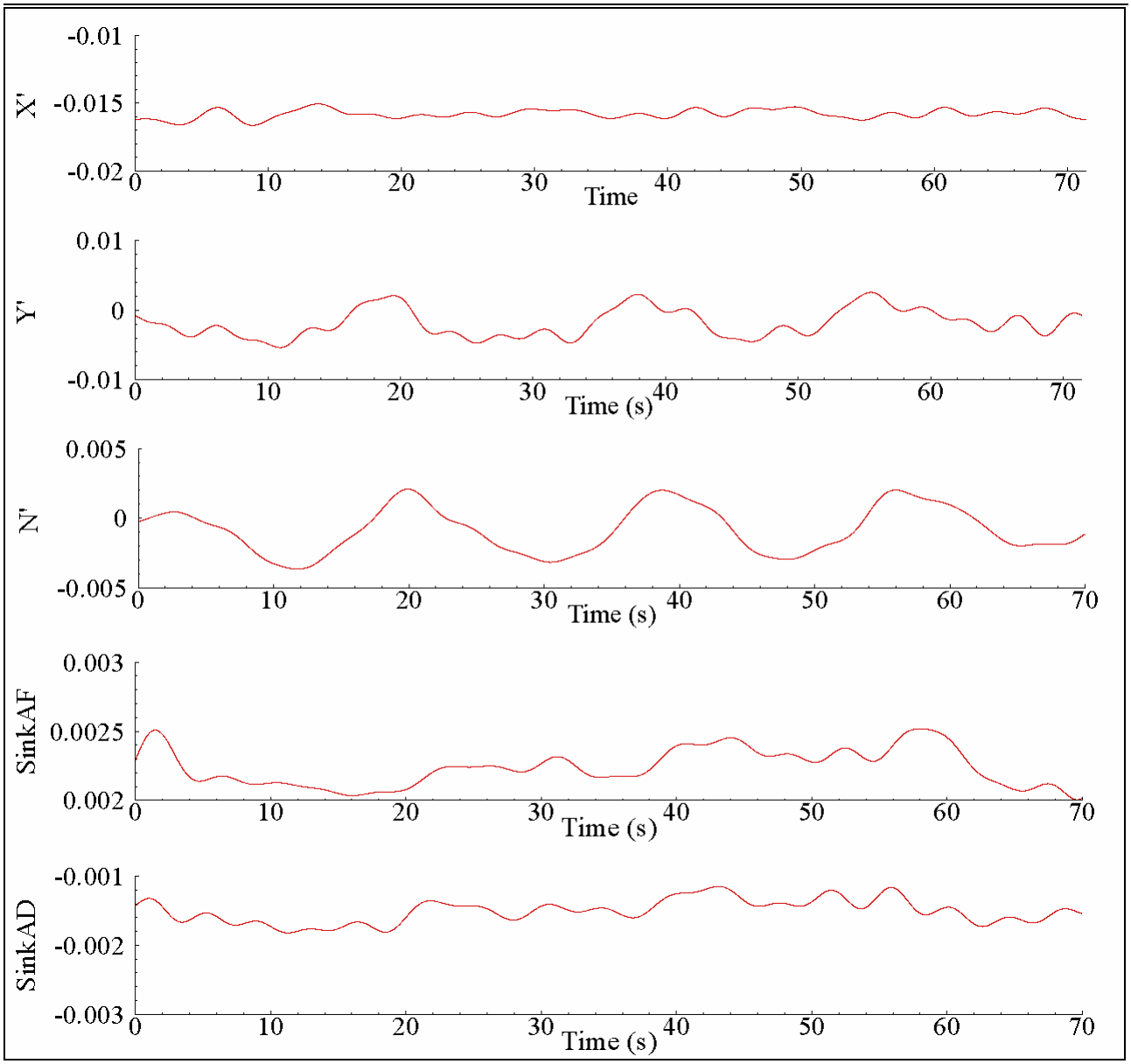

Figure C.6.1.2 Yaw_138_1 (part 2).

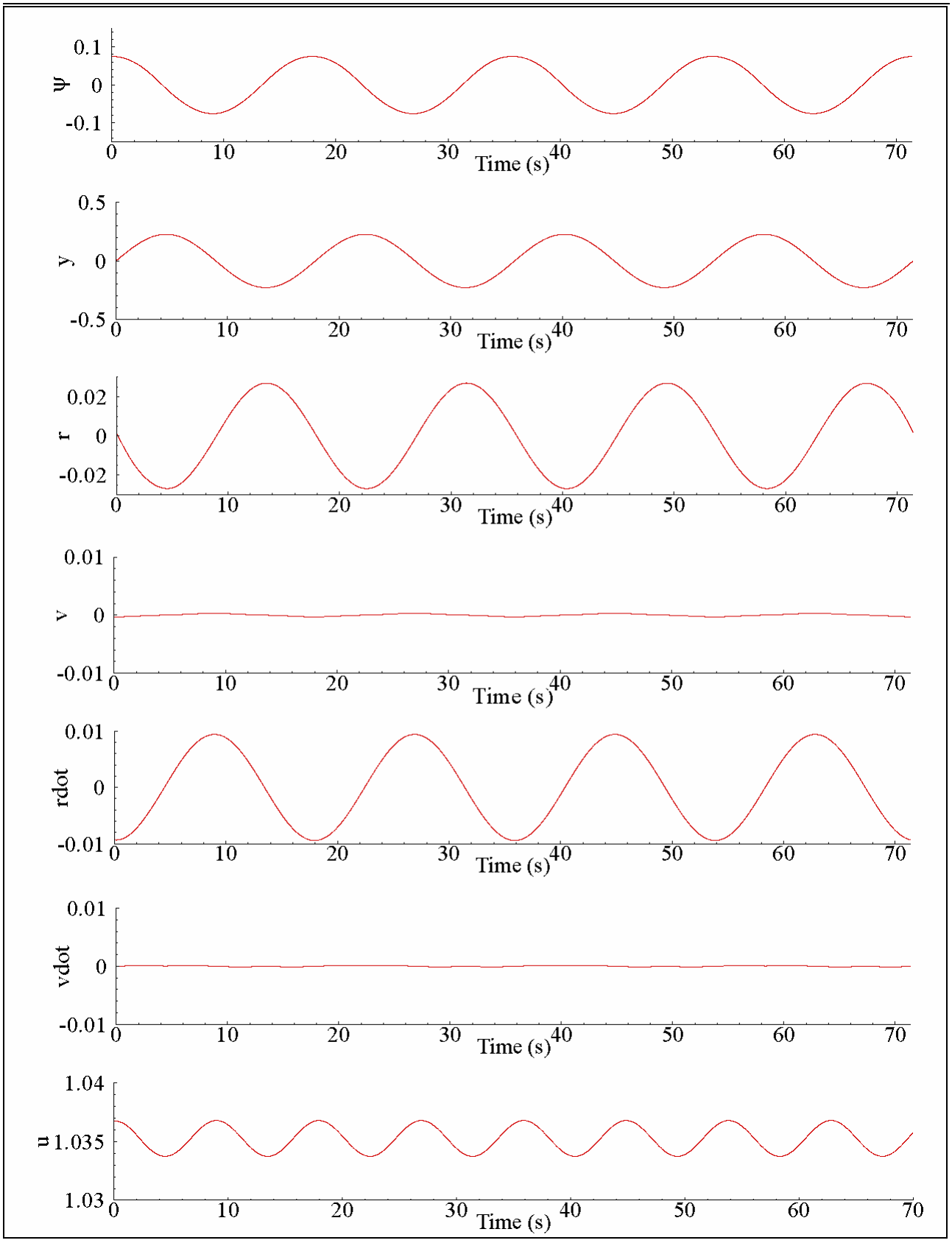

Figure C.6.1.3 Yaw_138_2 (part 1).

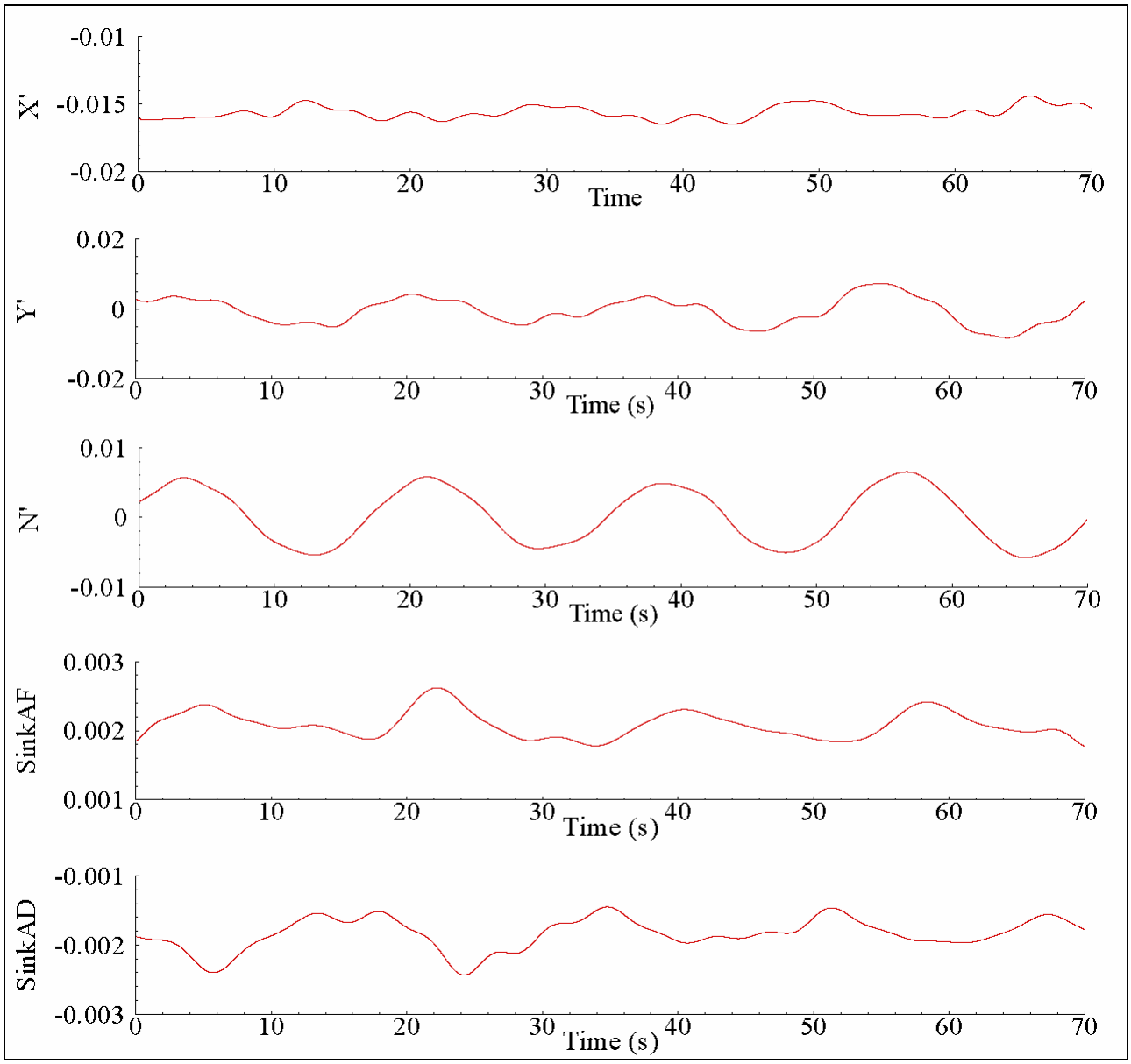

Figure C.6.1.4 Yaw_138_2 (part 2).

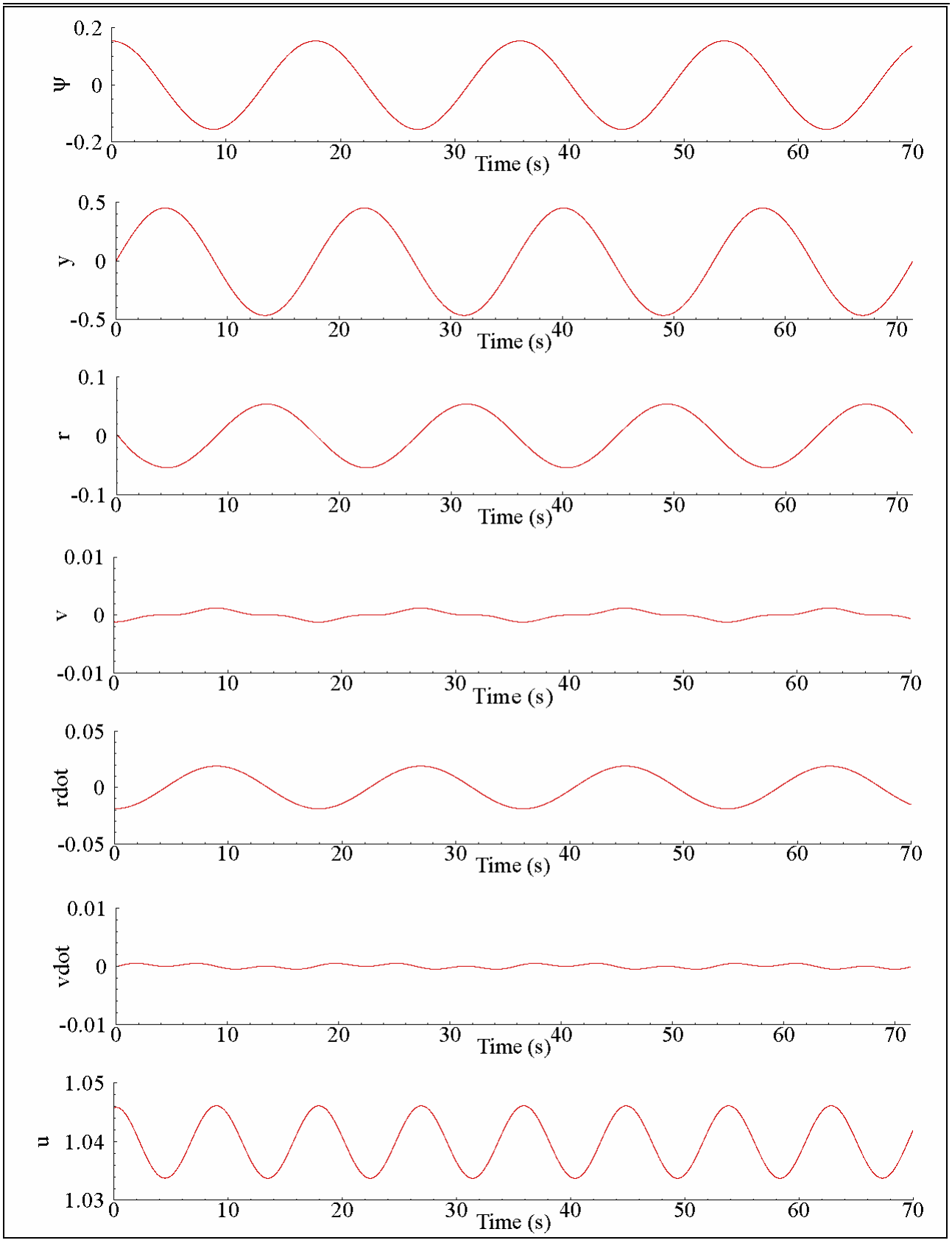

Figure C.6.1.5 Yaw_138_3 (part 1).

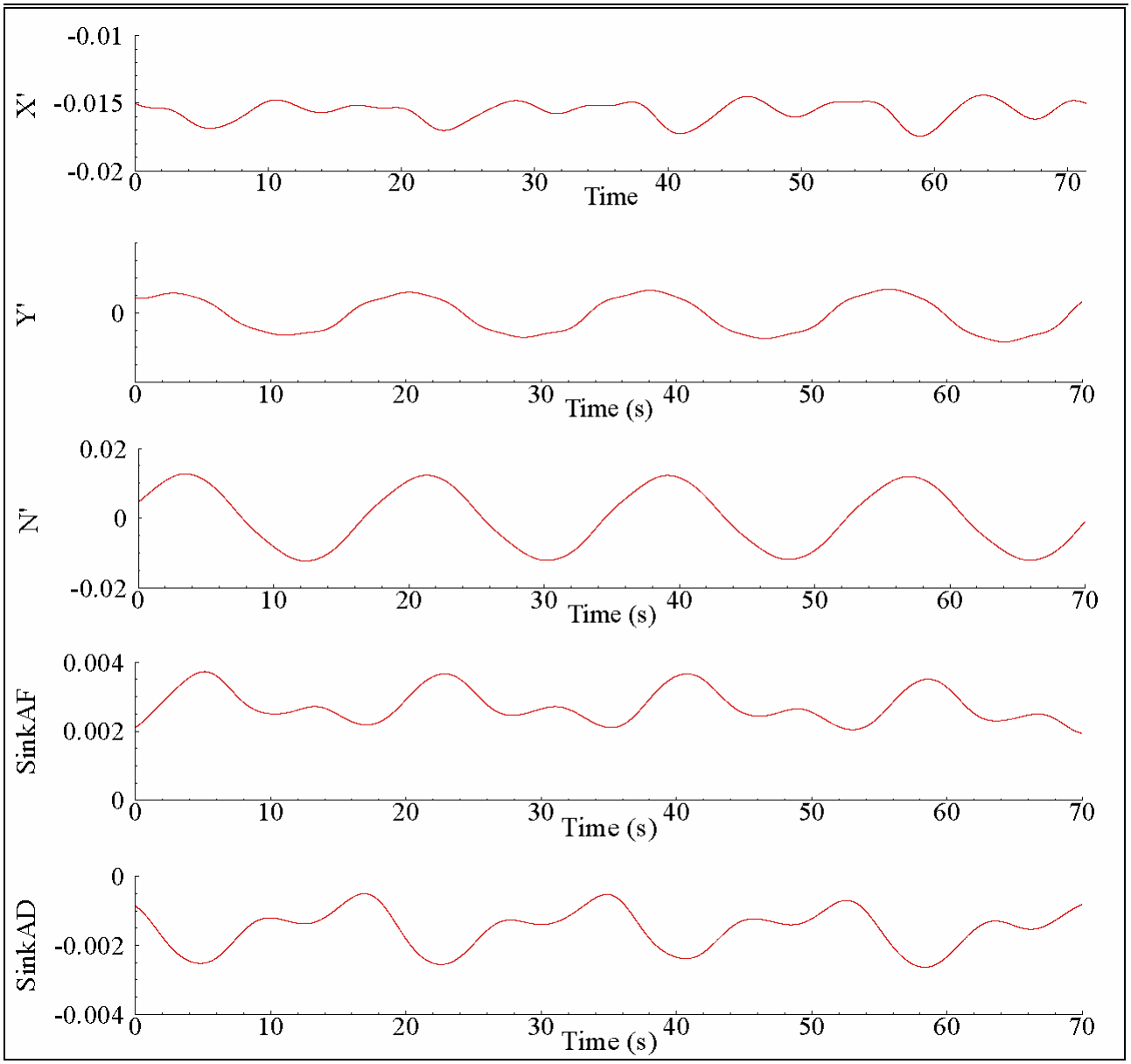

Figure C.6.1.6 Yaw_138_3 (part 2).

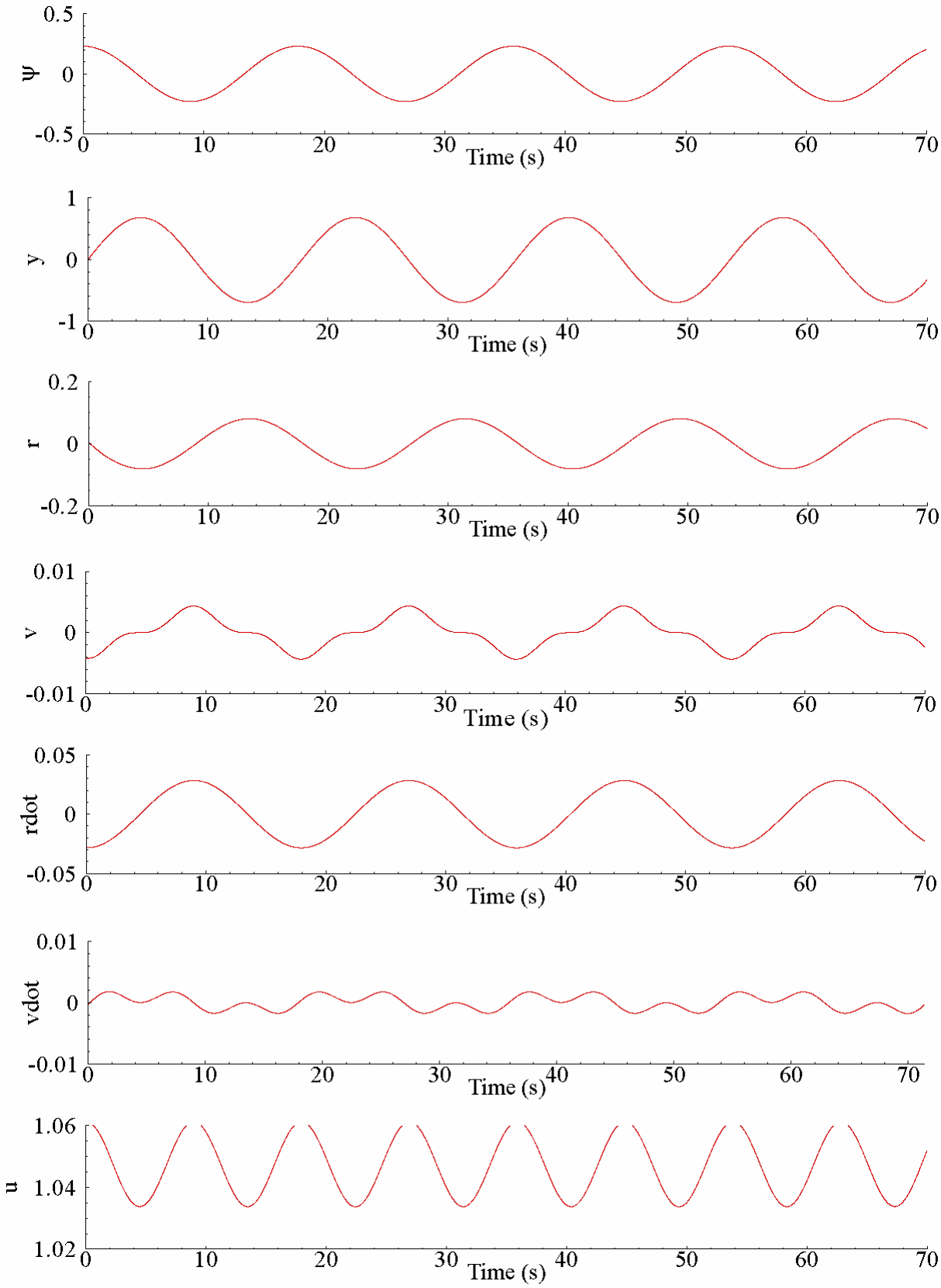

Figure C.6.1.7 Yaw_138_4 (part 1).

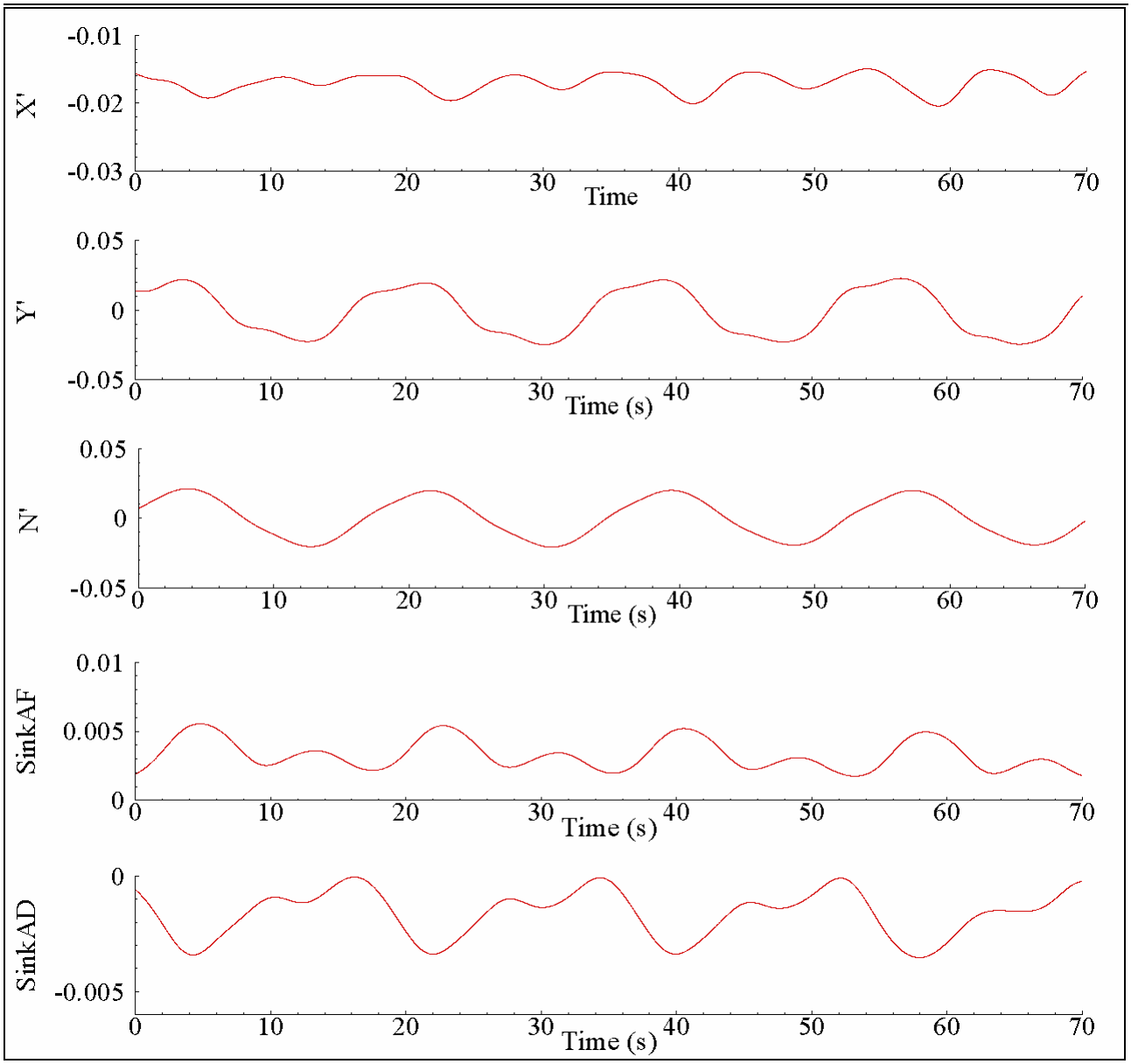

Figure C.6.1.8 Yaw_138_4 (part 2).

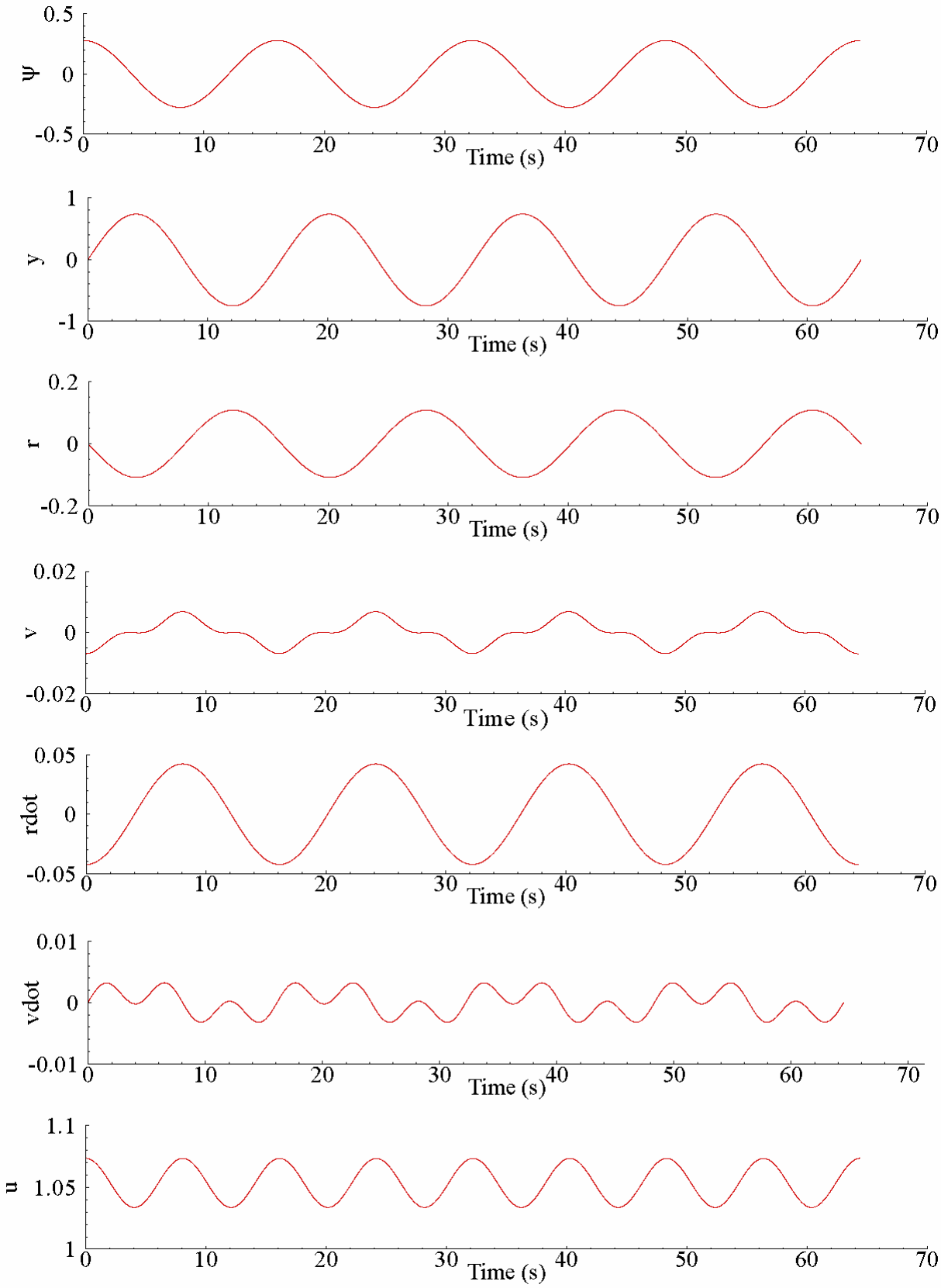

Figure C.6.1.9 Yaw_138_5 (part 1).

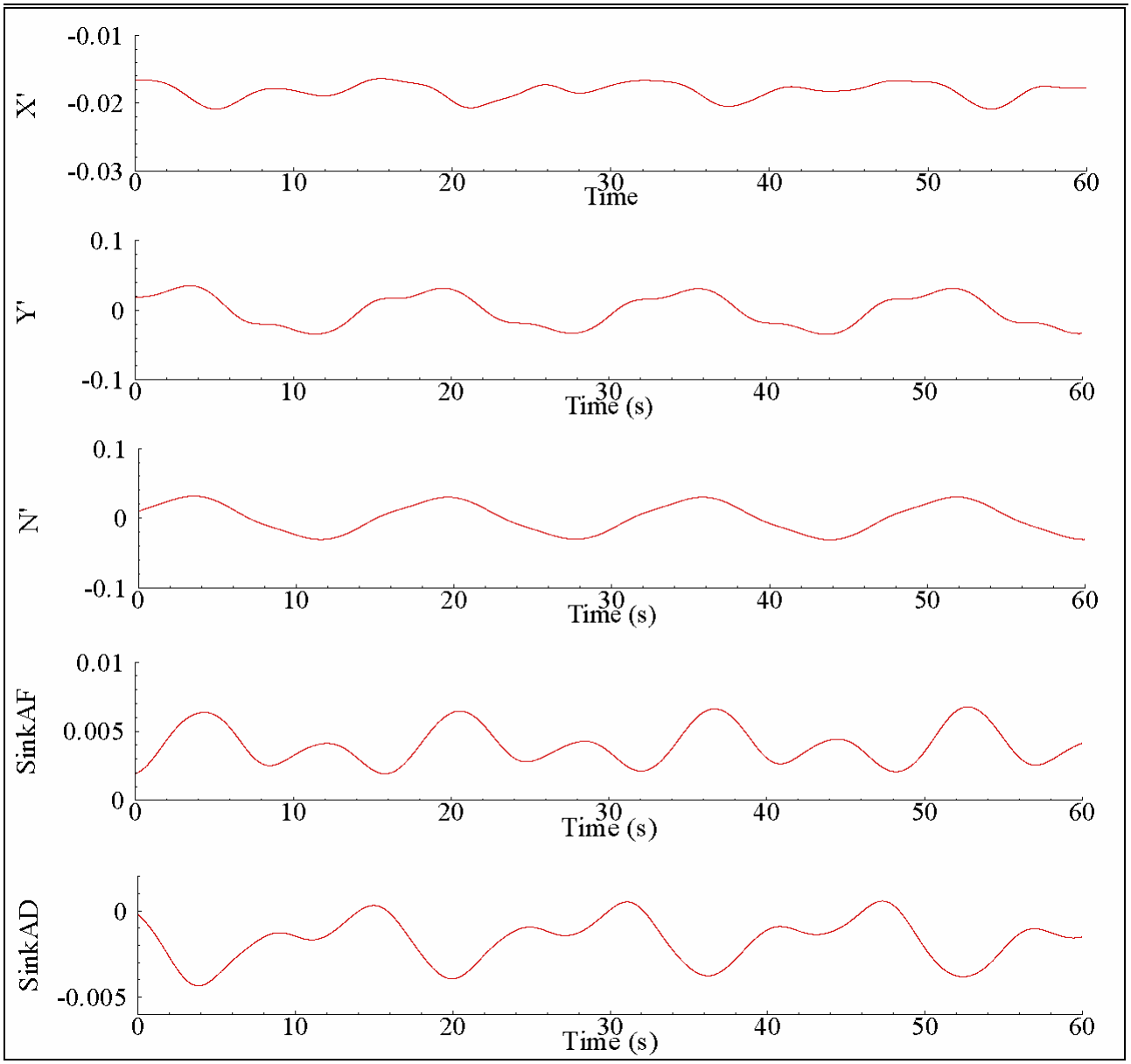

Figure C.6.1.10 Yaw_138_5 (part 2).

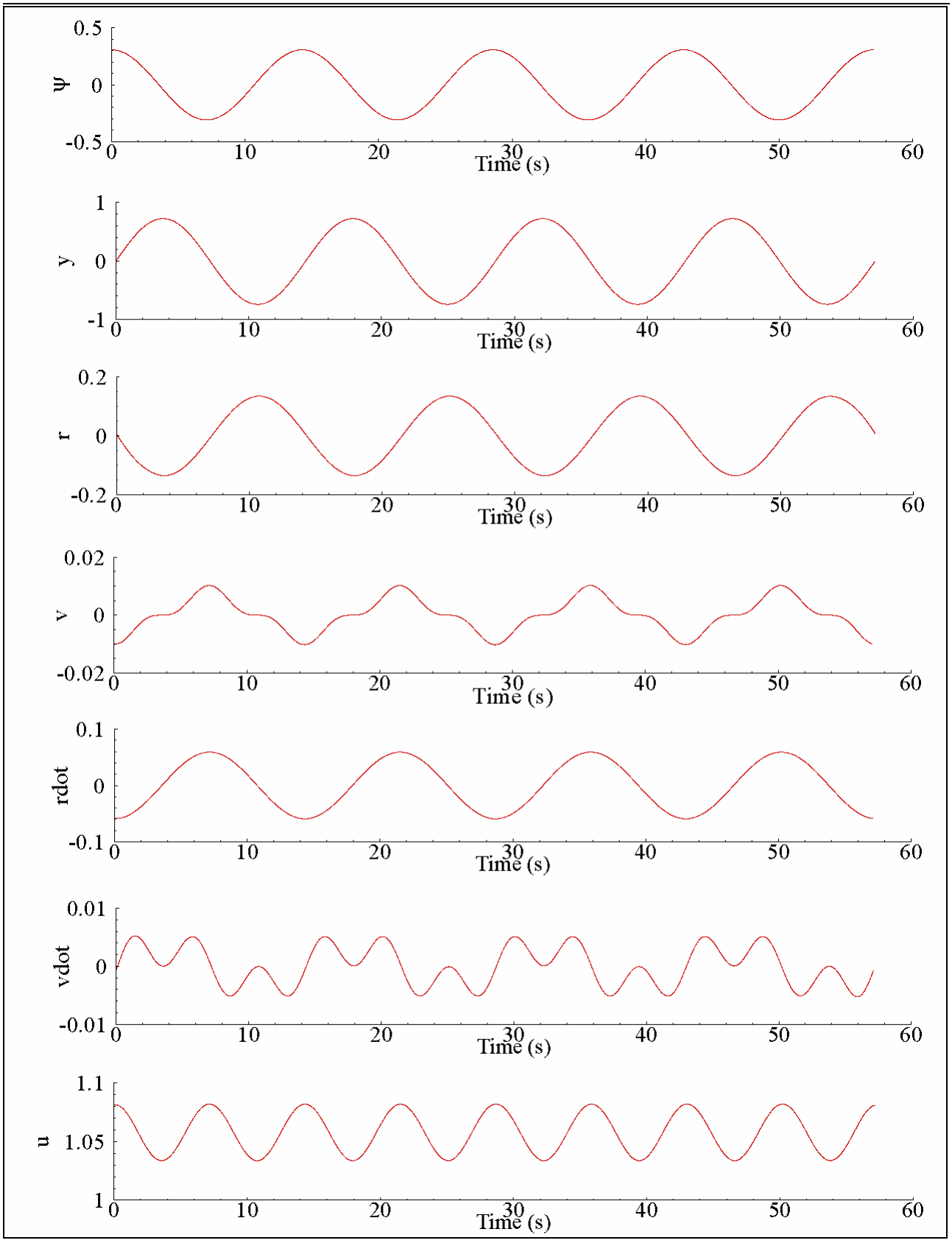

Figure C.6.1.11 Yaw_138_6 (part 1).

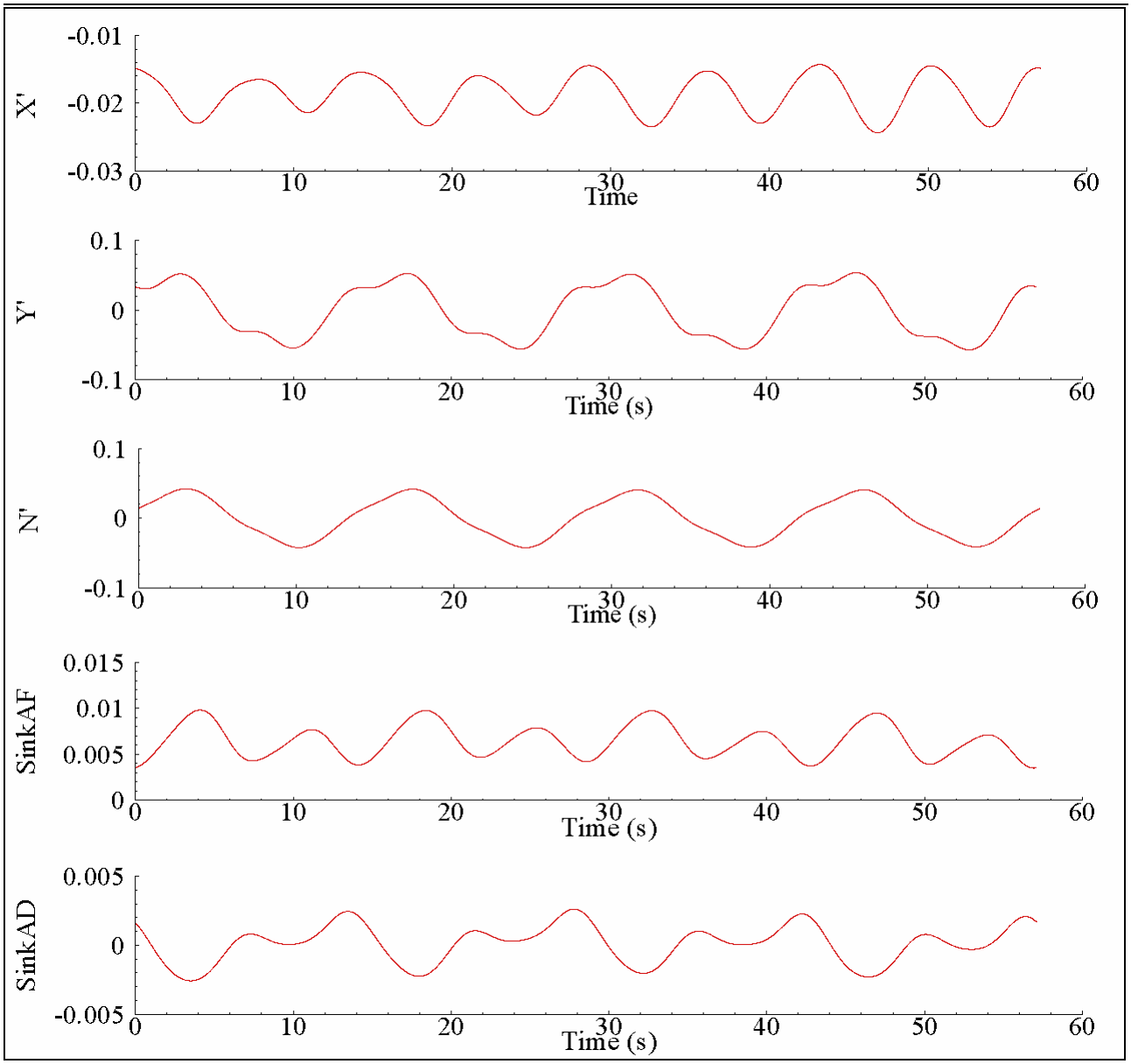

Figure C.6.1.12 Yaw_138_6 (part 2).

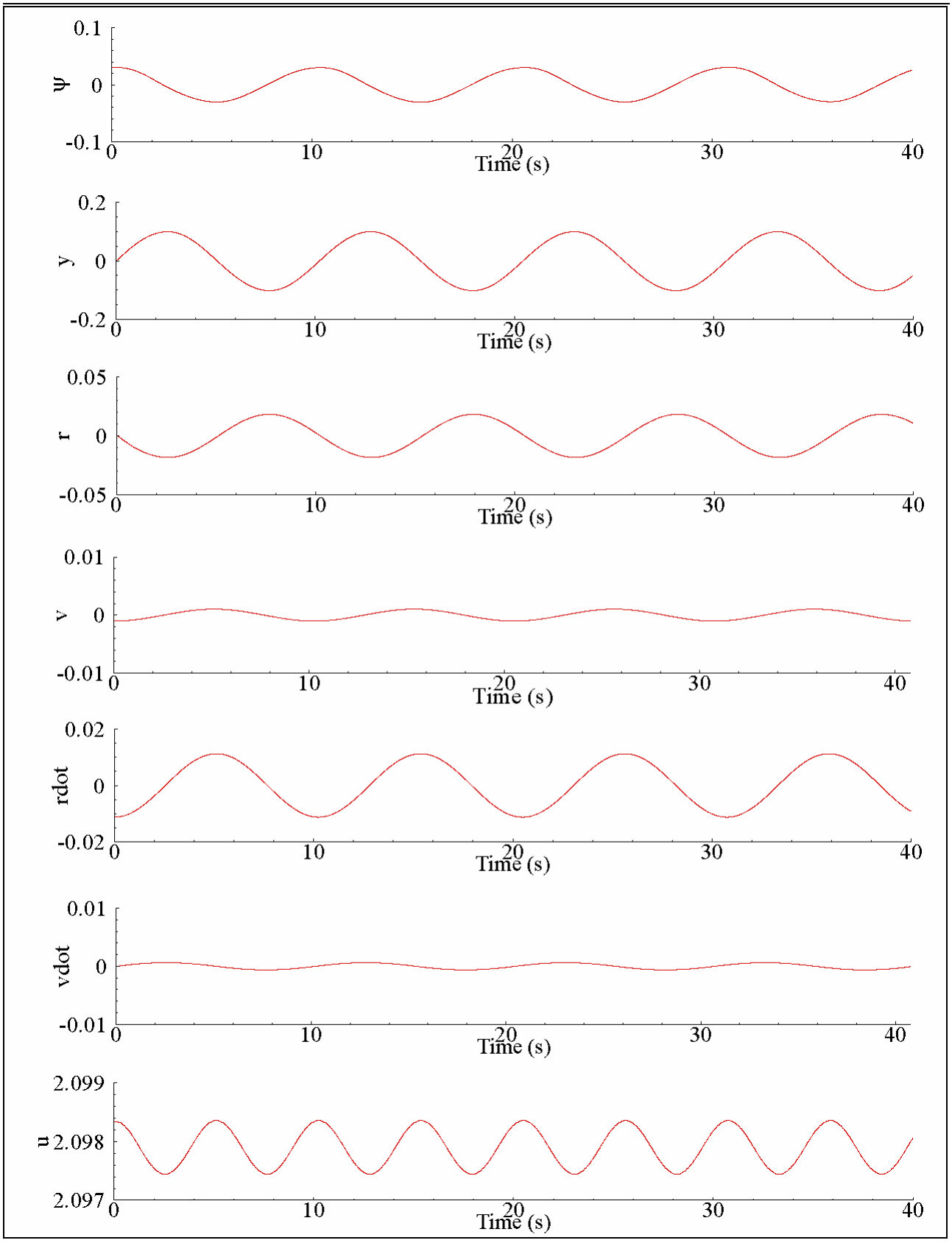

Figure C.6.1.13 Yaw_280_1 (part 1).

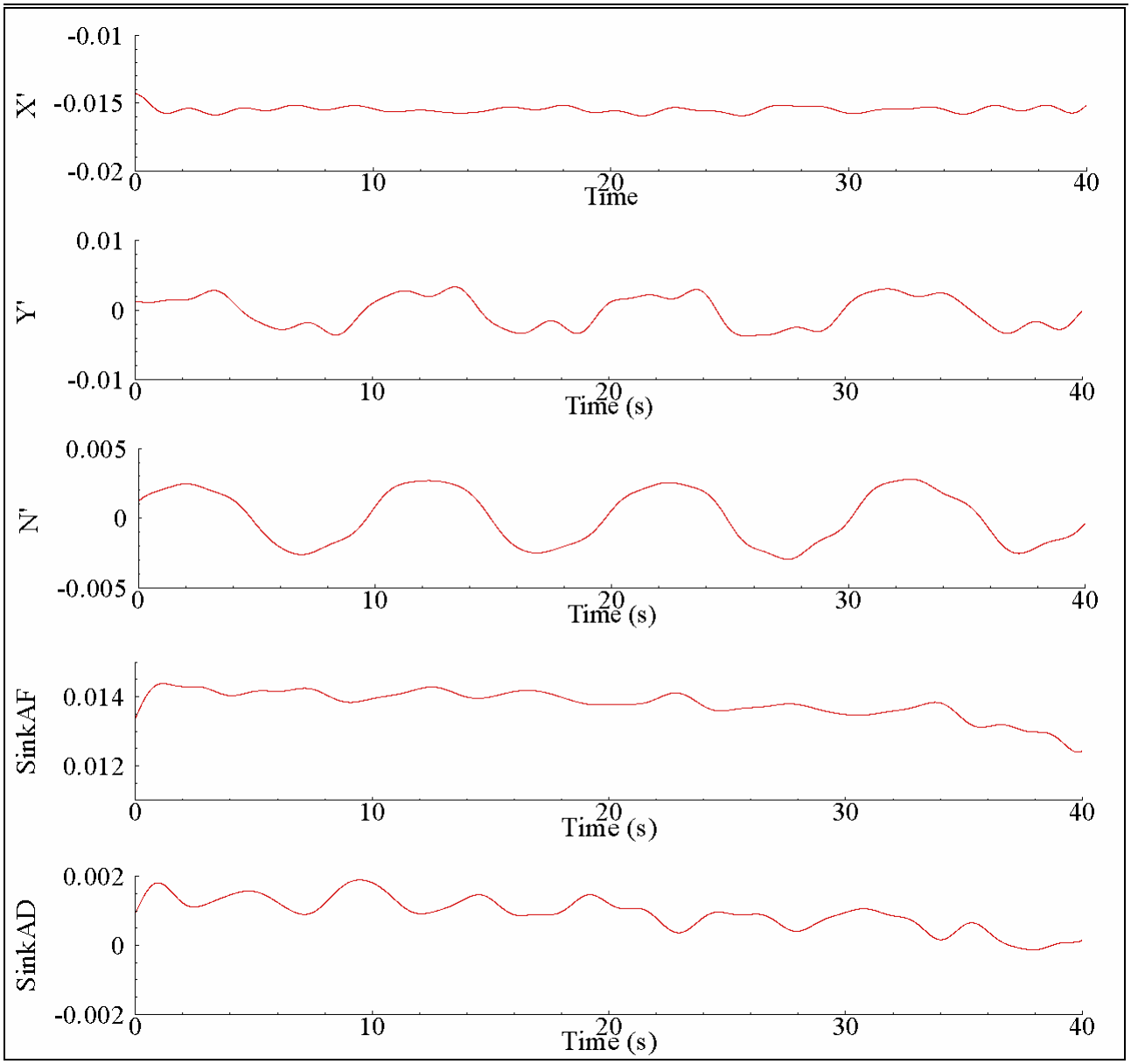

Figure C.6.1.14 Yaw_280_1 (part 2).

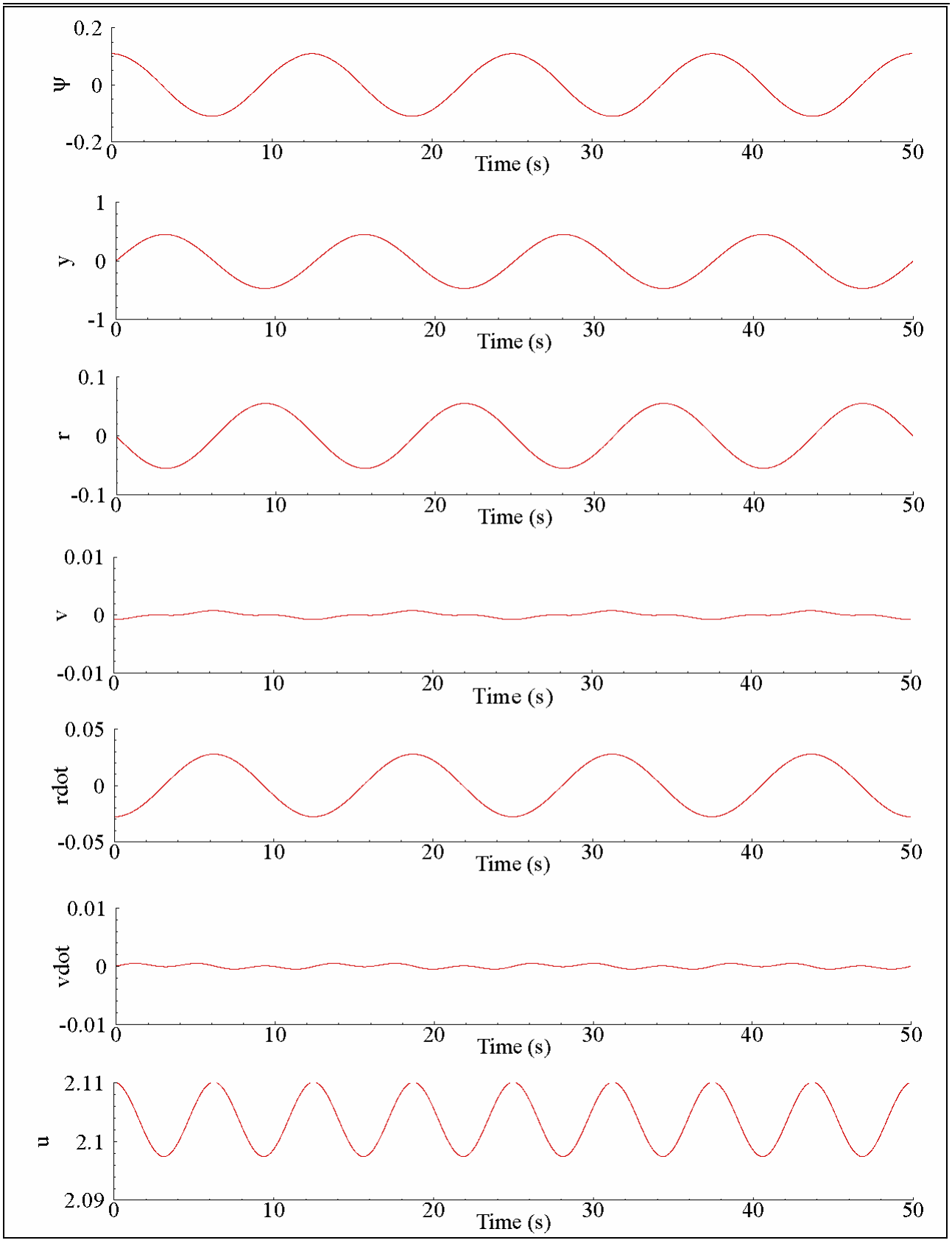

Figure C.6.1.15 Yaw_280_2 (part 1).

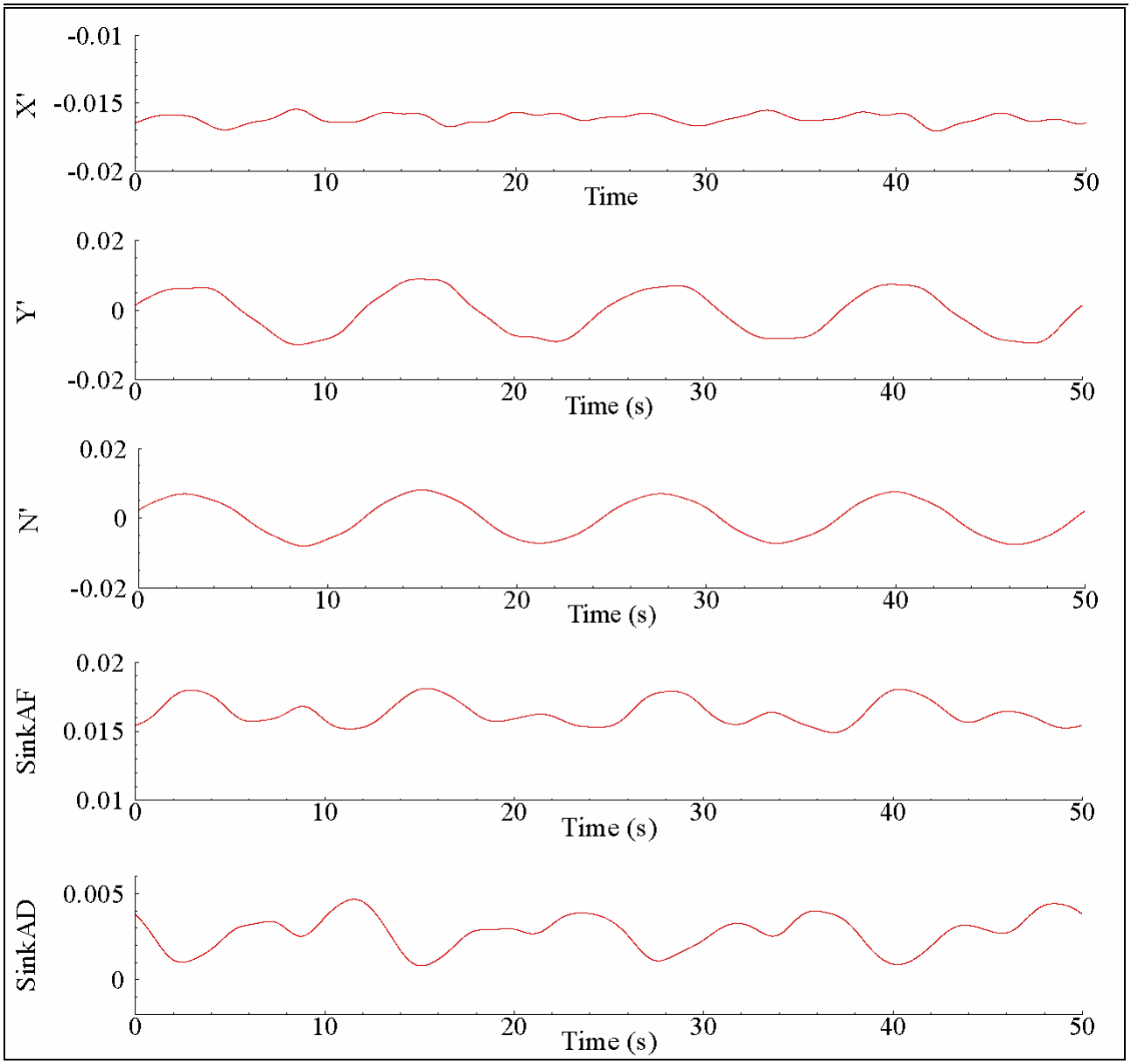

Figure C.6.1.16 Yaw_280_2 (part 2).

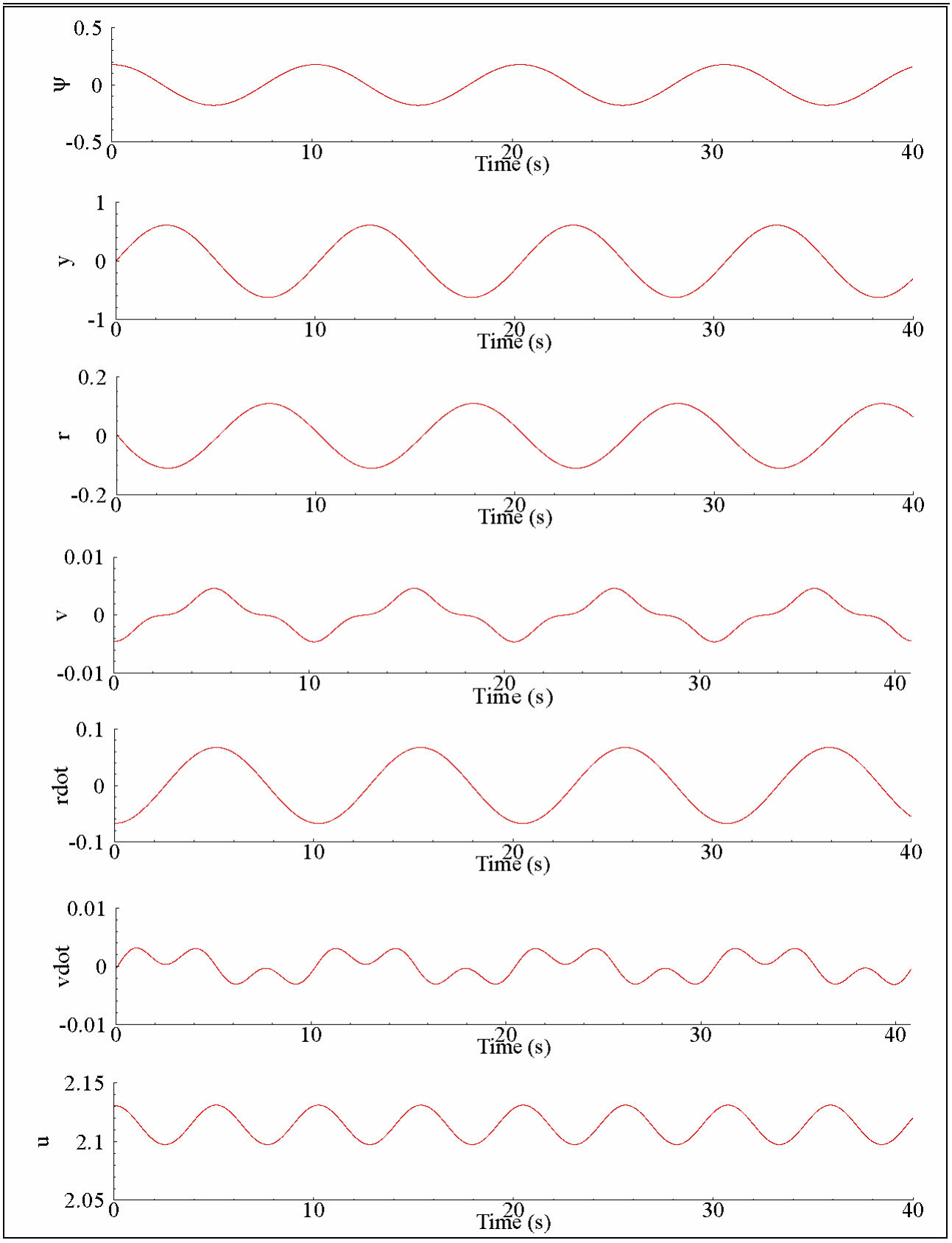

Figure C.6.1.17 Yaw_280_3 (part 1).

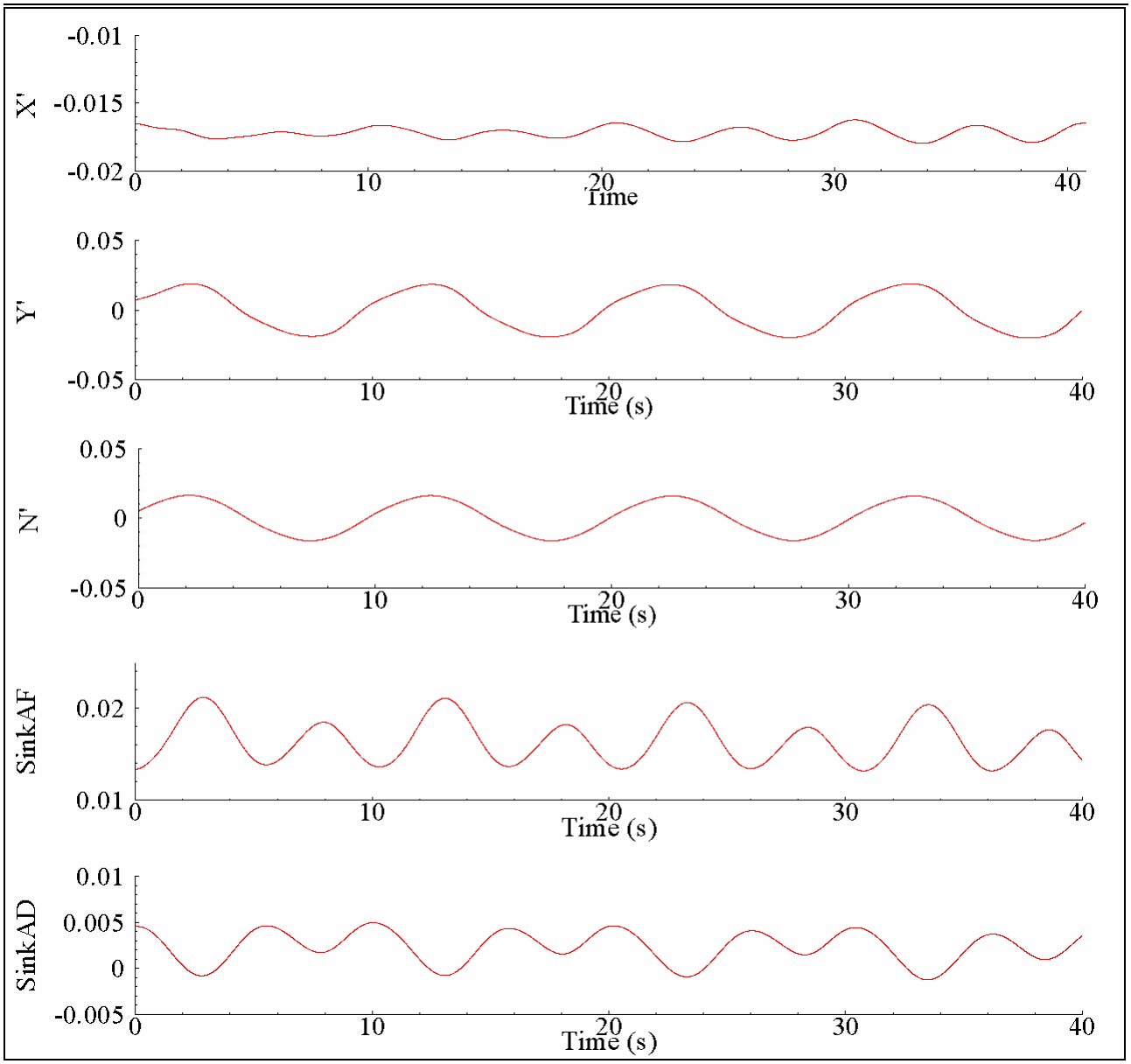

Figure C.6.1.18 Yaw_280_3 (part 2).

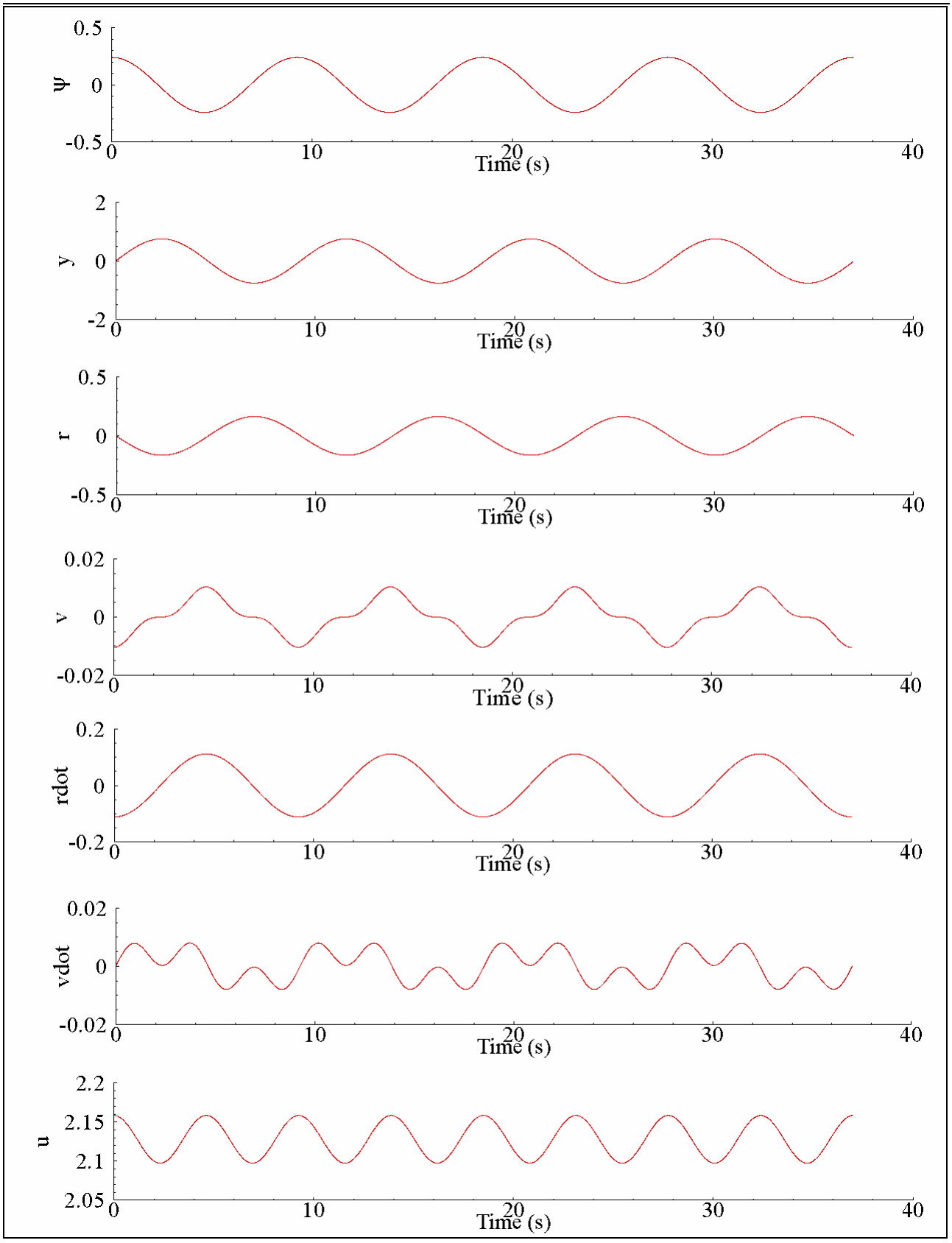

Figure C.6.1.19 Yaw_280_4 (part 1).

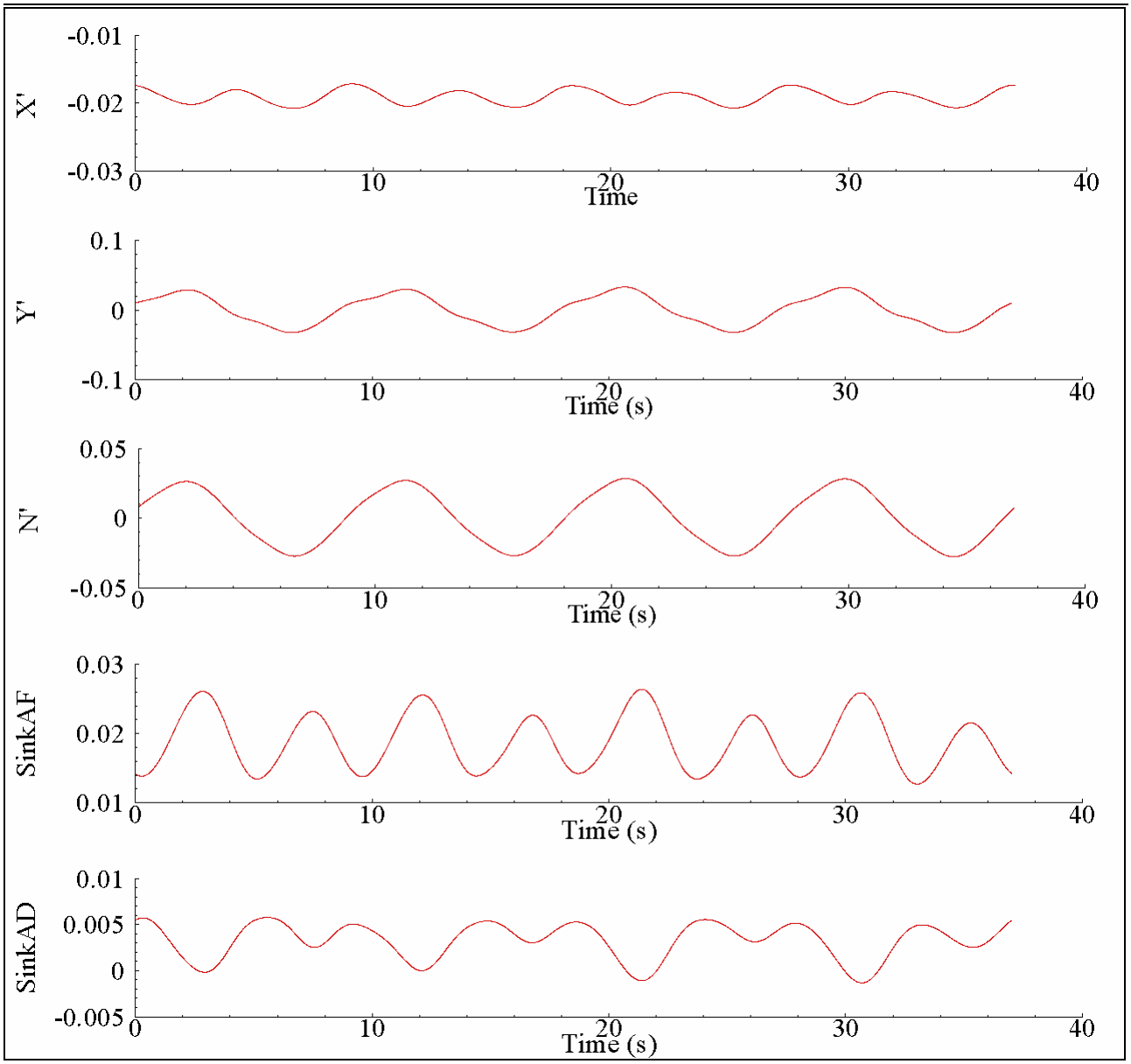

Figure C.6.1.20 Yaw_280_4 (part 2).

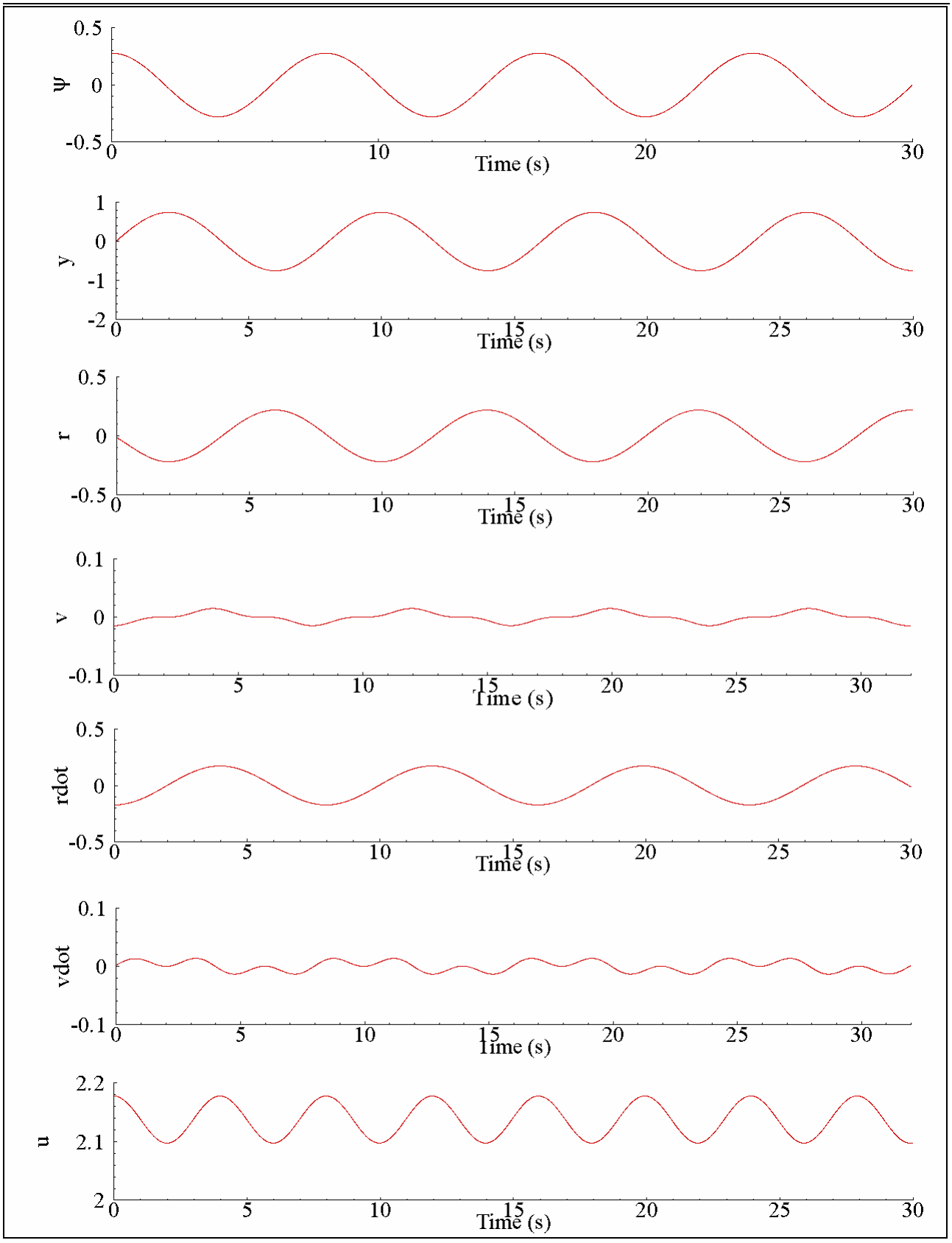

Figure C.6.1.21 Yaw_280_5 (part 1).

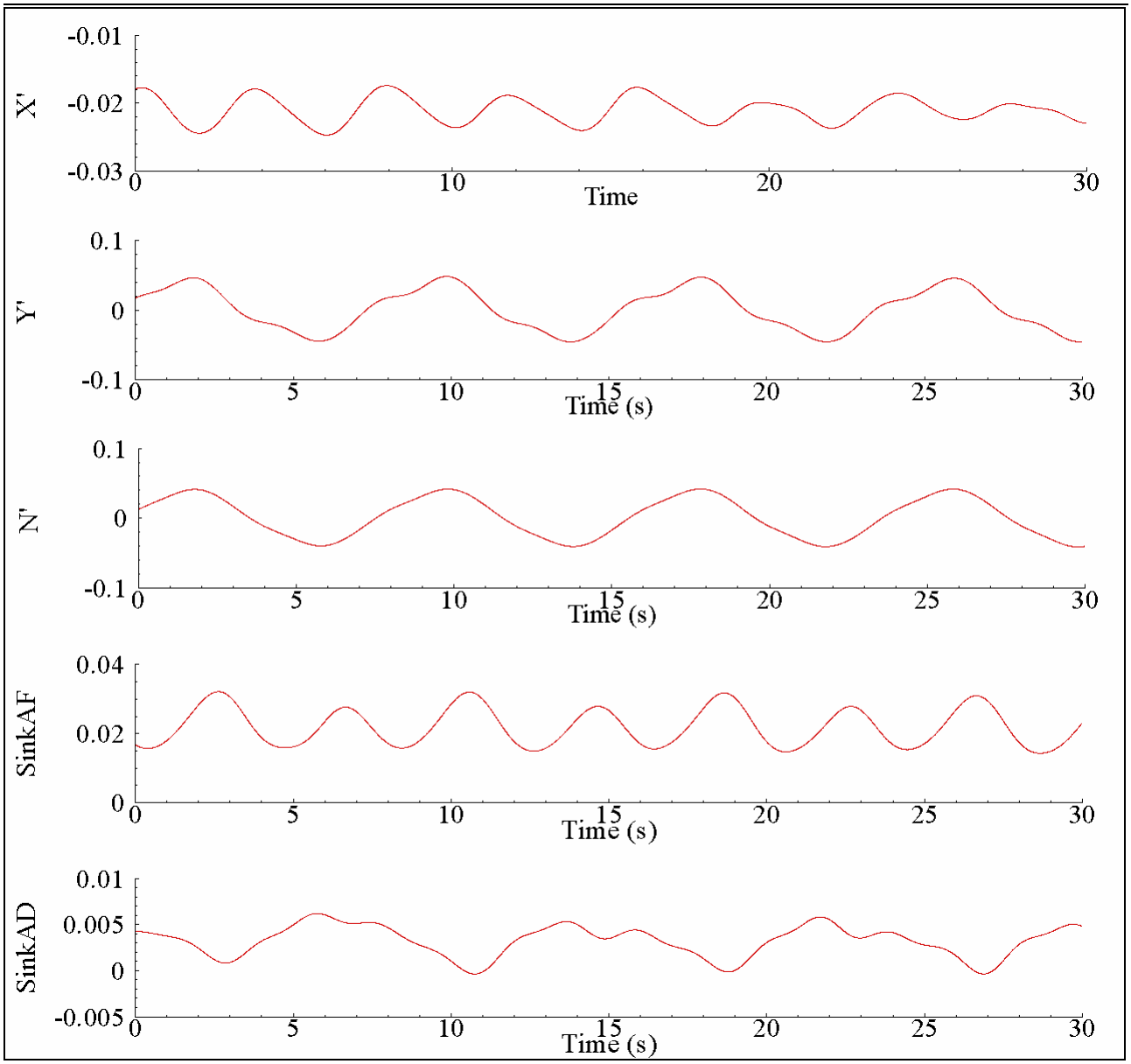

Figure C.6.1.22 Yaw_280_5 (part 2).

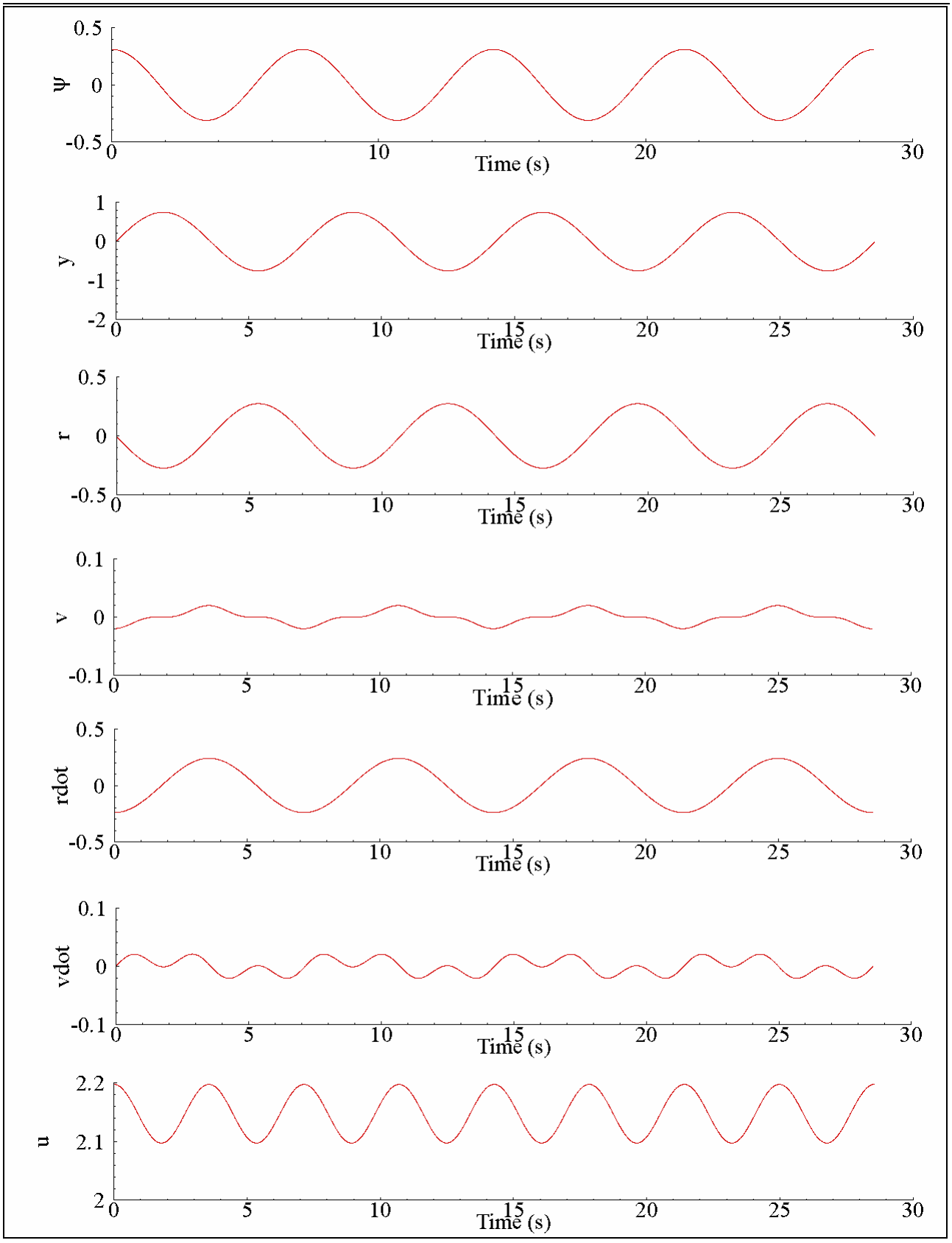

Figure C.6.1.23 Yaw_280_6 (part 1).

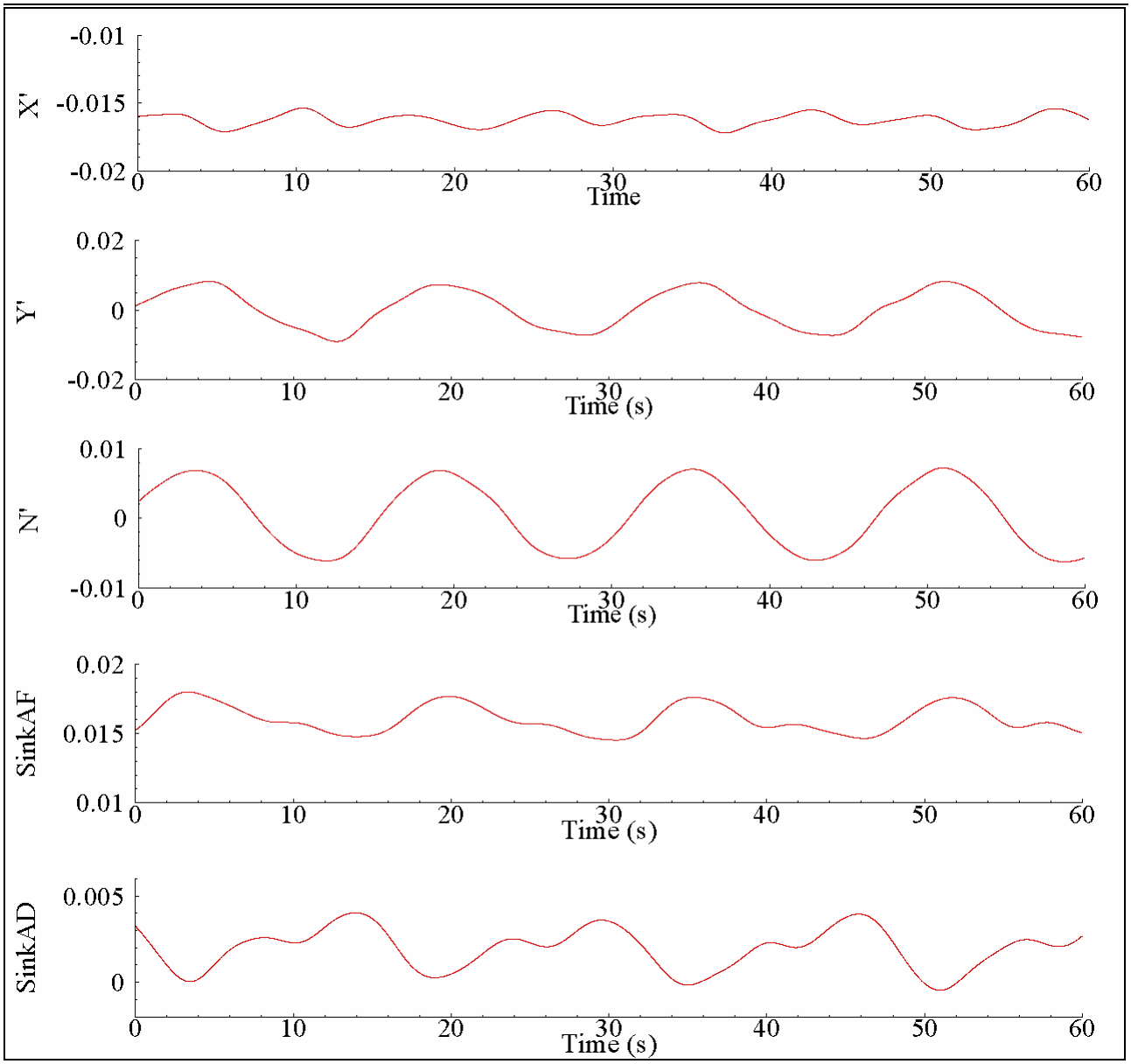

Figure C.6.1.24 Yaw_280_6 (part 2).

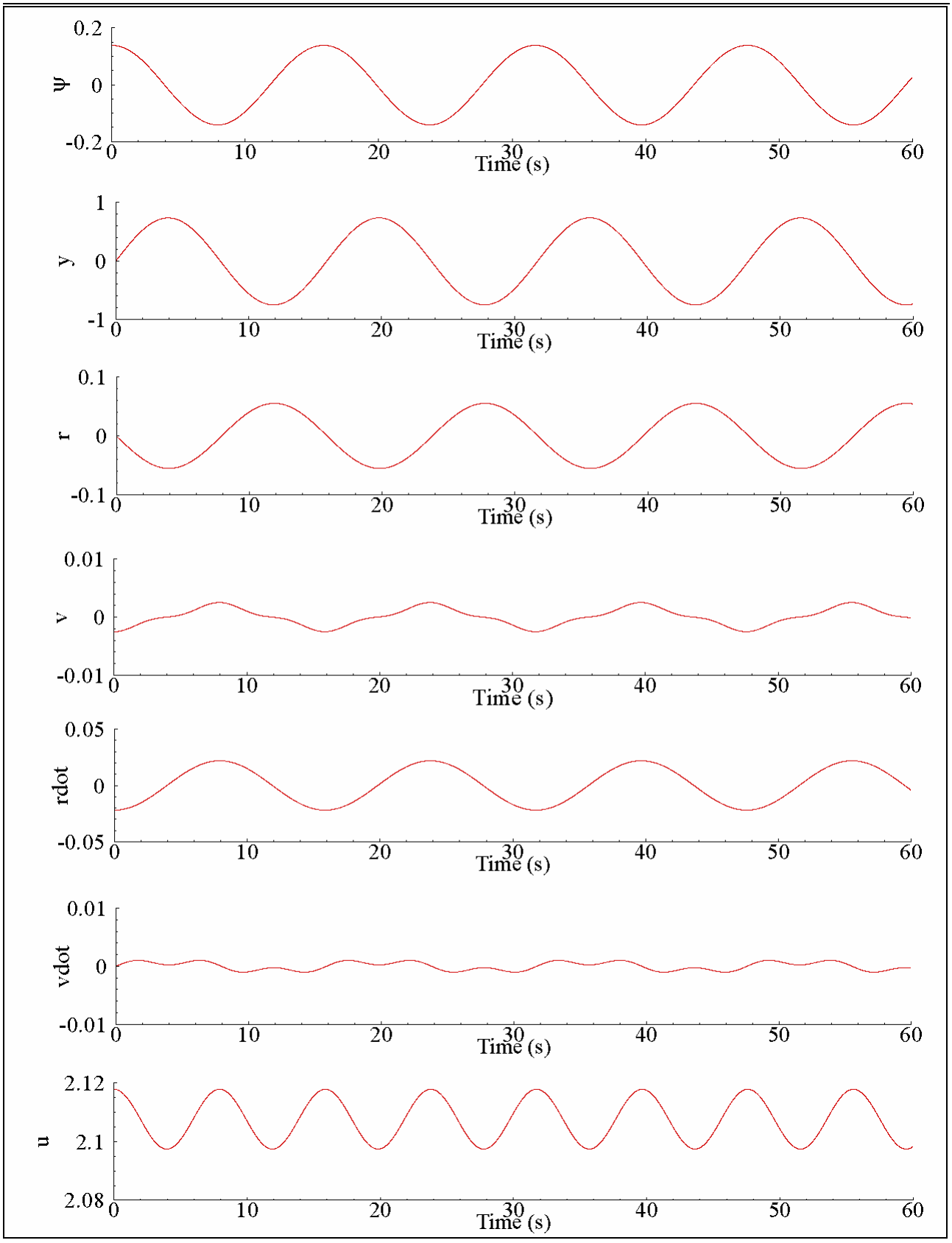

Figure C.6.1.25 Yaw_280_7 (part 1).

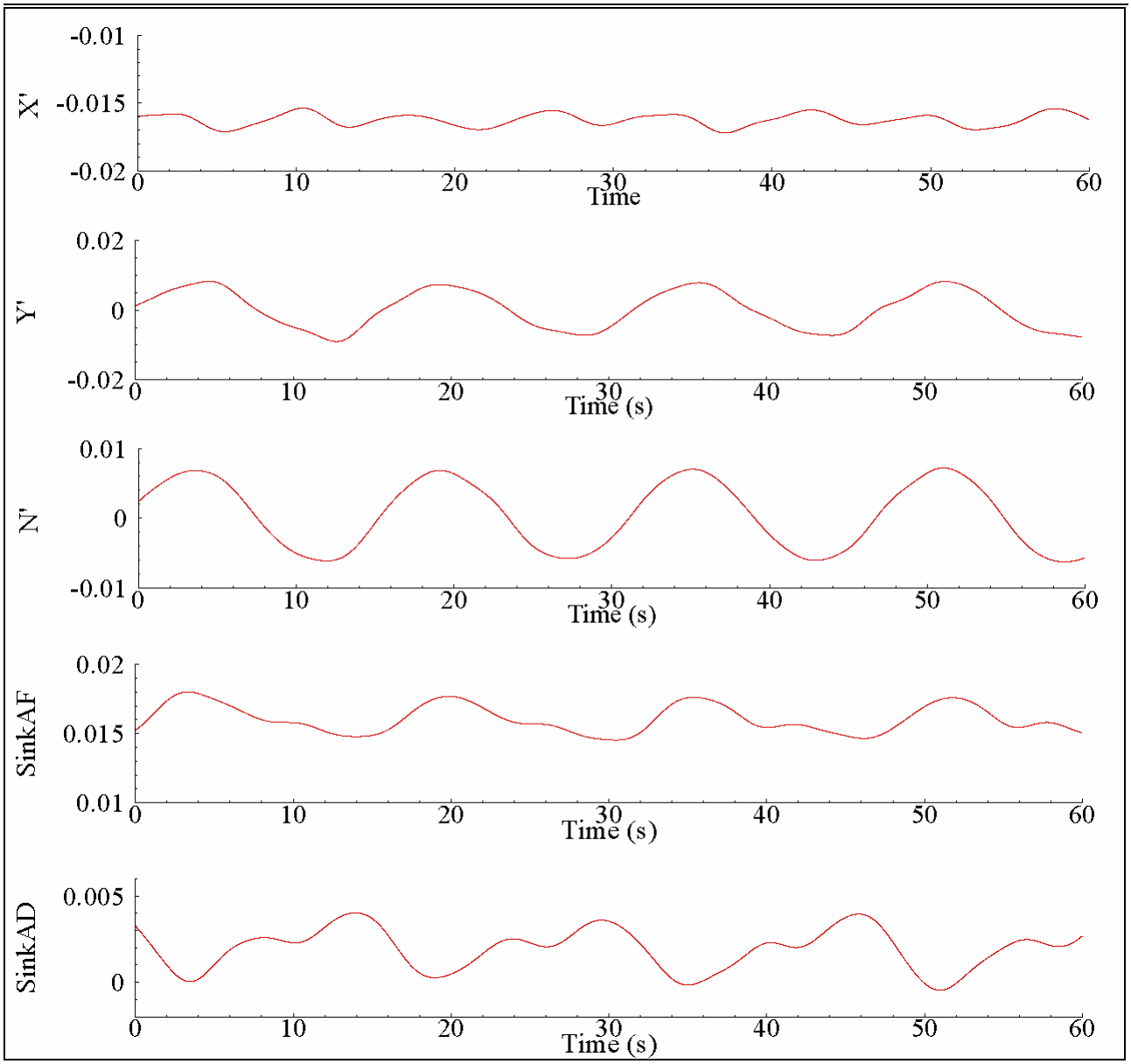

Figure C.6.1.26 Yaw_280_7 (part 2).

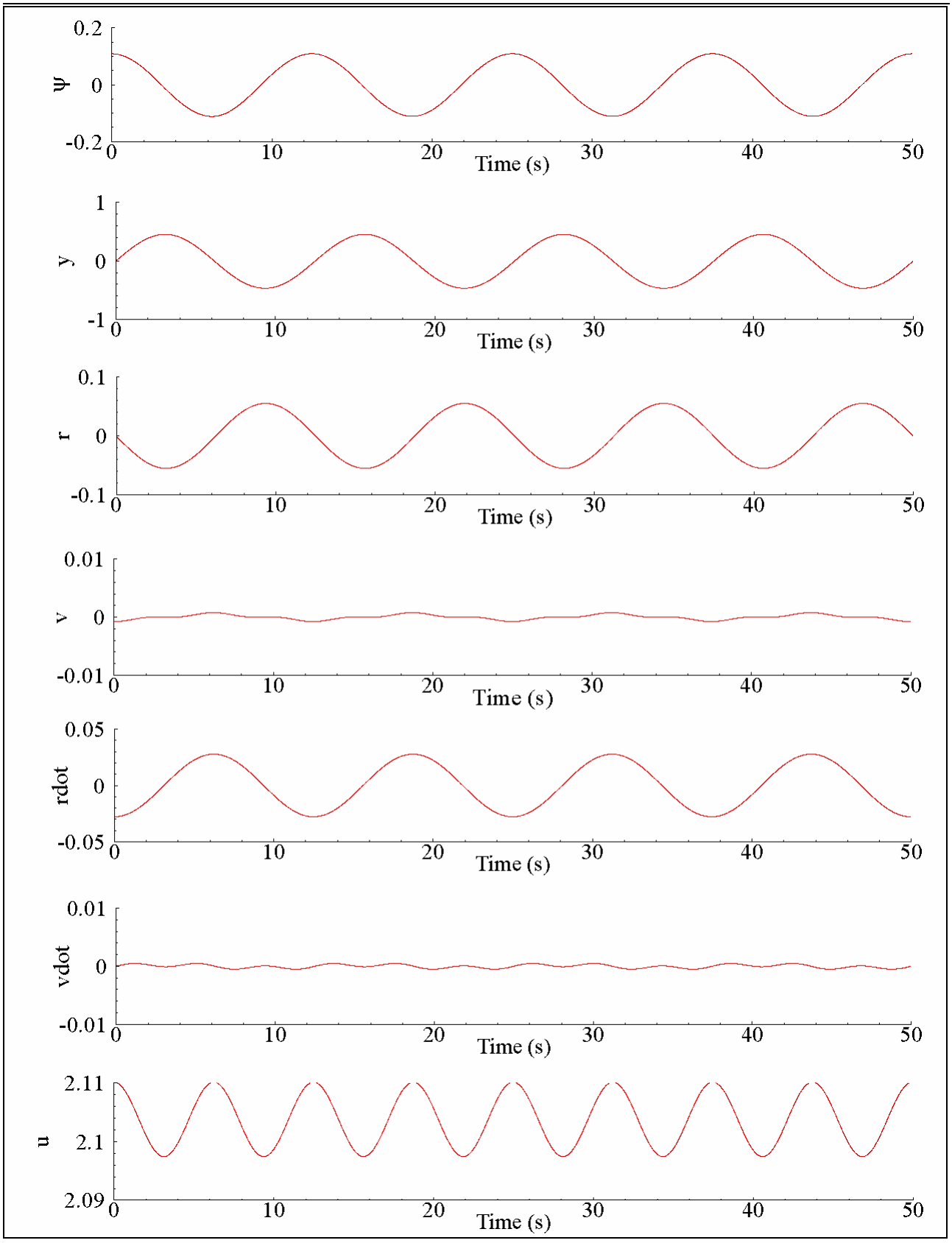

Figure C.6.1.27 Yaw_280_8 (part 1).

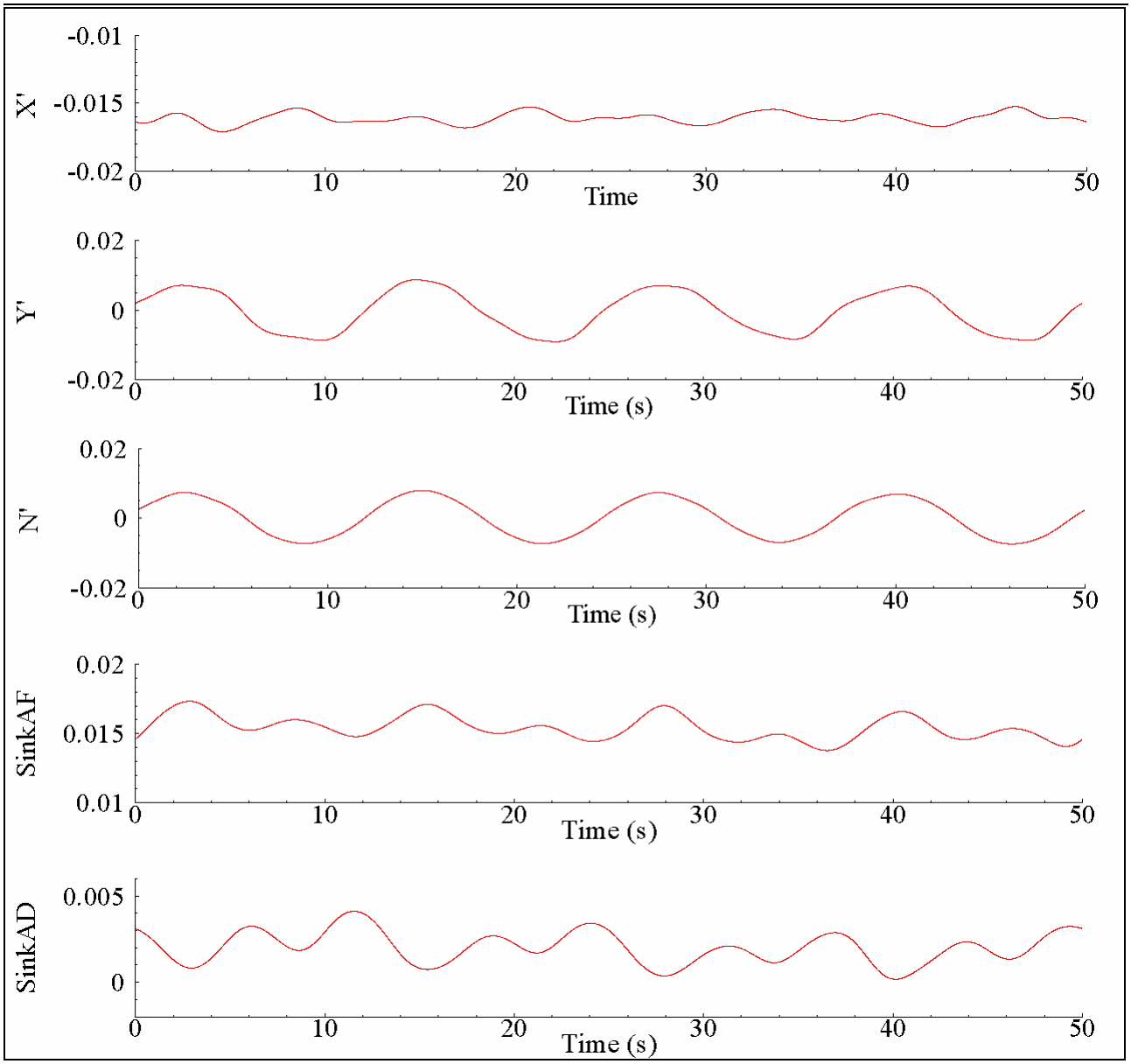

Figure C.6.1.28 Yaw_280_8 (part 2).

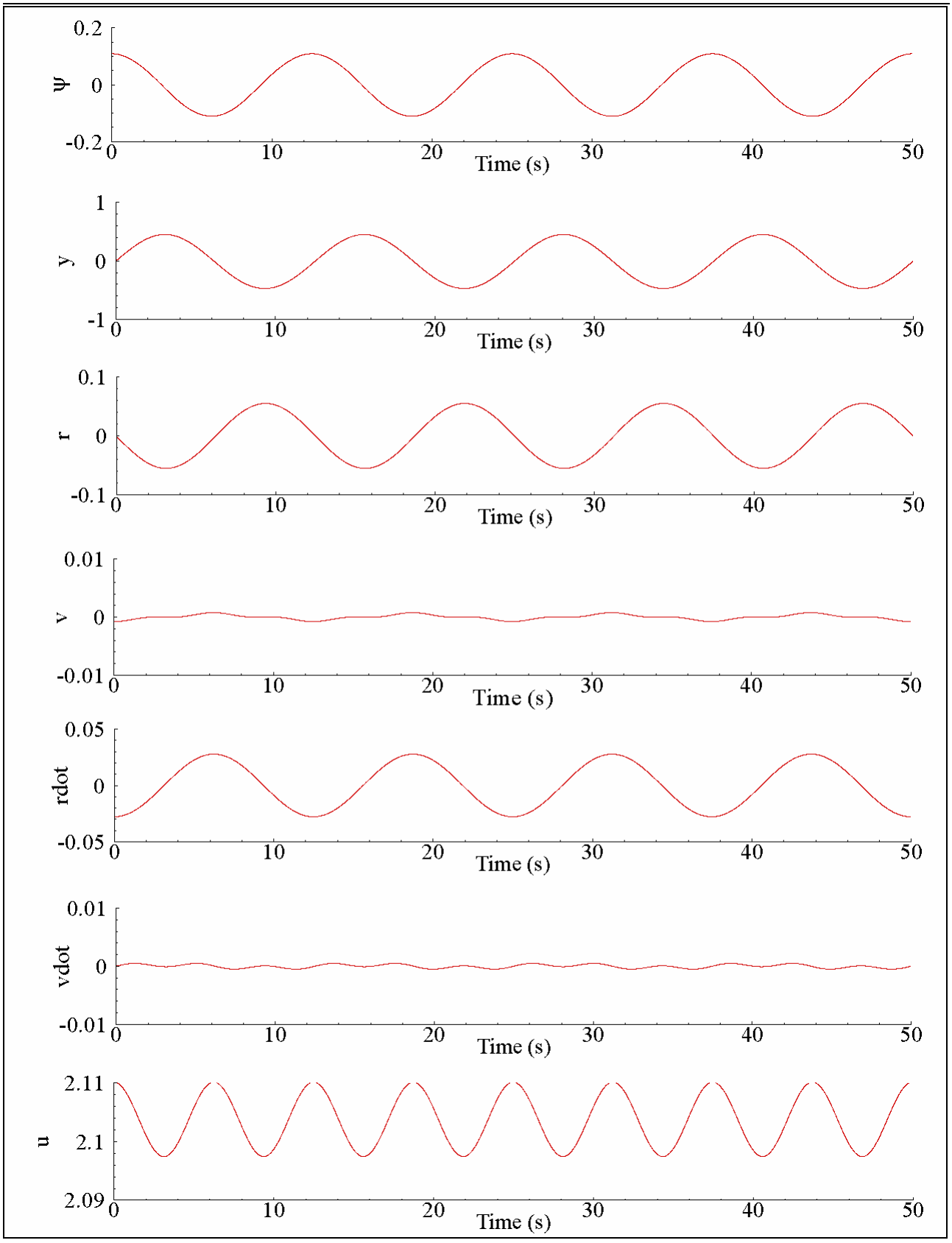

Figure C.6.1.29 Yaw_280_9 (part 1).

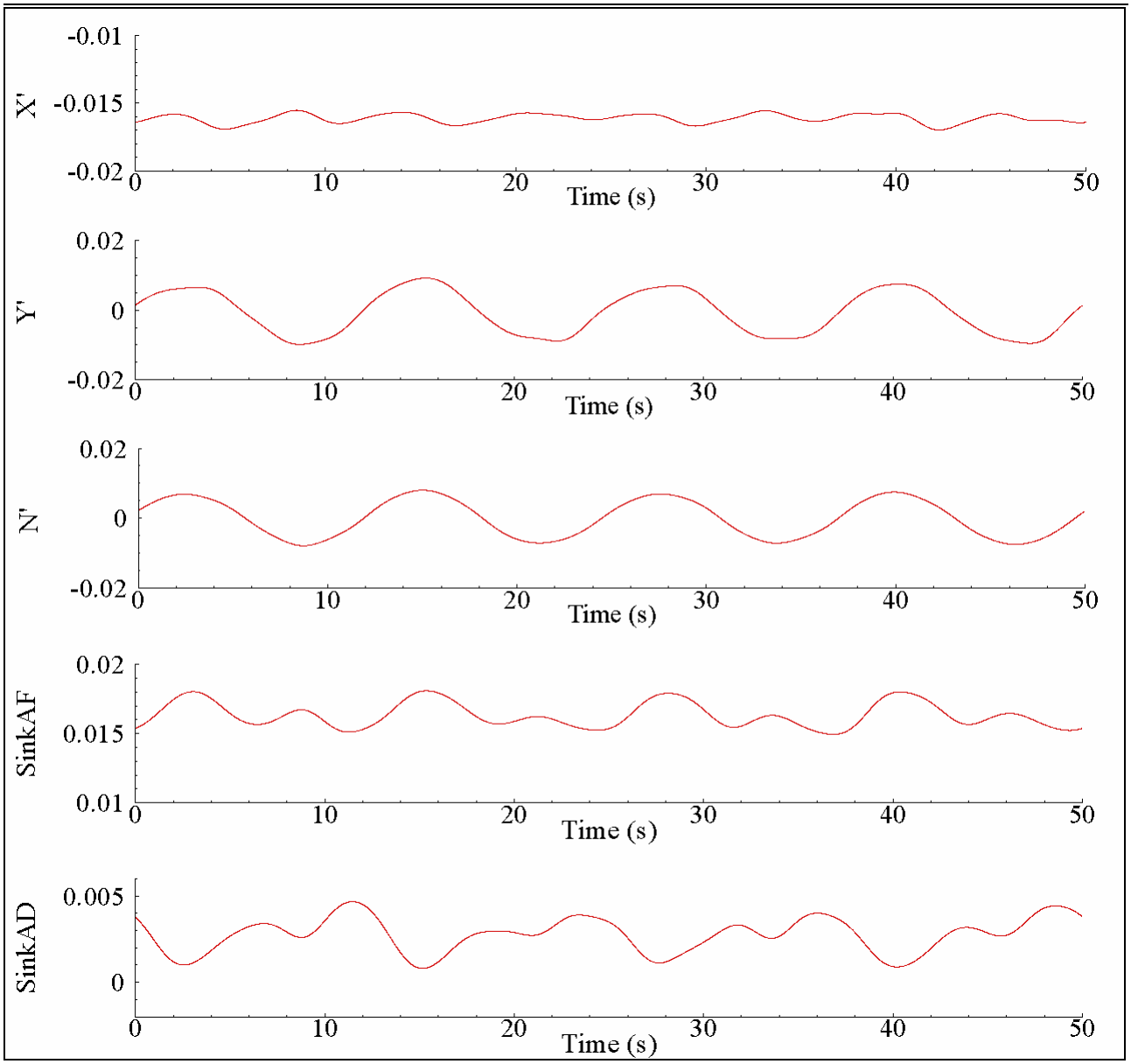

Figure C.6.1.30 Yaw_280_9 (part 2).

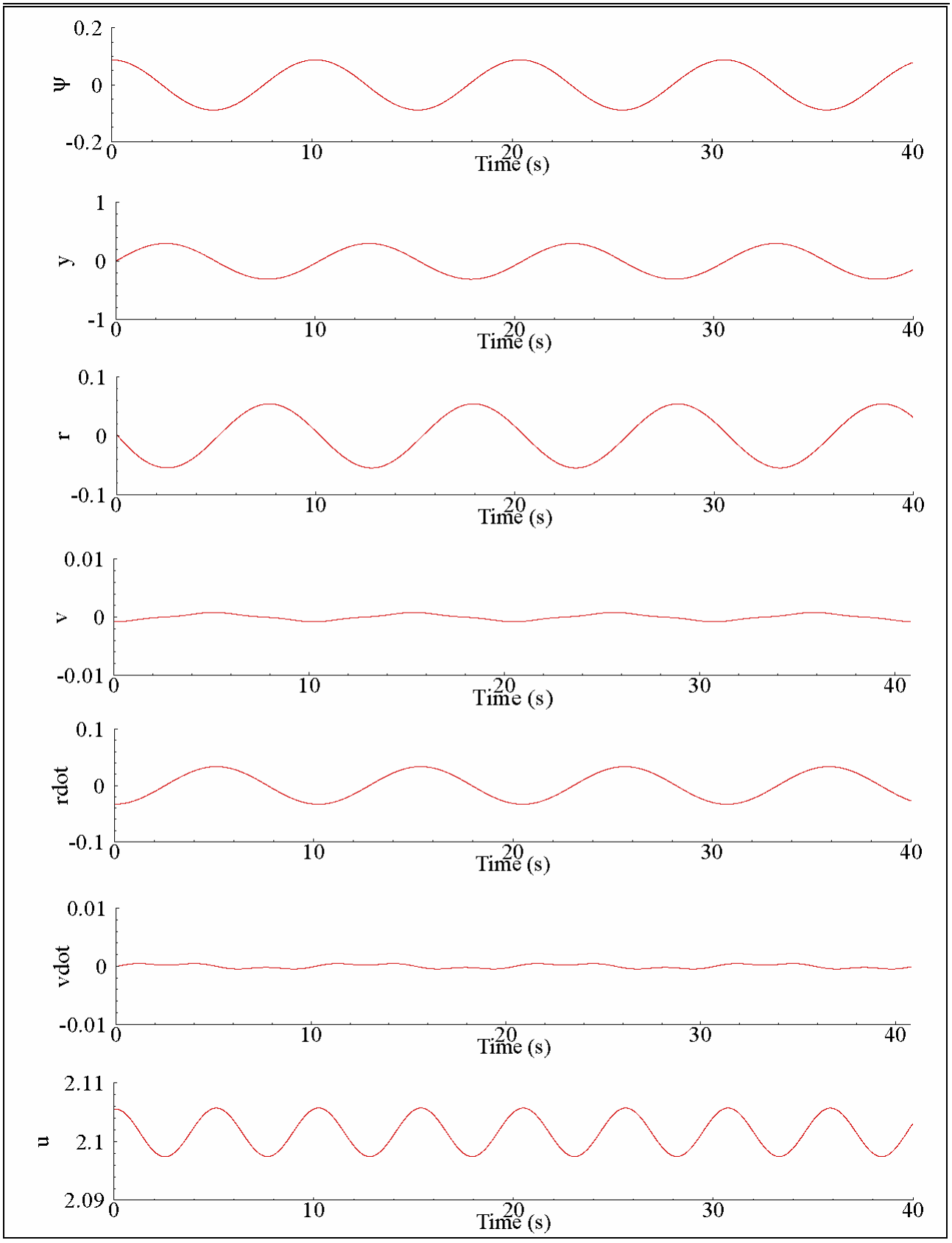

Figure C.6.1.31 Yaw_280_10 (part 1).

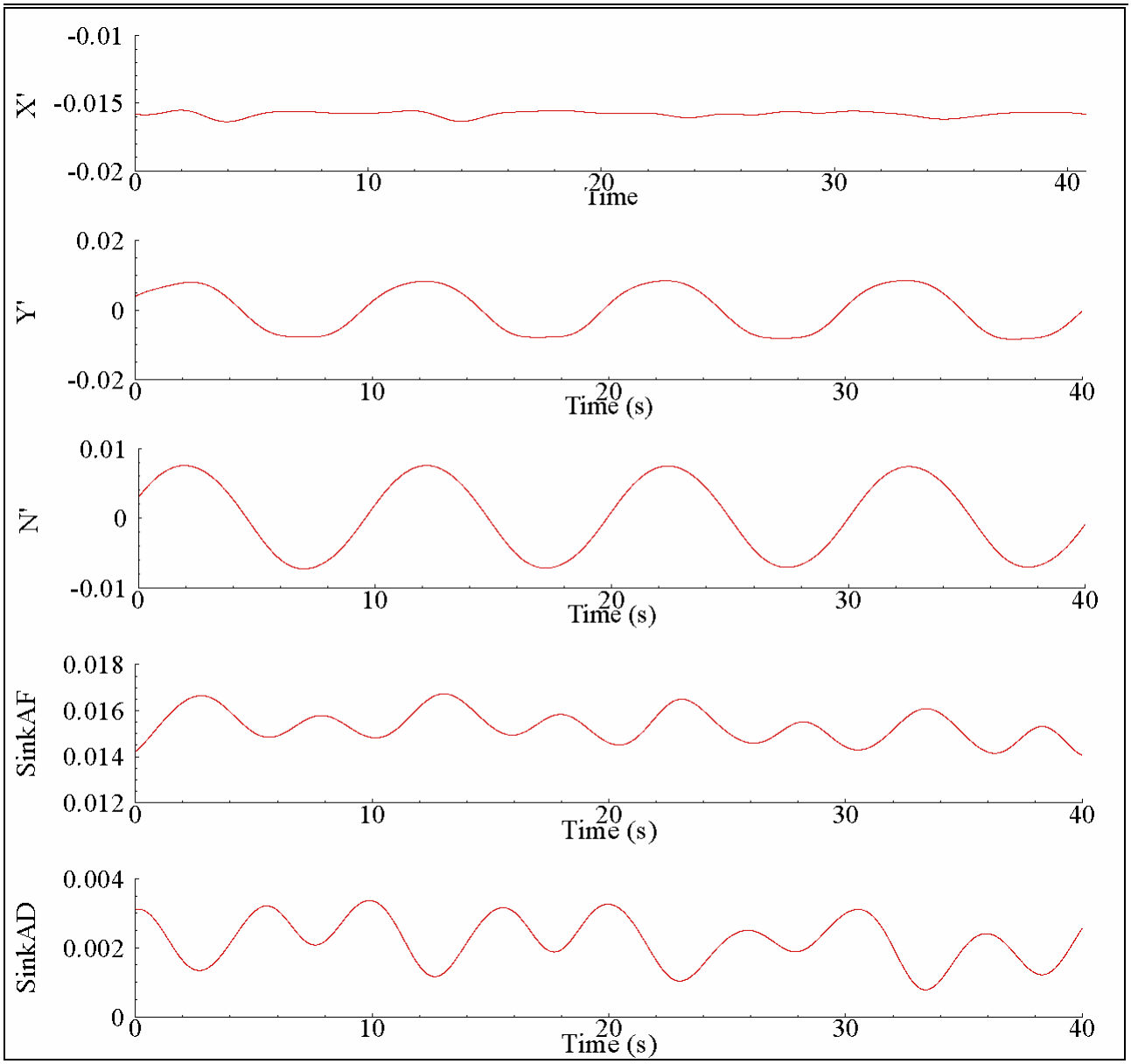

Figure C.6.1.32 Yaw_280_10 (part 2).

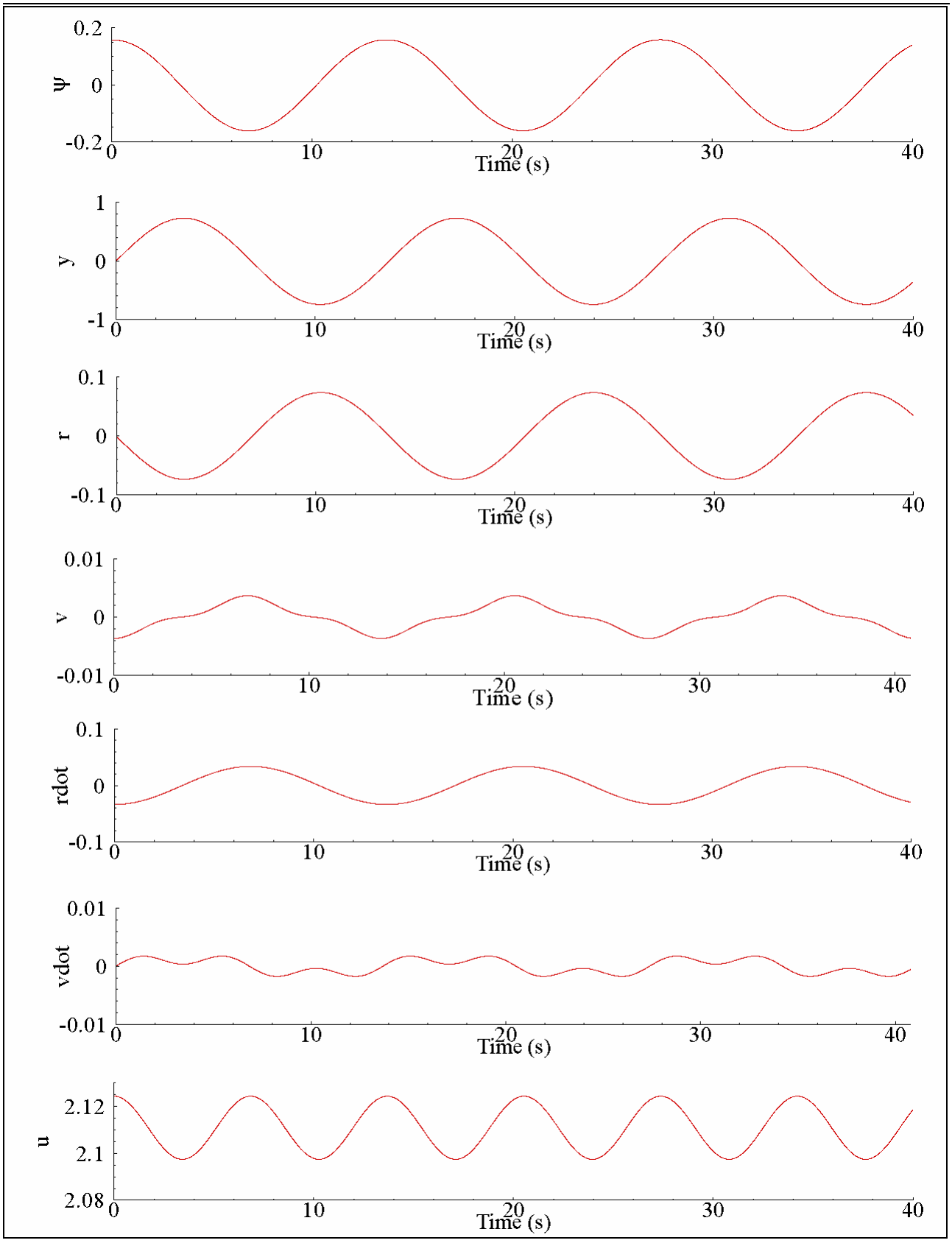

Figure C.6.1.33 Yaw_280_11 (part 1).

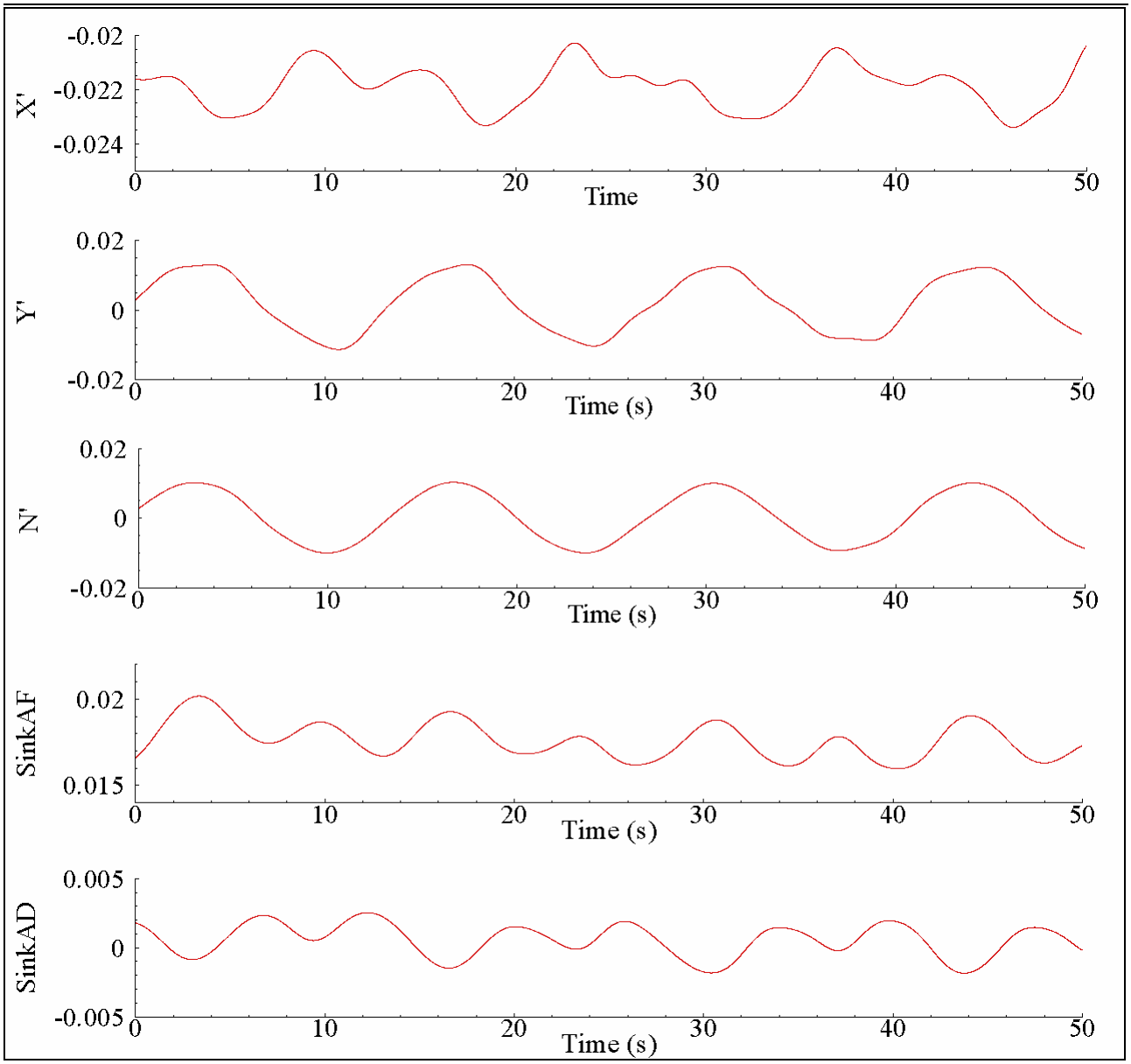

Figure C.6.1.34 Yaw_280_11 (part 2).

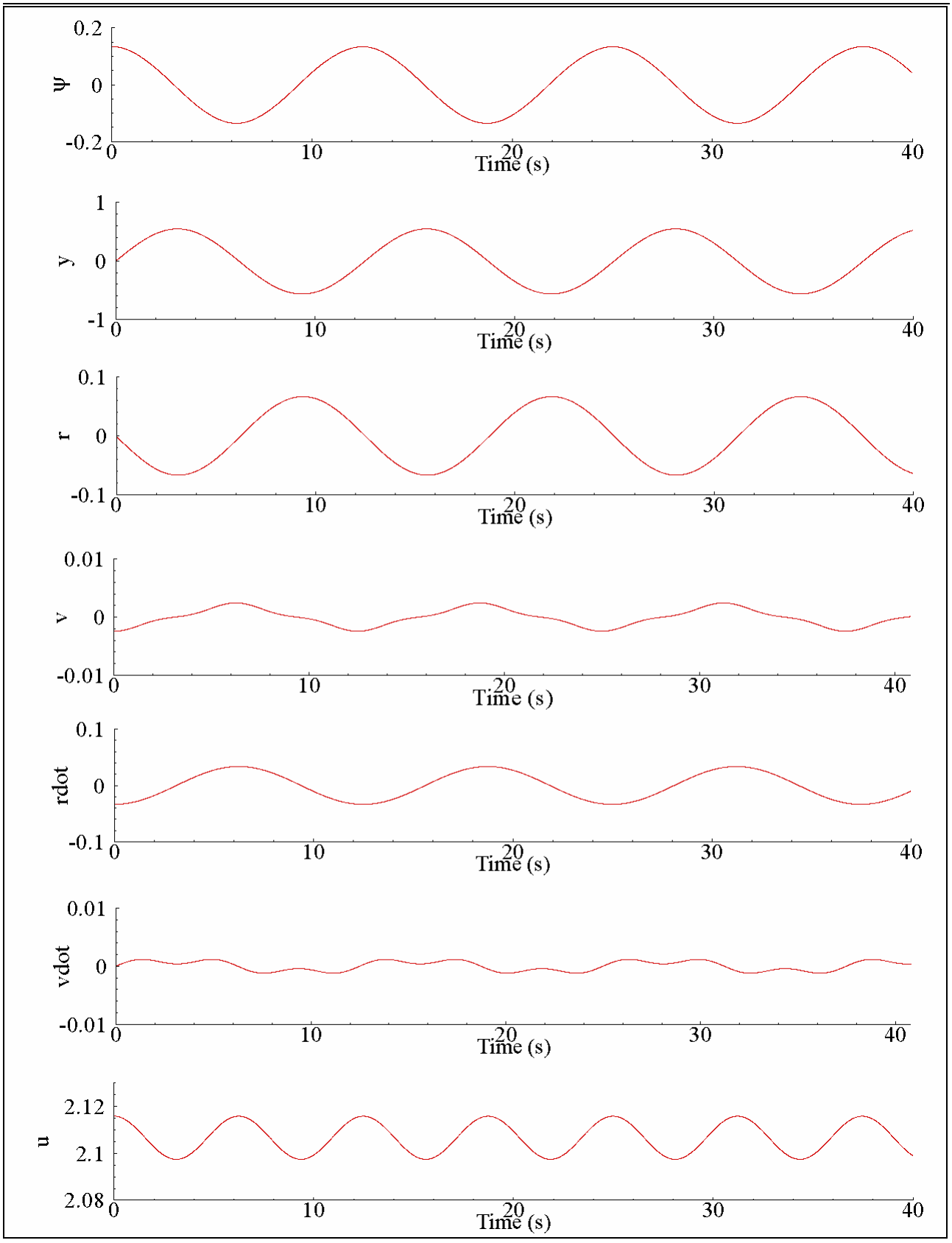

Figure C.6.1.35 Yaw_280_12 (part 1).

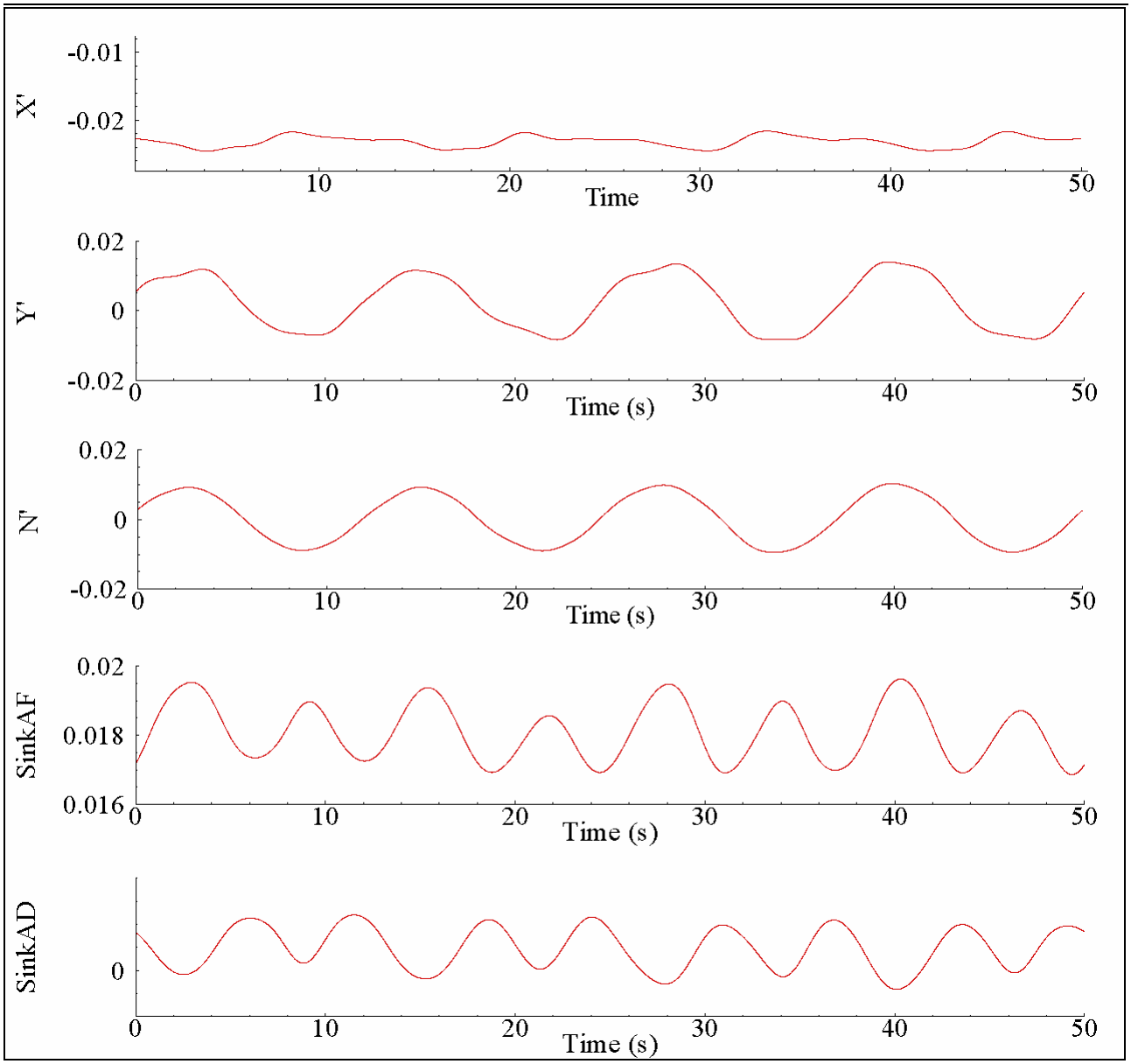

Figure C.6.1.36 Yaw_280_12 (part 2).

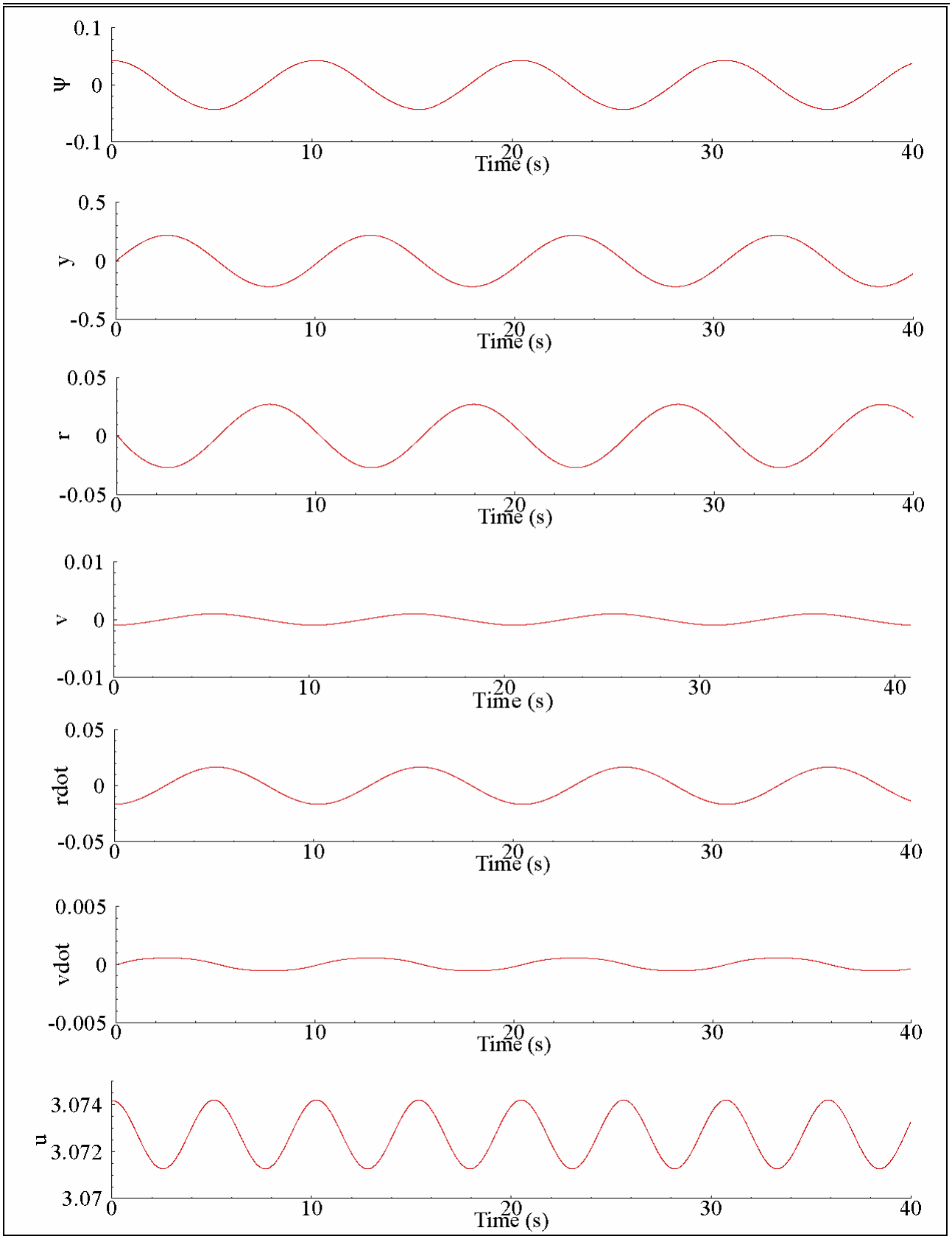

Figure C.6.1.37 Yaw_410_1 (part 1).

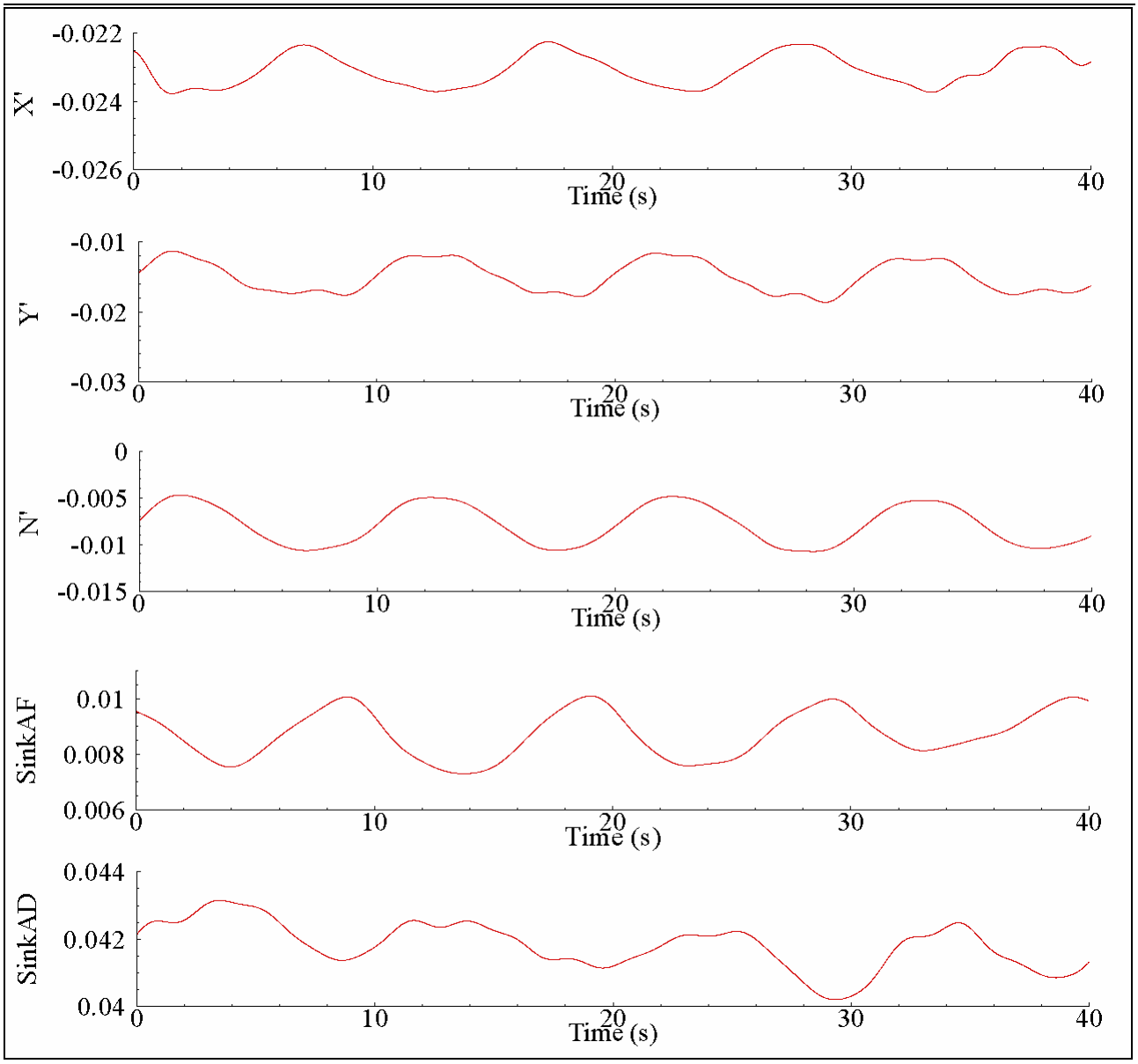

Figure C.6.1.38 Yaw_410_1 (part 2).

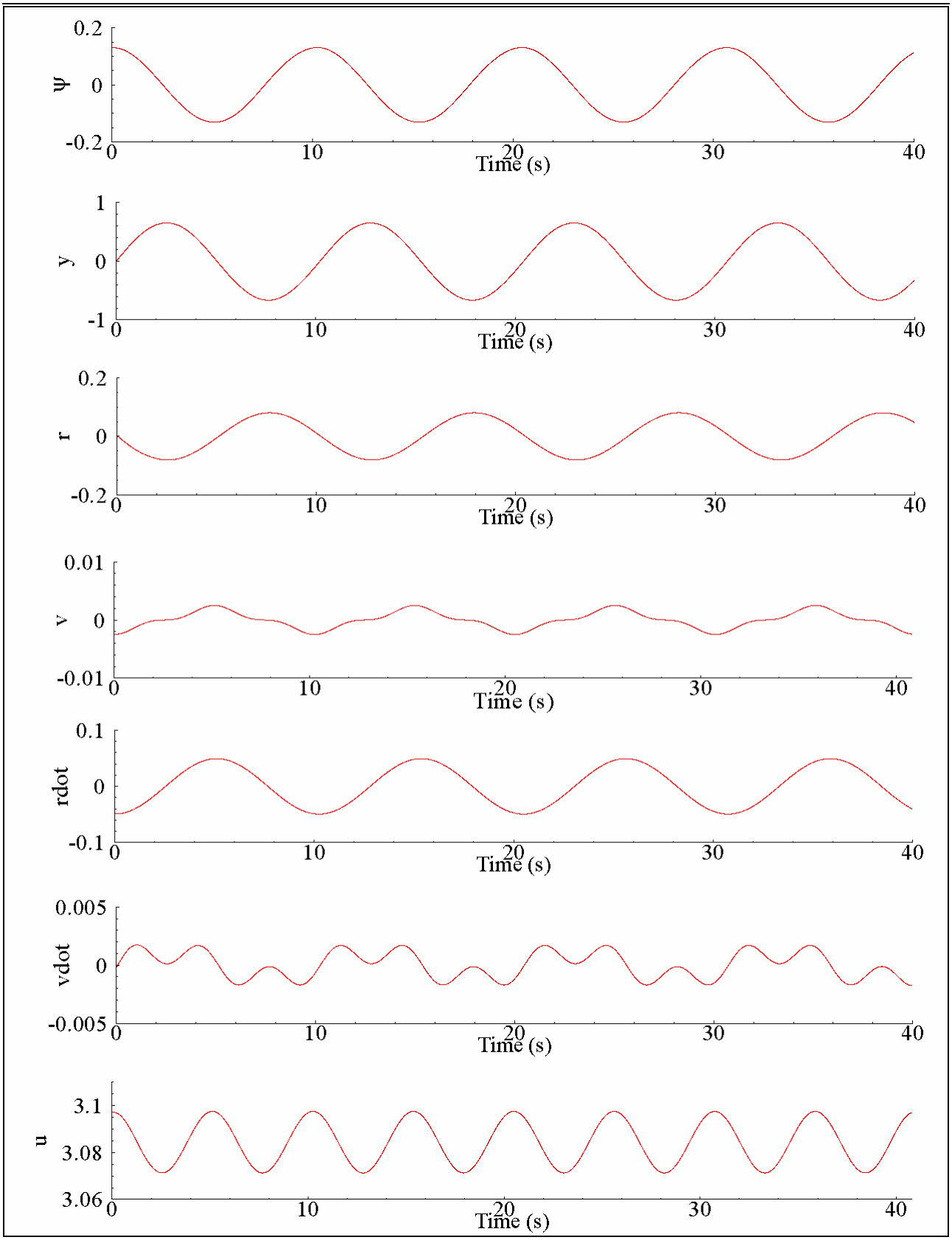

Figure C.6.1.39 Yaw_410_1 (part 2).

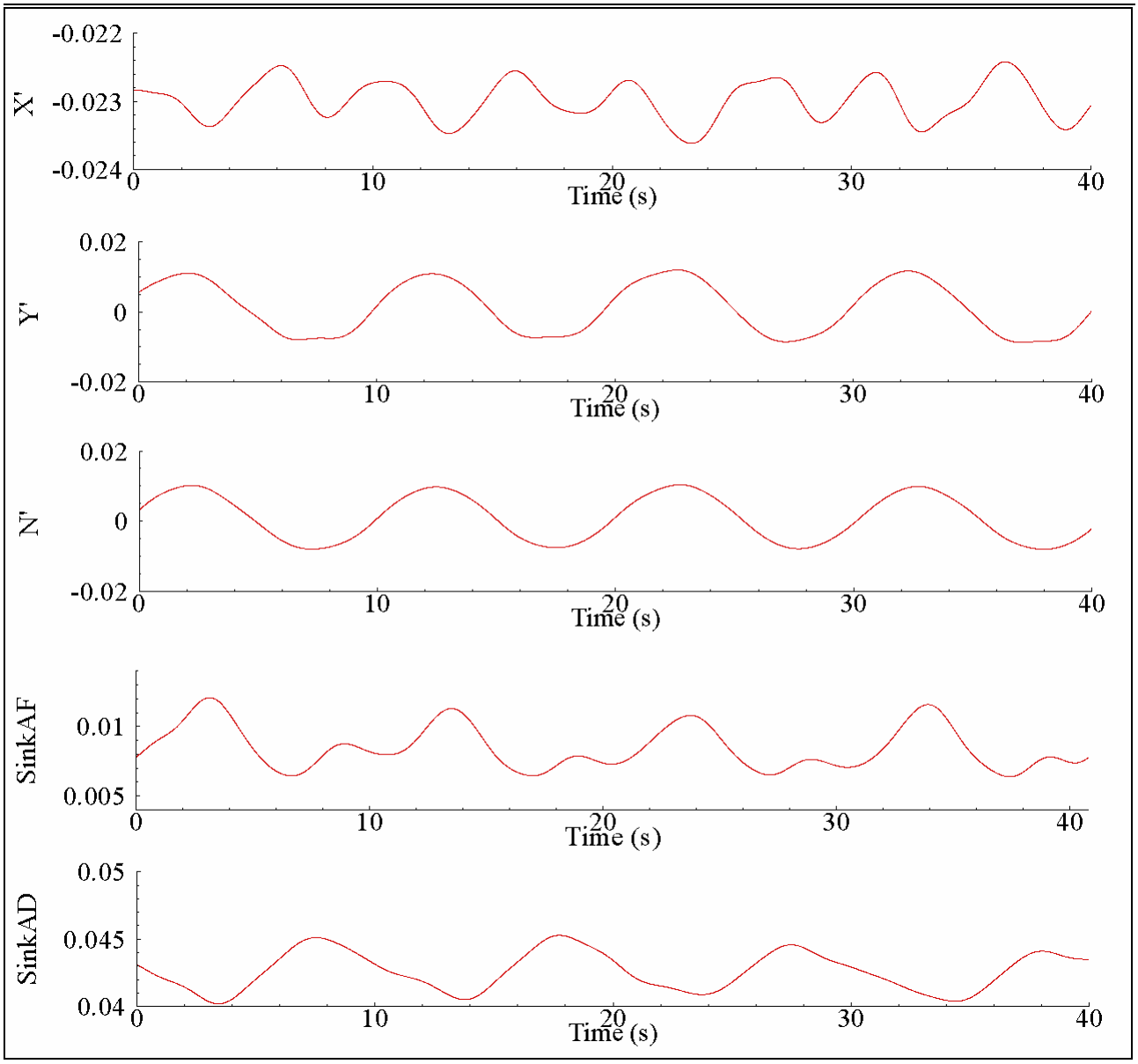

Figure C.6.1.40 Yaw_410_2 (part 2).

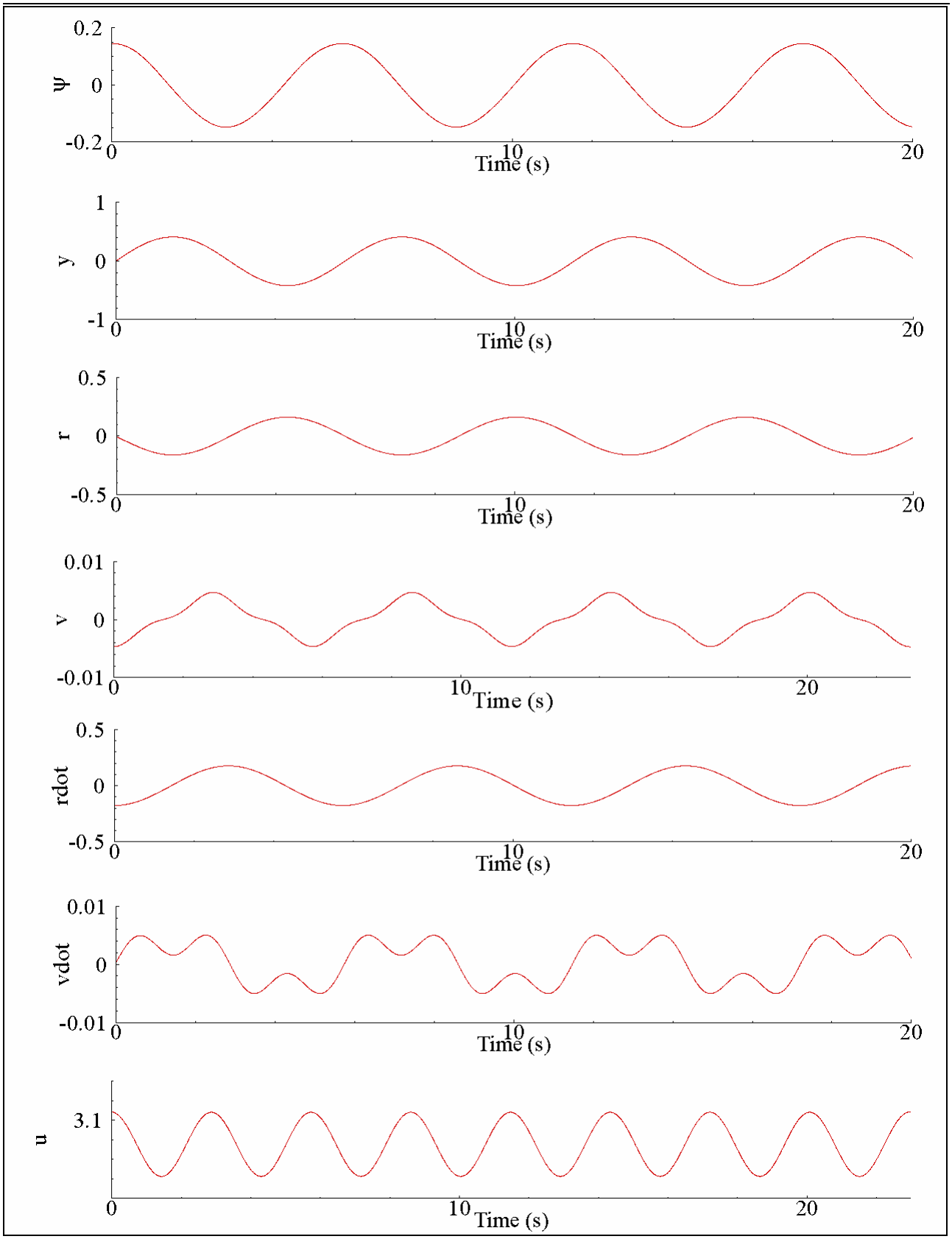

Figure C.6.1.41 Yaw_410_3 (part 1).

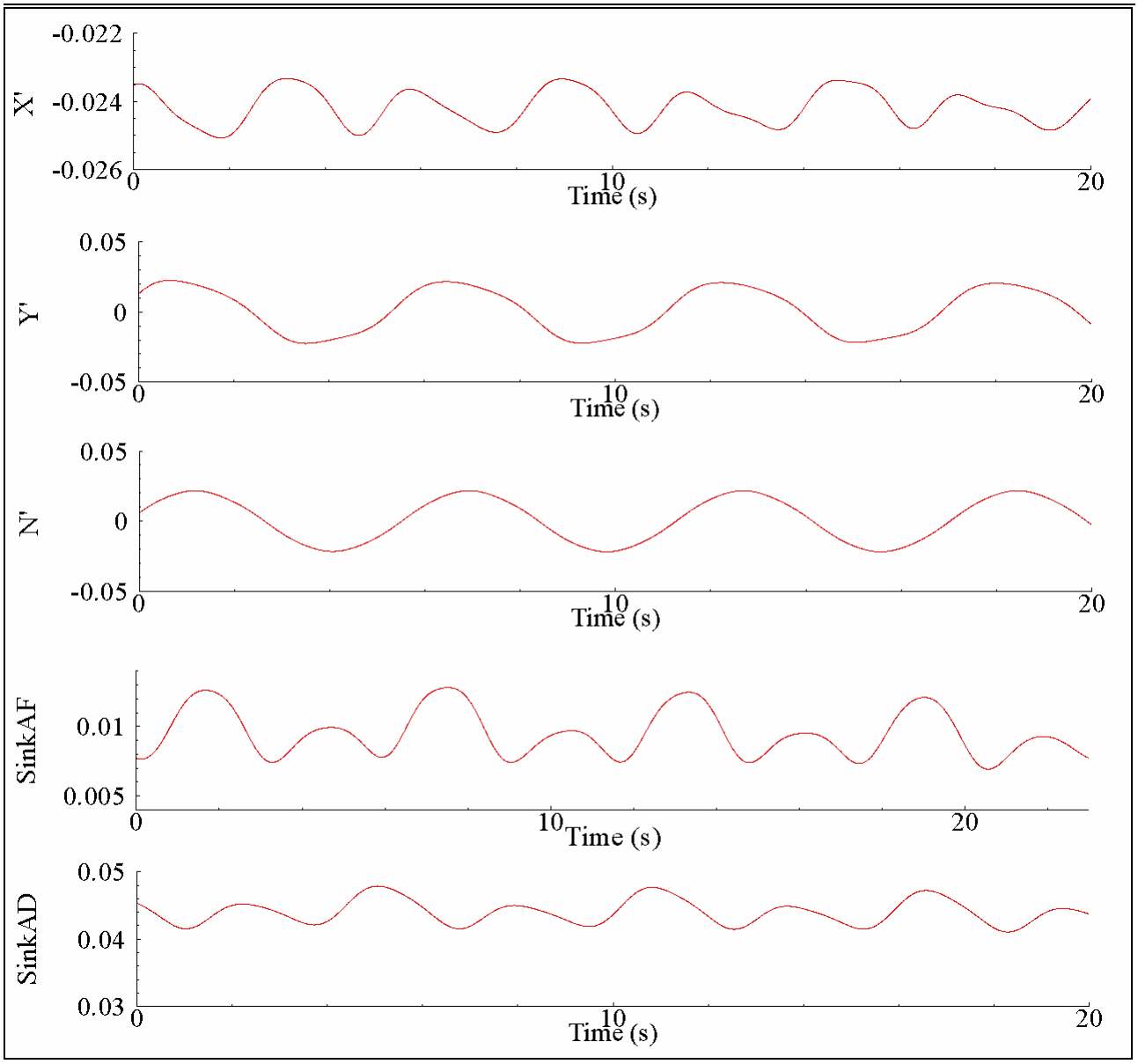

Figure C.6.1.42 Yaw_410_3 (part 2).

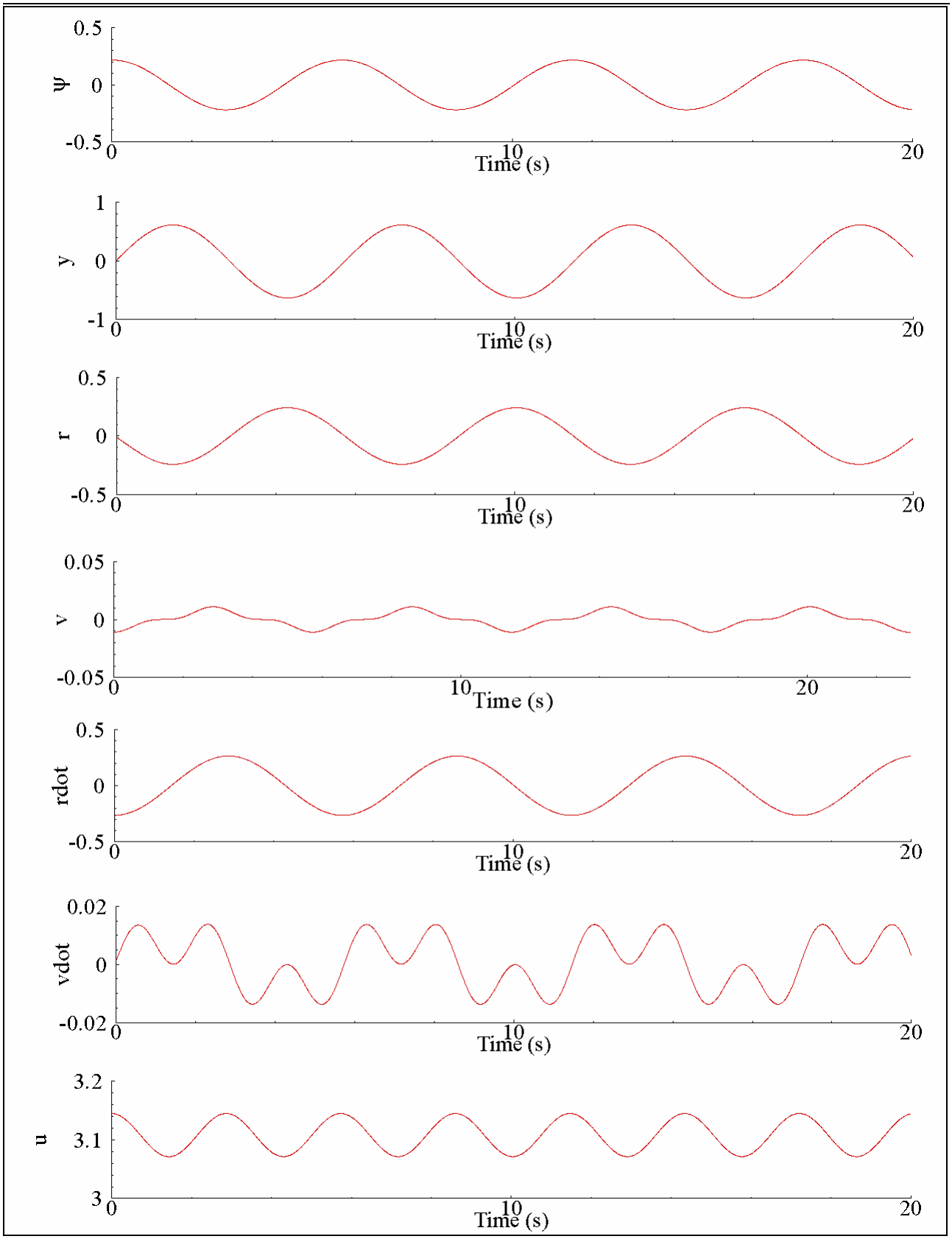

Figure C.6.1.43 Yaw_410_4 (part 1).

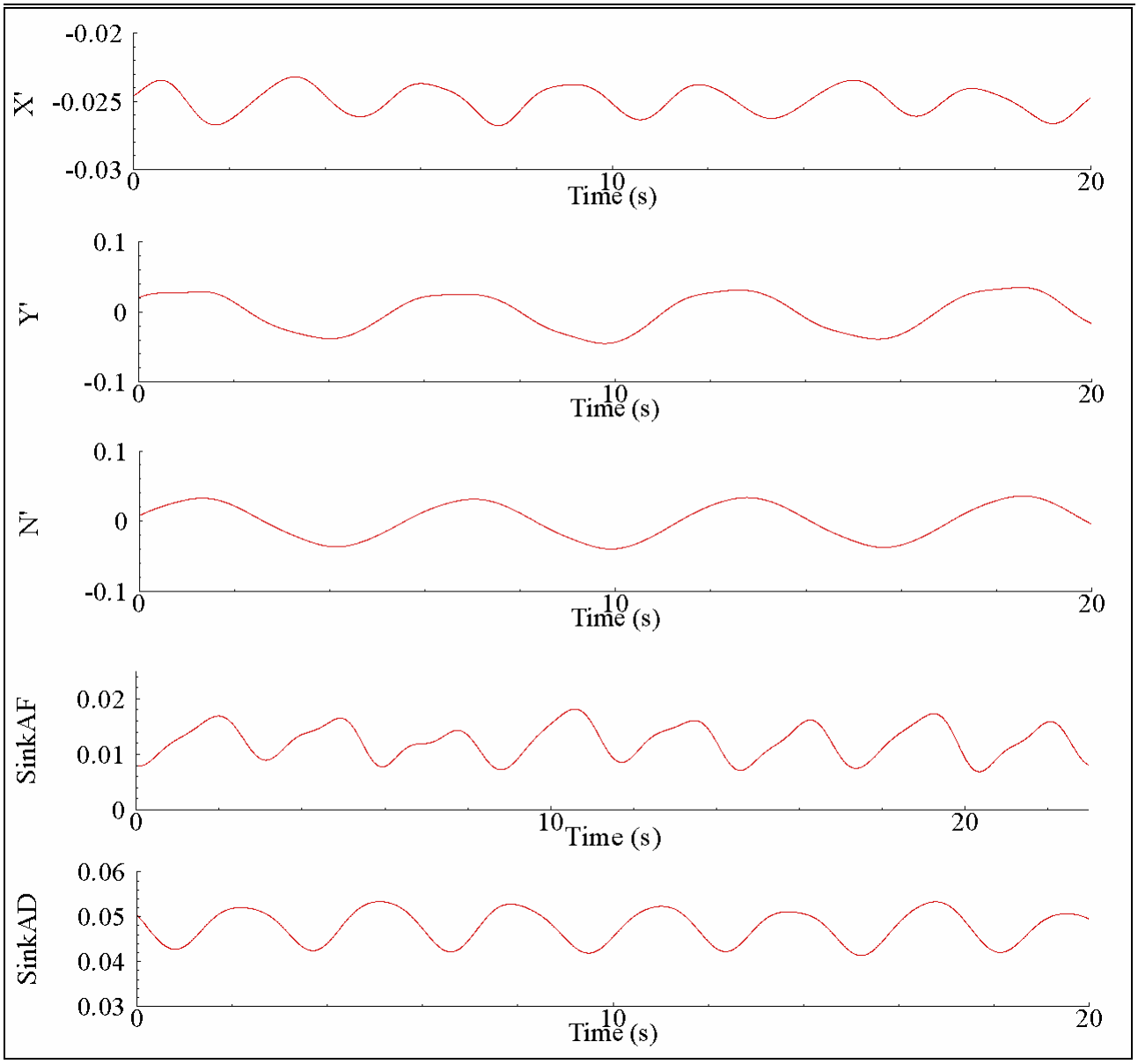

Figure C.6.1.44 Yaw_410_4 (part 2).

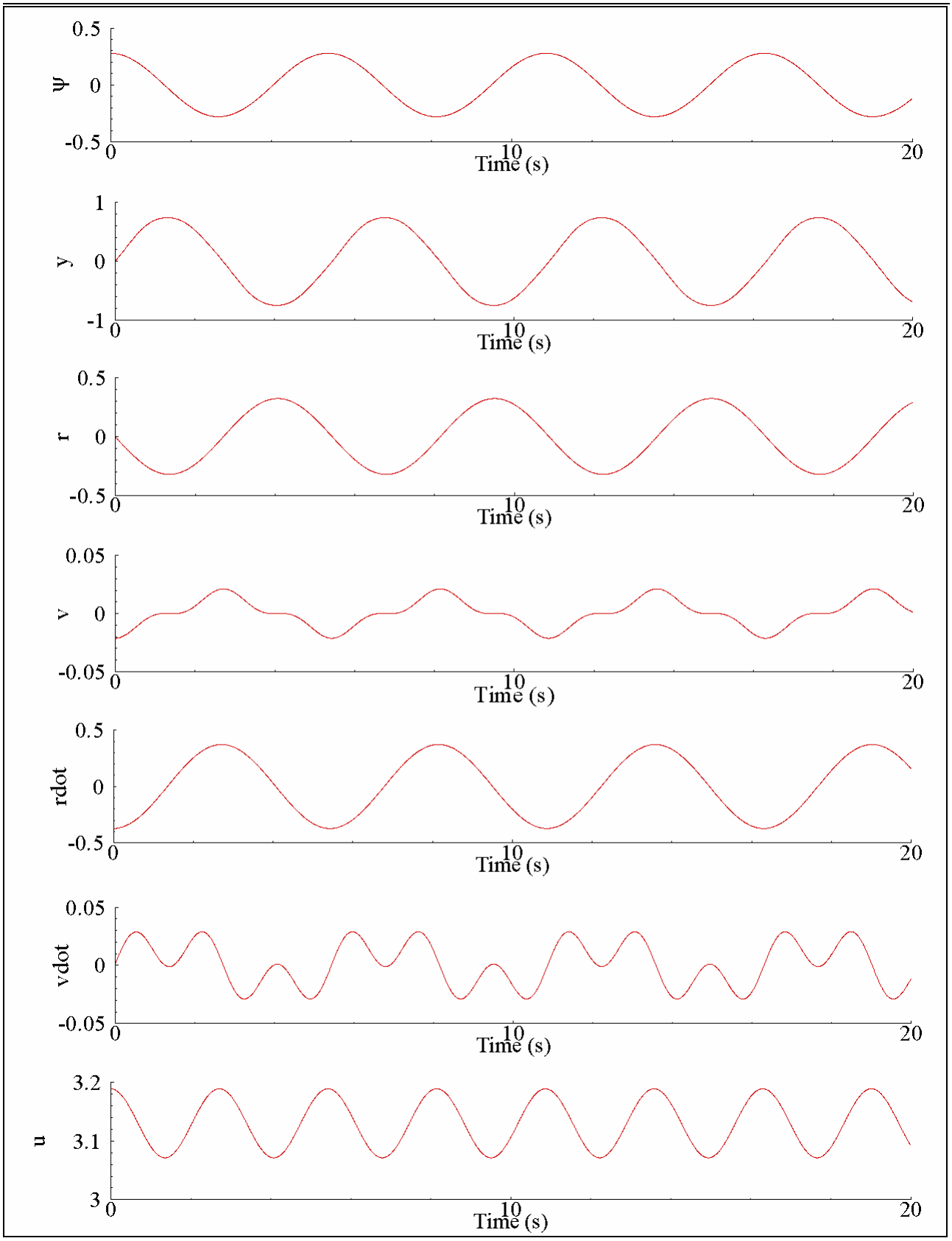

Figure C.6.1.45 Yaw_410_5 (part 1).

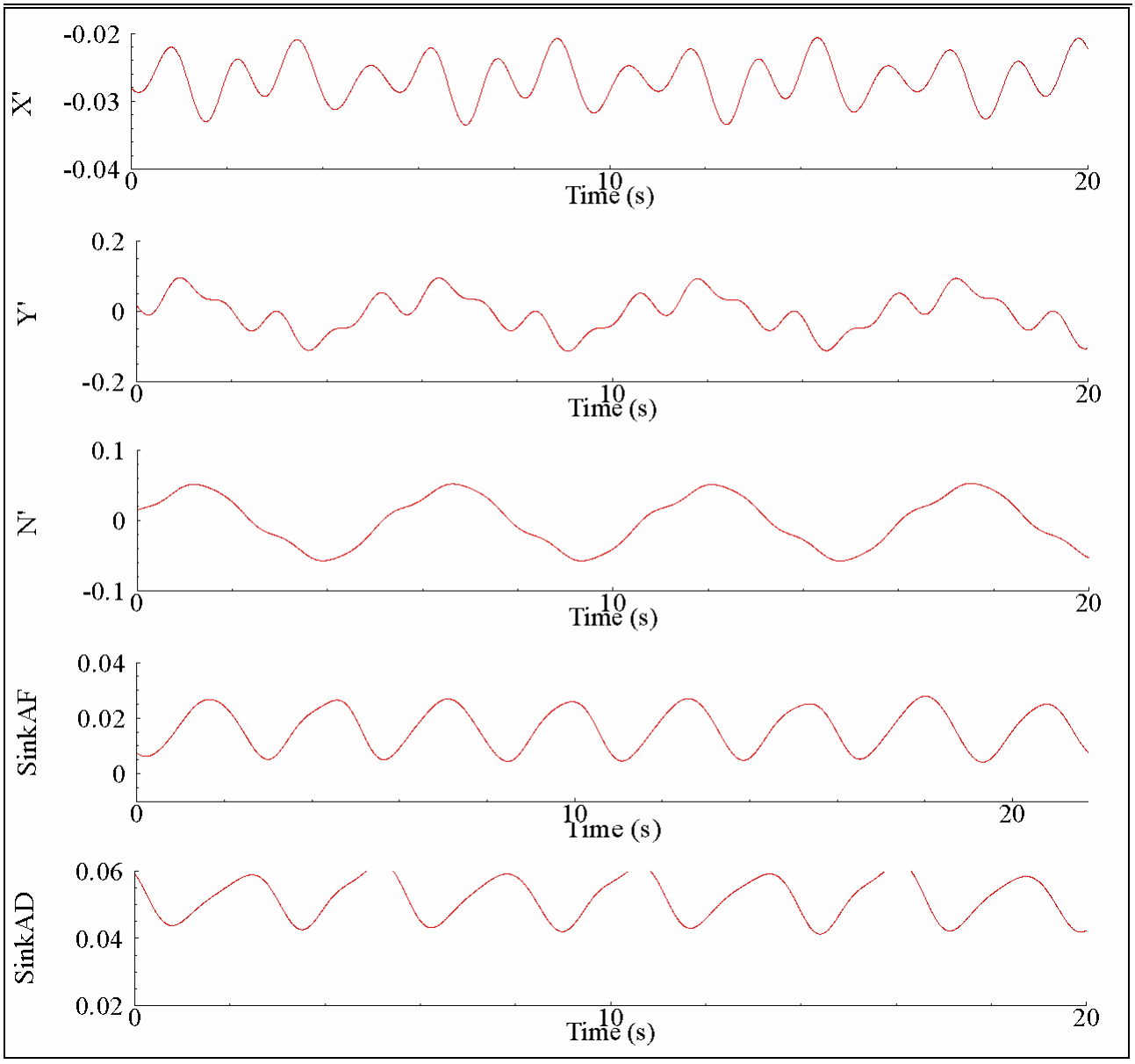

Figure C.6.1.46 Yaw_410_5 (part 2).

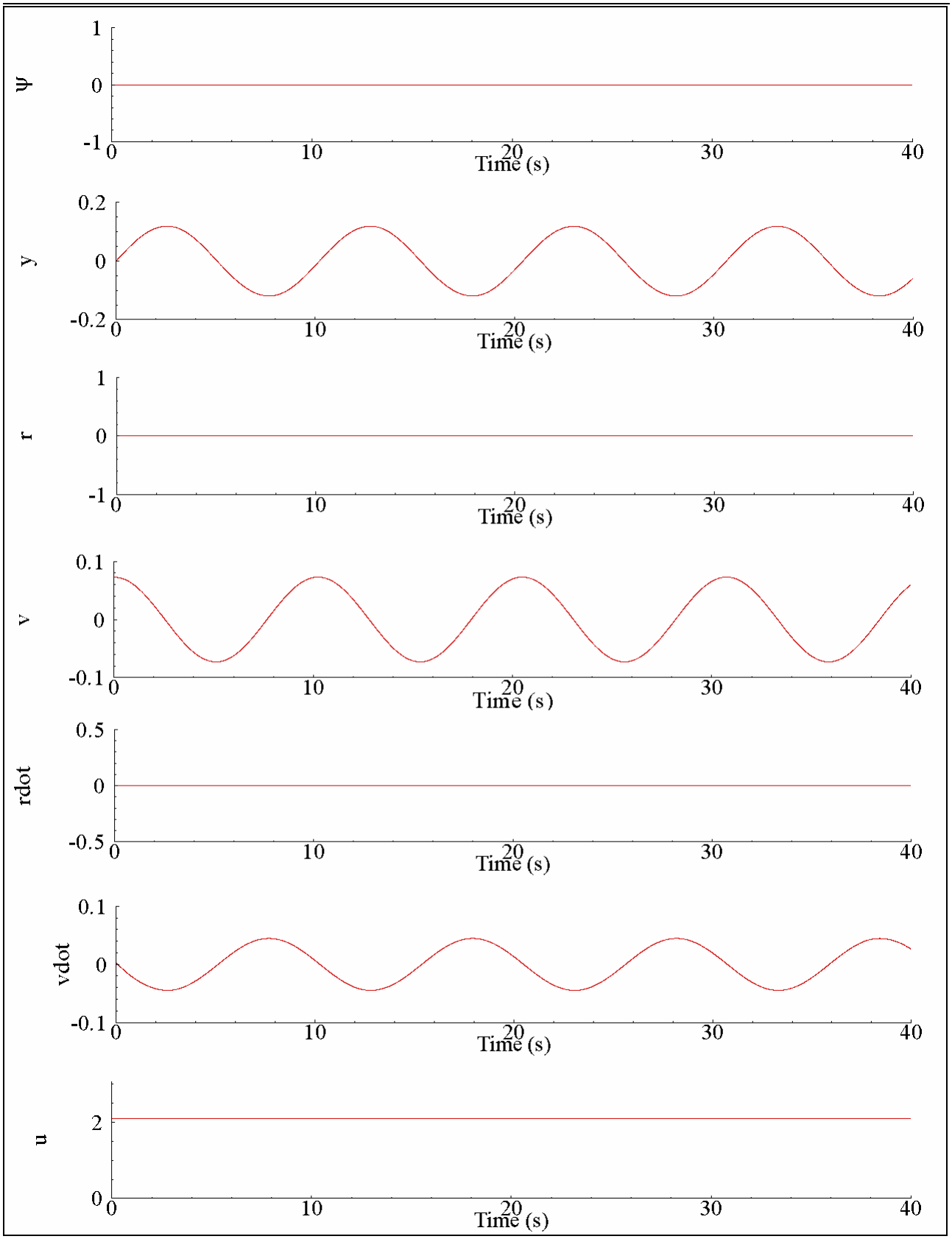

Figure C.6.1.47 Sway_280_1 (part 1).

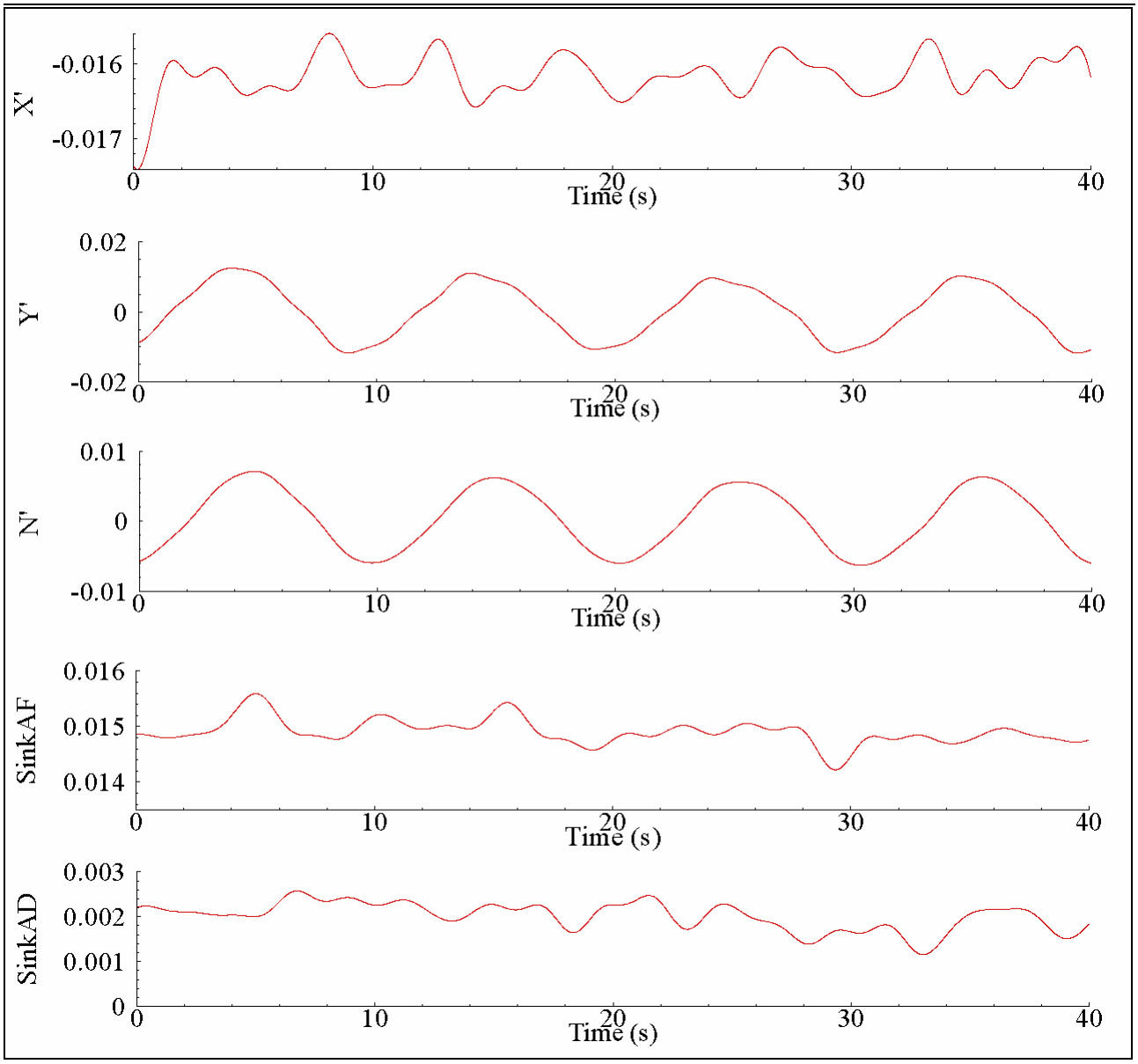

Figure C.6.1.48 Sway_280_1 (part 2).

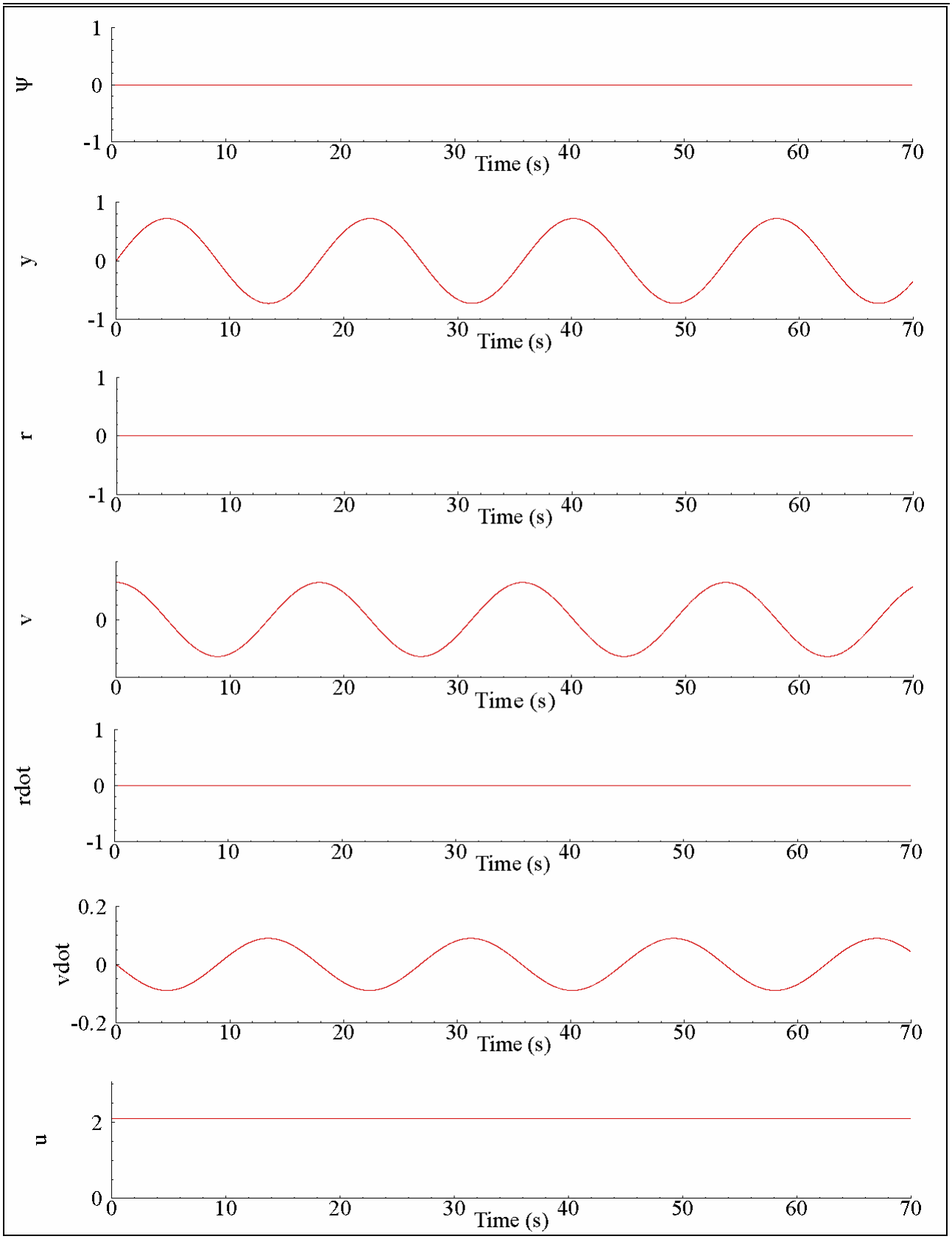

Figure C.6.1.49 Sway_280_2 (part 1).

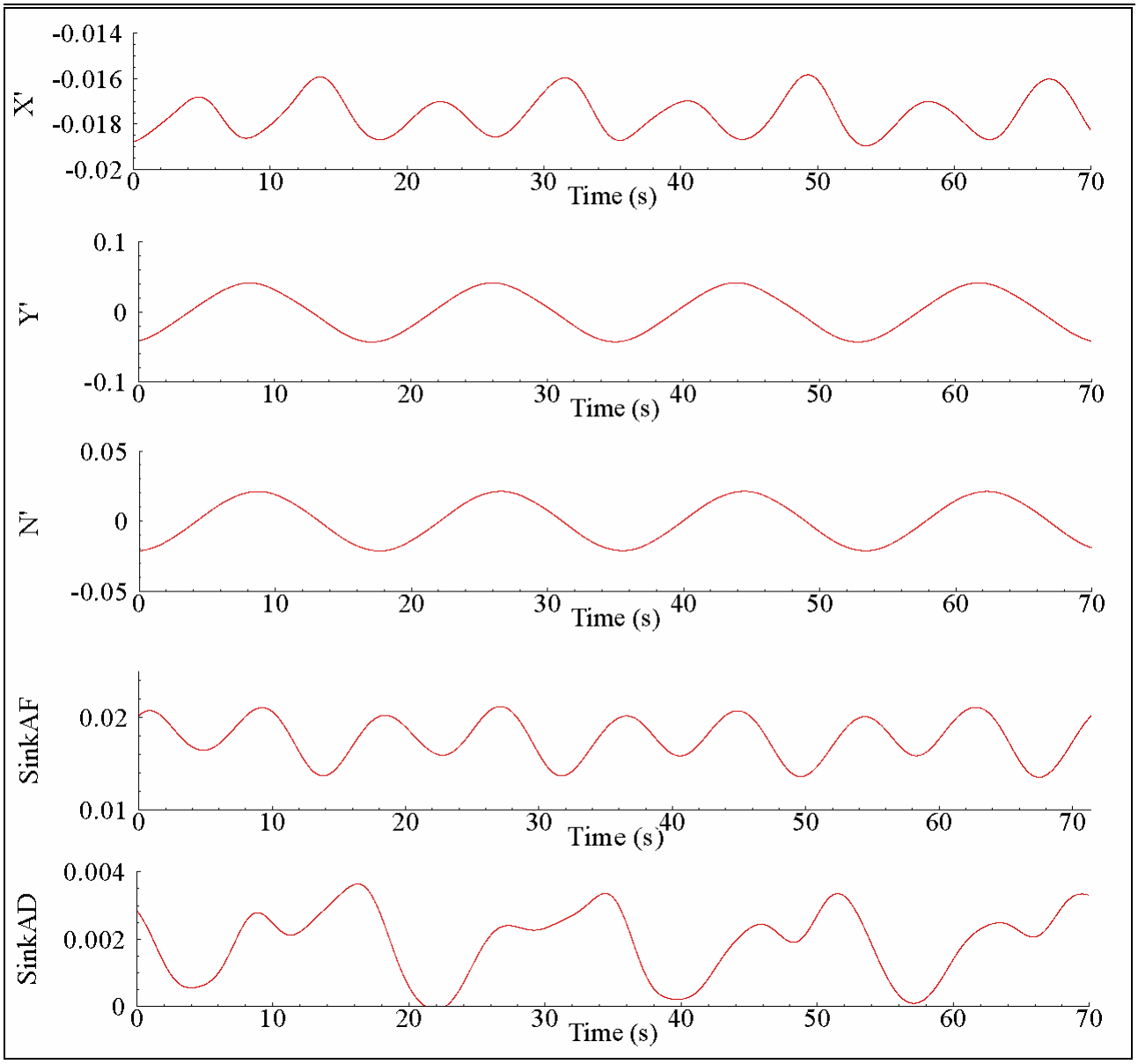

Figure C.6.1.50 Sway_280_2 (part 2).

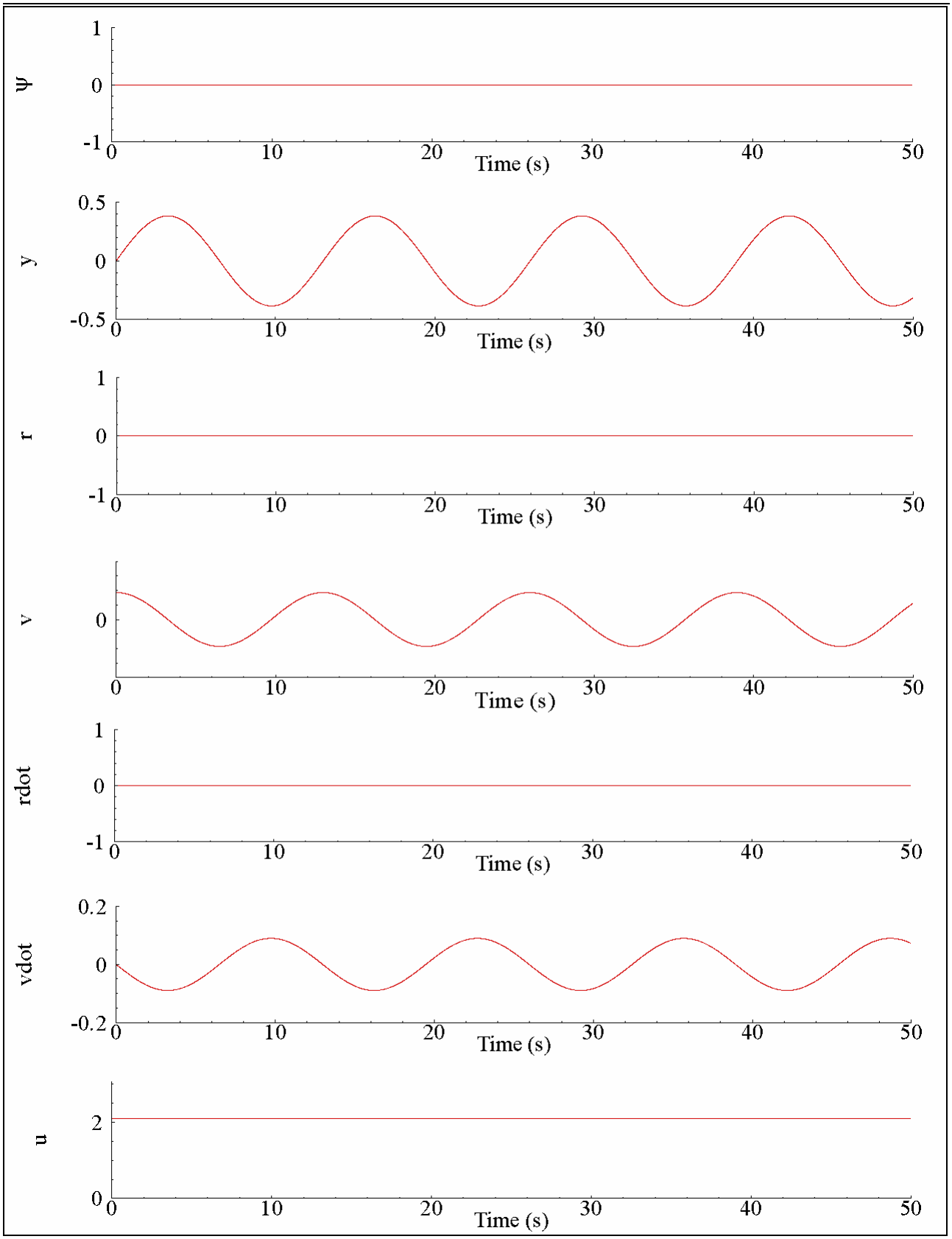

Figure C.6.1.51 Sway_280_3 (part 1).

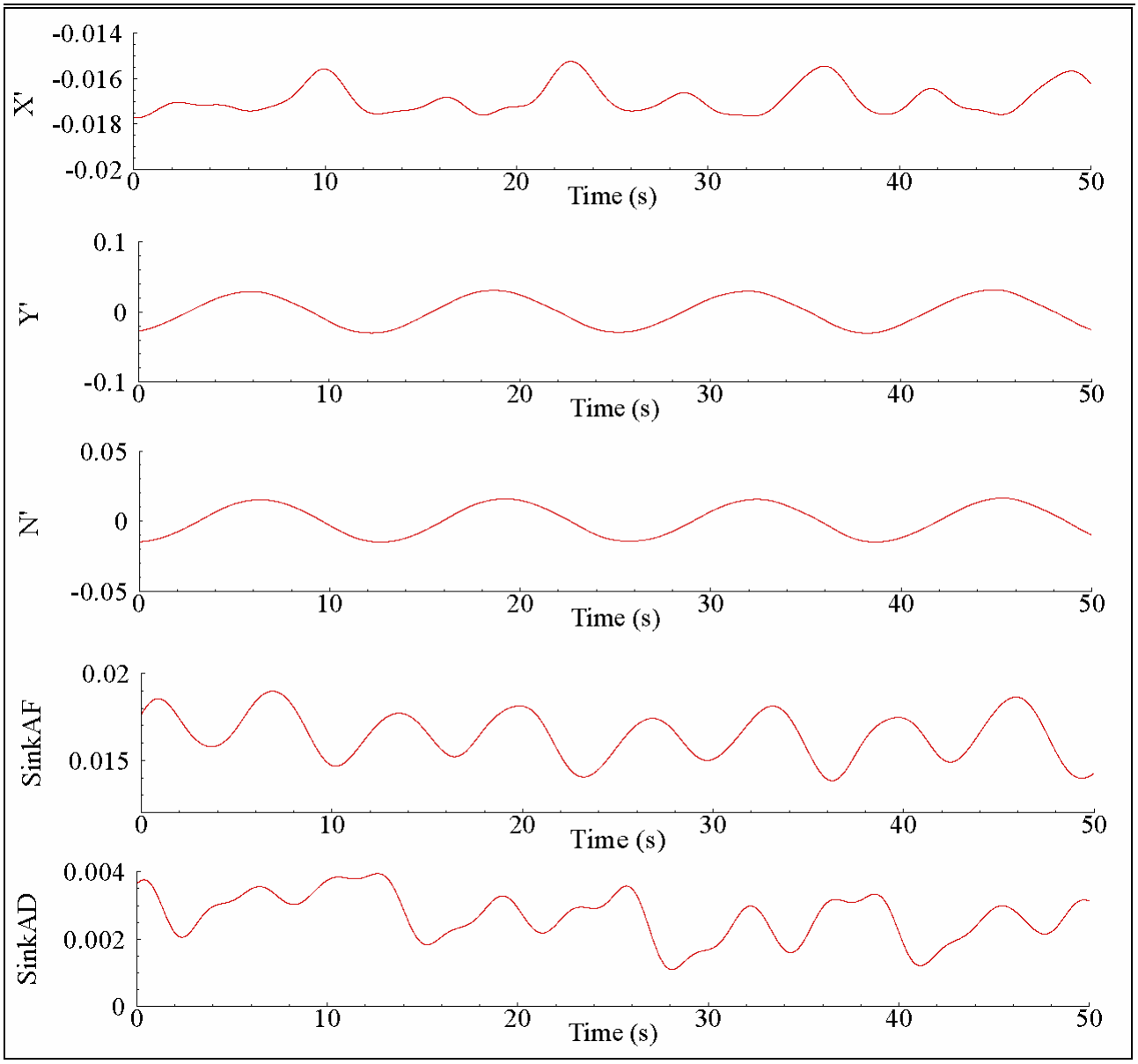

Figure C.6.1.52 Sway_280_3 (part 2).

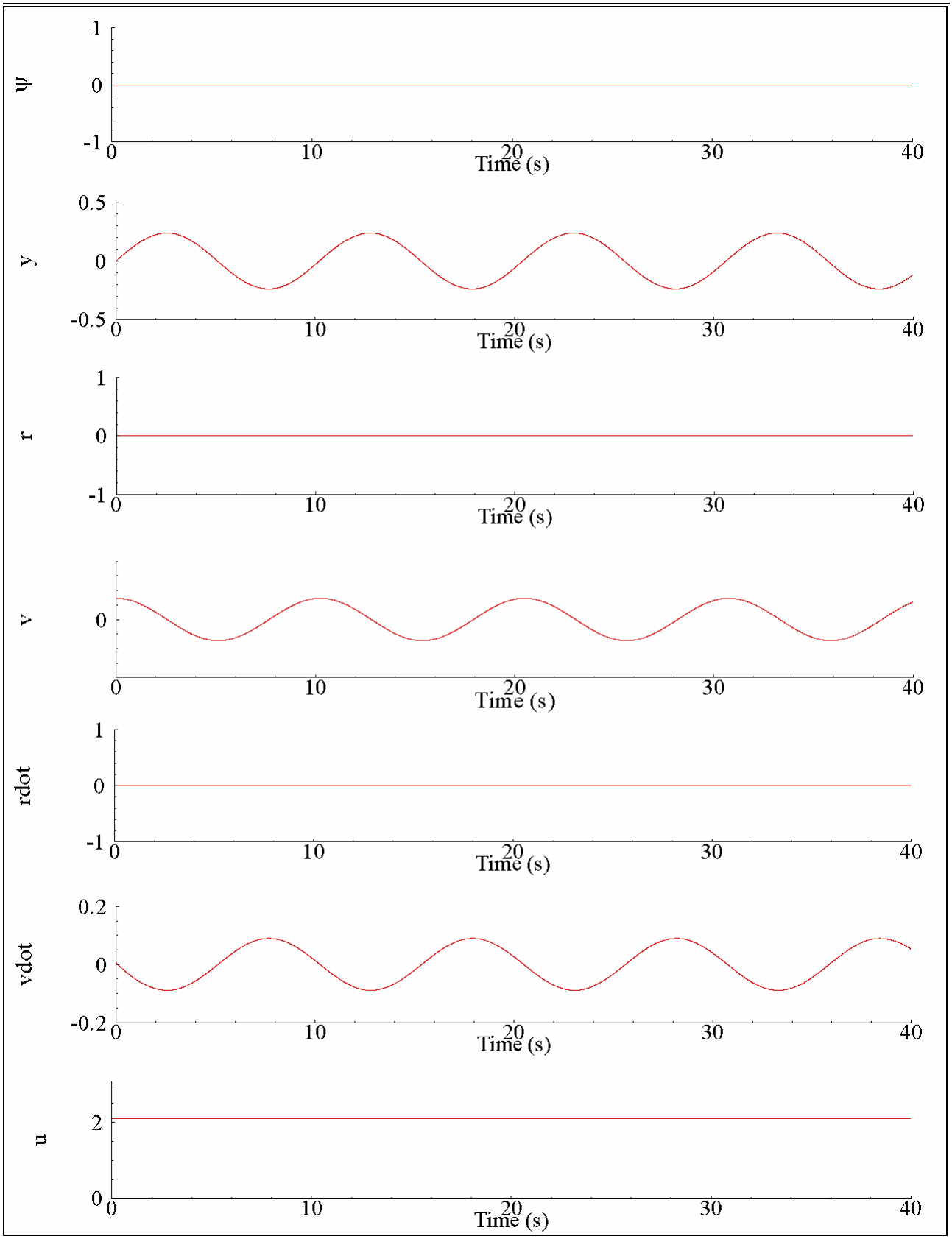

Figure C.6.1.53 Sway_280_4 (part 1).

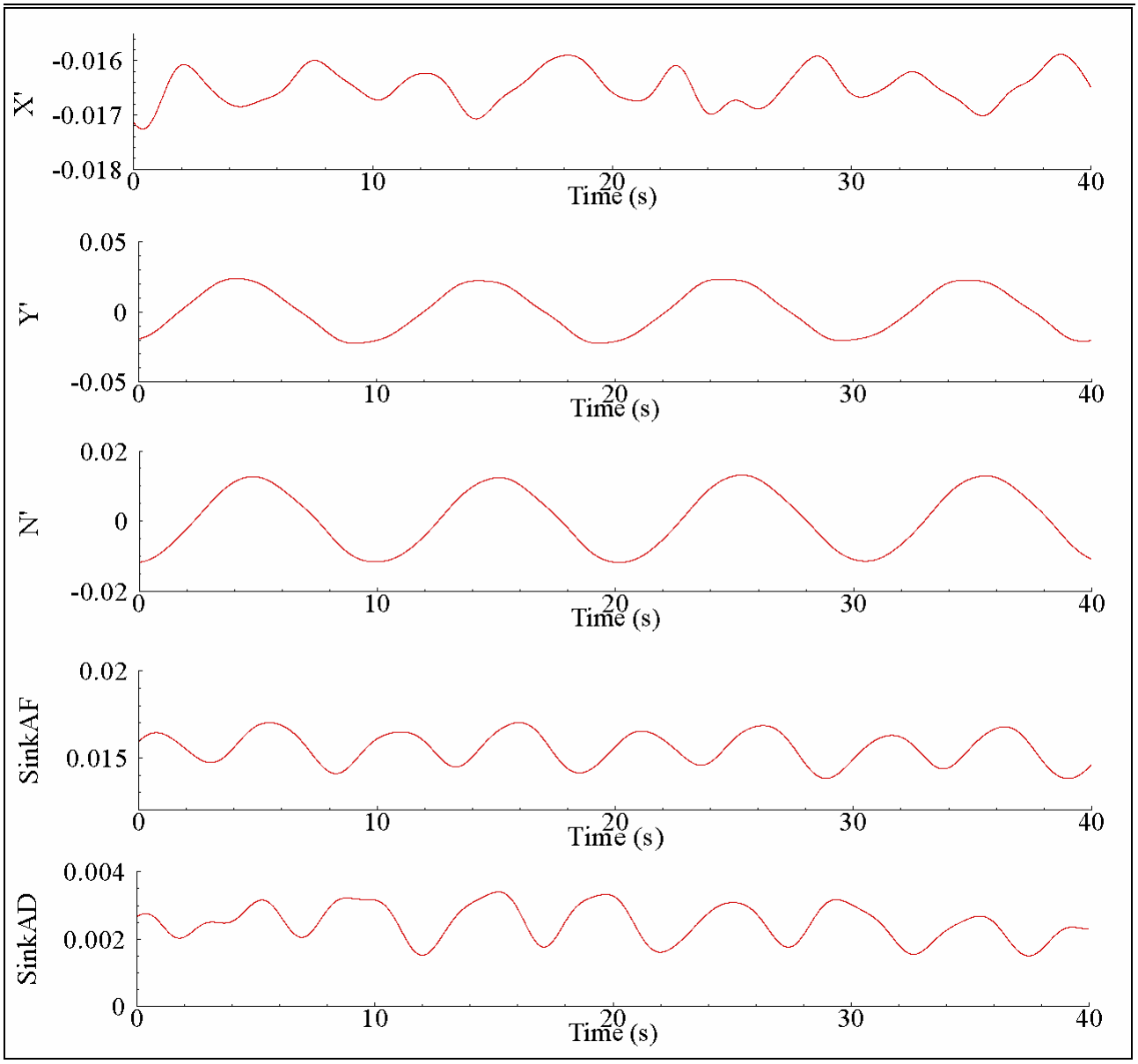

Figure C.6.1.54 Sway_280_4 (part 2).

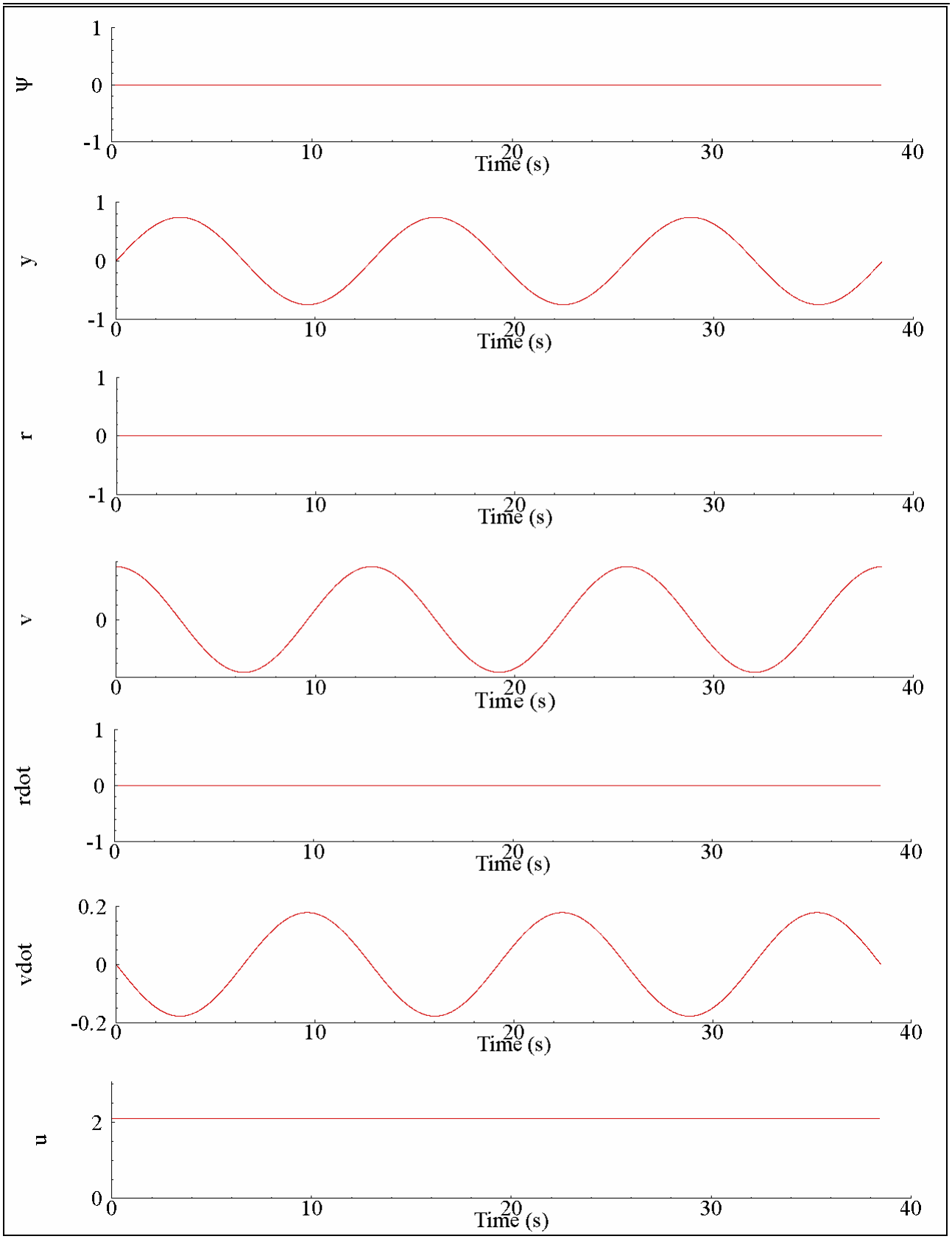

Figure C.6.1.55 Sway_280_5 (part 1).

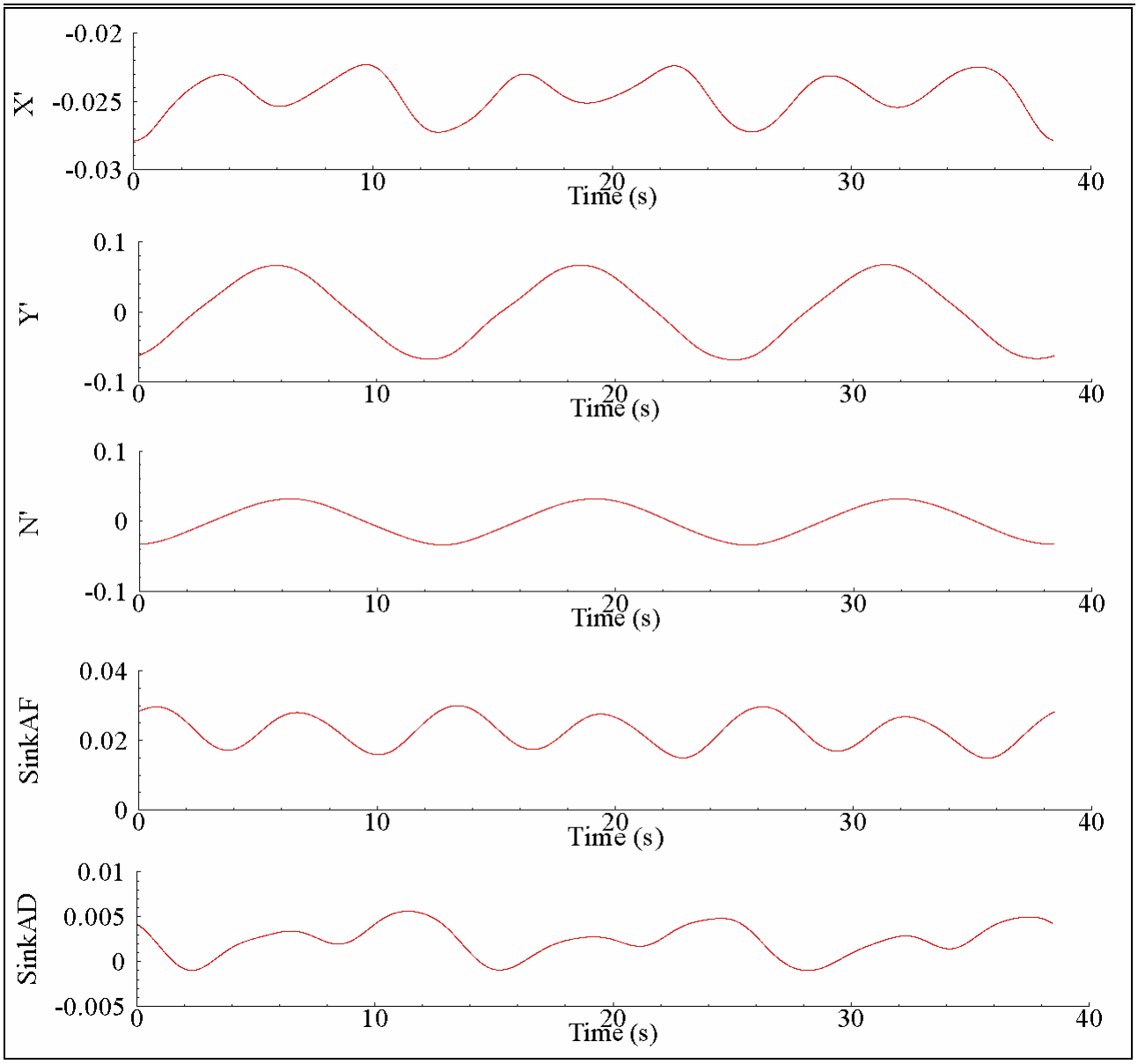

Figure C.6.1.56 Sway_280_5 (part 2).

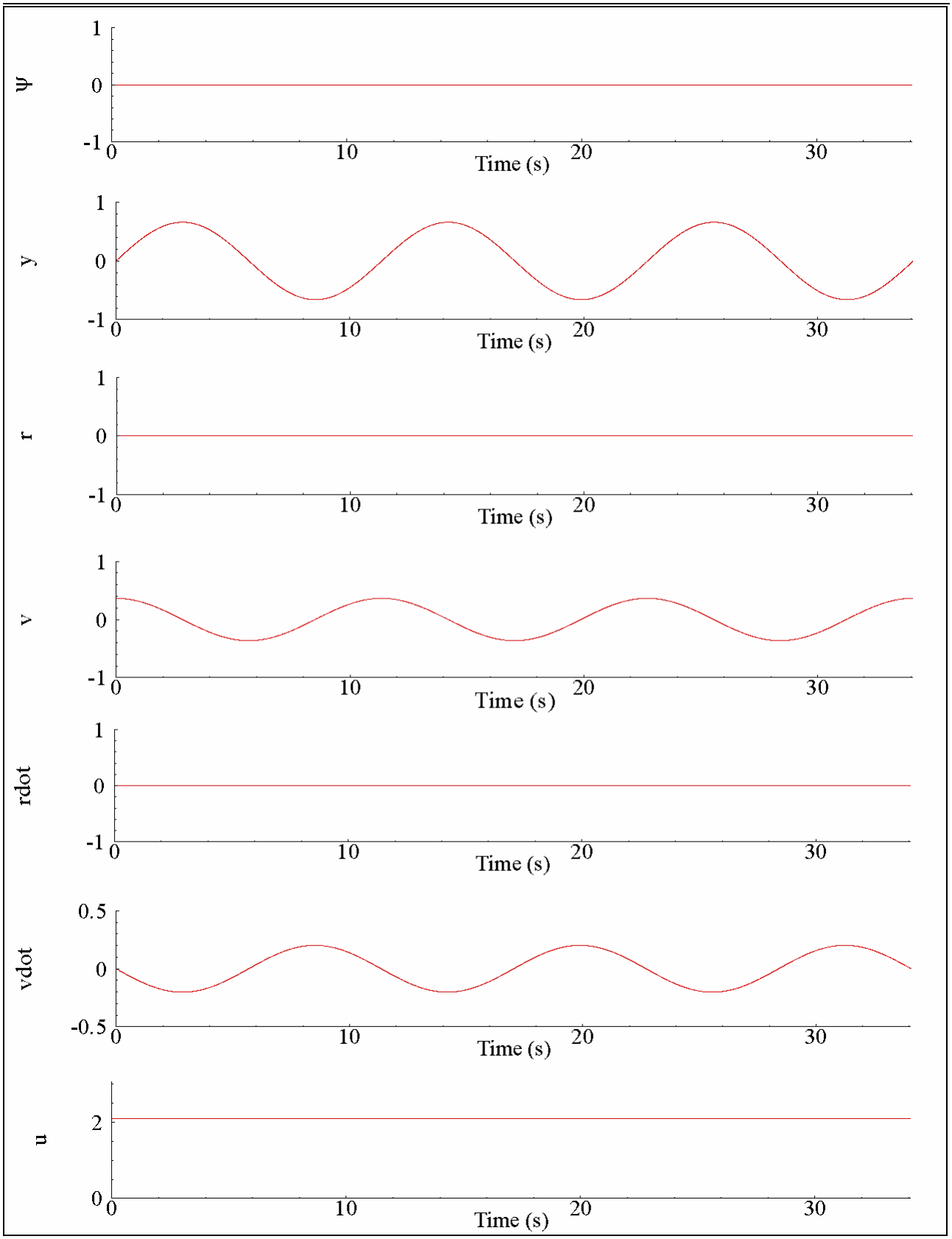

Figure C.6.1.57 Sway_280_6 (part 1).

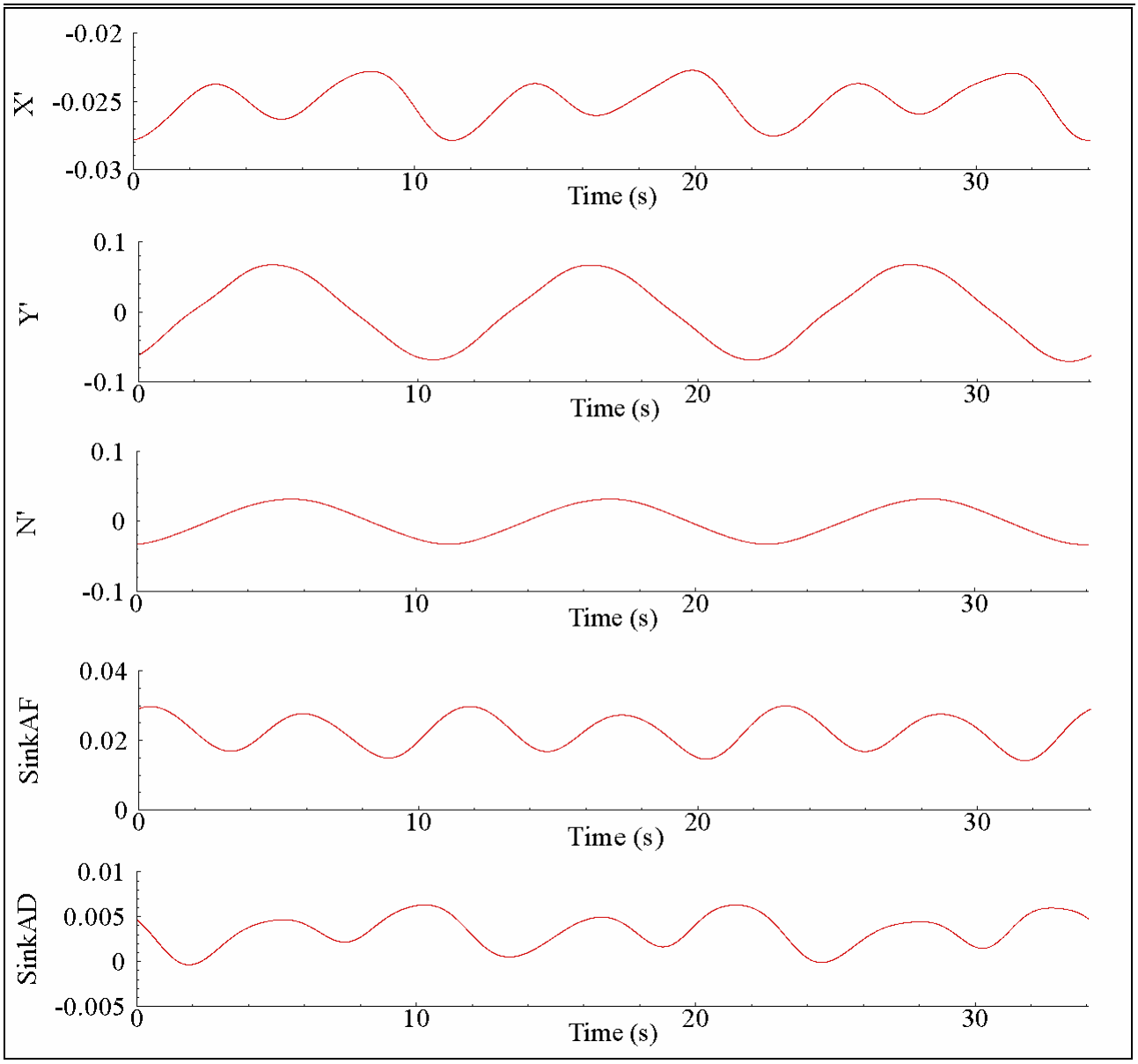

Figure C.6.1.58 Sway_280_6 (part 2).

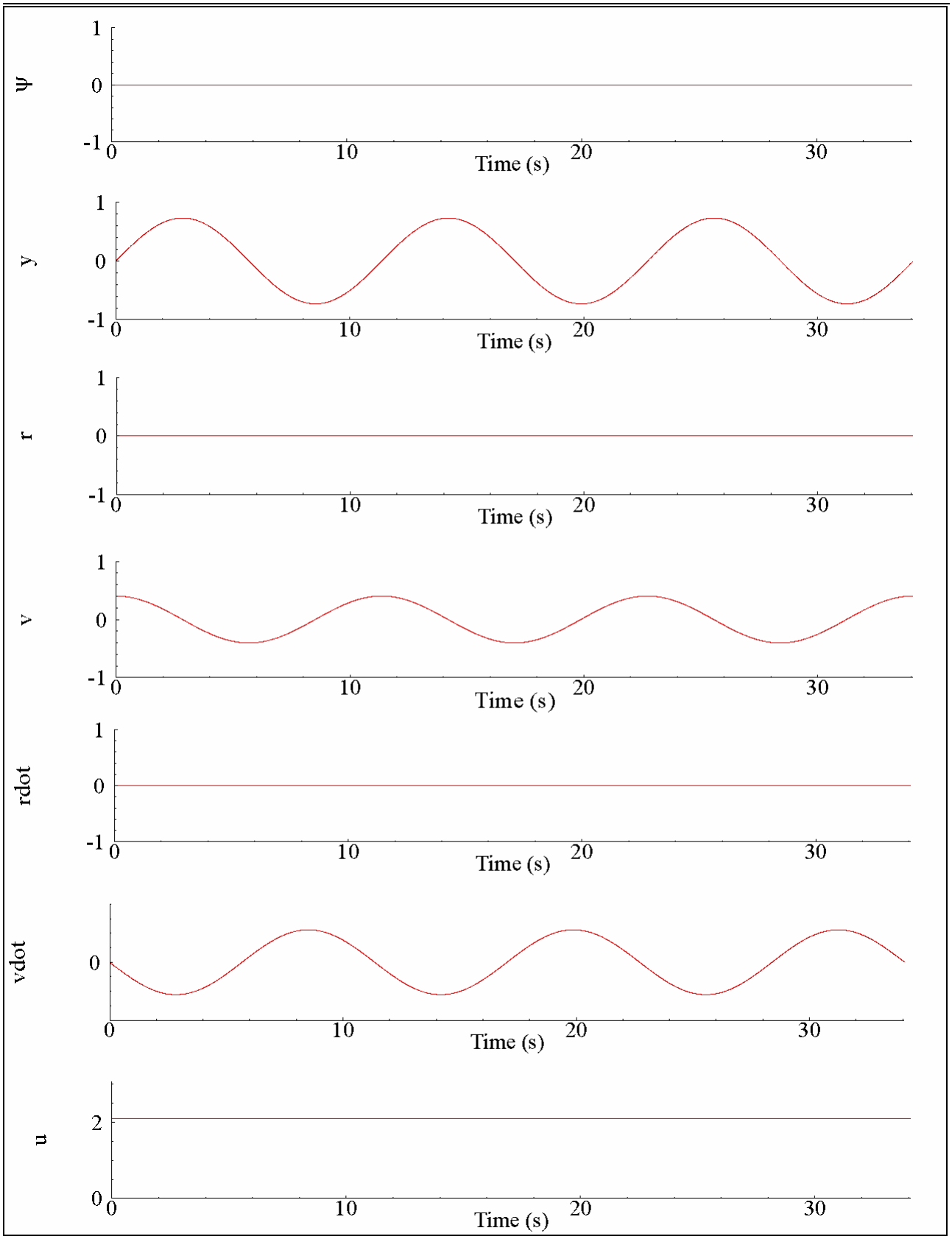

Figure C.6.1.59 Sway_280_7 (part 1).

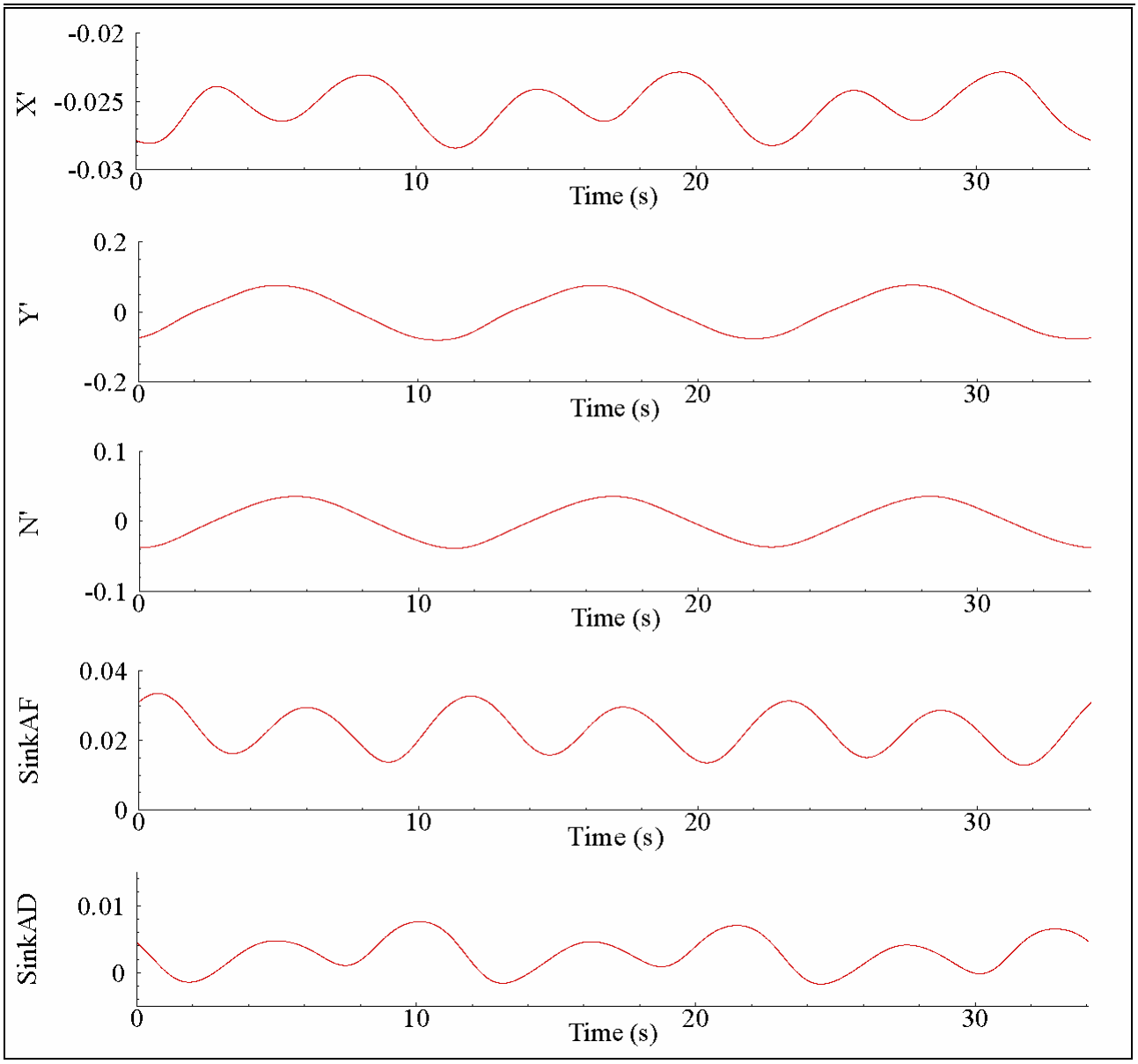

Figure C.6.1.60 Sway_280_7 (part 2).

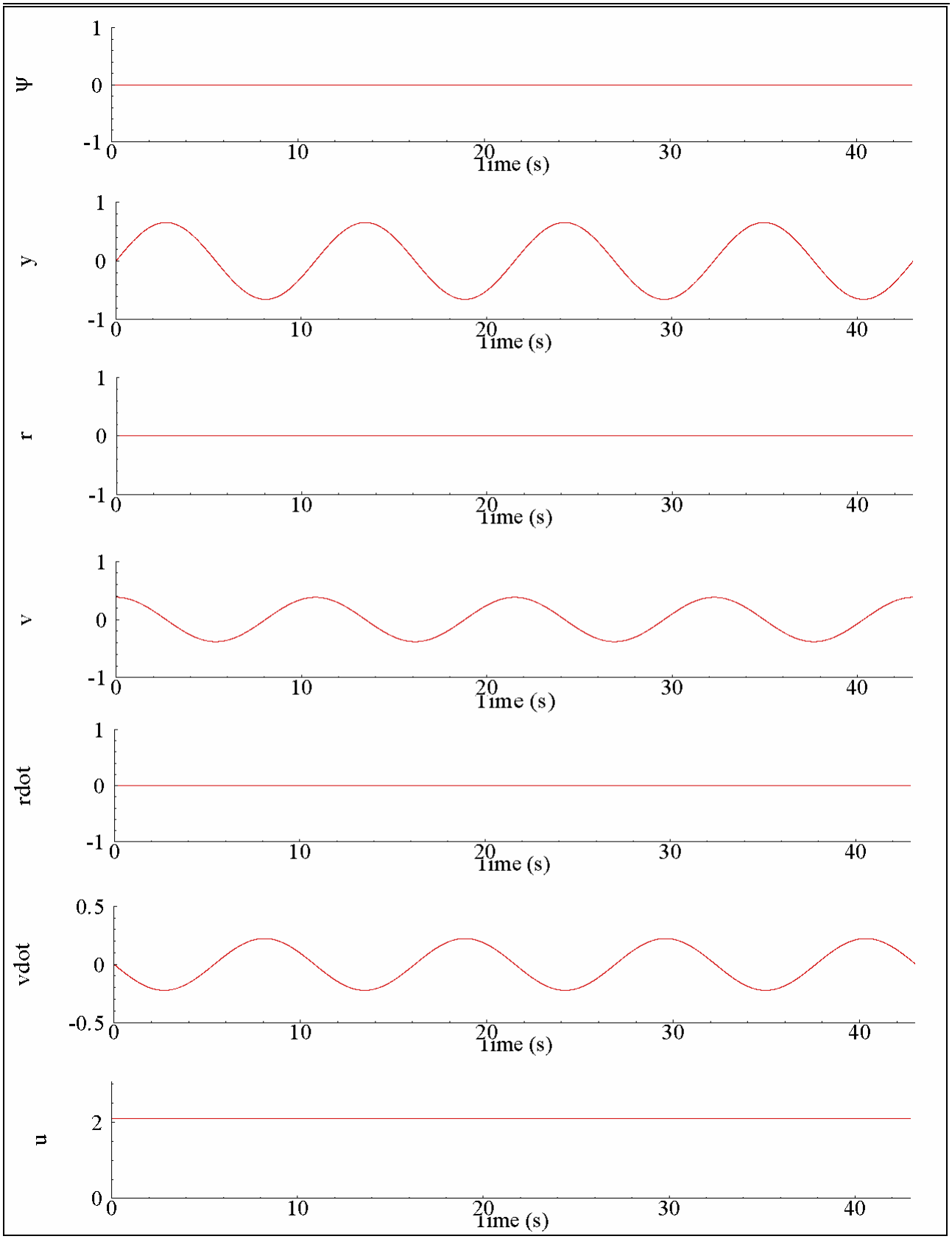

Figure C.6.1.61 Sway_280_8 (part 1).

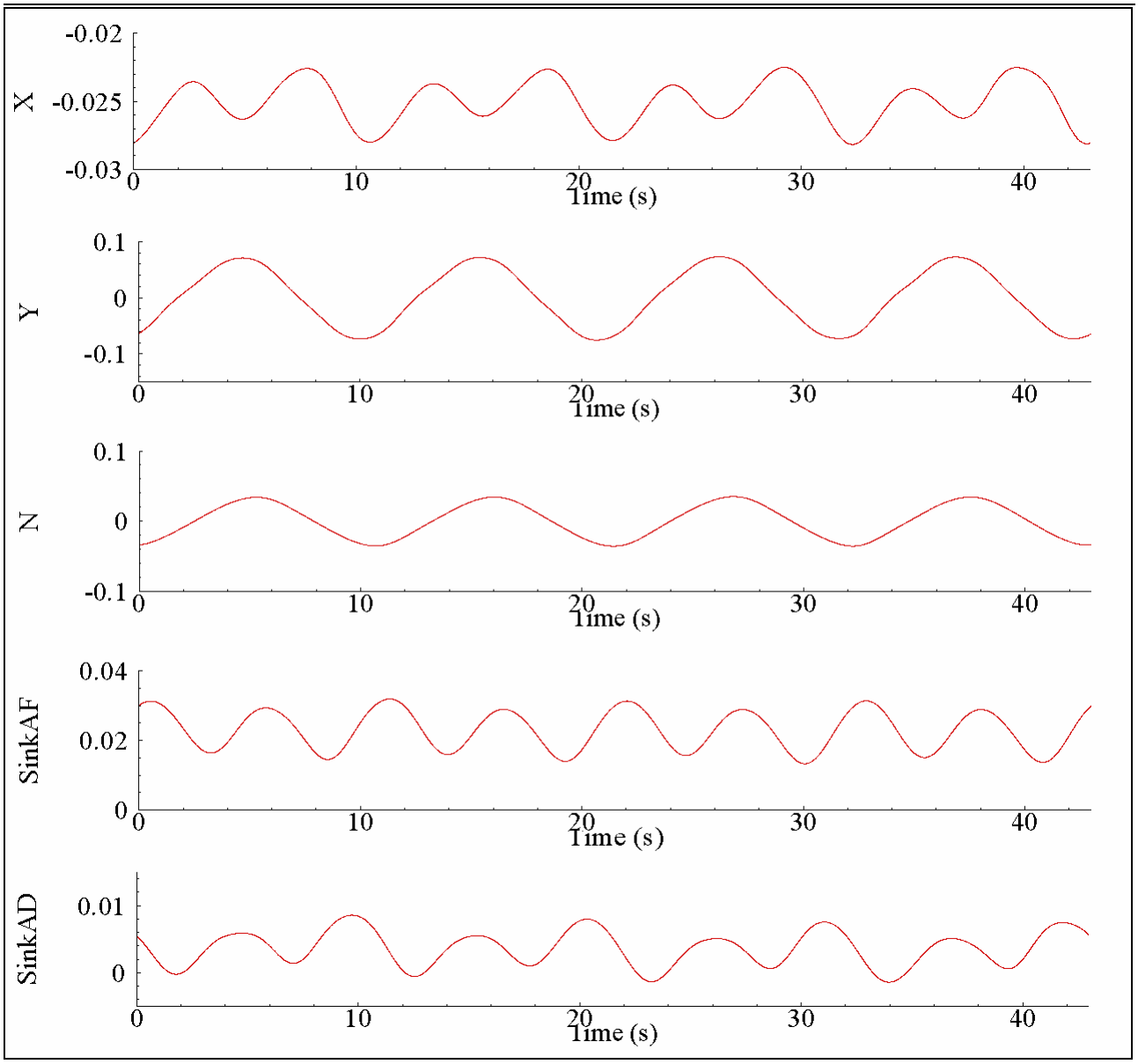

Figure C.6.1.62 Sway_280_8 (part 2).

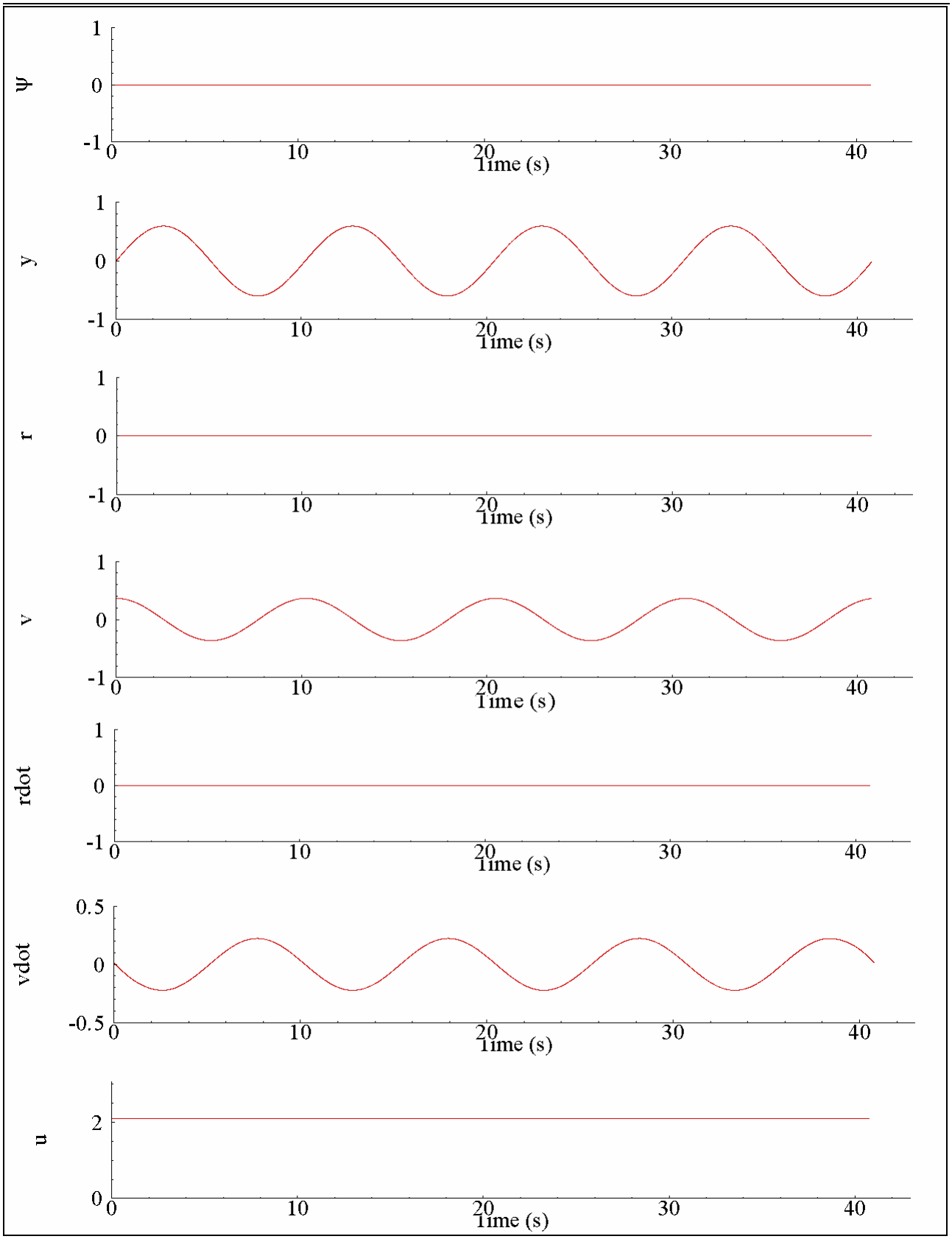

Figure C.6.1.63 Sway_280_9 (part 1).

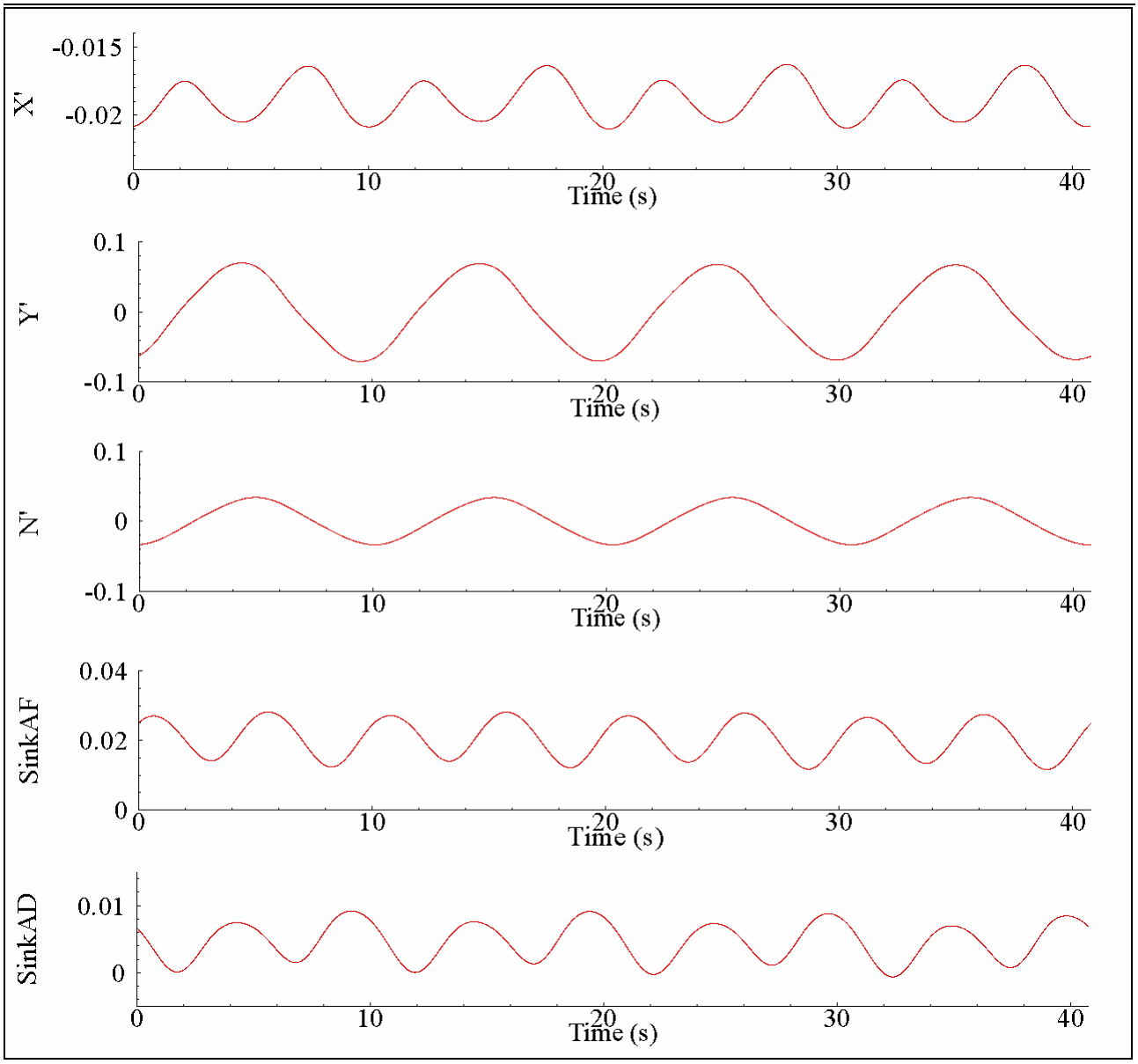

Figure C.6.1.64 Sway_280_9 (part 2).

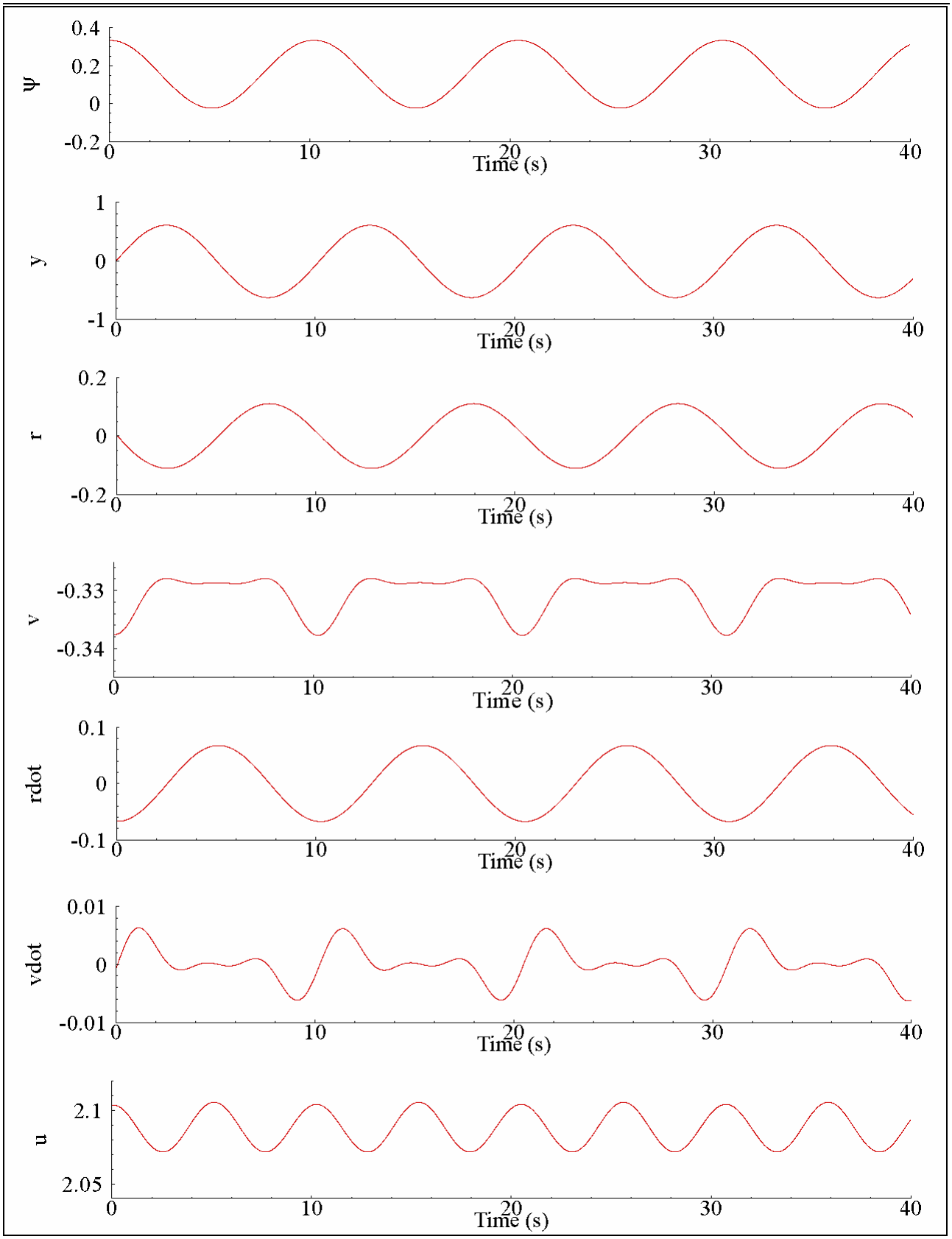

Figure C.6.1.65 Yaw&Drift_280_1 (part 1).

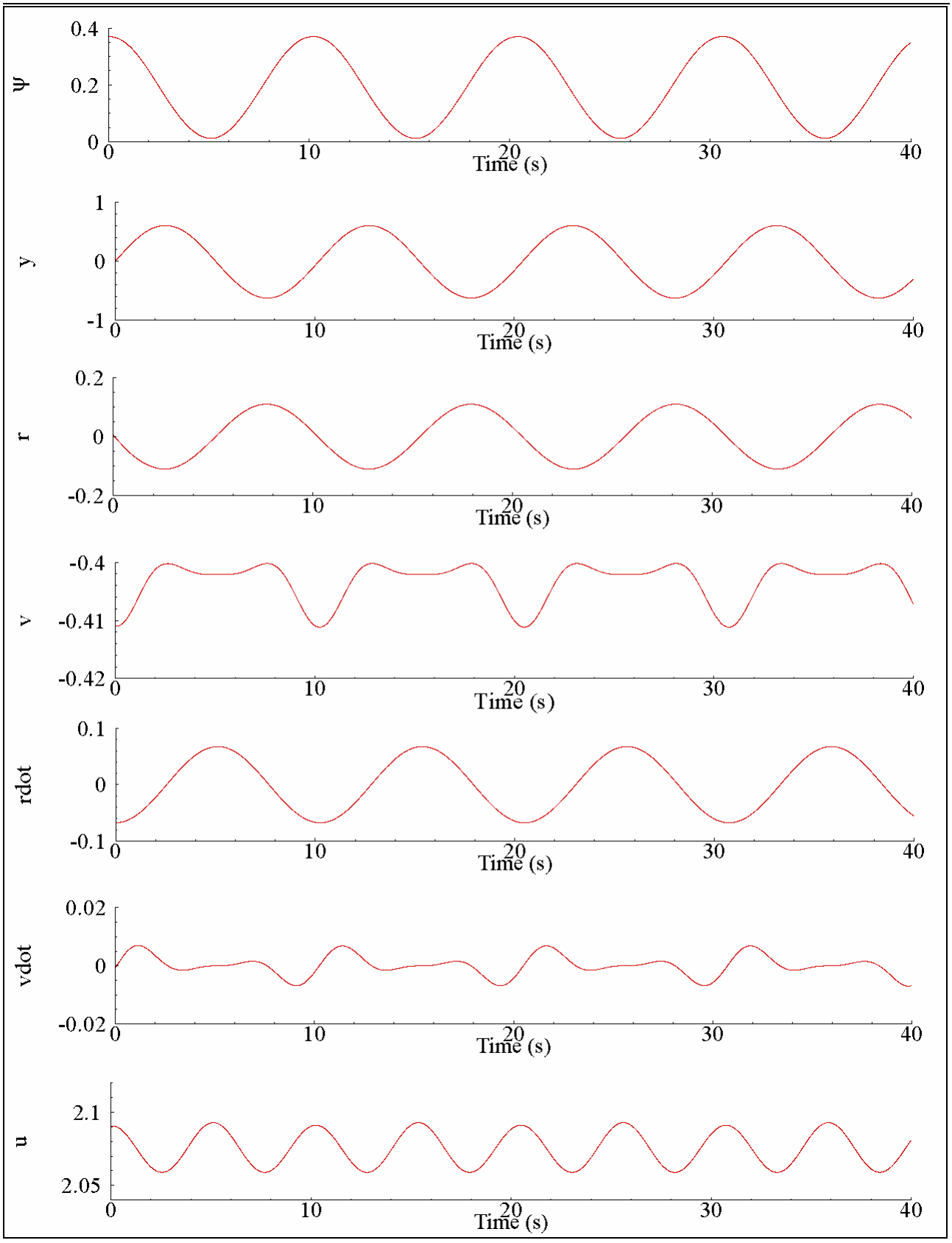

Figure C.6.1.66 Yaw&Drift_280_2 (part 1).

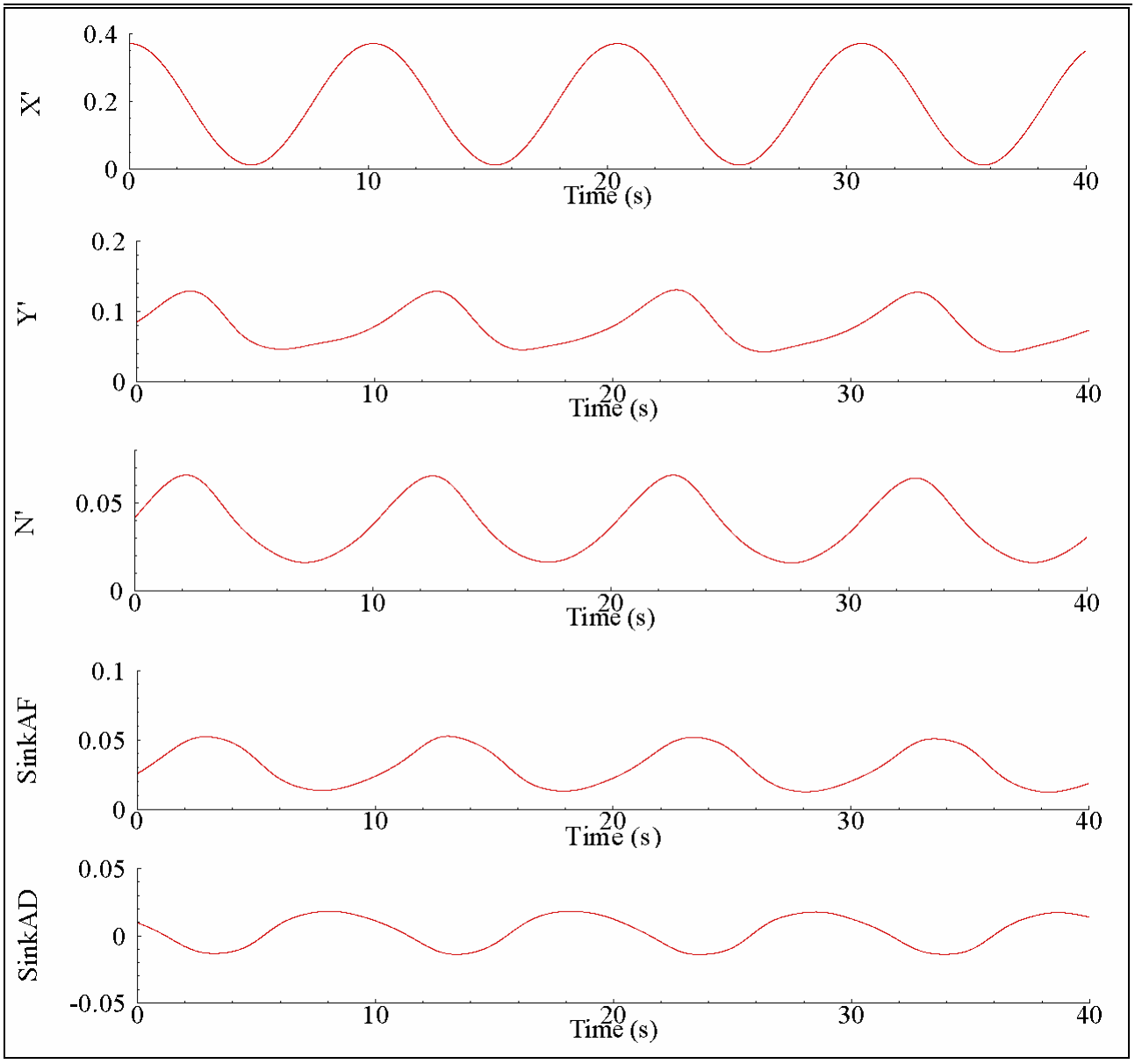

Figure C.6.1.67 Yaw&Drift_280_2 (part 2).

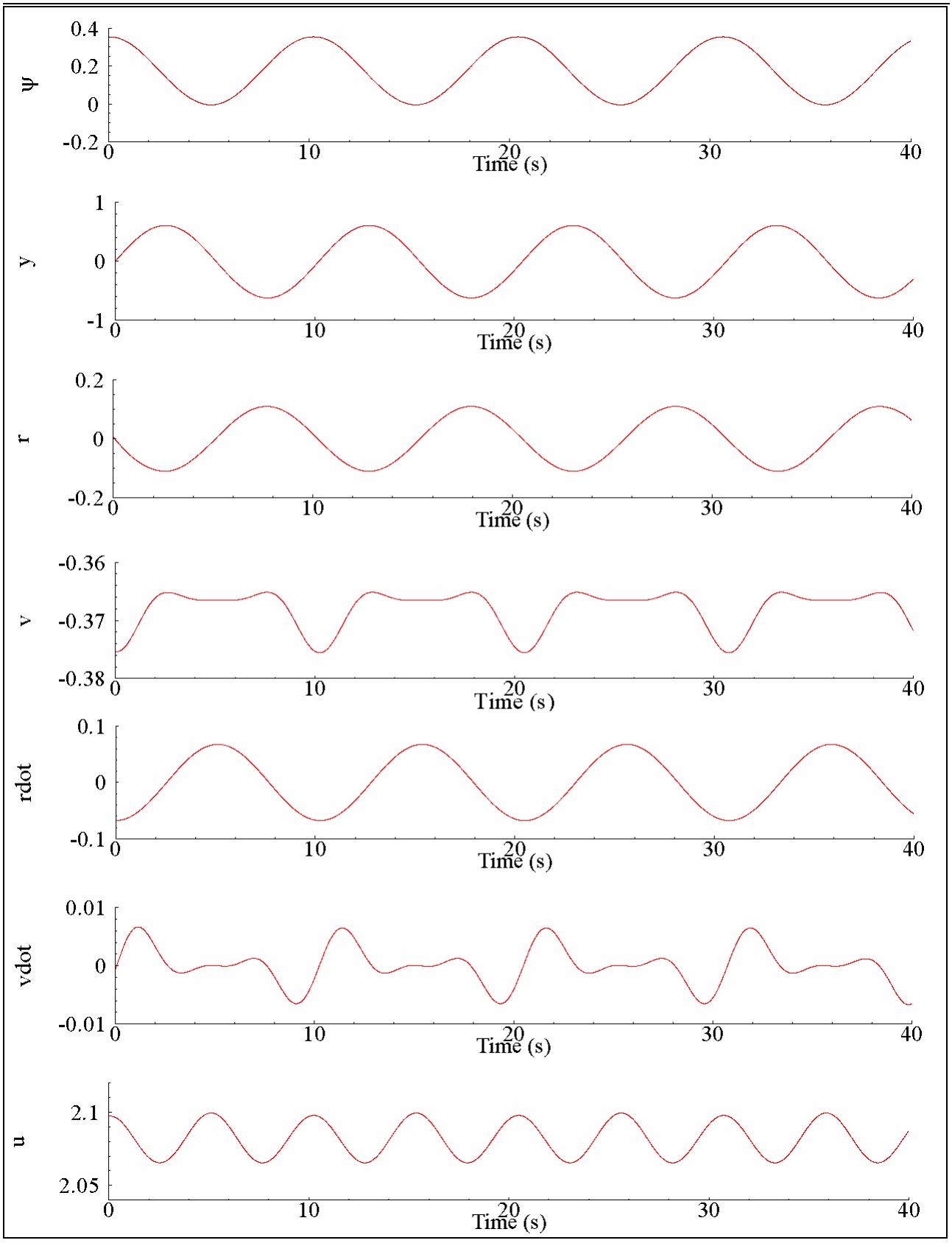

Figure C.6.1.68 Yaw&Drift_280_3 (part 1).

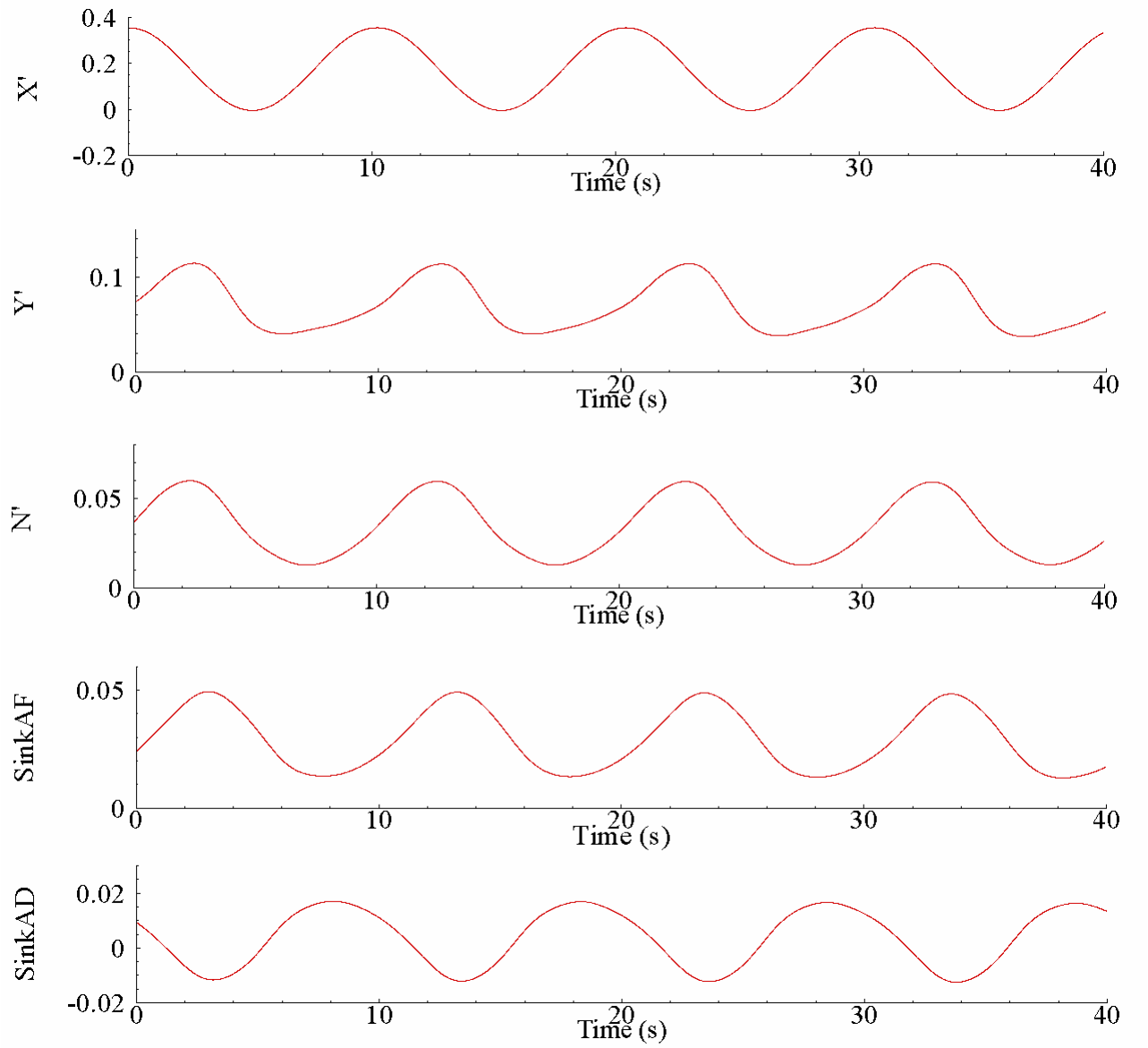

Figure C.6.1.69 Yaw&Drift_280_3 (part 2).